

Sheffield Hallam University

Raman and FTIR studies of the distribution and dynamics of active molecules in polymer films.

MURA, Carine.

Available from the Sheffield Hallam University Research Archive (SHURA) at:

<http://shura.shu.ac.uk/20101/>

A Sheffield Hallam University thesis

This thesis is protected by copyright which belongs to the author.

The content must not be changed in any way or sold commercially in any format or medium without the formal permission of the author.

When referring to this work, full bibliographic details including the author, title, awarding institution and date of the thesis must be given.

Please visit <http://shura.shu.ac.uk/20101/> and <http://shura.shu.ac.uk/information.html> for further details about copyright and re-use permissions.

LEARNING CENTRE
CITY CAMPUS, POND STREET,
SHEFFIELD, S1 1BZ.

101 610 830 3



Return to Learning Centre of issue
Fines are charged at 50p per hour

15 AUG 2007

Spn

24 AUG 2007 *Spn*

REFERENCE

ProQuest Number: 10697408

All rights reserved

INFORMATION TO ALL USERS

The quality of this reproduction is dependent upon the quality of the copy submitted.

In the unlikely event that the author did not send a complete manuscript and there are missing pages, these will be noted. Also, if material had to be removed, a note will indicate the deletion.



ProQuest 10697408

Published by ProQuest LLC (2017). Copyright of the Dissertation is held by the Author.

All rights reserved.

This work is protected against unauthorized copying under Title 17, United States Code
Microform Edition © ProQuest LLC.

ProQuest LLC.
789 East Eisenhower Parkway
P.O. Box 1346
Ann Arbor, MI 48106 – 1346

DECLARATION

The work described in this thesis was carried out by me in the Materials Research Institute at Sheffield Hallam University, between October 1995 and September 1998.

I declare that this work has not been accepted in substance for any degree, and is not being concurrently submitted in candidature for any other degree. The work is original except where indicated by reference.

Student _____

Supervisor _____

Date _____

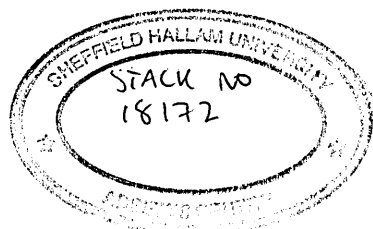
Raman and FTIR studies of the distribution and dynamics of active molecules in polymer films

Carine MURA

A thesis submitted in partial fulfilment of the requirements of
Sheffield Hallam University
for the degree of Doctor of Philosophy

November 1998

Collaborating Organisation : Zeneca Specialties



LEVEL 1

ABSTRACT

Fourier Transform Infrared Attenuated Total Reflection Spectroscopy (FTIR-ATR) and Raman microscopy were employed to study the distribution and leaching of the fungicide fluorfolpet in plasticised poly(vinyl chloride) (pPVC) matrixes, along with the diffusion and perturbation of water molecules in the matrixes.

Raman mapping and depth profiling were used to determine the molecular distribution of fluorfolpet on the surface and in the bulk of the films respectively. The films were examined both before and after treatment with water at 25°C, in order to study the effect of the leaching of fluorfolpet and its distribution and that of the plasticiser dioctylphthalate (DOP). It was found that the degree of leaching was strongly dependent upon the concentration of DOP in the films, and that leaching occurred from the surface (i.e. film/solvent interface). The distribution of the additives was determined to be "heterogeneous" on the microscopic scale, but "homogeneous" on the macroscopic scale.

Additional information such as the rate of migration of the biocide inside the film was obtained using FTIR spectroscopy and the rotating disc method in conjunction with UV spectroscopy.

FTIR-ATR was used to investigate the hydration and dehydration of plasticised PVC films. Monitoring of the time dependent change in the $\nu(\text{OH})$ mode of water was used to determine the mode of sorption of water into PVC. A dual-mode sorption model was found to fit the data well. Diffusion rates of water were found to be strongly dependent on the DOP concentration in the film. It was shown that the "free volume" and the "number of potential binding sites" were determining factors for the diffusion of water in PVC films.

A systematic FTIR-ATR study of the perturbation of water sorbed into PVC polymer as a function of plasticiser content and time is reported. The $\nu(\text{OH})$ band of water in the polymer has been fitted to individual components, corresponding to those recently found for pure water itself. A detailed quantitative analysis of the frequency shifts and relative intensities of these bands yields direct evidence for the breaking of the water network in the polymer matrix.

ACKNOWLEDGEMENTS

First, I would like to thank my supervisor Prof. Jack Yarwood at Sheffield Hallam University for his encouragement and advice throughout this project.

I am also grateful to Zeneca Specialties Manchester for sponsoring the project and I would like to acknowledge the help of Mr. Ron Swart, Dr. David Hodge and Dr. Jonathan Booth. I also would like to thank the other staff at Zeneca, especially Mr. Paul Rainsford who carried out the DSC work.

A special thanks goes to all my friends at Sheffield Hallam University, for putting up with me for so long, and making my stay in Sheffield so enjoyable. So thanks to Jane (also known as the "Sexy Jane"), Pierre (also known as the "Sexy Pierre"), Chris ("like the landscape artist"), Pete (the "Beer Monster"), France, Franny, Sohail, Chris S., Delphine, JPG, Sandry, Jeff, and Thierry.

I also would like to thank the "Teesside French connection", Alex, Carine, Evelyne, Claudine, and especially Isabelle and Andy for their support and encouragement.

Last but not least, I would like to thank my family and especially my parents, for their support throughout my academic years.

Finallement, mes derniers remerciements vont à ma famille et spécialement à mes parents, pour leurs support et encouragements durant toutes ces années.
Merci.

CONTENTS

CHAPTER 1. : INTRODUCTION.....	1
1. 1. POLYVINYL CHLORIDE.....	3
1. 2. PVC FORMULATIONS.....	4
1. 2. 1. PVC additives.....	4
1. 2. 2. Plasticisers.....	5
1. 2. 3. Resistance to biological attack	8
1. 3. BIODETERIORATION OF PLASTICISED PVC	9
1. 3. 1. Outward manifestations of biodeterioration	9
1. 3. 2. Attacking micro-organisms	10
1. 3. 3. Susceptibility of polyvinyl chloride to biodeterioration.....	11
1. 3. 4. Biofouling in industry.....	12
1. 3. 5. Formation of biofilms on medical devices.....	15
1. 3. 6. Economic problems and cost of biofouling	15
1. 3. 7. Mechanism of biodegradation.....	16
1. 4. PROTECTION AGAINST MICROBIAL ATTACK.....	18
1. 4. 1. Choice of biocide	18
1. 4. 2. Mechanism of microbiocidal action.....	19
1. 4. 3. Assessment of the biocide effect.....	20
1. 4. 4. Previous work on the leaching of biocides.....	22
1. 5. GENERAL AIMS.....	23
1. 6. REFERENCES.....	25
CHAPTER 2. : SPECTROSCOPY BACKGROUND	33
2. 1. INFRARED SPECTROSCOPY.....	36
2. 1. 1. Molecular vibrations.....	37
2. 1. 1. 1. The vibrating diatomic molecule	37
2. 1. 2. Intensities in infrared spectroscopy	41
2. 1. 2. 1. Selection rules for infrared.....	42

2. 1. 2. 3. Number of molecules in the sample	43
2. 1. 3. Fourier transform infrared spectroscopy	44
2. 1. 3. 1. The Michelson interferometer	44
2. 1. 3. 2. Advantages of Fourier transform	49
2. 1. 3. 3. Disadvantages of Fourier transform	52
2. 1. 3. 3. 1. Fellget disadvantage.....	52
2. 1. 3. 3. 2. Water vapour and carbon dioxide.....	53
2. 1. 4. Attenuated total reflectance infrared spectroscopy (ATR-FTIR).....	53
2. 1. 4. 1. Introduction	53
2. 1. 4. 2. Total internal reflection	54
2. 1. 4. 3. Advantages of ATR.....	64
2. 1. 4. 4. Disadvantages of ATR.....	64
2.1.5. Data analysis	64
2. 1. 5. 1. Derivative spectrometry	65
2. 1. 5. 2. Fourier self-deconvolution	66
2. 2. RAMAN.....	70
2. 2. 1. Introduction and history	70
2. 2. 2. The Raman effect.....	71
2. 2. 2. 1. Classical description of Raman spectroscopy	74
2. 2. 2. 2. Quantum theory.....	75
2. 2. 2. 3. Selection rules and intensities for Raman scatter.....	76
2. 2. 2. 4. Limitations	76
2. 2. 3. Raman microscopy.....	76
2. 2. 4. Quantitative Raman	84
2. 2. 5. Complementarity of Raman and IR spectroscopy	85
2. 3. REFERENCES.....	87

CHAPTER 3. : DIFFUSION OF WATER IN POLYMERIC MEMBRANES..... 92

3. 1. DIFFUSION OF WATER INTO POLYMERS	94
3. 1. 1. Diffusion behaviour.....	95
3. 1. 1. 1. Case I or Fickian diffusion	97
3. 1. 1. 2. Case II diffusion.....	97
3. 1. 1. 3. Case III or non - Fickian or anomalous diffusion	98

3. 1. 2. Dual - mode sorption	98
3. 2. WATER.....	100
3. .2 . 2. Water in polymeric membranes	101
3. 3. REFERENCES.....	103

CHAPTER 4. : EXPERIMENTAL TECHNIQUES 110

4. 1. SAMPLE PREPARATION	112
4. 1. 1. Materials	112
4. 1. 2. For ATR and Raman spectroscopy	114
4. 1. 3. For rotating disc experiment	116
4. 2. FTIR - ATR SPECTROSCOPY IN THE STUDY OF DIFFUSION	116
4. 2. 1. The method of sorption for the study of Fickian diffusion	116
4. 2. 2. Application of FTIR - ATR spectroscopy to the dual -mode sorption mode.....	120
4. 2. 3. Acquisition of the infrared diffusion data.....	122
4. 3. RAMAN MICROSCOPY	125
4. 3. 1. The Renishaw Ramascope 2000.....	125
4. 3. 2. Raman mapping and depth profiling.....	127
4. 3. 2. 1. Raman mapping	127
4. 3. 2. 2. Raman depth profiling.....	130
4. 3. 2. 3. Raman imaging.....	131
4. 4. THE ROTATING DISC METHOD.....	131
4. 4. 1. Experimental set - up.....	132
4. 5. EXPERIMENTAL PROCEDURE (FOR EACH SAMPLE).....	143
4. 6. REFERENCES.....	144

CHAPTER 5.: DETERMINATION OF THE DISTRIBUTION OF FLUORFOLPET
IN PLASTICISED PVC FILMS..... 146

5. 1. INTRODUCTION	149
5. 2. RAMAN MAPPING	150
5. 2. 1. Method.....	150

a) Polyvinyl chloride.....	152
b) Dioctylphthalate	153
c) Fluorfolpet.....	154
d) Fluorfolpet / DOP / PVC	155
5. 2. 2. Quantitative analysis of the maps.....	157
5. 2. 3. Results and discussion	159
5. 2. 3. 1. Distribution of Dioctylphthalate on the surface of the film.....	159
5. 2. 3. 2. Redistribution (by leaching of fluorfolpet) of DOP on the surface of the film	160
5. 2. 3. 3. Distribution of fluorfolpet on the surface of the film	166
5. 2. 3. 4. Redistribution of fluorfolpet on the surface of the films due to leaching	169
5. 3. DEPTH PROFILING	175
5. 3. 1. Method.....	175
5. 3. 2. Quantitative analysis.....	175
5. 3. 3. Results and discussion	177
5. 3. 3. 1. Distribution of DOP as a function of depth.....	177
5. 3. 3. 2. Redistribution of DOP due to leaching (of PA3) in water	181
5. 3. 3. 3. Distribution of fluorfolpet as a function of depth	185
5. 3. 3. 4. Redistribution as a function of depth of fluorfolpet due to leaching	190
5. 4. CONCLUSION.....	194
5. 5. REFERENCES.....	196

CHAPTER 6. : HYDRATION AND DEHYDRATION OF PLASTICISED PVC FILMS.....	197
6. 1. INTRODUCTION	199
6. 2. HYDRATION OF PLASTICISED PVC FILMS	200
6. 2. 1. Determination of the diffusion coefficients using the dual - mode sorption model	202
Diffusion coefficients :.....	204
Equilibrium water content of PVC films.....	208
Swelling of the matrix.....	211

6. 2. 2. Determination of the diffusion coefficients using sorption kinetics, and Fick's second law.....	215
6. 2. 3. Conclusions	221
6. 3. DEHYDRATION OF PLASTICISED PVC FILMS	224
Diffusion rates.....	226
Shrinking of the polymer matrix	228
Conclusion.....	231
6. 4. REFERENCES.....	232

CHAPTER 7. : FTIR-ATR STUDIES OF THE PERTURBATION OF WATER MOLECULES IN A POLY(VINYL CHLORIDE) MEMBRANE.....	237
--	-----

7. 1. INTRODUCTION	239
7. 2. METHOD	240
7. 2. 1. ATR measurements.....	240
7. 2. 2. Band fitting procedure.....	241
7. 2. 3. Quantitative measurement of the perturbation	246
7. 3. RESULTS AND DISCUSSIONS	248
7. 3. 1. Changes in band shape.....	248
7. 3. 2. Changes in band position	252
7. 3. 3. Changes in intensity	258
7. 4. REFERENCES.....	262

CHAPTER 8. : LEACHING STUDIES OF FLUORFOLPET.....	267
---	-----

8. 1. INTRODUCTION	269
8. 2. EXPERIMENTAL.....	270
8. 2. 1. FTIR-ATR spectroscopy	270
8. 2. 2. Rotating disc method	274
8. 3. RESULTS AND DISCUSSION	276
8. 3. 1. FTIR-ATR results.....	276
8. 3. 2. Rotating disc method	281

8. 4. SUMMARY AND CONCLUSIONS.....	289
8. 5. REFERENCES.....	290
CHAPTER 9. : FINAL CONCLUSIONS AND FUTURE WORK.....	292
CONFERENCES ATTENDED	296
PUBLICATIONS	298

CONTENTS

CHAPTER 1. : INTRODUCTION.....	1
1. 1. POLYVINYL CHLORIDE.....	3
1. 2. PVC FORMULATIONS	4
1. 2. 1. PVC additives.....	4
1. 2. 2. Plasticisers	5
1. 2. 3. Resistance to biological attack.....	8
1. 3. BIODETERIORATION OF PLASTICISED PVC	9
1. 3. 1. Outward manifestations of biodeterioration.....	9
1. 3. 2. Attacking micro-organisms	10
1. 3. 3. Susceptibility of polyvinyl chloride to biodeterioration	11
1. 3. 4. Biofouling in industry	12
1. 3. 5. Formation of biofilms on medical devices	15
1. 3. 6. Economic problems and cost of biofouling.....	15
1. 3. 7. Mechanism of biodegradation	16
1. 4. PROTECTION AGAINST MICROBIAL ATTACK	18
1. 4. 1. Choice of biocide.....	18
1. 4. 2. Mechanism of microbiocidal action	19
1. 4. 3. Assessment of the biocide effect	20
1. 4. 4. Previous work on the leaching of biocides	22
1. 5. GENERAL AIMS	23
1. 6. REFERENCES.....	25

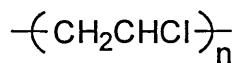
CHAPTER 1. : INTRODUCTION

Plasticised polyvinyl chloride (pPVC) is used in a wide range of applications including shower curtains, pool liners, cable and wire insulation, baby pants, wall coverings and medical devices. In the United States and Japan PVC is second in volume to polyethylene (PE), but in the other plastics - producing countries it is the leading plastic material. PVC use in packaging is growing fast in the United States, from 300 million pounds in 1987 for films and sheet forms in packaging to 360 million pounds in 1988, and up to 13.7 billion pounds in 1995 (Summers 1997). Use in bottles for a wide variety of household products is growing even faster, from 165 million pounds in 1987 to 225 million pounds in 1988 (Greek 1988).

1. 1. POLYVINYL CHLORIDE

Commercial PVC polymers are the products of polymerisation of vinyl chloride , $\text{CH}_2=\text{CHCl}$ (Titow 1990). Different polymerisation techniques are being used to produce PVC polymers : suspension polymerisation (about 80% of total commercial polymer production), emulsion polymerisation (about 10%) and solution polymerisation.

The basic repeat unit of the PVC polymer chain is :

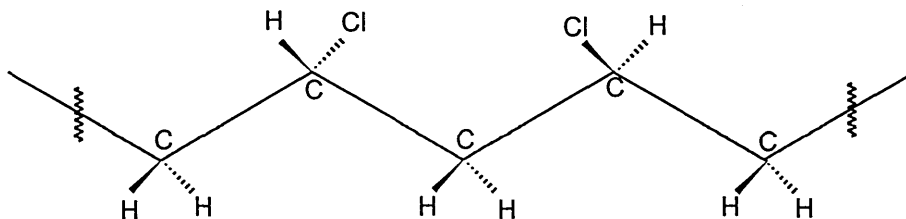


as the monomer units are for the most part joined head-to-tail (Krimm and Liang 1956, Fuller 1940).

The X-ray diffraction pattern of oriented crystalline specimens show that the fundamental repeat unit along the chain is about 5\AA , suggesting that, although the carbon chain backbone is in a planar zigzag, the chlorine atoms are

alternately on opposite side of the plane of the carbon chain (Gugelmetto et al. 1971, Abdel-Alim 1975).

Therefore the structure for crystalline polyvinyl chloride can be represented as follows :



Crystallinity of the films can be measured by Raman; using the sum of the areas of the peaks at 608 and 638 cm^{-1} expressed as the fraction of the total area under all the $\nu(\text{C-Cl})$ peaks, an approximate measure of crystallinity is obtained.

However commercial PVC polymers may be regarded as essentially amorphous in nature (Howard 1973, Lia et al. 1980), containing small crystallites (amounting to about 8-10% crystallinity). The glass transition temperature (T_g) of commercial homopolymers lies in the range 80-84°C.

1. 2. PVC FORMULATIONS

1. 2. 1. PVC additives

The combination between the basic polymer $(\text{CH}_2\text{CHCl})_n$ with a wide range of additives including plasticisers, fillers, lubricants, stabilisers, and pigments yields an infinite number of PVC plastics with physical, chemical and electrical properties that can be tailored to almost any requirement by simply varying the choice of additives (Davidsons and Gardner 1983, Titow 1990).

In the ideal case, the incorporation of a filler might confer the combined benefits of technical advantages in the properties and performance of the product; possibly improvement in appearance, product cost reduction, and improved or easier processing at no higher cost (Miles and Briston 1965). Examples of

such fillers are glass fibres used as reinforcing fillers. Other fillers act as flame retardants and smoke suppressants, or simply as pigments.

The role of stabilisers is to prevent thermal and photochemical degradation of PVC.

1. 2. 2. Plasticisers

The plasticiser is probably the additive conferring PVC its versatile character (Titow 1990) ; Without the incorporation of plasticisers, PVC forms a strong, but rigid material, unplasticised PVC (uPVC), applied for example in the production of window-frames and in pipe materials. The principal role of a plasticiser is to impart to the ultimate product the properties of flexibility, extensibility and softness. The characteristics of plasticising substances is that they lower the melting temperature, elastic modulus and second order transition temperature of polymers, but do not alter the chemical nature of the macromolecules. The plasticiser is responsible for lowering the glass-transition temperature (T_g dropped from 80°C down to -50°C in some cases) (Vergnaud 1991), reducing strength and increasing impact resistance. That means that PVC softens from a hard, glassy material to a softer, rubbery material at the T_g temperature. As the temperature increases, the molecules vibrate more. The vibrations separate the molecules, making them more mobile. At T_g , vibrations are sufficient to separate the molecules enough so that they can move past each other, thereby making the plastic soft and rubbery. Therefore as the plasticiser content in a polymer increases and the T_g decreases, the polymer films become more malleable at lower temperatures (i.e. room temperature).

The proportion of plasticiser in a PVC composition is always fairly substantial and may be very high in soft materials (up to 80% in wt).

The plasticiser or combination of plasticisers used must be compatible with the polymer matrix and must be cost effective. Generally, a combination of plasticisers is used, and the resulting properties will represent a combination of those normally conferred by each individual plasticiser when present alone.

In the practical context a distinction is commonly made between primary and secondary plasticisers. The former are those which are highly compatible with PVC polymers, whilst the latter, less compatible, are generally used in mixtures with primary plasticisers to confer some special balance of properties on the PVC composition, or simply to lower the costs (Titow 1990, Miles and Briston 1965). Dioctylphthalate (DOP) is an example of a relatively inexpensive, general-purpose plasticiser. Table 1. 1. shows a summary of some plasticisers effects (Titow 1990).

PVC plasticisers are mainly organic esters with high boiling points. Two thirds of the plasticisers in general use are diesters of phthalic anhydride with C₄-C₈ alcohols. The other classes of more specialised plasticisers are phosphoric esters (triarylphosphates), alkyl esters or dibasic alkyl acids, alkyl trimellitate esters, or high molecular weight polyesters (polymeric plasticisers) and epoxies.

Mechanism of plasticisation :

Mixtures of PVC and various plasticisers have been widely investigated by a wide range of state-of-the-art analytical techniques, including vibrational spectroscopy, molecular modelling, solid state nuclear magnetic resonance spectroscopy (Howick 1995). Several theories have been proposed to explain the mechanism of plasticiser action. These include :

- (i) the "lubricity theory" (Kickpatrick 1940, Clark 1941, Barron 1943),
- (ii) the "gel theory" (Doolittle 1954, Bruins 1965),
- (iii) the "free volume theory" (Howick 1995),
- (iv) "solvation - desolvation equilibrium",
- (v) "generalised structure theories",
- (vi) interaction parameters (Dessain and Anderson 1992),
- (vii) spectroscopic studies of specific interactions (Benedetti et al. 1985, Tabb and Koenig 1975).

Details of each are described in 'The technology of plasticiser' by Sears and Darby (Sears and Darby 1982).

From these studies it is clear that a single theory is insufficient to explain the overall plasticisation process, but that each of them contributes to explain the different steps involved in the plasticisation mechanism.

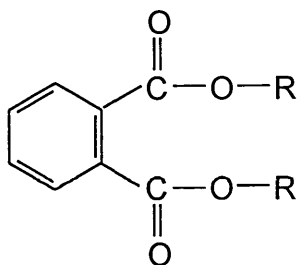
The main stages of plasticisation can be summarised as followed :

- (i) plasticiser is mixed with the PVC resin,
- (ii) absorption of the plasticiser and swelling of the resin particles,
- (iii) diffusion of the plasticiser within the polymer particles, i.e. polar groups in the PVC resin are freed from each other,
- (iv) plasticiser polar groups interact with the polar groups of the resin, so that polymer molecules are no longer rigidly held together but behave as a polymer in its rubbery rather than glassy state (i.e. the chemical nature of the polymer is not altered).

Table 1. 1.

Characteristics required	Typical relevant plasticiser type(s)	Examples of application
Price economy	Selected phthalates, extenders	Wide range of cheaper grade compositions
Important features of behaviour of plasticiser in composition : (a) high compatibility with PVC resins (b) Performance	Many phthalates, triaryl phosphates Polymeric plasticisers, high molecular weight phthalates	Paste mouldings and coatings shower curtains, upholstery
Processing properties: (a) Ease of solvation and gelation (b) Low viscosity (c) High viscosity	BBP, DBP, triaryl phosphates, phthalates Aliphatic diesters, extenders BBP, DBP, triaryl phosphates, polymeric plasticisers	Foamed coatings
End-use properties : (a) Good colour (b) Good chemical resistance (c) good low temperature properties (d) Electrical properties (e) Food contact applications (f) Mechanical properties	Phthalates Polymeric plasticisers Aliphatic diesters Triaryl phosphates, sebacates High-purity grade individual plasticisers Triaryl phosphates, sebacates	Clear compositions Protective clothing Tarpaulins, flexible tubing Packaging films

For the purpose of this PhD, the plasticiser dioctylphthalate (DOP) was used to obtain plasticised PVC films. Dioctylphthalate falls into the category of phthalate plasticisers which are compounds of the general formula :



For DOP, $R = \text{CH}_2\text{CH}(\text{C}_2\text{H}_5)(\text{CH}_2)_3\text{CH}_3$

The phthalates constitute the biggest and most widely used single chemical group of plasticisers.

1. 2. 3. Resistance to biological attack

It is a well known fact that plasticised PVC films can be attacked by micro-organisms, especially fungi (Berk 1950, Berk et al. 1957, Kurane 1998). Of the main PVC formulation components, those vulnerable to microbiological attack are : most plasticisers (in varying degrees, depending on the chemical nature, with epoxy compounds most highly susceptible and aryl phosphates and chlorinated extenders the least), some stabilisers, lubricants (especially epoxy compounds) and organic fillers such as wood flour (Klausmeier and Jones 1961).

Biofouling is recognised for the serious industrial and medical problems it causes constituting economic losses of 0.5% of the British gross national product in 1976. Developing methods to prevent biofouling is therefore of great importance.

1. 3. BIODETERIORATION OF PLASTICISED PVC

Biodeterioration or biofouling can be defined as : a process of degradation initiated by living organisms or by-products directly derived from such organisms.

1. 3. 1. Outward manifestations of biodeterioration

Symptoms of such degradation can be classified into categories, as shown below : (Hueck 1974, Gächter and Müller 1985).

Morphological symptoms :

- staining : growth of mildew as on clothing, paint, tents, out-doors furniture, bathroom furniture (shower curtains, bath mats),
- efflorescence and pitting : fouling of ships' hulls by barnacles and algae and pitting corrosion of ships' hulls associated with sulphate reducing bacteria,
- lesions and disfigurement : blistering of paints due to fungi, damage to wool by clothes moths,
- enhanced dirt uptake : results from surface roughness and stickiness, in vinyl hoses or wire jacketing for example,

Functional symptoms :

- changes in mechanical properties : change in elasticity modulus of pPVC,
- changes in electrical properties, especially insulating power,
- Changes in optical properties : opacity of glass caused by the etching activity of chemicals excreted by fungi,
- changes in permeability of solvents and gases of roofing membranes, protecting clothing, or sight shields for example,
- development of heat,
- development of odours,

hygienic effects : growth of micro-organisms also creates the danger of supporting and dispersing pathogenic organisms.

The essential mechanism of microbial attack is enzymatic degradation of the substrate on which the micro-organisms grow (Reese et al. 1955, Berk et al. 1957). Both bacteria and fungi produce enzymes (Williams 1985) capable of breaking down many carbon compounds to simpler substances usable as nutriment. Some of the products of the breakdown process can be coloured. Pink stains due to the pink/red pigment of *streptomyces rubrireticuli* or black spots are characteristic of PVC biodegradation.

As mentioned above., microbial growth also affects the physical properties of the films. The removal of plasticiser from pPVC results in undesirable physical changes such as increase tensile strength and decrease elasticity, loss of flexibility (Berk 1950). It also causes changes in the electrical insulation properties of the PVC resins (Luce and Mathes 1951, Leonard and Patouillet 1951, Teitell et al. 1955).

Cryo-SEM on pPVC has shown that fungi grow not only on the surface, but also within the film, making holes and therefore causing irreversible structural damage (Moryiama 1993).

Other outward manifestations of microbiological attacks are development of offensive odours, surface tackiness or surface cracking.

1. 3. 2. Attacking micro-organisms

Micro-organisms responsible for the biodeterioration of pPVC are mainly fungi (Brown 1945, Bessems 1979, Osmon et al. 1972). The ability of cultures of single fungi (Wellman and McCallan 1945), a mixture of four fungi (Molar and Leonard 1945), or a ten-culture composite, to utilise various plasticisers as nutriment source was examined. Species and strains of various genera such

as *Aspergillus*, *Penicillium*, *Rhizopus*, *Chaetonium*, *Memnoniella*, *Monilia* and *Stachybotrys* were identified as being able to grow on pPVC films (Klausmeier and Jones 1961). Moriyama et al. (Moriyama et al. 1992) isolated the following fungal strains : *Cladosporium*, *Phoma*, *Alternaria*, *Uclocladium*, *Aureobasidium*, *Trichoderma*, *Penicillium* and *Aspergillus* from Japanese bathrooms.

Numerous publications also show that pPVC can be damaged by bacteria (Pankhurst et al. 1971, Bessems 1988) , actinomycetes (Bessems 1979, Klausmeier and Osmon 1976, Williams 1985) and yeast (Osmon et al. 1979, Klausmeier and Jones 1961, Klausmeier 1966, Stahl and Pessen 1953).

1. 3. 3. Susceptibility of polyvinyl chloride to biodeterioration

Complete plastic formulation contains not only the polymer itself, but also fillers, plasticisers, pigments and stabilisers, but early reports (Brown 1945) tend to indicate that the resins themselves are essentially funginert (Pankhurst et al. 1971, Pankhurst and Davies 1968).

Numerous publications have demonstrated that microbial attack at flexible PVC must be attributed almost entirely to the presence of plasticisers (Klausmeier and Jones 1961, Osmon et al. 1970, Kaplan 1977, Klausmeier and Osmon 1976, Pankhurst et al. 1971, Booth and Robb 1968). The phthalates, the most commonly used group of plasticising agents are of low susceptibility, whilst the epoxidised natural oils are very vulnerable to microbial attack (Bessems 1988). But other additives such as starch fillers are also used by the micro-organisms as a source of carbon, and it has been shown that the extent of growth increases with presence of starch as a filler (Griffin and Mivetchi 1976).

The degradation of pPVC may be enhanced by UV, thermal and mechanical degradation during weathering of pPVC (Bacaloglu and Fisch 1994, Hillemans et al 1993, Bowden et al. 1991, Feldman 1989).

The resistance of PVC materials can vary widely depending on the formulation (Titow 1990). However, even resistant compositions can be affected indirectly if in contact with a material susceptible to attack , such as dust and other

substrates which accumulate on the surface of the film : thus, for example, bacteria and fungi can thrive in the cotton fabric lining of a pPVC-coated protective glove (especially if the lining is kept moist for appreciable periods by perspiration or condensation), or in a slightly moist adhesive (paste) layer of a PVC wall-covering, or in surface contaminants (grease, dirt) on uPVC cladding. This phenomenon is called dissimilation (Bessems 1979). The organic waste, various acids for instance, produced by the bacteria or fungi may attack or damage PVC.

1. 3. 4. Biofouling in industry

An industrial operation contains numerous environments where corrosion and fouling processes are potentially troublesome including cooling water systems (Bott 1992), storage tanks, water and waste water treatment facilities (Capdeville and Rols 1992), filters and piping (Herbert 1993). Microbial fouling and corrosion also occur on ship hulls (Henschel 1990), reverse osmosis membranes (Ridgway 1984), ion exchangers, drinking water systems (Characklis 1988, Block 1992). Biofouling has been reported in turbulent flows and stagnant waters, on smooth surfaces and crevices, and on metals, concrete, plastics and numerous other substrata.

Fouling biofilms impair the performance of process equipment. Table 1. 2. lists the principal industrial and environmental problems due to biofouling (Hamilton 1993, Characklis 1988).

Table 1. 3. Lists the typical micro-organisms and their associated problems (Bott 1992).

The food industry is obviously not immune from the phenomenon of microbial deterioration (Le Chevalier et al. 1987, Holah and Kearney 1992, Jones 1993, Carpentier and Cerf 1993). It has been observed that one heat-resistant micro-organism, *streptococcus thermophilus*, can contaminate pasteurised milk through the pasteuriser (by adhering to it) (Bouman et al. 1981, Ronner and Husmark 1992).

Table 1. 2.

Biofilm characteristics	Industrial and environmental problems	Concerns
<ul style="list-style-type: none"> • Surface growth • Growth on membranes, filters, porous media, sediments • Altered cell physiology • Site of high/unique chemical reactivities • Dynamic structure 	<ul style="list-style-type: none"> • Increased fluid frictional resistance in pipe flow causing energy losses • Accelerate corrosion • Heat exchanger (decreased heat transfer) • Biofilm formation on ships hull causing increased fuel consumption • Focal point for microbial growth leading to contamination downstream • Plugging of filters, reservoirs • Estuary and sea bed pollution • Loss of function (e.g. Membranes, exchange resins) • Souring of hydrocarbon reservoirs • Resistance to chemical biocides • Requirement for physical removal • Secondary oxidation of H₂S to H₂SO₄ in concrete sewerage pipes • Long term stability and regeneration after remedial treatments • Sloughing leading to infection downstream 	<ul style="list-style-type: none"> • Municipal utilities, power industry, chemical process industry, solar energy systems • Navy, shipping industry • Public health • Public health • Industrial water treatment • All industry • Chemical process industry • Public health

Table 1. 3.

Type of organism	Type of problem
<i>Bacteria</i> Slime forming bacteria Spore-forming bacteria Iron-depositing bacteria Nitrifying bacteria Sulphate-reducing bacteria	Form dense, sticky slime with subsequent fouling. Water flows can be impeded and promotion of other organism growth occurs. Become inert when their environment becomes hostile to them. Difficult to control if complete kill is required. Cause the oxidation and subsequent deposition of insoluble iron from soluble iron. Generate nitric acid from ammonia contamination. Can cause severe corrosion. Generate sulphides from sulphates and causes serious localised corrosion.
<i>Fungi</i> Yeast and mould	Cause spots on paper products, paints and plastics.
<i>Algae</i>	Grow in sunlit areas in dense fibrous mats. Can cause plugging of distribution holes on cooling tower decks or dense growths on reservoirs and evaporation ponds.

1. 3. 5. Formation of biofilms on medical devices

In medicine (Neu et al. 1992), biofilms form on catheters and implants (Sticker and Winters 1993, Reid and Busscher 1992, Pascual et al. 1986, Anwar and Strap 1992, Williams 1985, Fletcher 1992, Busscher et al. 1992). Skin flora such as *Staphilococcus epidermidis* are commonly found to be associated with device related infections. Formation of biofilms on medical devices is particularly serious in acute and chronic care settings (intensive care patients, premature new-borns, cancer and transplant patients) where ill patients can die from device related infections (Pascual et al. 1986), often due to *coagulase negative Staphilococci* (Willcox 1992, Reid and Busscher 1992).

1. 3. 6. Economic problems and cost of biofouling

An estimate of the economic consequences of fouling was presented by Pritchard (Pritchard 1981) for fouling in Britain and suggested the cost was between \$600-1000 million per year, which represents about 0.5% of the British 1976 BNP.

The technical problems arising from biodeterioration are accompanied by other problems (Characklis 1990) such as quality control problems, increased costs for excess equipment capacity to account for fouling, increased cost for premature replacement of equipment, cost of downtime resulting in loss of production (downtime can cost a power plant as much as \$ 1 million per day), and safety problems.

1. 3. 7. Mechanism of biodegradation

The growth of micro-organism depends primarily on the following factors (Feldman 1989, Bessems 1979, Osmon et al. 1972) :

- pH,
- temperature (Bessems 1988), it has been a constant observation that the hot-wet tropical environment favours microbial growth (Upsher 1984a and 1994b, Moriyama et al. 1993, Molar and Leonard 1949, Moriyama et al. 1992),
- availability of mineral nutrients,
- oxygen concentration,
- humidity (the presence of water being a prerequisite).

Biodeterioration is essentially limited at the interface at which all the above factors are mutually present. Osmon and co-workers (Osmon et al. 1972) have demonstrated that regardless of the shape of the pPVC sample, the growth of micro-organisms is concentrated at the periphery of the film, i.e. where water inorganic nutrients, oxygen and organic substrata are the most readily available. The rate limiting factor for biodeterioration seems to be the rate of plasticiser diffusion (Osmon et al. 1972), thus plastics containing a non-diffusing plasticiser could be considered microbially resistant.

The ability of plasticisers to support growth is due to the ability of the micro-organism to utilise them as carbon source. The micro-organisms are able , through enzymatic reactions, to decompose the plasticiser into smaller molecules used for growth. Many micro-organisms are capable of producing a wide variety of hydrolyases (such as amylases, chitinase, arabinase, xylases pectinase, keratinase, lipase etc...) (Williams 1985), which enables them to deesterify hydrolysable groups such as plasticisers in the main chain of the pPVC matrix.

Fouling biofilm accumulation can be considered the net result of the following physical, chemical, and biological processes (Characklis 1990, Videla and Characklis 1992, Carpentier and Cerf 1993) :

(i) Transport and adsorption of organics : organic molecules are transported from the bulk liquid to the substratum where some of them adsorb, resulting in a "conditioned substratum".

(ii) Transport on microbial cells : a fraction of the microbial cells are transported from the bulk water to the conditioned substratum. A fraction of the cells that strike the substratum adsorb to it for some finite time and then desorb. This process is termed reversible adsorption. Desorption may result from fluid shear forces, but other physical, chemical or biological factors may also influence the process.

(iii) Attachment of microbial cells : A fraction of the reversible adsorbed cells remain immobilised beyond a "critical" residence time and become irreversibly adsorbed.

(iv) Growth within the film : the irreversible adsorbed cells grow at the expense of substrate and nutrients in the bulk water, increasing biofilm cell numbers. The cells may also form a significant number of products, some of which may be excreted.

(v) Detachment : portions of the biofilm detach and are re-entrained in the bulk water. Detachment may be termed erosion or sloughing. Cell multiplication can also lead to the release of daughter cells into the bulk water.

1. 4. PROTECTION AGAINST MICROBIAL ATTACK

To prevent biodegradation special additives are added in PVC compositions. Those able to destroy fungi and bacteria are often referred to , respectively, as fungicides and bacteriocides, and collectively as biocides.

Adding biocides to PVC gives rise to several important aspects. Biocides may be added to destroy completely all micro-organisms, acting as a bacteriocide or fungicide, or to impede the growth of micro-organisms acting as a bacteriostat or fungistat. Biocides differ widely in the extent of the bactericidal or fungicidal effect (Kaplan 1970). They affect different species of micro-organisms and are therefore subdivided into what are called spectra. In order to obtain the desired spectrum, several different biocides are being used in combination.

1. 4. 1. Choice of biocide

The choice of biocides depends on many other factors and has to be considered carefully (Bott 1992). The ideal biocide for incorporation in PVC would be active against a wide range of micro-organisms, be active at low concentration (0.1-1% by weight of the composition) (Titow 1990, Bessems 1988), be compatible with other additives, be resistant in time (i.e. stability and long lasting effectiveness), have relatively low toxicity to other life forms, and economically friendly, and cost effective. It is extremely unlikely that any one biocide will meet all these criteria so that the final choice will be a combination of two or more different biocides (Rossmore 1995).

Various types of biocides are available and can be divided into chemical families (Bott 1992, Rossmore 1995), some of which are shown in table 1. 4. :

Table 1. 4.

Biocide type	Biocide	Usage
<ul style="list-style-type: none">• Chlorinated phenols• Copper salts (Copper sulphate)• Mercury compounds• Amines and ammonium compounds• Organo tin	<ul style="list-style-type: none">• Preventol CMK• Copper 8 hydroxy-quinolinolate• Aciticide MPM• Troysan 192	<ul style="list-style-type: none">• Adhesives• Plastic products
<ul style="list-style-type: none">• Organo sulphur compounds• Isothiazolones	<ul style="list-style-type: none">• Bioperse 201• Biocide 207• Skane M8	<ul style="list-style-type: none">• Adhesives• Latex paints, resin emulsions
<ul style="list-style-type: none">• Organo-dibrominated compounds	<ul style="list-style-type: none">• 5,4'-Dibromosalicylanilide	<ul style="list-style-type: none">• Cooling water systems• Cooling towers
<ul style="list-style-type: none">• Thiocynates	<ul style="list-style-type: none">• Metasol T-10	<ul style="list-style-type: none">• Latex and oil-based paints• latex paints, PVC plastics, acrylic paints adhesives
<ul style="list-style-type: none">• Arsenic compounds	<ul style="list-style-type: none">• Vinyzene (OBPA)	<ul style="list-style-type: none">• Paper slimes, cooling water systems• PVC plastics, fabric coatings, polyurethane
<ul style="list-style-type: none">• Zinc Compounds	<ul style="list-style-type: none">• Zinc Omadine	<ul style="list-style-type: none">• PVC plastics, metal working fluids

1. 4. 2. Mechanism of microbiocidal action

Biocides are of two types (Pujo and Bott 1992, Bessems 1988, Rossmore 1995) :

(i) oxidising biocides which comprise most of the halogenated compounds and halogens (chlorine and bromine for example). In the hypo-acid form these chemicals irreversibly oxidise protein and other organic constituents, resulting in a loss of normal enzyme activity, the hydrolysis of organic constituents and subsequently the rapid death of the cell.

(ii) non-oxidising biocides (Burchfield and Storrs 1976) which are either enzyme poisons that block the transfer of electrons in the respiration enzymes or block the organic synthesis in the cell. Cytoplasm damaging biocides (heavy metal-based biocides) destroy the protein or complex with other compounds to poison

the cell. Surfactant types of microbiocides damage the cell by virtue of their surface activity. They affect the cells' differential permeability, disrupting the normal flow of nutrients into the cell and the discharge of wastes from the cell. Cationic surfactant materials (quaternary ammonium compounds) absorbed on the surface of the cell membrane, chemically react with the negatively charged ions associated with the cell wall. Anionic surfactant compounds reduce cell wall permeability and can eventually dissolve the entire cell membrane. Chlorinated phenolic compounds penetrate the cell wall, forming a colloidal suspension with the cytoplasm. The suspension causes precipitation and denaturation of protein materials within the cell. Other chemicals such as the organo sulphur compounds complex with enzyme-metabolite, or non-competitively react with an enzyme in place of the normal metabolite, or non-competitively attach to an enzyme at a point different from the normal metabolite and prevent normal enzyme reaction.

1. 4. 3. Assessment of the biocide effect

The biocide effect can be assessed in various ways (Bessems 1988) :

- (i) visually,
- (ii) by measuring the weight increase of fungus,
- (iii) by measuring the weight loss of PVC film,
- (iv) by measuring the oxygen consumption of the attacking micro-organism. This method is called the "respirometric method",
- (v) by measuring the loss of flexibility or elasticity of the deteriorated pPVC film.

These measures can be performed on samples obtained by exposure of the test material via the zone of inhibition, soil burial or humidity tests (Cadmus 1978, Bessems 1988).

There are many standard methods for determining changes in the properties of plastics, such as :

- * ISO 846-1978 (1986) : evaluation of the effects of fungal and bacterial action,
- * BS 4618 : section 4.5:1974 : effect of soil burial and biological attack,
- * ASTM G21-70 (1985) : determination of resistance to fungi,
- * ASTM G22-76 (1985) : determination of resistance to bacteria.

It is not realistic to expect that biocide application alone will be sufficient to control biofilms formation (LeChevalier 1990, Bott 1992). A strategy for biofilm control should include consideration of :

(i) The engineered system, which should have smooth surfaces to reduce adhesion of micro-organisms (Cooksey and Wigglesworth-Cooksey 1992), plus it should be free of structures which might provide protection for attached bacteria. Materials susceptible to be used as nutrients by the micro-organisms should be avoided whenever possible.

(ii) The water chemistry : in order that a proper choice of biocide may be made, a complete analysis of the water will be necessary. The pH in the system is of great importance in the efficiency of the biocide. Also a turbulent flow is preferable to stagnation.

(iii) The type of micro-organism,

(iv) the biocide ; the biocide should be appropriate for the species of micro-organisms present.

The biocide must act on the surface of the pPVC in order to avoid adhesion of the attacking micro-organisms and/or to kill these micro-organisms. This means that the incorporated fungicide or bactericide must be able to migrate from the inside of the film to the film surface where its activity is required. On the other hand the leaching of the biocide into the surrounding aqueous media must be slow enough to allow the biocide to work and not be washed away and leave an exposed film. The migration process involved is expected to depend

on the other additives it contains, and on the distribution of the biocide in the PVC film.

1. 4. 4. Previous work on the leaching of biocides

The leaching of fungicides from paint films has mostly been studied using a “leaching chamber”, or the “static” leaching method, or most recently a rotating disc apparatus (Zeneca Specialties Manchester).

Using the “leaching chamber” method, leaching profiles were obtained by determination of fungicide concentration in leachate collected following the condensation of water onto samples under investigation. In the “leaching chamber”, the samples are exposed to intermittent drops of water. Leachate samples are removed at intervals and analysed using either UV spectroscopy or HPLC.

“Static leaching” :acrylic paint is coated on a filter paper substrate and placed in bottles containing distilled water. At various time intervals the water is changed and the concentration of fungicide determined using UV spectroscopy or HPLC.

“Rotating disc” method : the solid substrate under investigation is immersed in an aqueous solution, and rotated at fixed angular frequency. Samples of the water are analysed at regular intervals using UV spectroscopy and HPLC.

In all three cases the data are plotted as leaching time against weight of biocide released. These techniques can be very time consuming; from 48 hours (for a rotating disc experiment) to up to 3 months (for a “static experiment”) are required to collect the data.

1. 5. GENERAL AIMS

This project covers the initial phase in a research venture that aims to :

- (i) determine the distribution and redistribution of one particular biocide, fluorfolpet, in a pPVC film using Raman microspectroscopy ;
- (ii) investigate whether or not the active distribution is affected by the plasticiser diffusion and hence a change in the formulation of the film ;
- (iii) examine the migration of biocide molecules in the film using the rotating disc method and their leaching into water by Fourier-transform infrared attenuated total reflectance (FTIR-ATR) spectroscopy ;
- (iv) study the water uptake and removal in pPVC films ;
- (v) explore the water perturbation in these films using FTIR-ATR spectroscopy.

Raman microscopy revealed itself to be a very useful technique for obtaining information on the molecular level about the distribution (and redistribution) of biocide molecules in pPVC films, as well as determining the loss of biocide from leaching experiments.

FTIR-ATR spectroscopy was used as an *in-situ* tool for monitoring the sorption and desorption of water in unplasticised and plasticised PVC films, and their consequences on the dynamics of leaching of biocide fluorfolpet.

This thesis describes how Raman microscopy and FTIR-ATR spectroscopy were used to reach the aims identified above and the results achieved doing so. Therefore it is divided into nine chapters where :

Chapter 1 gives a general introduction to the subject ;

Chapters 2, 3, and 4 outline the theoretical backgrounds to Raman microscopy, FTIR-ATR spectroscopy, the study of diffusion in a polymer film, and other techniques used such as the rotating disc method ;

Chapter 5, 6, 7 and 8 are results chapters in which results on the determination of the distribution of fluorfolpet in pPVC, study of water ingress

and removal, fluorfolpet leaching, as well as, the water perturbation in pPVC films are presented and discussed,

Chapter 9, gives a summary of the main conclusions and interpretations, as well as a forward look.

1. 6. REFERENCES

Abdel-Alim A.H., *J. Appl. Polym. Sci.*, 1975, **19**(8), 2179.

Anwar H., Strap J.L., *Int. Biodet. and Biodeg.*, 1992, **30**, 177.

Bacaloglu R. and Fisch M., *Polym. Degrad. and Stability.*, 1994, **45**, 301.

Barron H., *Plastics*, 1943, **7**, 449.

Benedetti E., Posar F., D'Alessio A. And Vergamini P., *J. of Polym. Sci. : Polym. Phys. Ed.*, 1985, **23**, 1187.

Berk S., *ASTM Bull.*, 1950, **168**, 53.

Berk S., Ebert H. and Teitell, *Ind. Eng. Chem.*, 1957, **49**, 1115.

Bessems E., *J.of Coated Fabrics*, 1979, **9**, 26.

Bessems E., *J. of Vinyl Tech.*, 1988, **10**(1), 3.

Block J.C., in *Biofilms - Science and Technology*, ed. : Melo L.F., Bott T.R., Fletcher M., Capdeville B., Kluwer Academic Publishers, Netherlands, 1992, 469-485.

Booth G.H. and Robb J.A., *J.of Appl. Chem.*, 1968, **18**, 194.

Bott T.R., in *Biofilms - Science and Technology*, ed. : Melo L.F., Bott T.R., Fletcher M., Capdeville B., Kluwer Academic Publishers, Netherlands, 1992, 3-11 and pp 567-581.

Bouman S., Driessen E.M., Schmidt D.G., *Proceedings of the 9th Congress on Fundamentals and Applications of Surface Phenomena Associated with Fouling and Cleaning in Food Processing*, 1981, pp 190-203.

Bowden M., Donaldson P., Gardiner D.J., Birnie J., Gerrard D.L., *Anal. Chem.*, 1991, **63**, 2915.

Brown A.E., *The Problem of Fungal Growth on Synthetic Resins, Plastics and Plasticisers*, OSRD report no 6067, 1945.

Bruins P.F., *Plasticiser Technology*, Reinhold, New York, 1965.

Burchfield H.P. and Storrs E.E., in *Proceedings of the 3rd International Biodegradation Symposium*, ed. : Sharpey J.M., Kaplan A.M., Applied science publishers Ltd., London, 1976, pp1043-1055.

Busscher H.J., Schakenraad M.J., Van der Mei H.C., in *Biofilms - Science and Technology*, ed. : Melo L.F., Bott T.R., Fletcher M., Capdeville B., Kluwer Academic Publishers, Netherlands, 1992, 309-326.

Cadmus E.L., in *Additives for Plastics : State of the Art 1.*, ed. : Seymour R.B., Academic Press Inc., 1978, pp 219-231.

Capdeville B. and Rols J.L., in *Biofilms - Science and Technology*, ed. : Melo L.F., Bott T.R., Fletcher M., Capdeville B., Kluwer Academic Publishers, Netherlands, 1992, 13-20.

Carpentier B. and Cerf O., *J. of Appl. Bacteriology.*, 1993, **75**, 499.

Characklis W.G., in *Final Report, American Water Works Association Resource Foundation*, Denver, CO, 1988.

Characklis W.G., in *Biofouling and Biocorrosion in Industrial Water Systems, Proceedings of the International Workshop on Industrial Biofouling and Biocorrosion (Stuttgart)*, Springer Verlag, Berlin, 1990, pp 7-28.

Clark F.W., *Chem. in Ind.*, 1941, **60**, 225.

Cooksey K.E. and Wigglesworth-Cooksey B., in *Biofilms - Science and Technology*, ed. : Melo L.F., Bott T.R., Fletcher M., Capdeville B., Kluwer Academic Publishers, Netherlands, 1992, 529-549.

Dessain E.C. and Anderson D., *Appl. Spec.*, 1992, **46**(1), 152.

Doolittle A.K., *The Technology of Solvents and Plasticisers*, John Willey, New York, 1954

Davidson J.A. and Gardner K.L., *Vinyl Polymers* in *Encyclopedia of Chemical Technology 3rd edition*, ed. by Grayson M., Eckroth D., Mark H.F., Othmer D.F., Overberger C.G. and Seaborg G.T., 1983, pp 798-979.

Feldman D., *Polymeric Building Materials*, Elsevier Applied Science, London, 1989, pp 496-556.

Fletcher M., in *Biofilms - Science and Technology*, ed. : Melo L.F., Bott T.R., Fletcher M., Capdeville B., Kluwer Academic Publishers, Netherlands, 1992, 299-308.

Fuller C.S. and Liang C.Y., *Chem. Revs.*, 1940, **26**, 143.

Gächter R., Müller H., in *Plastics Additives Handbook*, Hanser publishers, München, Wien 1985.

Greek E., *C. and Engings. News.*, 1988, November 15-17.

Griffin G.J.L., Mivetchi H., *Proceedings of the 3rd International Biodegradation Symposium*, ed. Sharpley J.M., Kaplan A.M., Applied Science Publishers Ltd, London, 1976, pp 807-813.

Gugelmetto P., Pezzin G., Cerri E., and Zinelli, *Plast. Polym.*, 1971, **34**(144), 398.

Hamilton W.A., in *Bacterial Biofilms and their Control in Medicine and Industry*, ed. : Wimpenny J., Nichols W., Stickler D., Lappin-Scott H., Cardiff Bioline, 1993, pp 109-112.

Henschel J.R., Branch G.M., Cook P.A., *South-African J. of Marine Sci.*, 1990, **9**, 299.

Herbert B.N., in *Bacterial Biofilms and their Control in Medicine and Industry*, ed. : Wimpenny J., Nichols W., Stickler D., Lappin-Scott H., Cardiff Bioline, 1993, pp 117-120.

Hillemans J.P.H.M., Colemonts C.M.C.J., Meier R.J., Kip B.J., *Polym. Degrad. and Stability*, 1993, **42**, 323.

Holah J.T. and Kearney L.R., in *Biofilms - Science and Technology*, ed. : Melo L.F., Bott T.R., Fletcher M., Capdeville B., Kluwer Academic Publishers, Netherlands, 1992, 35-41.

Howard R.N., *The physics of Glassy Polymers*, Applied Science Publisher, London, 1973, pp 201-206.

Howick C., *Plastics, Rubber and Composites Processing and Applications*, 1995, **23**, 56.

Hueck H.J., *Int. Biodet. Bull.*, 1974, **10**, 87.

Jones M., in *Bacterial Biofilms and their Control in Medicine and Industry*, ed. : Wimpenny J., Nichols W., Stickler D., Lappin-Scott H., Cardiff Bioline, 1993, pp 113-116.

Kaplan A.M., *Develop. in Ind. Microbiology*, 1977, **18**, 203.

Kirkpatrick A., *J. of Appl. Phys.*, 1940, **11**, 255.

Klausmeier R.E., *S.C.I. Monograph 23, Microbiological Deterioration. in the Tropics*, 1966, pp 232-243.

Klausmeier R.E. and Jones W.A., *Develop. in Ind. Microbiology.*, 1961, **2**, 47.

Klausmeier R.E. and Osmon J.L., *Proc. of the Int. Biodeg. Symp.*, 1976, 815.

Krimm S. and Liang C.Y., *J. of Polym. Sci.*, 1956, **22**, 95.

Kurane R., *Biosci. Indust.*, 1988, **46**, 3173.

LeChevalier M.W., in *Biofouling and Biocorrosion in Industrial Water Systems, Proceedings of the International Workshop on Industrial Biofouling and Biocorrosion (Stuttgart)*, Springer Verlag, Berlin, 1990, pp113-132.

LeChevalier M.W., Babcock T.M., Lee R.G., *Appl. and Environ. Microbiology.*, 1987, **53**, 2714.

Leonard J.M. and Patouillet C., *Product. Eng.*, 1951, **22**(12), 158.

Lia N. I., Tong S. N., Koenig J. L., *J. Appl. Sci.*, 1980, **25**, 2205.

Luce R.H. and Mathes K.N., *Annual report, 1950 Conference on Electrical Insulation, National Research Council*, 1951, pp 27-29.

Miles D.C. and Briston J.H. *Plasticiser, Stabilisers and Related Additives*, in *Polymer Technology*, Temple press book Ltd, London, 1965, pp 321-332.

Molar D.M. and Leonard J.M., *Tropical Deterioration of Materials for Electronic Equipment, part I. : Plasticisers*, Naval Research Laboratory report no P-2492, 1949.

Moriyama Y., Kimura N., Inoue R., Kawaguchi A., *Int. Biodet. and Biodeg.*, 1993, **31**, 231.

Moriyama Y., Nawata N., Tsuda T., Nitta M., *Int. Biodet. and Biodeg.*, 1992, **30**, 47.

Neu T.R., Van der Mei H.C., Busscher H.J., in *Biofilms - Science and Technology*, ed. : Melo L.F., Bott T.R., Fletcher M., Capdeville B., Kluwer Academic Publishers, Netherlands, 1992, 21-34.

Osmon J.L., Klausmeier R.E., Jamison E.I., *Biodet. of Materials*, 1972, **2**, 66-75.

Osmon J.L., Klausmeier R.E., Jamison E.I., *Develop. in Ind. Microbiology.*, 1970, **11**, 447.

Pankhurst E. S., Davies M. J., *Investigations into the effects of micro-organisms on PVC pressure-sensitive tape and its constituents*, in *Proceedings of the 1st International Biodeterioration Symposium*, ed., Walters A. N., Elphick J. J., 302 : Applied Science Publisher Ltd., London, 1968.

Pankhurst E.S., Davies M.J., Blake H.M., in *Biodeterioration of Materials 2.*, ed. Walters A.H., Vanderplis H., Applied Science Publisher Ltd, London, 1971, pp 76-90.

Pascual A., Fler A., Westerdal N.A.C., Verhoef J., *European J. of Clinical Microbiology*, 1986, 5(5), 518.

Pritchard A.M., in *Fouling of Heat Transfert Equipment*, ed. : Somescales F.F.C., Knuden J.G., Hemisphere Publishing Corporation, Washington, DC, 1981, pp 513-523.

Pujo M.D. and Bott T.R., *Biofilms - Science and Technology*, ed. : Melo L.F., Bott T.R., Fletcher M., Capdeville B., Kluwer Academic Publishers, Netherlands, 1992, 583-588.

Reese E.T., Cravetz H., Mandels G.R., *Farlowia*, 1955, 3, 45.

Reid G., Busscher H.J., *Int. Biodet. and Biodeg.*, 1992, 30, 105.

Ridgway H.F., Justice C.A., Whittaker C., Argo D.G., Olson B.H., *J. of American Water Works Association*, 1984, 76, 94.

Rönner U., Husmark U., in *Biofilms - Science and Technology*, ed. : Melo L.F., Bott T.R., Fletcher M., Capdeville B., Kluwer Academic Publishers, Netherlands, 1992, 403-406.

Rossmore H. W., in *Handbook of Biovide and Preparative Use*, Blackie Academic and Professional, Glasgow, 1995.

Sears J.K. and Darby J.R., *The Technology of Plasticisers*, John Willey, New York, 1982.

Summers J. W., *J. of Vinyl and Additive Tech.*, 3(2), 130.

Stahl H.W., Pessen H., *Appl. Microbiology*, 1953, 1, 30.

Sticker D. and Winters C., in *Bacterial Biofilms and their Control in Medicine and Industry*, ed. : Wimpenny J., Nichols W., Stickler D., Lappin-Scott H., Cardiff Bioline, 1993, pp 97-104.

Tabb D.L. and Koenig J.L., *Macromolecules*, 1975, 8(6), 929.

Teitell L., Berk S., Kravitz A., *Appl. Microbiology*, 1955, 3, 75.

Titow W.V., *PVC Plastics : Properties, Processing and Applications*, Elsevier Applied Science, 1990.

Upsher F.J., *Int. Biodet.*, 1984a, 20(2), 73.

Upsher F.J., *Int. Biodet.*, 1984b, 20(3), 157.

Vergnaud J. M., *Liquid Transport Processes in Polymeric Materials : Modeling and Industrial Applications*, Prentice-Hall Inc., 1991.

Videla H.A. and Characklis W.G., *Int. Biodet. and Biodeg.*, 1992, 29, 195.

Wellman R.H. and McCallan S.E.A., *Fungus Resistance of Plastics*, OSRD report no 5683, 1945.

Wilcox M.H., in *Biofilms - Science and Technology*, ed. : Melo L.F., Bott T.R., Fletcher M., Capdeville B., Kluwer Academic Publishers, Netherlands, 1992, 363-370.

Williams S.T., *Int. Biodet.*, 1985, 21(3), 201.

CHAPTER 2. :
SPECTROSCOPY BACKGROUND

CONTENT

CHAPTER 2. : SPECTROSCOPY BACKGROUND.....	33
2. 1. INFRARED SPECTROSCOPY	36
2. 1. 1. Molecular vibrations	37
2. 1. 1. 1. The vibrating diatomic molecule.....	37
2. 1. 2. Intensities in infrared spectroscopy.....	41
2. 1. 2. 1. Selection rules for infrared	42
2. 1. 2. 3. Number of molecules in the sample	43
2. 1. 3. Fourier transform infrared spectroscopy	44
2. 1. 3. 1. The Michelson interferometer.....	44
2. 1. 3. 2. Advantages of Fourier transform.....	49
2. 1. 3. 3. Disadvantages of Fourier transform.....	52
2. 1. 3. 3. 1. Fellget disadvantage	52
2. 1. 3. 3. 2. Water vapour and carbon dioxide	53
2. 1. 4. Attenuated total reflectance infrared spectroscopy (ATR-FTIR).....	53
2. 1. 4. 1. Introduction	53
2. 1. 4. 2. Total internal reflection.....	54
2. 1. 4. 3. Advantages of ATR.....	64
2. 1. 4. 4. Disadvantages of ATR	64
2.1.5. Data analysis.....	64
2. 1. 5. 1. Derivative spectrometry.....	65
2. 1. 5. 2. Fourier self-deconvolution.....	66
2. 2. RAMAN	70
2. 2. 1. Introduction and history.....	70
2. 2. 2. The Raman effect.....	70
2. 2. 2. 1. Classical description of Raman spectroscopy	71
2. 2. 2. 2. Quantum theory	74

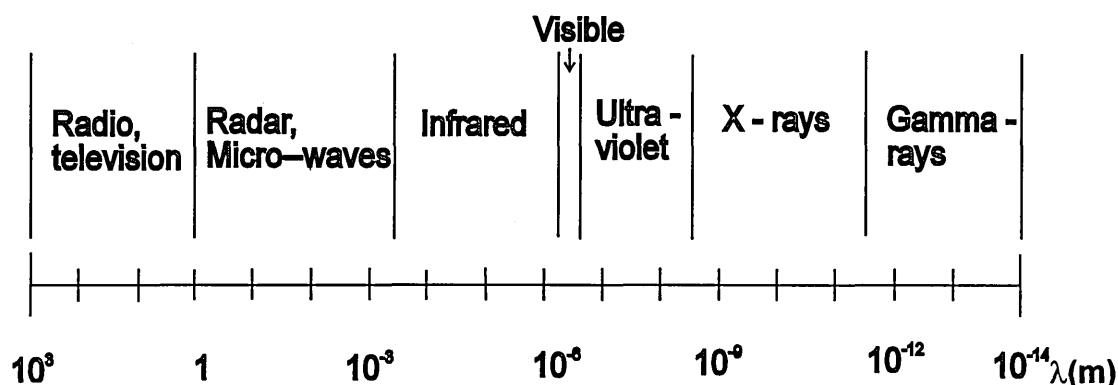
2. 2. 2. 3. Selection rules and intensities for Raman scatter	75
2. 2. 2. 4. Limitations	76
2. 2. 3. Raman microscopy.....	76
2. 2. 4. Quantitative Raman	84
2. 2. 5. Complementarity of Raman and IR spectroscopy.....	85
2. 3. REFERENCES.....	87

CHAPTER 2. : SPECTROSCOPY BACKGROUND

2. 1. INFRARED SPECTROSCOPY

We are all familiar with the various kinds of electromagnetic radiation : light (visible, ultraviolet, infrared), x-rays, radio and radar waves. These are simply part of a broad spectrum that stretches from gamma rays to radiowaves. This is illustrated in *Figure 2. 1.*

Figure 2. 1. : Electromagnetic radiation domain.



The region of interest in this work is the infrared, IR, region. As shown in *Table 2. 1.* the IR region can be subdivided in three smaller regions : near-IR, mid-IR, and far-IR.

Table 2. 1. : IR region.

Region	Wavenumber range	Vibrational / rotational changes
Near-IR	14000 - 4000	Changes in vibrational and rotational levels
Mid-IR	4000 - 400	Changes in fundamental vibrational levels
Far-IR	400 - 20	Changes in vibrational and rotational levels

A summary of infrared theory is given below (Mackenzie 1988, Griffiths and De Haseth 1986, Banwell 1983, Ferraro and Basile 1978).

2. 1. 1. Molecular vibrations

2. 1. 1. 1. The vibrating diatomic molecule

Real molecules do not have simple harmonic motions; bonds between atoms, although flexible, do not stretch elastically but have a much more complicated behaviour.

In an idealistic system, two atoms may be regarded as linked by a spring. When you pull the atoms apart, attractive forces (like in a spring) pull the atoms back closer, and likewise, if the atoms were to be pushed together, repulsive forces would keep them apart. This system follows Hookes law (eq. 2. 1.).

$$f = -k(r - r_e) \quad (\text{eq. 2. 1.})$$

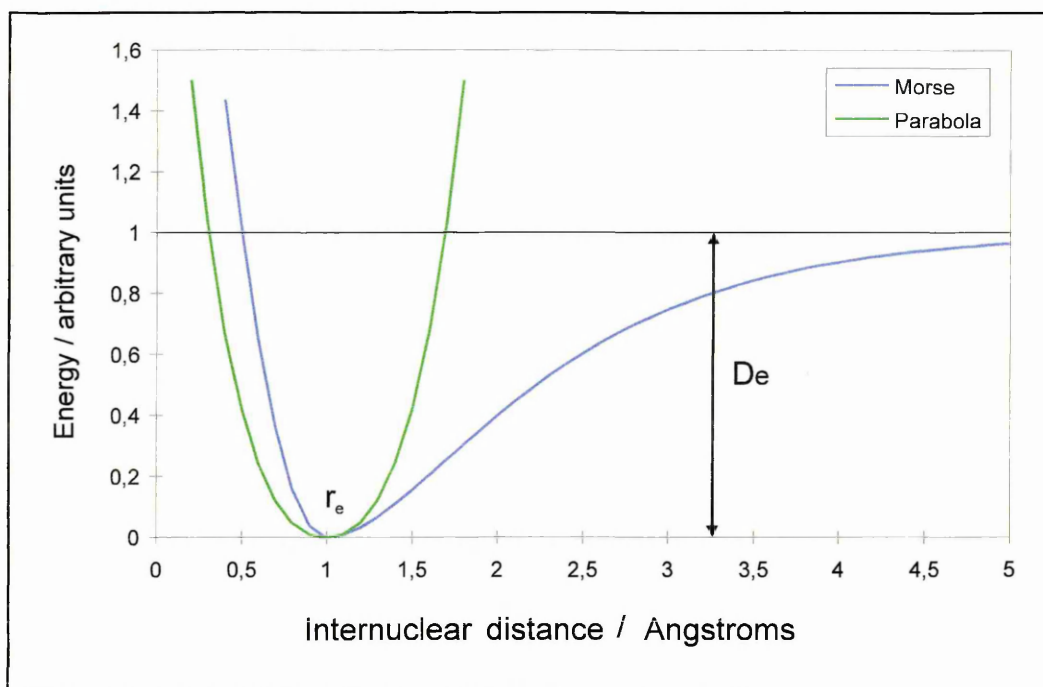
Where,

- f = the restoring force,
- k = the force constant,
- r = the internuclear distance,
- r_e = the internuclear distance at equilibrium or bond length.

In a real situation if the atoms are pulled apart , a point can be reached were the bond breaks, leading to the dissociation of the atoms.

Figure 2. 2A. shows the shape of the energy curve of a diatomic molecule undergoing anharmonic extensions and compressions (the Morse curve).

Figure 2. 2A. : Morse curve.



The Morse function is an empirical expression which fits the observed behaviour to a good approximation :

$$V = D_e \left[1 - \exp\{a(r_e - r)\} \right]^2 \quad (\text{eq. 2. 2.})$$

Where D_e = dissociation energy,
 a = constant for a particular molecule,
 r_e = equilibrium distance, or bond length,
 r = internuclear distance.

When eq. 2. 2. in used to solve the Schrödinger equation, the permitted energy levels are found to be :

$$E_v = \left(v + \frac{1}{2} \right) \omega_e - \left(v + \frac{1}{2} \right)^2 \omega_e x_e \quad (\text{eq. 2. 3.})$$

Where ω_e = equilibrium oscillation frequency,

$$x_e = \text{anharmonicity constant and } x_e = \frac{a^2}{2\mu\omega_e}$$

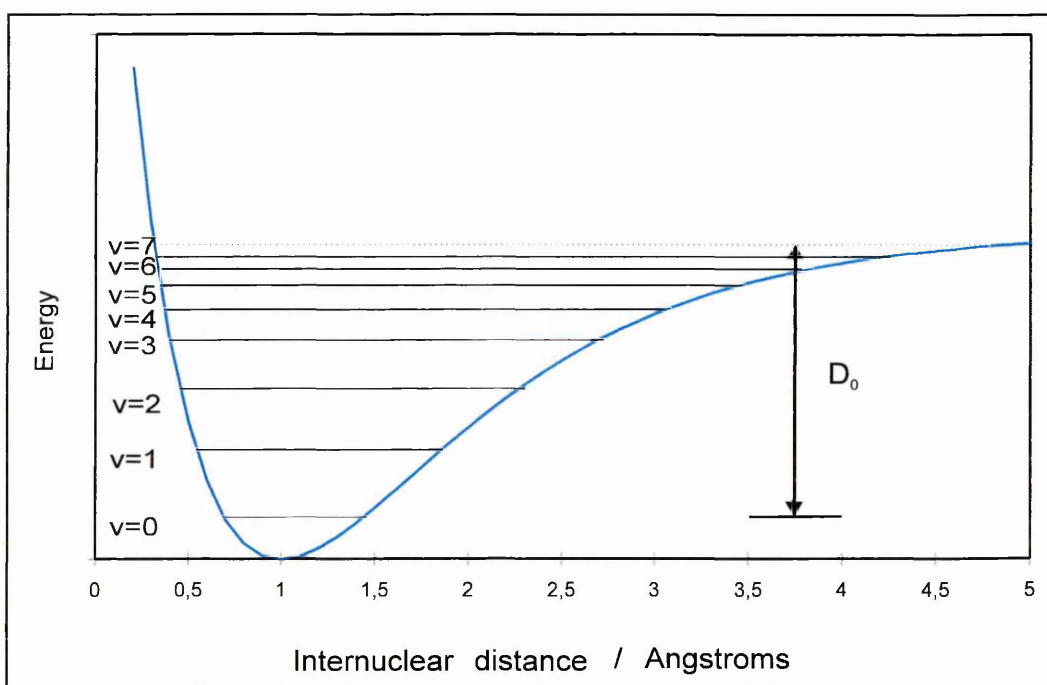
$$v = 0, 1, 2, \dots$$

μ = reduced mass

The selection rules for the anharmonic oscillator undergoing vibrational changes are :

$$\Delta v = \pm 1, \pm 2, \pm 3, \dots$$

Figure 2. 2B. : Diagram of the allowed energy levels and some transitions between them for a diatomic molecule undergoing anharmonic vibrations.



The lowest energy level is called the ground state $v = 0$, although the energy is not zero, but is termed the zero point energy which can be calculated from (eq. 2. 3.). (Eq. 2. 3.) is an approximation only. The more general equation for the energy levels, used to fit the experimental data and find the dissociation energy of the molecule is :

$$E_v = \left(v + \frac{1}{2}\right)\omega_e - \left(v + \frac{1}{2}\right)^2 \omega_e x_e + \left(v + \frac{1}{2}\right)^3 \omega_e y_e \dots \dots \quad (\text{eq. 2. 4.})$$

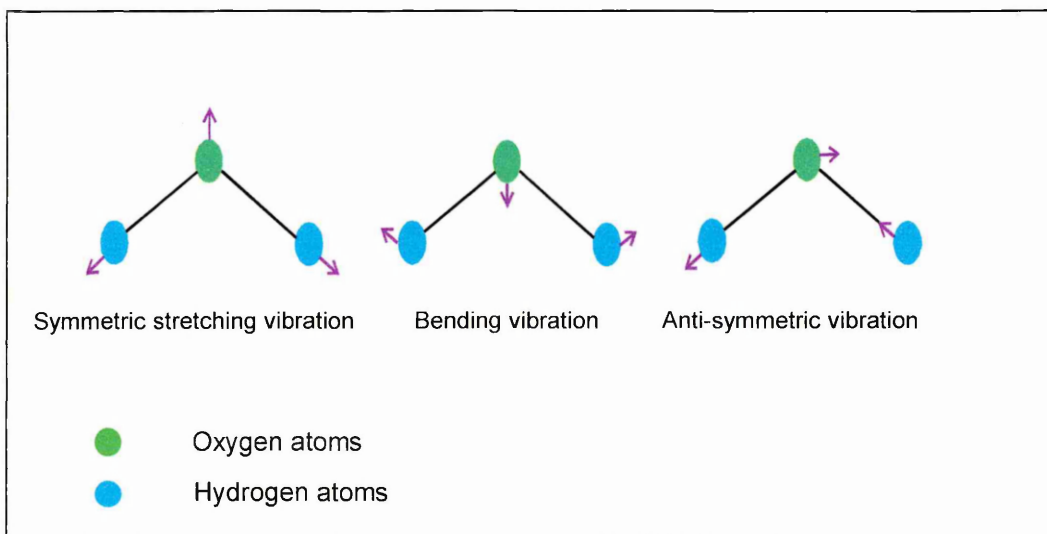
2. 1. 1. 2. The vibrations of polyatomic molecules

Normal modes :

For a molecule containing N atoms, we can refer to the position of each atom by specifying their three Cartesian co-ordinates. Therefore the total number of co-ordinate values is $3N$ and we say the molecule has $3N$ degrees of freedom. Three co-ordinates are needed to specify the translational motion of the molecule as a whole, leaving $3N-3$ non-translational 'internal' modes of the molecule. Three co-ordinates (for a non-linear molecule) and two co-ordinates (for a linear molecule) are needed to specify the orientational displacement of the molecule. Thus this leaves $3N-6$ vibrational modes for non-linear molecules and $3N-5$ for linear molecules.

Figure 2. 3. shows the normal modes of vibration of water.

Figure 2. 3. : Normal modes of vibration of water.



The relevant transitions that are generally observed are :

$v = 1 \leftarrow 0$ fundamental transition (the first harmonic),

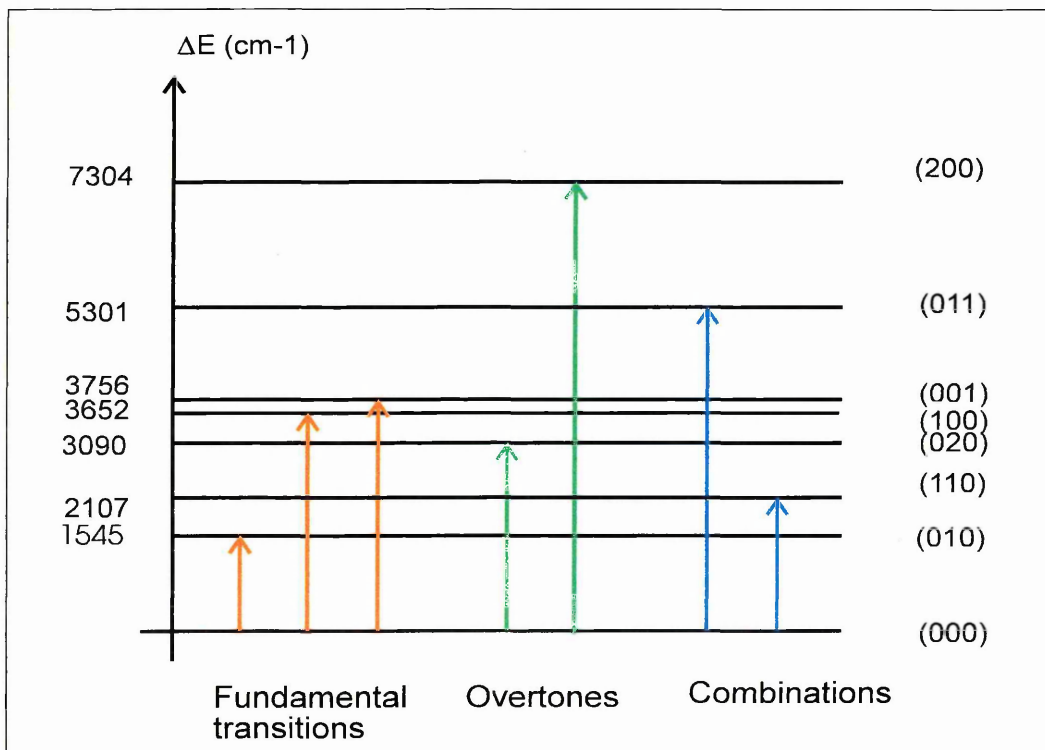
$v = 2 \leftarrow 0$ or $v = 3 \leftarrow 0$ which are overtones, occurring at frequencies $2\nu_1$ and $3\nu_1$, where ν_1 is a fundamental mode.

In addition, the selection rules permit combination bands. Combination bands arise from the addition of two or more fundamental frequencies or overtones,

and similarly the difference bands arise from the subtraction of two or more fundamental frequencies or overtones. However such combination and difference bands have very small intensities.

Figure 2. 4. shows an energy level diagram for water.

Figure 2. 4. : Energy level diagram for water.



2. 1. 2. Intensities in infrared spectroscopy

The intensities of infrared bands depend primarily on the three following factors:

- (i) the change in the permanent electric dipole of the molecule,
- (ii) the population of the initial state at thermal equilibrium,
- (iii) the number of molecules in the sample.

2. 1. 2. 1. Selection rules for infrared

The selection rules determine whether a transition is 'allowed' or 'forbidden'. They are derived from the transition probability $P^{v'v''}$.

$$P^{v'v''} \propto N_i \left[\int \psi_{v'} \hat{H} \psi_{v''} dQ \right]^2 \quad (\text{eq. 2. 5.})$$

Where \hat{H} is the corresponding operator, in this case μ_k , the dipole moment of the molecule, and Q represents for the normal co-ordinate describing the motion of the atoms during a normal vibration.

$$\mu_k = (\mu_0) + \left(\frac{\partial \mu}{\partial Q} \right) Q + \left(\frac{\partial^2 \mu}{\partial Q^2} \right) Q^2 + \dots \quad (\text{eq. 2. 6.})$$

A vibration is infrared active only if the molecular dipole is modulated by the normal vibration,

$$\left(\frac{\partial \mu}{\partial Q} \right) \neq 0 \quad (\text{eq. 2. 7.})$$

and the intensity of the transition is proportional to the square of the transition dipole moment :

$$I \propto \left(\frac{\partial \mu}{\partial Q} \right)^2 \quad (\text{eq. 2. 8.})$$

2. 1. 2. 2. The population factor

The intensities of the transition at thermal equilibrium are proportional to the population of the initial vibrational state. The population N_i of the level i is given by the Boltzmann distribution :

$$\frac{N_i}{N_0} = \frac{g_i}{g_0} \exp(-\Delta E / kT) \quad (\text{eq. 2. 9.})$$

Where N_i = number of molecules of a particular state,

N_0 = number of molecules of the ground state,

ΔE = difference in energy between the states,

k = Boltzman constant,

T = temperature,

g_i and g_0 = the degeneracies of the particular levels.

For most systems at room temperature, it is found that the ground state is the most heavily populated.

2. 1. 2. 3. Number of molecules in the sample

The intensity is governed by the number of molecules in the beam (sample thickness or concentration). The relationship connecting the intensity of the transmitted and incident radiation to the number of molecules is known as the Beer-Lambert law, which is :

$$I = I_0 e^{-\epsilon cl} \quad (\text{eq. 2. 10.})$$

Usually a logarithmic form is used :

$$\log\left(\frac{I_0}{I}\right) = \epsilon cl \quad (\text{eq. 2. 11.})$$

Where I_0 = the intensity of radiation falling on the sample,

I = the transmitted radiation,

c = the sample concentration,

l = the path-length,

ϵ = the extinction coefficient at given wavelength.

2. 1. 3. Fourier transform infrared spectroscopy

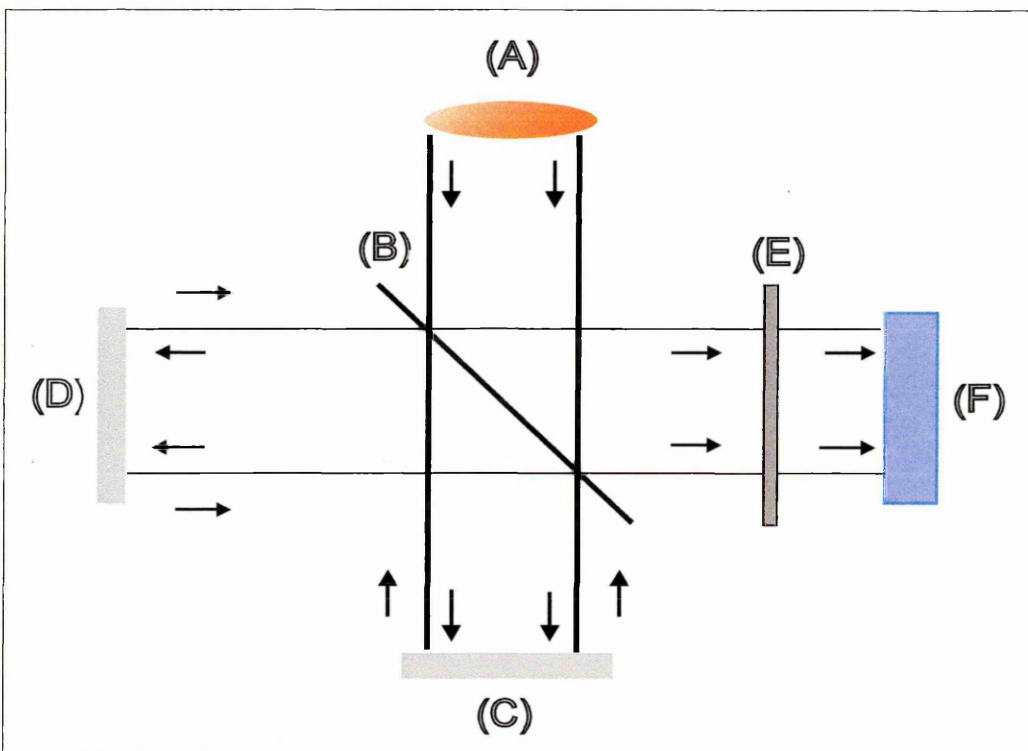
There are two types of spectrometer available for producing infrared spectra. These are the dispersive double beam, (diffraction grating or prism), spectrometer and the interferometer. The design of most interferometers for infrared spectrometry today is based on that of the interferometer originally designed by Michelson in 1891.

2. 1. 3. 1. The Michelson interferometer

A schematic of the Michelson interferometer can be seen in **figure 2. 5**.

The light from an infrared source (A), usually a silicon carbide ('Globar') source or a mercury lamp, is collimated and directed to the beam splitter (B), made of a material transparent to infrared light, such as KBr. The beam is divided, part going to the moving mirror (C), and part to the fixed mirror (D). The movable mirror can move along an axis perpendicular to its plane, at known constant velocity. The return beams recombine at the beam splitter and the reconstructed beam is then directed through the sample (E) and focused onto the detector (F). The detector may be a liquid nitrogen cooled mercury cadmium telluride (MCT) detector, or a thermal detector such as a Golay detector or a pyroelectric bolometer.

Figure 2. 5. : The Michelson interferometer.



A laser beam, undergoing the same change of optical path as the infrared beam, serves to reference the position of the mirror during the scan and initiates the collection of data points from the signal of the infrared detector at uniform intervals of mirror travel, Δx , called the sampling interval. The result is an interferogram, which is a record of the signal of the infrared detector as a function of the difference in path (retardation) for the two beams in the interferometer. The averaged interferogram undergoes computational mathematics; phase correction, apodisation and Fourier transformation in order to obtain a single beam spectrum.

The ratio of a single beam spectrum of the sample and the background will give the transmittance spectrum of the sample (the transmittance spectrum can then be converted into an absorbance spectrum).

The Fourier transform

The Fourier transform is a mathematical procedure which converts the signal as a function of retardation to a signal as a function of frequency.

The intensity of the radiation at the detector can be written as follows :

$$I(x) = 2 \int_0^{\infty} S(\bar{\nu}) \cos(2\pi\bar{\nu}x) d\bar{\nu} \quad (\text{eq. 2. 12.})$$

Where $S(\bar{\nu})$ = spectral density,

x = retardation.

In practice the mirror does not travel an infinite distance but has a maximum x_{max} , which means that there is a maximum permitted frequency,

$$\nu_{\text{max}} = \frac{1}{2x_{\text{max}}} \quad (\text{eq. 2. 13.})$$

which is known as the aliasing frequency.

And the relation for the intensity becomes :

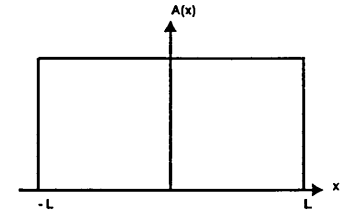
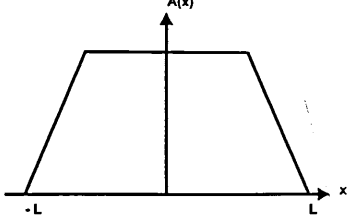
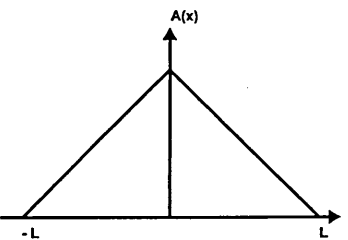
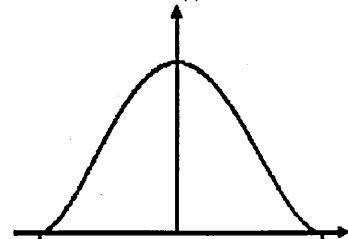
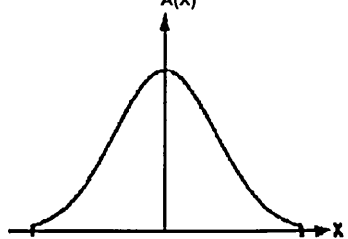
$$I(x) = 2 \int_0^{x_{\text{max}}} S(\bar{\nu}) \cos(2\pi\bar{\nu}x) d\bar{\nu} \quad (\text{eq. 2. 14.})$$

Apodisation

The limits of integration for taking the Fourier transform of a function properly cover all values of the independent variable from 0 to ∞ , but because there is a maximum mirror travel x_{max} , the interferogram is truncated which results in some loss of definition in the spectrum after Fourier transformation in the form of side lobes on the bands.

The application of a weighting function, known as the apodisation function, minimises the small oscillation on either side of the peak. Many apodisation functions are available. A few are shown on **figure 2. 6.**, but the most commonly used apodisation function is the triangular apodisation function.

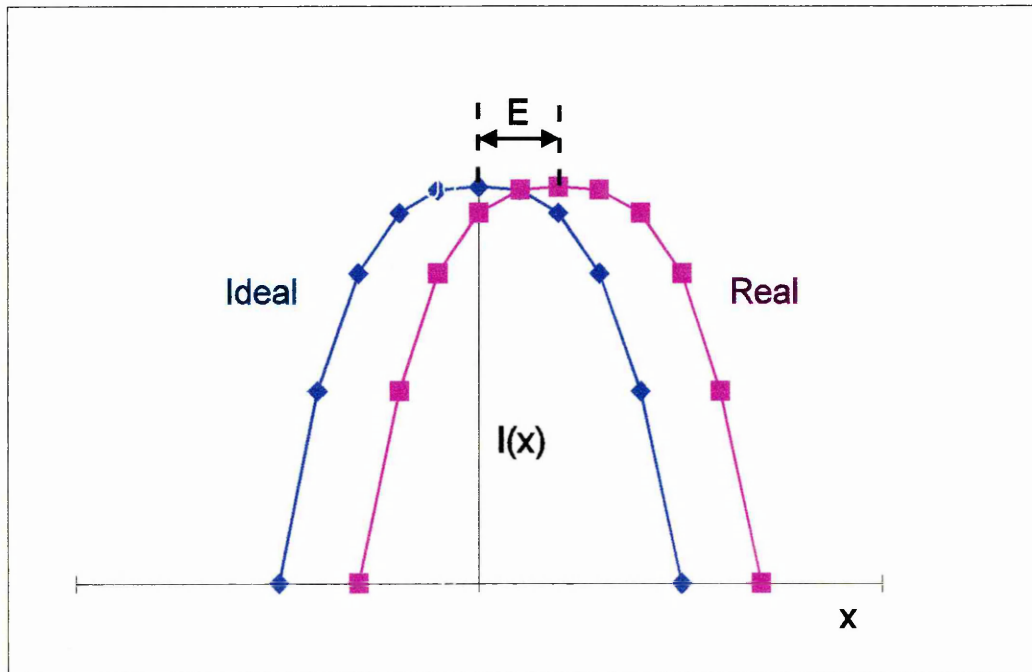
Figure 2. 6. : Apodisation functions.

Apodisation functions	Equations	Functions
Boxcar	$A(x) = \begin{cases} 1 & x \leq L \\ 0 & x > L \end{cases}$	
Trapezoidal	$2A(x) \times \left[1 - \frac{ x }{L} \right] - A(2x) \times \left[1 - \frac{2 x }{L} \right]$	
Triangular	$A(x) \times \left[1 - \frac{ x }{L} \right]$	
Bessel	$A(x) \times \left[1 - \left(\frac{x}{L} \right)^2 \right]^2$	
Gaussian	$A(x) \times \exp \left[\frac{\pi^2}{\text{Ln}2} \left(\frac{x}{2L} \right)^2 \right]$	

Phase corrections

A combination of optical, electronic and sampling effects leads to an asymmetric interferogram (see **figure 2. 7.**).

Figure 2. 7. : Phase correction



so,

$$I(x) = \int_0^{\infty} S(\bar{\nu}) \cos 2\pi\bar{\nu}(x - E) d\bar{\nu} \quad (\text{eq. 2. 15.})$$

Where E = phase correction.

or more generally :

$$I(x) = \int_0^{\infty} S(\bar{\nu}) \cos 2\pi\bar{\nu}(x - \theta_{\nu}) d\bar{\nu} \quad (\text{eq. 2. 16.})$$

Where θ_{ν} = phase angle.

Rearranging (eq. 2. 16.) :

$$I(x) = \int_0^{\infty} S(\bar{\nu}) \cos(2\pi\bar{\nu}x) \cos(2\pi\bar{\nu}\theta_v) + \sin(2\pi\bar{\nu}x) \sin(2\pi\bar{\nu}\theta_v) d\bar{\nu} \quad (\text{eq. 2. 17.})$$

So the computed spectrum $S(\bar{\nu})$ has both real (cosine transform) and imaginary (sine transform) parts.

The interferogram can be made symmetric by removal of the sine components.

The phase angle is calculated by :

$$\theta_v = \arctan \left\{ \frac{\text{Imag}S(\bar{\nu})}{\text{Real}S(\bar{\nu})} \right\} \quad (\text{eq. 2. 18.})$$

and can be used to make a phase correction.

2. 1. 3. 2. Advantages of Fourier transform

The following sections will discuss the advantages of Fourier transform infrared spectroscopy over the dispersive technique.

The throughput (Jacquinot) advantage

An improved signal-to-noise ratio (S/N) is achieved as a consequence of the larger optical throughput of the interferometer relative to that of a grating spectrometer ; the signal reaching the detector is much larger in the case of an interferometer. This is because there are no slits in the spectrometer (unlike in a dispersive instrument).

The spectral optical conductance of a grating instrument can be expressed as :

$$G_v^G = \frac{hH}{f\nu} R_0 \quad (\text{eq. 2. 19.})$$

Where $G_{\bar{\nu}}^G$ = optical conductance per wavenumber of grating,

H = height of the grating,

h = length of the entrance slit,

f = focal length of the collimator,

R_0 = theoretical resolving power.

For comparison purposes, we chose the beam area of the interferometer F_1 to be equal to the beam area of the grating H^2 .

Thus the optical conductance in an interferometer can be expressed as :

$$G_{\bar{\nu}}^I = \frac{2\pi H^2}{\bar{\nu}} \quad (\text{eq. 2. 20.})$$

Therefore the ratio of the two optical conductances is :

$$\frac{G_{\bar{\nu}}^I}{G_{\bar{\nu}}^G} \approx \frac{2\pi f}{h} \approx 200 \quad (\text{eq. 2. 21.})$$

The multiplex (Fellgett) advantage

The multiplex advantage of an FT-IR spectrometer arises from the fact that the detector sees all the spectral elements (N) 'at the same time'.

$$N = \frac{\bar{\nu}_H - \bar{\nu}_L}{\Delta \bar{\nu}_R} \quad (\text{eq. 2. 22.})$$

Where $\bar{\nu}_H$ = highest wavenumber,

$\bar{\nu}_L$ = lowest wavenumber,

$\Delta \bar{\nu}_R$ = resolution.

In the FT-IR spectrometer the signal-to-noise ratio (S/N), is proportional to the square root of the time of observation of each element :

$$(S/N)_{FT} \propto T^{1/2} \quad (\text{eq. 2. 23.})$$

In the dispersive instrument :

$$(S/N)_D \propto \frac{T^{1/2}}{N^{1/2}} \quad (\text{eq. 2. 24.})$$

Therefore there is a S/N gain of $N^{1/2}$.

The Connes advantage

In FT-IR spectroscopy absolute control of spectral wavelength is achieved. This is due to the fact that the sampling is controlled by a laser whose wavelength is fixed at 632.81646 nm (15798.002 cm^{-1}). This offers the advantage of very accurate spectral subtraction.

Spectral subtraction

The linear equation that applies is :

$$X - fY = D, \quad (\text{eq. 2. 25.})$$

Where X = a mixture spectrum,

Y = a component spectrum,

f = the scaling factor,

D = the resulting difference spectrum.

Absorbance subtraction is a process by which it is possible to remove a component from the spectrum of a mixture, thus making it possible to observe the spectra of other components.

Artefacts in the subtraction obtained spectra may appear in the shape of a first derivative of a peak. There are a number of reasons why this might occur. For example this may be due to excessive subtraction, a shift in the frequency position of a specific band in the mixture compared to the spectrum of the pure component, interactions in the mixture (i.e. hydrogen bonding), or a change in refractive index for example.

This method is very useful in the removal of water vapour bands from spectra. One of the major problems of water vapour spectral removal is due to the shifts in position, and in relative height, and width of water vapour bands with temperature. As the temperature increases, the number of collisions between the molecules increases. Since the width of the bands is proportional to the number of collisions, changes in band width occur. These changes are minimal, but have a profound effect upon spectral subtraction.

2. 1. 3. 3. Disadvantages of Fourier transform

There are few disadvantages to using Fourier transform spectrometry and they are outweighed by the advantages.

2. 1. 3. 3. 1. Fellgett disadvantage

If source noise varies with frequency and is significant, the detector will detect noise at all frequencies, since the detector integrates over all frequencies, even if the noise only occurs within a certain frequency range.

2. 1. 3. 3. 2. Water vapour and carbon dioxide

One of the most important problems in day-to-day work is associated with the presence of bands due to CO₂ and water vapour, from the air, in the spectrum. This can be avoided by purging the system using dry air, or nitrogen, although it can be a time consuming procedure. Another remedy is to use interactive subtraction of those bands.

2. 1. 4. Attenuated total reflectance infrared spectroscopy (ATR-FTIR)

2. 1. 4. 1. Introduction

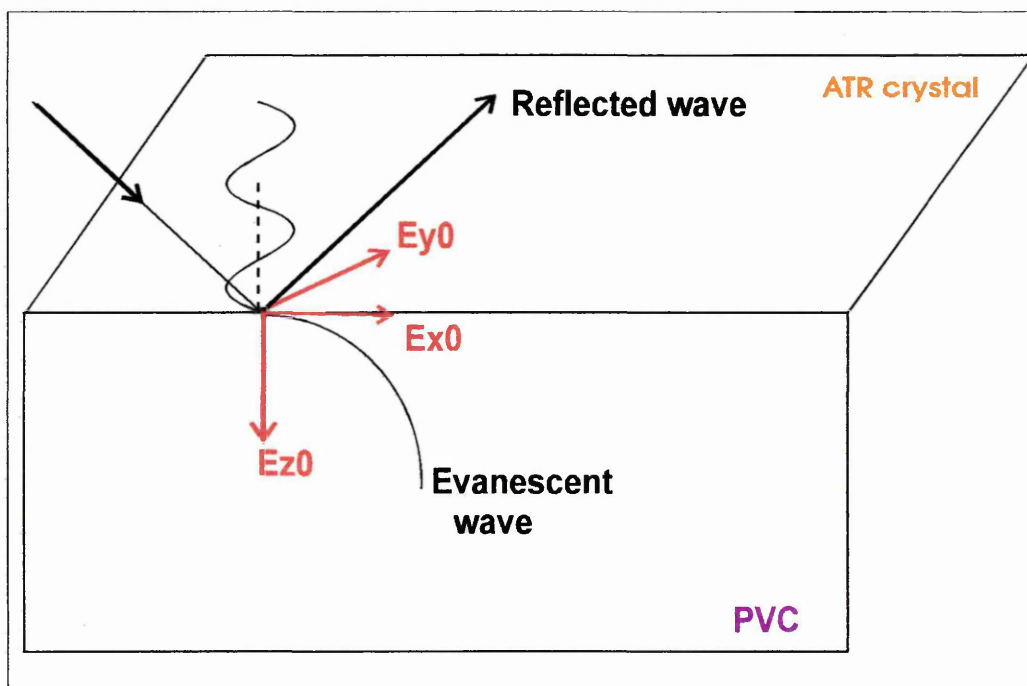
Attenuated total reflectance (ATR) or internal reflectance spectroscopy (IRS) is a popular sampling technique used for the infrared analyses of a wide variety of samples, ranging from very thin films (monolayers) to thick materials (Walls 1991, Walls and Coburn 1992, Belali and Vigoureux 1994), pastes, liquids, fibres (Sun et al. 1997, Yang and Kim 1997), polymer laminates (Pereira and Yarwood 1994, Boven et al. 1992). FTIR-ATR has also proven itself to be a very useful tool for *in-situ* examination of processes such as curing (Skourlis and McCulloch 1994), clay solvent interactions (Billingham et al. 1997) and the diffusion of small molecules into polymers. In addition the ability to control the sampling depth has allowed depth profiling of polymer laminates.

There are excellent texts by Harrick and Mirabella or Urban (Harrick 1987, Mirabella 1993, Urban 1996) which detail the theory and background of Fourier transform attenuated total reflectance spectroscopy, so only a brief summary of the theory will be given here.

2. 1. 4. 2. Total internal reflection

The history of ATR began nearly 200 years ago when Newton observed that when radiation is propagating from an optically denser medium 1 (an ATR prism), with refractive index n_1 , it undergoes total internal reflection at the interface with the optically rarer medium 2 (the sample), with refractive index n_2 , when the angle of incidence θ exceeds the critical angle θ_c (see **figure 2. 8.**).

Figure 2. 8. : Schematic of the ATR experiment.



The angle of incidence θ is defined as the angle with respect to the normal.

The critical angle is defined by :

$$\theta_c = \sin^{-1} n_2/n_1 \quad (\text{eq. 2. 26.})$$

As the critical angle is dependent upon the two media, it is important experimentally that the ATR prism should be of high refractive index and infrared transparent in the region of interest.

Some of those ATR prism materials and their range are shown in **table 2. 2.**

Table 2. 2. : ATR prisms

Material	Refractive index	IR window
ZnSe (Zinc Selenide)	2.4	450 - 20000 cm ⁻¹
KRS5	2.4	250 - 20000 cm ⁻¹
Ge (Germanium)	4.0	600 - 5500 cm ⁻¹
Si (Silicon)	3.4	110 - 8300 cm ⁻¹

At the point of attenuated total reflection, a standing wave is present in the denser medium and an evanescent field is produced in the rarer medium. The evanescent field is confined to the vicinity of the surface of the rarer medium and decays exponentially with distance from the interface along the z-axis. It has components in all spatial directions (x, y, and z), which can interact with transition dipoles $\left(\frac{\partial\mu}{\partial Q}\right)$ in the rarer medium.

The rate of decay of the evanescent field is dependent on :

- (i) the wavelength of the incident light,
- (ii) the angle of incidence of the light,
- (iii) the refractive indices of both the rarer and denser media.

The decrease in intensity of the evanescent field can be expressed as :

$$E = E_0 \exp\left[-\frac{2\pi}{\lambda_1}(\sin^2 \theta - n_{21}^2)^{1/2} z\right] \quad (\text{eq. 2. 27.})$$

Where E = the value of the electrical field at distance z into rarer medium,

E_0 = the electric field amplitude at the surface of rarer medium,

$\lambda_1 = \lambda/n_1$ = the wavelength of radiation in denser medium,

θ = the angle of incidence,

$n_{21} = n_2/n_1$.

This equation can be rewritten as :

$$E = E_0 \exp[-\gamma z] \quad (\text{eq. 2. 28.})$$

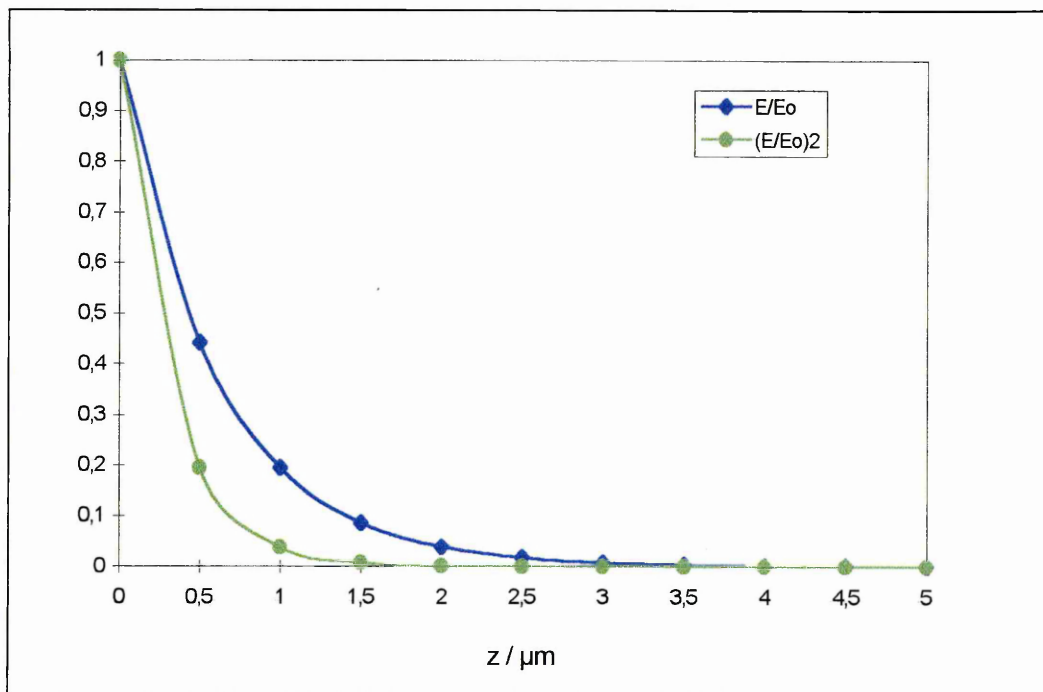
so that :

$$\gamma = \frac{2\pi(\sin^2 \theta - n_{21}^2)^{1/2}}{\lambda_1} \quad (\text{eq. 2. 29.})$$

Where γ is called the electrical field amplitude decay coefficient.

Figure 2. 9. shows a plot of the exponential decay of the electrical field amplitude (E/E_0) and the intensity $(E/E_0)^2$ as a function of depth into the surface, z , for $k = 0$.

Figure 2. 9. : (E/E_0) and $(E/E_0)^2$ versus z .



The reciprocal of γ is called the depth of penetration d_p , at which E decays to a value of $E_0 \exp[-1]$.

$$d_p = \frac{1}{\gamma} = \frac{\lambda}{2\pi n_1 (\sin^2 \theta - n_{21}^2)^{1/2}} \quad (\text{eq. 2. 30.})$$

Although d_p is used experimentally as a measure of the sampling depth, it should be noted that E is not zero at d_p , but that the real sampling depth d_e , is about three times d_p . In this case it is assumed that the rarer medium is non-absorbing, which is clearly non-realistic, since absorption of energy must occur if a measurement is to be made.

The effect of absorption turns out to be relatively small for most organic compounds, and especially for the case of polymers. Therefore (eq. 2. 28.) is still valid.

The case of an absorbing rarer medium can be treated in terms of the intensity loss per reflection, and the reflectivity R can be described as :

$$R = \frac{I}{I_0} = \exp(-\alpha d_e) \cong (1 - a) \quad (\text{eq. 2. 31.})$$

Where I = the reflected intensity,

I_0 = the incident intensity,

α = the absorption coefficient,

a = the absorption parameter $\cong \alpha d_e$ for a single reflection.

It is important to note that α is identical for transmission spectroscopy and IRS in the case of weak absorbers.

The absorption coefficient (α) is related to the attenuation index (κ) :

$$\alpha = \frac{4\pi n \kappa}{\lambda} \quad (\text{eq. 2. 32.})$$

For an absorbing sample the general expression of the penetration depth (d'_p) is needed, using a complex index of refraction :

$$d'_p = \frac{\lambda}{2\pi n_1} \frac{1}{\omega_2^+} \tag{eq. 2. 33.}$$

Where :

$$\omega_2^+ = \frac{1}{\sqrt{2}} \left(\sqrt{v_2^2 + \mu_2^2} + v_2 \right)^{1/2} \tag{eq. 2. 34.}$$

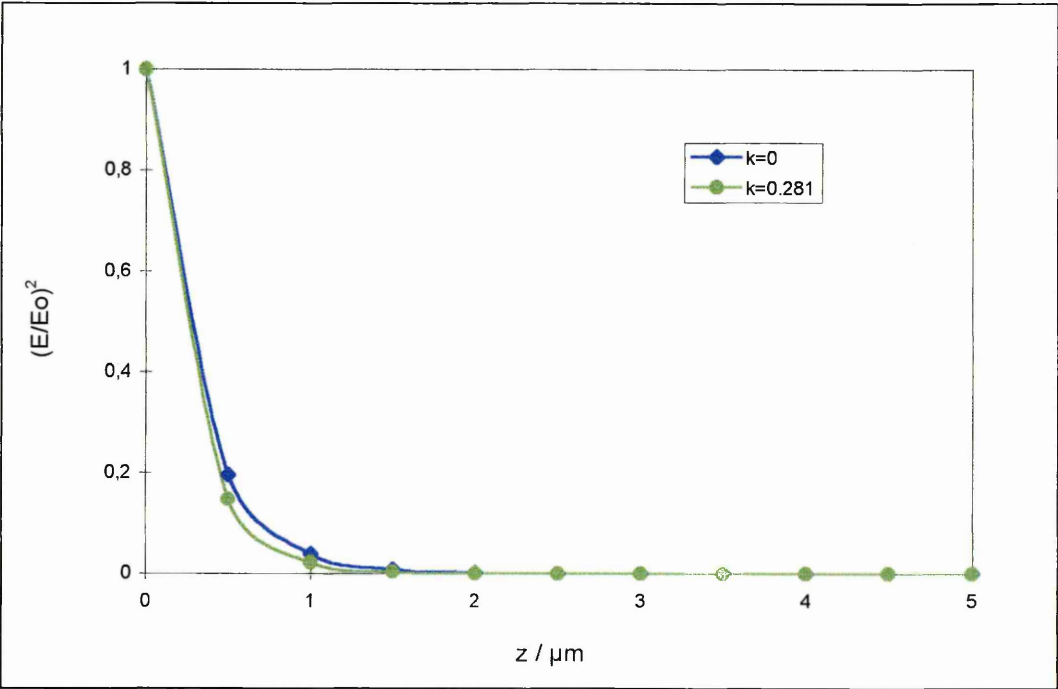
$$v_2 = \sin^2 - n_{21}^2 (1 - \kappa_2^2) \tag{eq. 2. 35.}$$

$$\mu_2 = 2n_{21}^2 \kappa_2 \tag{eq. 2. 36.}$$

N.B. : For $\kappa = 0$, one recovers the “non-absorbing” case.

Figure 2. 10. shows the decay of the electric field in the case of $\kappa = 0$ and $\kappa = 0.281$ (for water).

Figure 2. 10. : Electric field decay for non-absorbing and absorbing media.



In order to calculate d_e it is necessary to consider the two polarisations of the electromagnetic wave :

(i) the one parallel to the plane of incidence is called 'transverse magnetic' (TM), which has components in the x and z planes, i.e. the electric field amplitudes E_{x0} and E_{z0} are associated with it.

(ii) the one perpendicular to the plane of incidence is called 'transverse electric' (TE), which has components in the y plane only (E_{y0}).

$$TE = E_{\text{perpendicular}} = E_{y0} \quad (\text{eq. 2. 37.})$$

$$TM = E_{\text{parallel}} = \sqrt{|E_{x0}|^2 + |E_{z0}|^2} \quad (\text{eq. 2. 38.})$$

Because the properties of the evanescent field in the rarer medium depend on the thickness of that medium, we must distinguish between two cases ; namely the semi-infinite bulk case and the thin film case (Mirabella 1993).

In the semi-infinite bulk case the electric field amplitude falls to a very low value within the thickness of the rarer medium t , such that $t \gg 1/\gamma$ or $t \gg d_p$.

In the thin film case, the electric field amplitude remains essentially constant over the thickness t , such that $t \ll 1/\gamma$ or $t \ll d_p$.

The semi-infinite bulk case ($t \gg 1/\gamma$) :

TE wave,

$$E_{\perp} = E_{y0} = \frac{2 \cos \theta}{(1 - n_{21}^2)^{1/2}} \quad (\text{eq. 2. 39.})$$

TM wave,

$$E_{x0} = \frac{2(\sin^2 \theta - n_{21}^2)^{1/2} \cos \theta}{(1 - n_{21}^2)^{1/2} [(1 + n_{21}^2) \sin^2 \theta - n_{21}^2]^{1/2}} \quad (\text{eq. 2. 40.})$$

$$E_{z0} = \frac{2 \sin \theta \cos \theta}{(1 - n_{21}^2)^{1/2} [(1 + n_{21}^2) \sin^2 \theta - n_{21}^2]^{1/2}} \quad (\text{eq. 2. 41.})$$

and,

$$E_{||} = \sqrt{|E_{x0}|^2 + |E_{z0}|^2} \quad (\text{eq. 2. 42.})$$

The thin film case ($t \ll 1/\gamma$) :

In this case medium 3, with refractive index n_3 , behind medium 2 controls the decay of the field.

TE wave,

$$E_{\perp} = \frac{2 \cos \theta}{(1 - n_{31}^2)^{1/2}} \quad (\text{eq. 2. 43.})$$

TM wave,

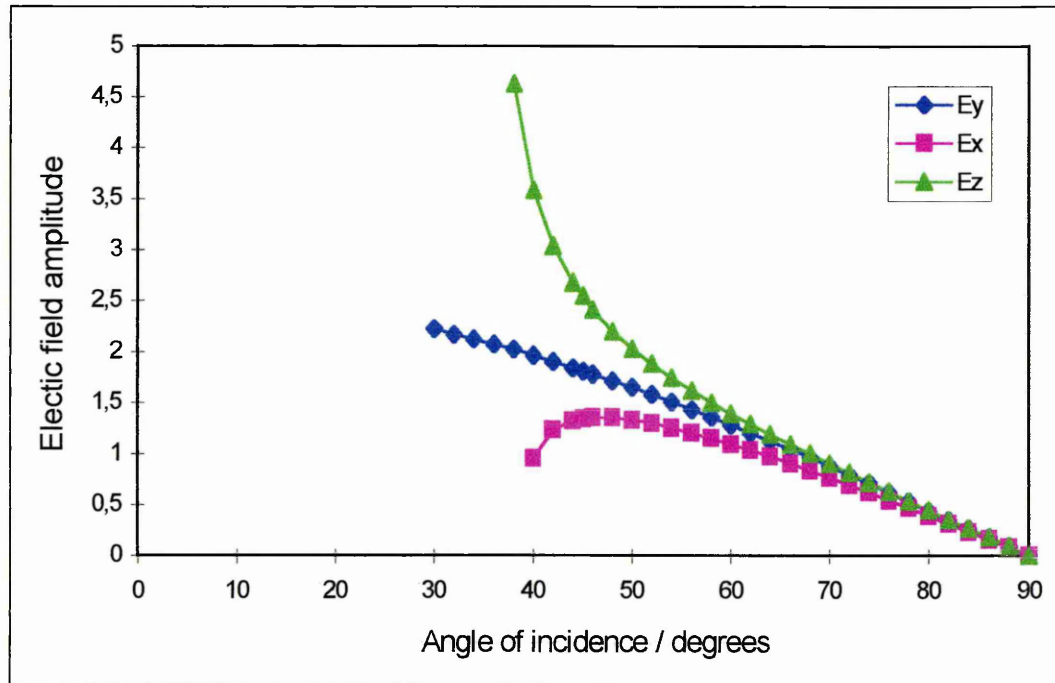
$$E_{||} = \frac{2 \cos \theta [(1 + n_{32}^4) \sin^2 \theta - n_{31}^2]^{1/2}}{(1 - n_{31}^2)^{1/2} [(1 + n_{31}^2) \sin^2 \theta - n_{31}^2]^{1/2}} \quad (\text{eq. 2. 44.})$$

Where $n_{31} = \frac{n_3}{n_1}$

$$n_{32} = \frac{n_3}{n_2}$$

Figure 2. 11. shows a plot of the electric field amplitudes as a function of angle of incidence θ for the semi-infinite bulk case where $n_1 = 2.4$ (for ZnSe) and $n_2 = 1.5$ (for PVC).

Figure 2. 11. : Electric field amplitudes as a function of angle of incidence.



From this plot it is interesting to note that the values of E_{y0} and E_{z0} reach a maximum at the critical angle, E_{x0} falls to 0 at θ_c .

The relationship between the absorption parameter a , and the electric field E for a weak absorber can be written as :

$$a = \frac{n_{21}\alpha}{\cos\theta} \int_0^t E^2 dz \quad (\text{for a thin film}) \quad (\text{eq. 2. 45.})$$

$$a = \frac{A}{N} = \frac{n_{21}\alpha c}{\cos\theta} \int_0^\infty E^2 dz \quad (\text{for a semi-infinite bulk}) \quad (\text{eq. 2. 46.})$$

Where A = the absorbance,

N = the number of reflections,

α = the molar absorption coefficient,

c = the concentration.

Solving this gives :

$$a = \frac{n_{21}\alpha E_0^2}{2\gamma \cos \theta} \quad (\text{for the semi-infinite bulk case}) \quad (\text{eq. 2. 47.})$$

$$a = \frac{n_{21}\alpha t E_0^2}{2\gamma \cos \theta} \quad (\text{for the thin film case}) \quad (\text{eq. 2. 48.})$$

Since $a = \alpha d_e$, by multiple substitutions and rearrangements, we find that :

For the semi-infinite bulk case :

TE wave,

$$d_{e\perp} = \frac{n_{21}\lambda_1 \cos \theta}{\pi(1-n_{21}^2)(\sin^2 \theta - n_{21}^2)^{1/2}} \quad (\text{eq. 2. 49.})$$

TM wave,

$$d_{e\parallel} = \frac{n_{21}\lambda_1(2\sin^2 \theta - n_{21}^2)\cos \theta}{\pi(1-n_{21}^2)[(1+n_{21}^2)\sin^2 \theta - n_{21}^2](\sin^2 \theta - n_{21}^2)^{1/2}} \quad (\text{eq. 2. 50.})$$

For the thin film case :

TE wave,

$$d_{e\perp} = \frac{4n_{21}t\cos\theta}{(1-n_{31}^2)} \quad (\text{eq. 2. 51.})$$

TM wave,

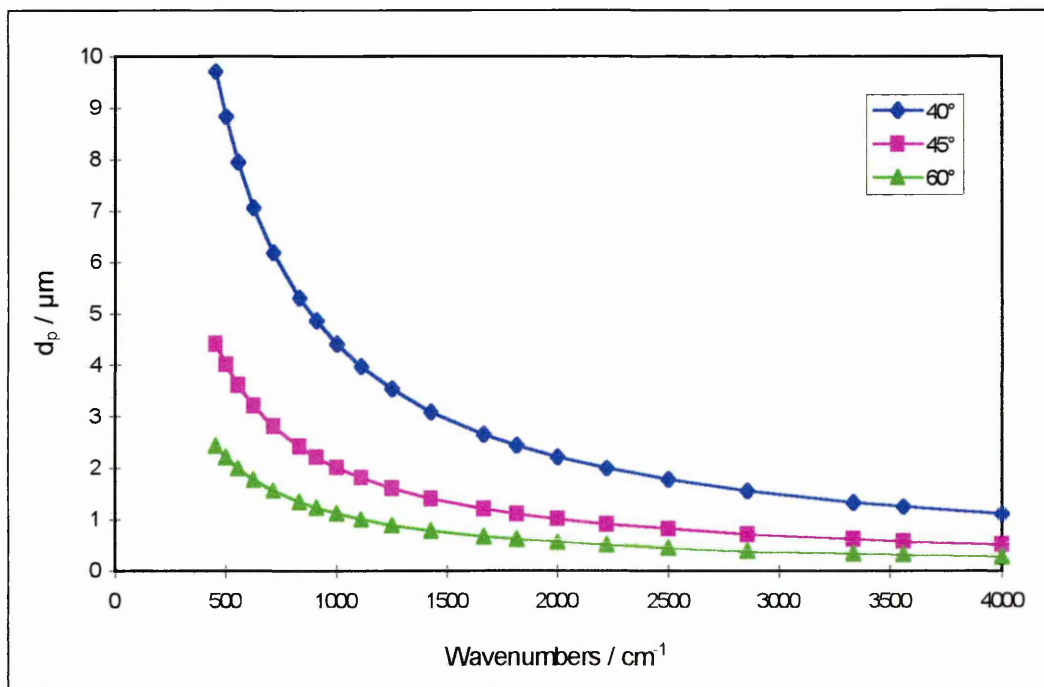
$$d_{e\parallel} = \frac{4n_{21}t\cos\theta\left[(1+n_{32}^4)\sin^4\theta - n_{31}^2\right]}{(1-n_{31}^2)\left[(1+n_{31}^2)\sin^2\theta - n_{31}^2\right]} \quad (\text{eq. 2. 52.})$$

The effective thickness for unpolarised radiation d_{eu} is given by :

$$d_{eu} = \frac{d_{e\perp} + d_{e\parallel}}{2} \quad (\text{eq. 2. 53.})$$

It is important to note that d_e is strongly dependent on θ and wavelength, as shown on **figure 2. 12.**

Figure 2. 12. : A plot of the effective thickness for various angles of incidence in a typical polymer sample as a function of wavelength.



2. 1. 4. 3. Advantages of ATR

1. There is a large sampling number, due to many reflections in the IRE element (14 reflections in a macro-ATR crystal, and 38 reflections in a micro-ATR crystal), so
2. ATR is a very sensitive technique (monolayers can be detected),
3. interference effects are eliminated,
4. depth profiling of polymer laminates is possible by varying the angle of incidence.
5. d_p (or d_e) can be changed by using different IRE materials.
6. highly absorbing materials can easily be studied, such as water, because d_p (or d_e) is small and absorbance therefore small,
7. *in-situ* experiments can be performed,
8. very little sample preparation is needed.

2. 1. 4. 4. Disadvantages of ATR

1. Very good optical contact is needed between the sample and the IRE.
2. The distribution of electric fields is complicated.
3. The total internal reflection wave loses energy at each reflection.

2.1.5. Data analysis

The analysis and interpretation of spectral data can be made difficult due to the presence of overlapping bands in the spectra.

Numerical methods can be applied, such as derivative spectroscopy, Fourier self-deconvolution, and band fitting routines.

For better and more accurate results it is recommended to use these techniques in conjunction with one another. For example, it is good practice to

use the second derivative and Fourier self-deconvolution (FSD) of the spectrum to obtain the bands positions and relative intensities, before proceeding to the band fitting procedure.

2. 1. 5. 1. Derivative spectrometry

When a single-sided interferogram is multiplied by a function of the form ax^n :

$$F(x) = ax^n \quad (\text{eq. 2. 54.})$$

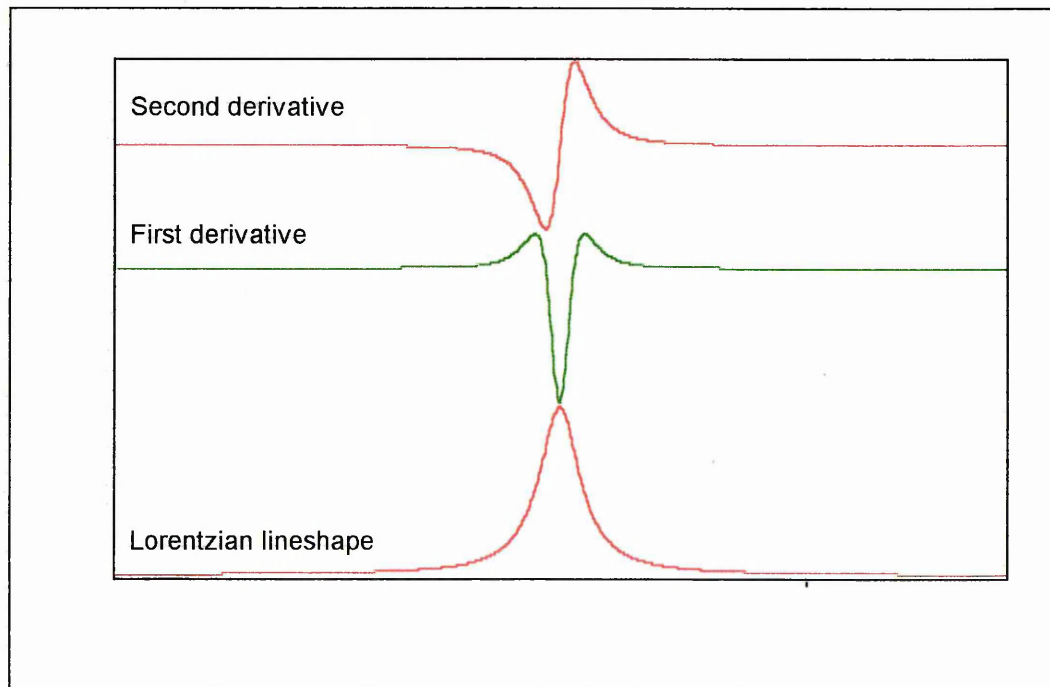
the calculation of the forward transform gives the n^{th} derivative of the spectrum.

The second derivative is the more often used one.

By taking the 2nd derivative of the spectrum, the band width is reduced by 20 %, and one obtains the number of components in the band, their centres and relative intensities.

The process of calculating the 2nd derivative is shown on **figure 2. 13.**

Figure 2. 13. : The second derivative of a Lorentzian band.



2. 1. 5. 2. Fourier self-deconvolution

Let us consider, that any spectrum is a convolution of a spectrum ($E'(\bar{\nu})$) (band position) with a line shape function ($G(\bar{\nu})$).

$$E(\bar{\nu}) = E'(\bar{\nu}) * G(\bar{\nu}) \quad (\text{eq. 2. 55.})$$

The relationship between $I(x)$ (the interferogram), and $E(\bar{\nu})$ (the spectrum), are as follows :

$$I(x) = \int_{-\infty}^{+\infty} E(\bar{\nu}) \exp(2\pi\bar{\nu}x) d\bar{\nu} = F^{-1}[E(\bar{\nu})] \quad (\text{eq. 2. 56.})$$

and,

$$E(\bar{\nu}) = \int_{-\infty}^{+\infty} I(x) \exp(2\pi\bar{\nu}x) dx = F[I(x)] \quad (\text{eq. 2. 57.})$$

Where F is the Fourier transform and F^{-1} the inverse Fourier transform.

Recalling that convolution in the spectrum is equivalent to multiplication in the interferogram, we can write from (eq. 2. 56.) and (eq. 2. 57.) :

$$I(x) = F^{-1}[E(\bar{\nu})] = F^{-1}[E'(\bar{\nu})] \bullet F^{-1}[G(\bar{\nu})] \quad (\text{eq. 2. 58.})$$

or,

$$I(x) = I'(x) \bullet F^{-1}[G(\bar{\nu})] \quad (\text{eq. 2. 59.})$$

Where,

$$I'(x) = F^{-1}[E'(\bar{\nu})] \quad (\text{eq. 2. 60.})$$

Therefore we have :

$$E'(\bar{\nu}) = F[I'(x)] \quad (\text{eq. 2. 61.})$$

and,
$$I'(x) = \frac{I(x)}{F^{-1}[G(\bar{\nu})]} \quad (\text{eq. 2. 62.})$$

If (2. 62.) is multiplied by an appropriate apodisation function, $D(x)$, the deconvoluted spectrum, $E'(\bar{\nu})$ can be obtained using :

$$E'(\bar{\nu}) = F[D(x) \bullet I'(x)] \quad (\text{eq. 2. 63.})$$

and the following result is obtained :

$$E'(\bar{\nu}) = F^{-1}[D(x) \bullet I'(x)] \quad (\text{eq. 2. 64.})$$

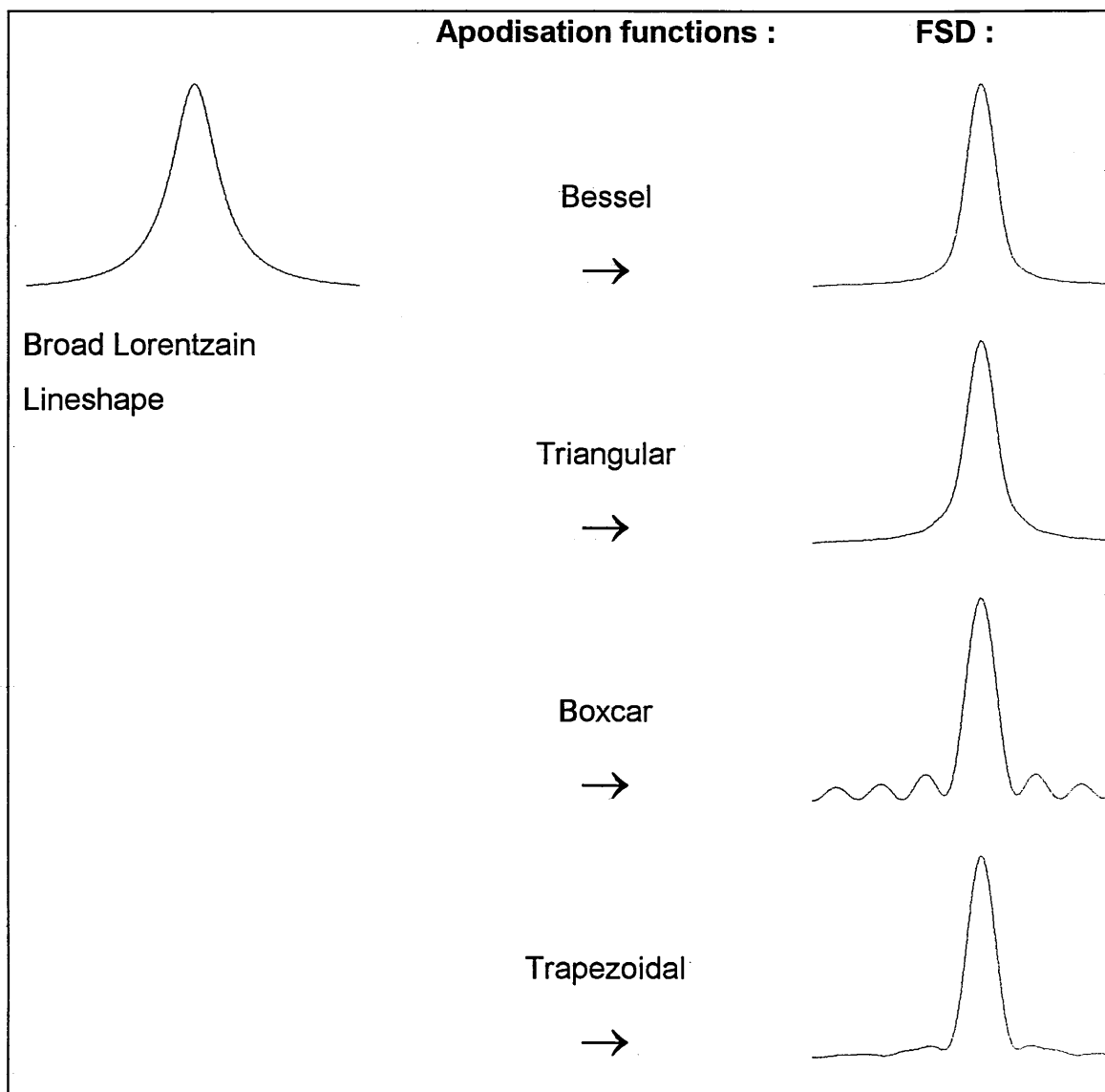
The final line shape $E'(\bar{\nu})$ depends highly on the form of the apodisation function used.

Figure 2. 14. illustrates the FSD process starting with a Lorentzian line and applying different apodisation functions.

When doing FSD three parameters need to be specified in the software :

1. an estimate of the average of the bandwidth (ω) of original bands,
2. the enhancement factor k , k can be estimate by $k \cong \log_{10}(S/N)$
3. the choice of apodisation function $D(x)$.

Figure 2. 14. : The Fourier self-deconvolution process.



2. 1. 5. 3. Band fitting

Band fitting or curve fitting is a powerful application in which a complex set of overlapping peaks are fitted to a number of ideal peaks. The method used here is based on the original algorithm of non-linear peak fitting as described by Marquardt and known as the Levenberg-Marquardt (Marquardt 1963) method. The information that one can obtain from curve fitting is as follows :

1. exact peak positions,
2. peaks widths, heights and areas,

But one needs to feed the following estimate of the information to the

program :

1. an accurate determination of the number of peaks,
2. knowledge of the true peak shapes,
3. an approximate estimate of the peak parameters, such as width, height, position etc...

The program then adjusts these starting values to obtain the best fit of the sum of the calculated peaks, to that of the measured peaks.

The quality of fit in this case is observed as follows (Grams software program) :

$$\chi^2 = \frac{\sum_{i=0}^n \left(\frac{\text{Actual}_i - \text{Calculated}_i}{\text{RMSNoise}} \right)^2}{(n-f)} \quad (\text{eq. 2. 65.})$$

Where Actual_i = measured data,

Calculated_i = calculated data,

RMS Noise = estimated root mean squared noise in the actual data over the fitted region,

n = number of data points in the fitted region,

f = total number of variables from all the peak and baseline functions.

The Levenberg-Marquardt algorithm iteratively adjusts every variable for each peak in order to minimise the χ^2 .

2. 2. RAMAN

2. 2. 1. Introduction and history

Simply stated the Raman effect can be described as the inelastic scattering of light by matter. The Raman effect was first predicted theoretically by Brillouin in 1922 and by Smekal in 1923. The first experimental observation however was made by Raman and Krishnam in 1928, and a complete semi-classical theory of the Raman effect was published a few years later by Placzek (in 1934). But despite the initial excitement the spectroscopic application of the Raman effect only really started to make progress in the late 50's, early 60's with the invention of lasers. Since then constant instrumental progress has been made, with the fabrication of high quality holographic gratings, improved detectors (such as CCD cameras (Williams et al. 1994)), and the development of PC-based computer power.

Raman spectroscopy can be used to obtain structural information, orientation, conformation and crystallinity (Robinson et al. 1976), to identify small inclusion in bulk materials (Boyer and Smith 1984, Purcell and White 1983, Jawhari et al. 1992), to study the effect of stress and strain on materials (Birnie et al. 1992, Blanpain et al. 1993), etc.

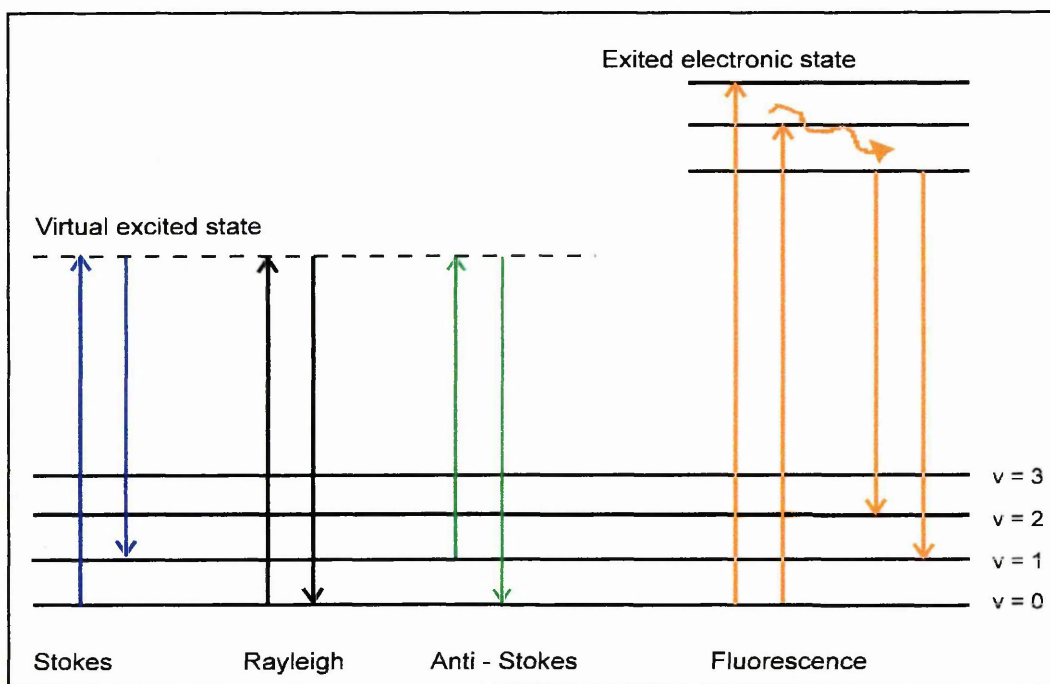
2. 2. 2. The Raman effect

When a molecule is irradiated with a beam of light of single frequency, most of the photons are scattered elastically with no change in energy, thus no change in frequency, the so called Rayleigh scattering. A very small portion of the incident photons (<0.1%), however, undergoes inelastic scattering and either gains (anti-Stokes) or loses (Stokes) energy to give a range of frequencies in the scattered light beam which constitutes the Raman spectrum of the particular molecule being examined.

For most purposes the Stokes scattering is used as this is considerably more intense than the anti-Stokes scattering. This intensity difference arises because of the population difference between the different vibrational energy levels of the molecule. At room temperature there will be many more molecules in the ground vibrational state (from which the Stokes lines arise) than in the higher vibrational states, and therefore the incoming light is more likely to interact with a molecule in the ground state.

Figure 2. 15. shows the Rayleigh and Raman scattering as well as fluorescence.

Figure 2. 15. : Rayleigh and Raman scattering model according to the quantum theory.



2. 2. 2. 1. Classical description of Raman spectroscopy

When a molecule is placed into an electric field, there is a change in the shape of the electron cloud, nuclei being attracted towards the negative pole of the

field, the electrons to the positive pole. This separation of charges causes an induced electric dipole moment to be produced.

The induced dipole moment μ is proportional to the field strength E .

$$\mu = \alpha E \quad (\text{eq. 2. 66.})$$

Where α is the polarisability of the molecule, which is the ease with which the electron cloud can be distorted. The polarisability can be represented by an ellipsoid.

When a molecule is subjected to a beam of radiation of frequency ν , the electric field experienced by the molecule varies according to the equation :

$$E = E_0 \cos 2\pi\nu_0 t \quad (\text{eq. 2. 67.})$$

thus,

$$\mu = \alpha E_0 \cos 2\pi\nu_0 t \quad (\text{eq. 2. 68.})$$

Where E_0 = equilibrium field strength,

ν_0 = angular frequency of the radiation,

t = time.

Because both μ and E are time dependent, the induced dipole moment will oscillate in time and emit or scatter radiation of frequency ν_0 . This is Rayleigh scattering.

The expression for μ can be written in terms of Cartesian components :

$$\mu_x = \alpha_{xx}E_x + \alpha_{xy}E_y + \alpha_{xz}E_z$$

$$\mu_y = \alpha_{yx}E_x + \alpha_{yy}E_y + \alpha_{yz}E_z$$

$$\mu_z = \alpha_{zx}E_x + \alpha_{zy}E_y + \alpha_{zz}E_z$$

or as a matrix equation :

$$\begin{bmatrix} \mu_x \\ \mu_y \\ \mu_z \end{bmatrix} = \begin{bmatrix} \alpha_{xx} & \alpha_{xy} & \alpha_{xz} \\ \alpha_{yx} & \alpha_{yy} & \alpha_{yz} \\ \alpha_{zx} & \alpha_{zy} & \alpha_{zz} \end{bmatrix} \begin{bmatrix} E_x \\ E_y \\ E_z \end{bmatrix} \quad (\text{eq. 2. 69.})$$

A molecule vibrating at a frequency ν_v also has internal (vibrational) motions, which can be described by normal co-ordinates (Q). Therefore the internuclear distance can be written as :

$$Q_v = Q_v^0 \cos(2\pi\nu_v t) \quad (\text{eq. 2. 70.})$$

Where Q_v^0 is the amplitude of vibration. Hence,

$$\alpha = \alpha_0 + \left(\frac{\partial \alpha}{\partial Q_v} \right)_v Q_v + \text{higher order terms} \quad (\text{eq. 2. 71.})$$

or,

$$\alpha = \alpha_0 + \left(\frac{\partial \alpha}{\partial Q_v} \right)_v Q_v^0 \cos(2\pi\nu_v t) \quad (\text{eq. 2. 72.})$$

and the expression for μ now becomes

$$\mu = \alpha_0 E_0 \cos 2\pi\nu_0 t + E_0 \left(\frac{\partial \alpha}{\partial Q_v} \right)_v Q_v^0 \cos(2\pi\nu_0 t) \cos(2\pi\nu_v t) \quad (\text{eq. 2. 73.})$$

or, (eq. 2. 74) :

$$\mu = \alpha_0 E_0 \cos(2\pi\nu_0 t) + \left(\frac{\partial \alpha}{\partial Q_v} \right)_v \frac{E_0 Q_v^0}{2} \{ \cos[2\pi(\nu_0 - \nu_v)t] + \cos[2\pi(\nu_0 + \nu_v)t] \}$$

The first term on the right-hand side of (eq. 2. 74.) represents the oscillation of the induced dipole at the frequency ν_0 of the incident light, resulting in Rayleigh scattering. The second term represents the Raman scattering, at frequencies $\nu_0-\nu_v$ (Stokes) and $\nu_0+\nu_v$ (anti-Stokes).

(eq. 2. 74.) shows that for Raman scattering to occur, the polarisability must change during the vibration, i.e.

$$\left(\frac{\partial \alpha}{\partial Q_v} \right) \neq 0 \quad (\text{eq. 2. 75.})$$

2. 2. 2. 2. Quantum theory

Quantum theory treats radiation of frequency ν as being a stream of photons of energy $h\nu$. Therefore each vibration of the molecule can be characterised by its energy E_v .

$$E_v = h\nu(v+1/2) \quad (\text{for SHO}) \quad (\text{eq. 2. 76.})$$

Where v is the vibrational quantum number. v can have values of 0, 1, 2, 3...etc.

During Raman scattering, the molecule can gain or lose energy in accordance with the following conditions : if the molecule gains energy ΔE , the photon will be scattered with energy $h\nu-\Delta E$, and if the molecule loses energy ΔE , the photon will be scattered with energy $h\nu+\Delta E$. This is shown in **figure 2. 15.**

2. 2. 2. 3. Selection rules and intensities for Raman scatter

There are $3N-6$ normal modes of vibrations for a non-linear molecule and $3N-5$ for a linear molecules. However not all these modes are Raman active.

First of all for a vibration to be Raman active there must be a change in the polarisability during the vibration ;

If $\left(\frac{\partial\alpha}{\partial Q_v}\right)_0 = 0$, then the normal mode of vibration is Raman inactive.

A general method to determine if a mode is Raman active or inactive involves determining the symmetry class via a group theory treatment of the molecule (Davidson 1991).

The best known selection rule for IR and Raman spectroscopy is the 'rule of mutual exclusion'. If a molecule has a centre of symmetry, then vibrations are either Raman or IR active, but not both. This rule is useful when determining if a molecule has a centre of symmetry or not. Empirically bands which have a high intensity in Raman, will give weak infrared bands, and vice versa.

Nishimura et al. in 1978 and Carey in 1982 have summarised the common observations about relative band intensities in Raman spectroscopy :

1. stretching vibrations are more intense than deformation vibrations,
2. the intensity of a band due to the stretching of a covalent bond increases with bond order,
3. the intensity of a band due to the stretching of a covalent bond increases with the atomic number of the bonded atoms,
4. bands due to in-phase stretching vibrations are more intense than bands due to out-of-phase vibrations.

2. 2. 2. 4. Limitations

Thermal sample degradation

Thermal decomposition of the sample may occur due to intense focused laser beam, this is especially a problem in Raman microscopy, when high powered lasers are used. Biological samples are especially sensitive to thermal decomposition.

Fluorescence

The fluorescence spectrum can mask the Raman spectrum of the sample. Fluorescence is a phenomenon approximately 10^6 - 10^8 times stronger than Raman scattering. The presence of additives, trace impurities etc., are often responsible for this phenomenon.

This problem may be overcome by diverse methods :

1. 'burning-out' of fluorescence, which involves leaving the sample under the laser light for a long period of time until the fluorescence level decreases to an acceptable level,
2. using UV or near-IR excitation,
3. using fluorescence-quenching agents,
4. using the time scale difference between the fluorescence process and the Raman process. The Raman process is almost instantaneous, whereas the fluorescence process requires more than 10^{-9} seconds in a typical case.
5. Where the fluorescence background is not too severe, it is possible to subtract it from the spectrum.
6. Fluorescence is reduced for anti-Stokes scattering.

2. 2. 3. Raman microscopy

A Raman micro-spectrometer results from coupling a microscope to a Raman spectrometer. One area which has greatly benefited from micro-Raman is that of semi-conductors (Abstreiter 1991, Tang and Rosen 1991), but many other

areas have also progressed such as biological systems (Barron et al. 1991), fibres (Lewis et al. 1996, Bard et al. 1997), PVD coatings (Chen et al. 1994, Blanpain et al. 1993), and polymer samples (Garton et al. 1993, Meier and Kip 1994, Huong 1996, Gerrard 1994, Maddams 1986).

By using a x100 objective one can achieve a spatial resolution of about 1 μ m. The spatial resolution is mainly a function of the wavelength of the illumination laser, which lies between 0.3 μ m and 0.7 μ m. This spatial resolution is obtained by using a confocal arrangement.

Confocal microscopy

The confocal 'set-up' of a Raman microscope enables one to discriminate between parts of the sample which are not at the same depth and allows the detection of scattered Raman light from inside the focal volume only, thereby eliminating most of the fluorescence and stray light coming from outside the focal volume. Therefore the confocal set-up can be used to depth-profile a sample. In effect this allows one to obtain spectra of sections of a sample at various depths. However one can encounter various problems. These include heating and burning of the sample, or a net decrease in the intensity of the spectra, due to the smaller volume sampled. One of the major disadvantages is due to the confocal profile being convoluted with the result of the depth-profile ; this will be discussed further in chapter 4.

The intensity of a given Raman line at the wavelength λ reaching the detector is:

$$S \approx I_0 \tau_\lambda N \Omega T_\lambda S_\lambda \quad (\text{eq. 2. 77.})$$

Where I_0 = the laser irradiance at the sample ,

τ_λ = the differential cross-section for the Raman line analysed,

N = the number of molecules in the probed volume,

Ω = the solid angle of collection of the Raman light,

T_λ = the throughput of the instrument,

s_λ = the sensitivity of the detector at the wavelength λ .

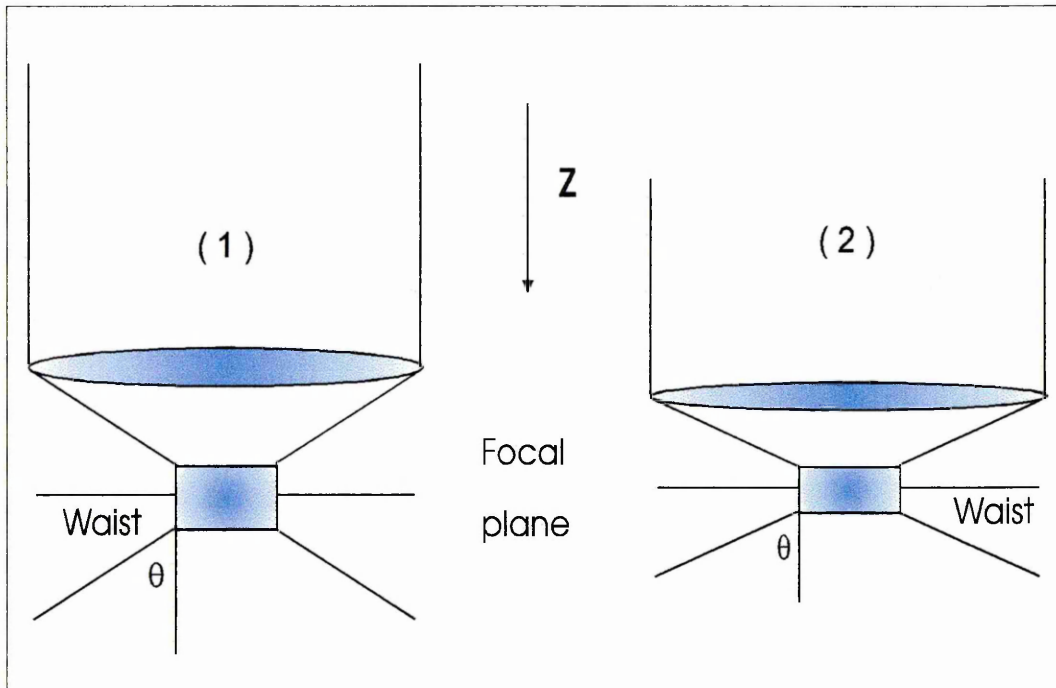
The best way to decrease the probed volume while increasing Ω and I_0 , is to use a microscope objective with high numerical aperture (NA).

$$NA = n \sin(\theta/2) \quad (\text{eq. 2. 78.})$$

Where θ = the angle of entrance,
 n = the refractive index of transmitting medium.

The NA determines the distribution of the laser field around the focus, a high NA resulting into a short waist and a low NA in a large waist. **Figure 2. 16.** shows the distribution of laser light around focus.

Figure 2. 16. shows the distribution of laser light around the focus for a high NA (2) and a low NA(1).



The length of the waist (ω), also known as the depth of focus is defined by :

$$\omega = 6.4(\lambda/2\pi)(1/\tan\theta)^2 \cong \lambda(1/\tan\theta)^2 \quad (\text{eq. 2. 79.})$$

Table 2. 3. shows the value of NA for several objectives.

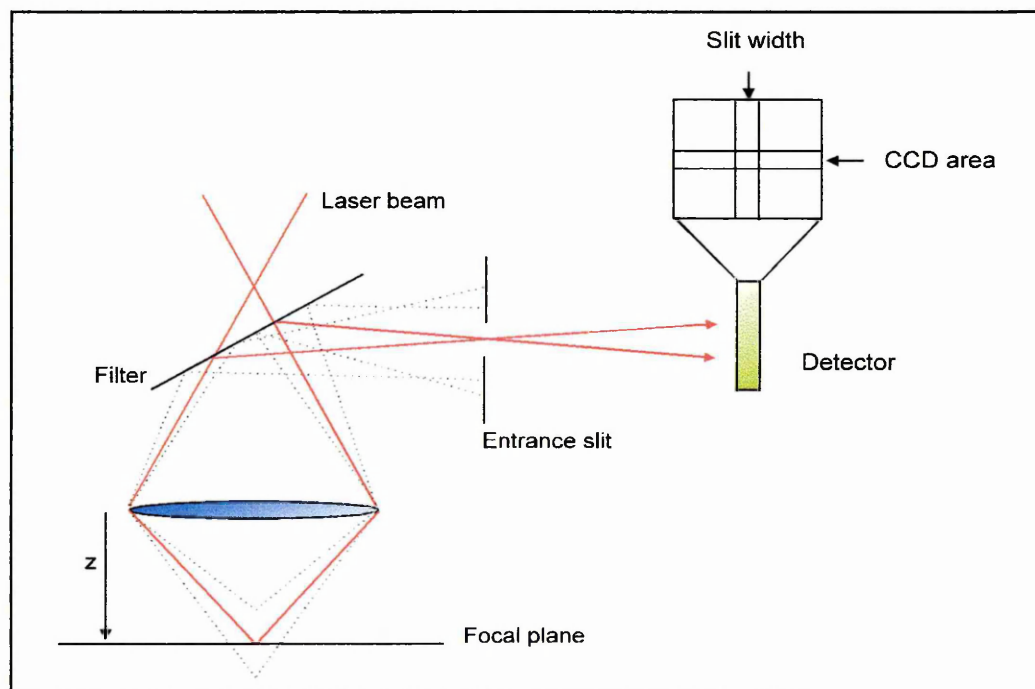
Table 2. 3. : Values of NA for several objectives.

Objective	NA	θ (degrees)	ω (μm)
x100	0.95	71.8	0.1
x50	0.80	53.13	0.4
x20	0.46	27.39	2.4
x20(long working)	0.40	23.58	3.3
x10	0.30	17.46	6.4

The performance of a confocal Raman microscope is not only determined by the optical properties of the microscope objective (numerical aperture, magnification power, and focal length), but also by the size of the pinhole placed in the back image plane of the microscope, or simulated using the combination of the spectrometer slit and a small area of the CCD camera.

The long axis of the CCD detector (576 pixels) is used to describe the spectral dimension, and the shorter axis (closed to about 5 pixels, corresponding to 100 μm) describes the image height. Combined with the spectrometer slit opened to approximately 15 μm , a pinhole effect is created. This is shown in **figure 2. 17.**

Figure 2. 17. : The confocal arrangement.



And the size of the laser spot can be expressed as :

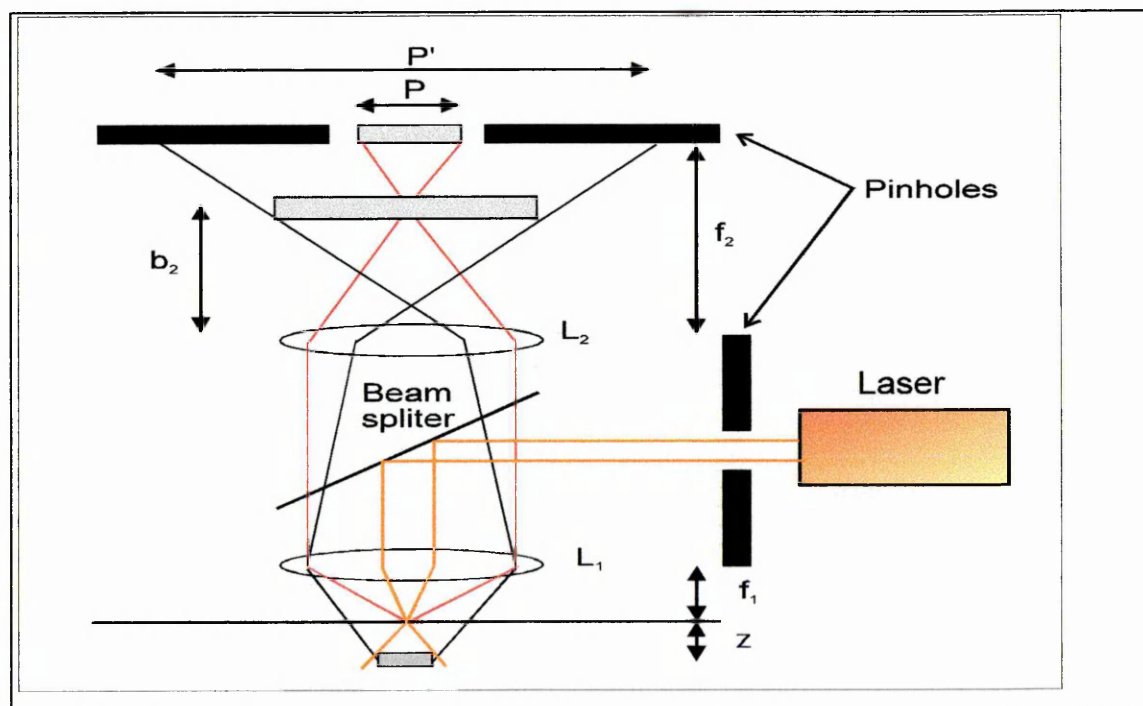
$$s(f_1 \pm z) = sf_1 \quad \text{for } z < \omega/2 \quad (\text{eq. 2. 80.})$$

$$s(f_1 \pm z) = sf_1 + 2(z - \omega/2) \tan\theta \quad \text{for } z > \omega/2 \quad (\text{eq. 2. 81.})$$

In a confocal arrangement a pinhole or slit is situated at the back image plane of the microscope, and out-of-focus laser spot of size $s(f_1 \pm z)$ will be imaged outside of the back focal plane at a distance b_2 from the second lens L_2 . (see **figure 2. 18.**)

$$b_2 = \left\{ \frac{1}{f_2} - \frac{1}{\left(f_2 - \left[\frac{1}{f_1} - \frac{1}{(f_1 \pm z)} \right]^{-1} \right)} \right\}^{-1} \quad (\text{eq. 2. 82.})$$

Figure 2. 18. : Principle of confocal Raman microspectroscopy.



Where f_1 = the focal length of objective lens L_1 ,

f_2 = The focal length of slit focusing lens L_2 .

This image is projected on the back image plane of the microscope. It is bigger than the laser spot of the microscope on the focal plane. The diameter of the out-of-focus plane projection, P' is equal to :

$$P' = \frac{f_2 M s (f_1 \pm z)}{b_2} \quad (\text{eq. 2. 83.})$$

Where M = the magnification.

This projection P' is larger than the projection caused by a laser spot in the focal plane of lens L_1 , therefore by placing a pinhole with diameter $P < P'$ in the back image plane, the light coming from out-of-focus plane is cut off without blocking out light from the in-focus planes (see **figure 2. 18.**).

Figure 2. 19. shows a comparison between intensity distribution as a function of distance from the object focal plane for a confocal and a conventional Raman microscope.

Figure 2. 19A. : Confocal Raman microscope versus conventional Raman microscope for the x50 objective.

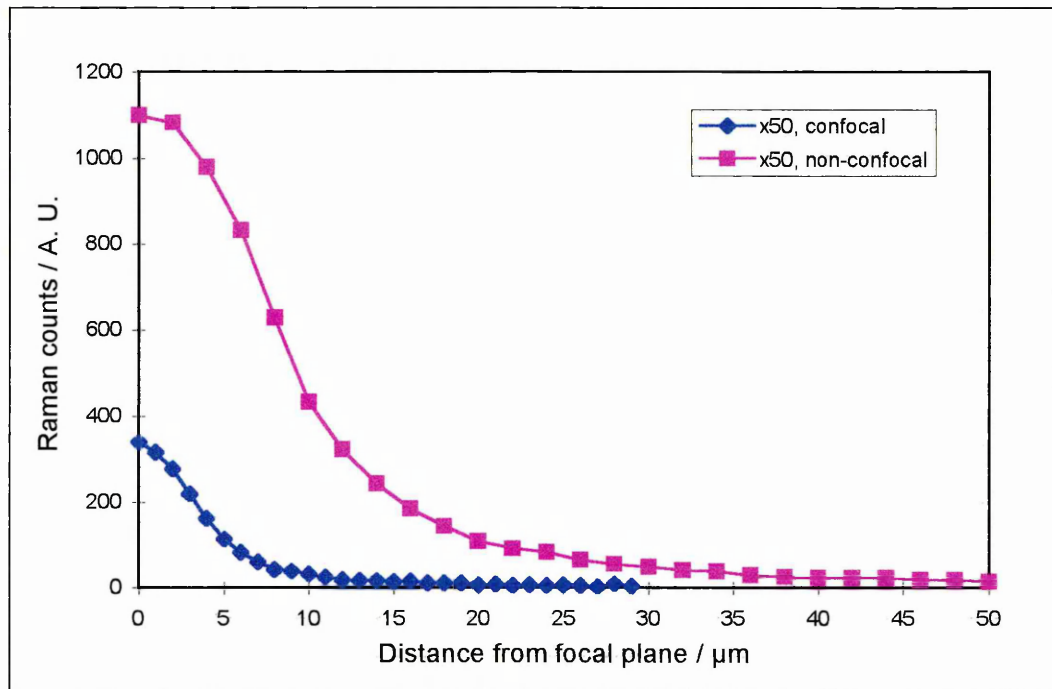
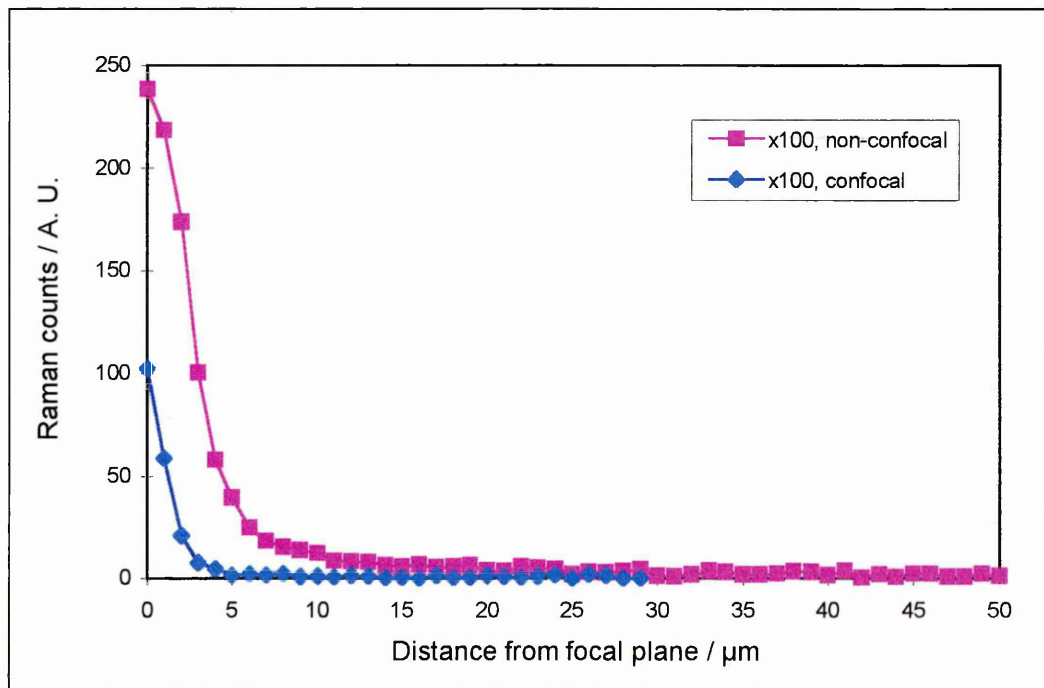


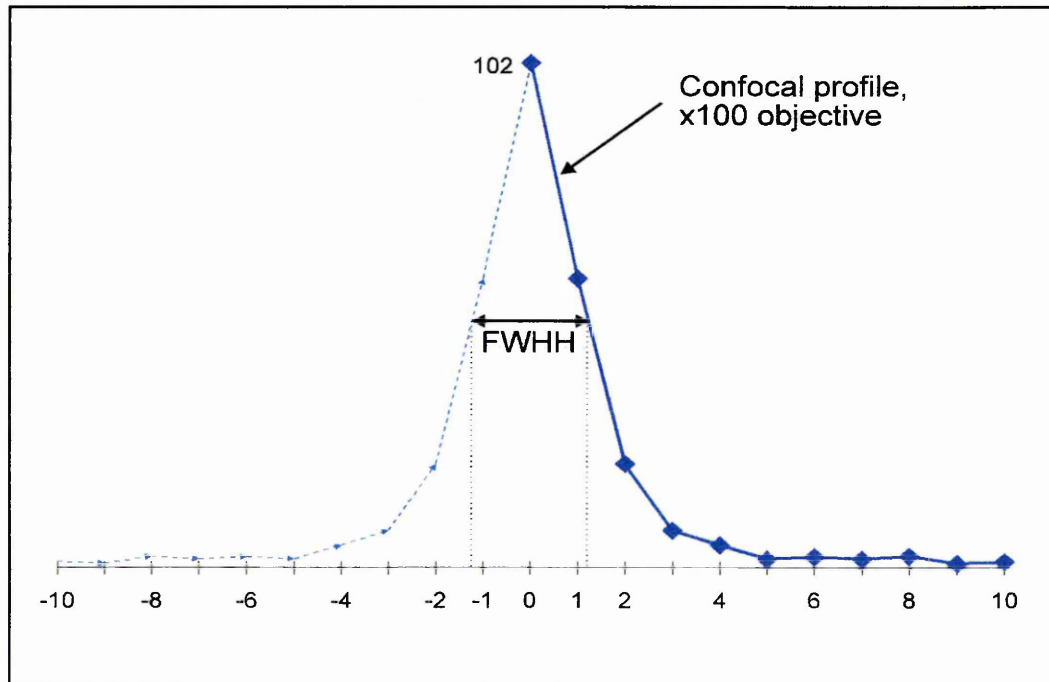
Figure 2. 19B. : Confocal Raman microscope versus conventional Raman microscope for the x100 objective.



It is possible to determine the confocal response at different magnifications of a Raman spectrometer. This is done experimentally, by moving the objective away from a silicon wafer in steps of $1\mu\text{m}$, taking a spectrum at each step. The Raman response is then plotted as a function of distance away from the wafer (the Si band at 520 cm^{-1} is used).

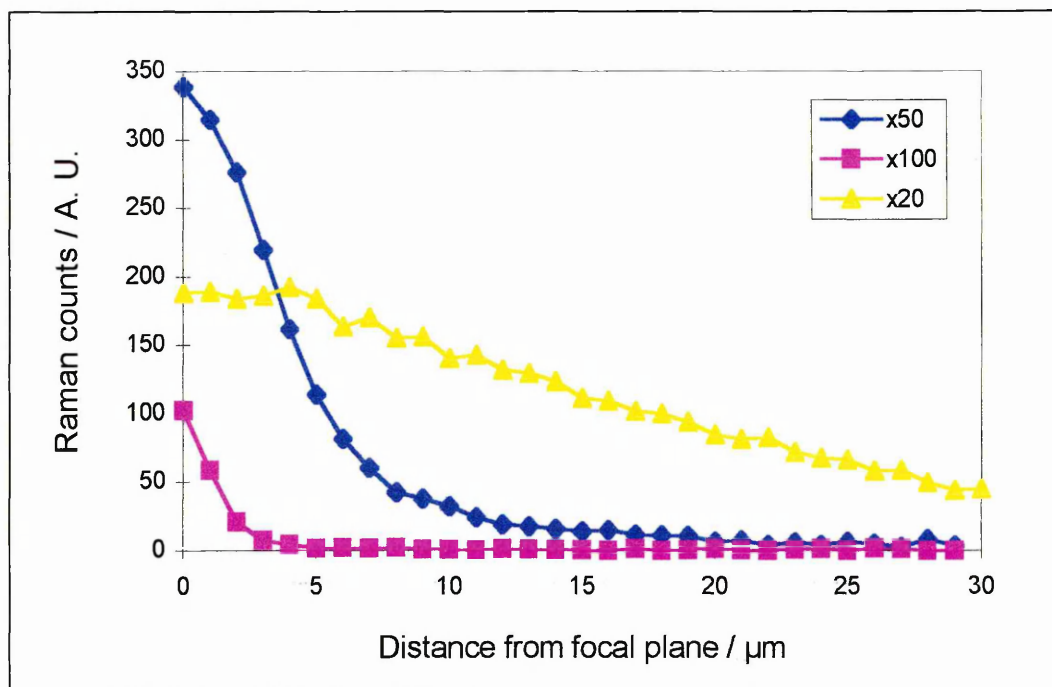
The FWHH of this profile gives the depth resolution for the objective used, as shown on **figure 2. 20A.** .

Figure 2. 20A. : Spatial resolution.



The confocal response for various objectives is shown in **figure 2. 20B.**. From this figure it is clear that the best confocal response is obtained with a x100 objective.

Figure 2. 20. : Confocal response of various objectives.



2. 2. 4. Quantitative Raman

The intensity of the Raman scattering of a functional group is linearly related to its concentration. The linear relationship is most useful in obtaining an accurate measure of the ratio of two or more components in a mixture, i.e. determining the relative concentrations of the different species. But an internal standard has to be used for the determination of absolute concentrations.

The difficulty of measuring absolute concentration in Raman spectroscopy arises from various sources : variations in the source, sample and optics, the inherent weakness of the Raman process, strong fluorescence for many samples.

Quantitative analysis by Raman spectroscopy started in the late 60's, early 70's, with the introduction of lasers, replacing the mercury-vapour lamps as the excitation source.

Grasselli, Snavely and Bulkin (Grasselli et al 1981) cite a dozen applications of quantitative Raman spectroscopy for the period from 1970 to 1979. There are also many reports of use of quantitative Raman spectroscopy in routine analysis in the determination of pollutants in water (Reeves et al. 1973, Cunningham et al. 1977, Miller 1977) There have been further applications of quantitative analysis in Raman spectroscopy, including the determination of azodyes (Womack et al. 1987), pharmaceutical products (Sato et al. 1980), or ethanol in fermentation broth for example (Shope et al. 1987).

Internal standards :

In solution measurements, the solvent is often chosen as the internal standard, for example the case of water in aqueous solutions. With solid samples a major component is selected as the internal standard.

However using an internal standard might not be sufficient, and the method may fail due to changes in shape or position of the relevant bands as there are changes in sample composition, non-linearity of the instrument response, differences in sample scattering at the analyte and standard lines. Wavenumber errors may also be introduced, rendering subtraction of spectra difficult.

Various techniques are available for quantifying peaks, such as peak height, cross correlation, and least square fitting.

2. 2. 5. Complementarity of Raman and IR spectroscopy

Due to the difference in selection rules between Raman and IR, in order to obtain complete vibrational (and rotational) information, it is imperative to have the Raman and IR spectrum of the sample of interest.

Also, it is possible using Raman spectroscopy to record low frequency vibrations, down to ca 5 cm^{-1} . The spatial resolution in Raman is greater, $1\ \mu\text{m}$ (in confocal mode) compared to IR, $10\ \mu\text{m}$.

Although Raman scattering is a weak effect enhancement techniques such as resonance Raman or SERS can be used in certain cases. Techniques such as Raman mapping (Hayward et al. 1995, Gardiner and Bowden 1990, Batchelder et al. 1991) and imaging (Williams et al. 1994, Hayward et al. 1994, Hayward et al. 1995, Batchelder et al. 1991) are also available.

2. 3. REFERENCES

Abstreiter G., *Appl. Surf. Sci.*, 1991, **50**, 73.

Banwell C.N., *Fundamentals of Molecular Spectroscopy*, third edition, Mc Graw - Hill Book Company (UK) Limited, 1983

Bard D., Yarwood J., Tylee B., *J. of Raman Spec.*, 1997, **28**, 803.

Batchelder D.N., Cheng C., Pitt D., *Adv. Materials*, 1991, **3**(11), 566.

Belali R., J.M. Vigoureux, *Appl. Spec.*, 1994, **48**(4), 465.

Billingham J., Breen C., Yarwood J., *Vib. Spec.*, 1997, **14**(1), 19.

Birnie J., Craggs C., Gardiner D.J., Graues P.R., *Corros. Sci.*, 1992, **33**(1), 1.

Blanpain B., Franck M., Mohrbacher H., Vancoille E., Celis J.P., Roos J.R., *Micro - Raman Spectroscopy for the Characterisation of Wear Induced Surface Modifications on Hard Coatings in : Thin films in Tribology*, eds. : Dowson D., Elsevier Publishers, 1993, pp623 - 630.

Barron L.D., Gargaro A.R., Hecht L., Wen Z.Q., Hug W., *Proc. SPIE - Int. Soc. Opt. Eng.*, 1991, **1403**(1), 66.

Boven G., Brinkhuis R.H.G., Vorenkamp E.J., Challa G., Schouten A.J., *Polymer*, 1992, **33**(6), 1150.

Boyer H., Smith D.C., *Microbeam Anal.*, 1984, **26**, 33.

Brillouin L., *Ann. Phys.*, 1922; **88**, 17.

Carey P.R., *Biochemical Applications of Raman and Resonance - Raman Spectroscopies*, Press, Toronto, 1982.

Chen C., Liang N.T., Tse W.S., Chen I.Y., Duh J.G., *Chinese J. of Phys.*, 1994, **32**(2), 205.

Cunningham K.M., Goldberg M.C., Weiner E.R., *Anal. Chem.*, 1977, **49**, 70.

Davidson G, *Group Theory for Chemists*, McMillan, Physical Science Series, 1991.

Ferraro J.R., Basile L.J., *Fourier Transform Infrared Spectroscopy : Applications to Chemical Systems*, Volume 1., Academic Press, London, 1978.

Gardiner D.J., Bowden M., *Microscopy and Analysis*, 1990, **27**.

Garton A., Batchelder D.N., Cheng C., *Appl. Spec.*, 1993, **47**(7), 922.

Gerrard G.L., *Anal. Chem.*, 1994, **66**(12), 547R.

Grasselli J.G., Snavely M.K., Bulkin B.J., *Chemical Application of Raman Spectroscopy*, Willey (Interscience), New York, 1981, pp24 - 28.

Griffiths P.R, De Haseth J.A, *Fourier Transform Infrared Spectrometry*, John Willey and Sons, 1996.

Harrick N.J., *Internal Reflection Spectroscopy*, third edition, Harrick Scientific Corporation, New York, 1987.

Hayward I.P., Baldwin K.J., Hunter D.M., Batchelder D.N., Pitt G.D., *Diamond and Related Materials*, 1995, **4**, 617.

Hayward I.P., Batchelder D.N., Pitt G.D., *Anal. Magazine*, 1994, **22**(10), M28.

Huong P.V., *Vib. Spec.*, 1996, **11**, 17.

Jawhari T., Merino J.C., Rodriguez - Cabello J.C., Pastor M., *Polymer*, 1992, **33**, 4199.

Lewis I.R., Chaffin N.C., Gunter M.E., Griffiths P.R., *Spectrochimica Acta part A*, 1996, **52**, 315.

Mackenzie M.W., *Advances in Applied Fourier Transform Infrared Spectroscopy*, John Willey and Sons, 1988.

Maddams W.F., *American Laboratory*, 1986, 58.

Marquardt D.W., *J. Soc. Ind. Appl. Math.*, 1963, **11**, 431.

Meier R.J., Kip B.J., *Microbeam Anal.*, 1994, **3**, 61.

Miller A.G., *Anal. Chem.*, 1977, **49**, 2044.

Mirabella Jr. F.M., *Internal Reflection Spectroscopy : Theory and Applications*, Marecel Dekker Inc., 1993.

Mirabella Jr. F.M., Harrick N.J., *Internal Reflection Spectroscopy : Review and Supplement*, Harrick Scientific Corporation, 1985.

Nishimura Y., Hirakawa A., Tsuboi M., *Advances in Infrared and Raman Spectroscopy*, 1978, **5**, 217.

Pereira M.R., Yarwood J., *J. of Polym. Sci. : part B : Polym. Phys.*, 1994, **32**, 1881.

Placzek G., *Rayleigh Streuung und Raman Effekt* in : *Handbuch der Radiologie*, eds. Marx E., Akademische - Verlag, Leipzig, 1934, pp205.

- Purcell F.J., White W.B., *Microbeam Anal.*, 1983, **26**, 107.
- Raman C.V., Krishnam K.S., *Nature*, 1928, **121**, 50.
- Raman C.V., Krishnam K.S., *Proc. Roy. Soc. Lond.*, 1929, **122**, 23.
- Reeves J.M., Bradley E.B., Frenzel C.A., *Water Resources*, 1973, **7**, 1417.
- Robinson M.E.R., Bower D.I., Maddams W.F., *Polymer*, 1976, **17**, 355.
- Sato S., Higuchi S., Tanaka S., *Anal. Chimi. Acta*, 1980, **120**, 209.
- Shope T.B., Vickers T.J., Mann C.K., *Appl. Spec.*, 1987, **41**, 908.
- Skourlis, McCulloch R.L., *J. of Appl. Polym. Sci.*, 1994, **52(9)**, 1241.
- Smekal A., *Naturwissenschaften*, 1923, **11**, 873.
- Sun Y.Y., Zhao Z.Z., Ma M.H., Hu P., Liu Y.S., Yu T.Y., *J. of Polym. Sci.*, 1997, **65(5)**, 959.
- Tang W.C., Rosen H.J., *Microbeam Anal.*, 1991, **26**, 101.
- Urban M.W., *Attenuated Total Reflectance Spectroscopy of Polymers : Theory and Practice*, Polymer Surfaces and Interfaces Series, American Chemical Society, Washington, DC, 1996.
- Yang Y., Kim H., *Polym. Composite*, 1997, **67(7)**, 486.
- Walls D.J., *Appl. Spec.*, 1991, **45(7)**, 1193.
- Walls D.J., J.C. Coburn, *J. of Polym. Sci. part B, Polym. Phys.*, 1992, **30**, 887.

Williams K.P.J., Smith B.J.E., Hayward I.P., *Appl. Spec.*, 1994, **48**(2), 232.

Womack J.D., Vickers T.J., Mann C.K., *Appl. Spec.*, 1987, **41**, 117.

CHAPTER 3. :
DIFFUSION OF WATER IN POLYMERIC
MEMBRANES.

CONTENTS :

CHAPTER 3. : DIFFUSION OF WATER IN POLYMERIC MEMBRANES.	92
3. 1. DIFFUSION OF WATER INTO POLYMERS.....	94
3. 1. 1. Diffusion behaviour	95
3. 1. 1. 1. Case I or Fickian diffusion.....	97
3. 1. 1. 2. Case II diffusion	97
3. 1. 1. 3. Case III or non - Fickian or anomalous diffusion.....	98
3. 1. 2. Dual - mode sorption.....	98
3. 2. WATER	100
3. .2 . 2. Water in polymeric membranes.....	101
3. 3. REFERENCES.....	103

CHAPTER 3. : DIFFUSION OF WATER IN POLYMERIC MEMBRANES

3. 1. DIFFUSION OF WATER INTO POLYMERS

Polyvinyl chloride (PVC) is one of the leading plastic materials in the world. It is extensively used in packaging and bottles, or in ion - selective membranes (Li et al. 1996 and 1996a, Chan et al. 1992, Okuno et al. 1995) in contact with aqueous solutions and biological samples such as blood (Widmer 1993, Armstrong and Horvai 1990). In addition, many polymer films are being used as barriers to toxins in protective clothing equipment or sealant (Finch 1983, Vieth 1991). The barrier properties of the films are related to the rate of molecular diffusion. Polymeric materials absorb water at varying rates, and various properties such as mechanical properties, vary with the absorption of water. Absorption of water is often accompanied by desorption or leaching of various additives in the polymer, such as fillers (Balik and Xu 1994), plasticisers (Vergnaud 1994) and biocides (Cadmus and Brophy 1982).

The diffusion of solvent or small molecules into polymer films can be studied using various methods ; such as gravimetric analysis (Bouzon and Vergnaud 1991, Storey et al. 1991, Southern and Thomas 1980, Hopfenberg et al. 1975, Shailaja and Yaseen 1993, Gray and Gilbert1975) (or pat and Weigh method), using fluorescent tracers (Krongauz et al. 1995), by TGA (Ogawa et al. 1993), using a spatial imaging spectrometer (Li et al. 1996, Chan et al 1992), Raman spectroscopy (Klier and Peppas 1986), stray field magnetic resonance imaging (Lane and McDonald 1997), FTIR - ATR spectroscopy (Pereira and Yarwood 1996 and 1996a, Fieldson and Barbari 1993 and 1995, Cogan - Farinas et al. 1994, Van Alsten 1995, Hadjatdoost and Yarwood 1997), HPLC (Parker and Ranney 1994) or UV spectroscopy (Vergnaud 1994).

Different sorption processes have been reported for different species and polymers. They have been categorised in three types : Case I or Fickian diffusion mode, Case II diffusion and non - Fickian or anomalous diffusion (Verghnaud 1991, Crank 1994, Comyn 1993).

3. 1. 1. Diffusion behaviour

Sorption describes the penetration and dispersal of penetrant in a polymeric matrix. Sorption process may include penetrant adsorption, absorption, incorporation into micro-voids, cluster formation, solvation-shell formation and other modes of mixing. More than one concurrent or sequential mode of sorption may happen in a given polymer material. The diffusion mode of penetrant may change with changes in sorbed concentration, temperature, swelling induced structural states, time of sorption to equilibrium and other factors.

Polymers usually have a wide spectrum of relaxation times, associated with structural changes. They all decrease with increase of temperature or increase in penetrant concentration or increase in polymer segmental motion.

Classification of sorption process can be made according to the relative rates of diffusion and polymer relaxation.

The mathematical treatment of diffusion is based on Fick's discovery that like transfer of heat conduction, diffusion is due to random molecular motion, and therefore the following equation can be applied :

$$F = -D \left(\frac{\partial C}{\partial z} \right) \quad (\text{eq. 3. 1.})$$

also known as Fick's first law.

Where F = the flux in the z - direction,
 $\partial C / \partial z$ = the concentration gradient,
 D = the diffusion coefficient.

For one - dimensional molecular diffusion in a polymer film with a constant diffusion coefficient, the equation for the diffusing species reduces to :

$$\frac{\partial C}{\partial t} = D \left(\frac{\partial^2 C}{\partial z^2} \right) \quad (\text{eq. 3. 2.})$$

or Fick's second law.

Where D = the diffusion coefficient,
 C = the concentration of the diffusing material,
 t = the time,
 z = the space co -ordinate measured normal to the diffusion.

The mass of molecules diffused at time t in a plane sheet of thickness L is described by,

At short times :

$$\frac{M_t}{M_\infty} = \frac{2}{L} \left(\frac{D}{\pi} \right)^{1/2} t^{1/2} \quad (\text{eq. 3. 3.})$$

where M_t = the amount of material transported at time t ,
 M_∞ = the amount of material transported at equilibrium.

and at long times :

$$\frac{M_t}{M_\infty} = 1 - \frac{8}{\pi^2} \exp\left(\frac{-D\pi^2 t}{4L^2} \right) \quad (\text{eq. 3. 4.})$$

usually used in the form :

$$\ln\left(1 - \frac{M_t}{M_\infty}\right) = \ln\left(\frac{8}{\pi^2}\right) - \frac{D\pi^2 t}{4L^2} \quad (\text{eq. 3. 5.})$$

3. 1. 1. 1. Case I or Fickian diffusion

During Fickian diffusion the rate of diffusion is much less than that of relaxation, and the polymer-penetrant systems obey Fick's law. This type of behaviour is characterised experimentally by a $t^{1/2}$ time dependence at short times of the concentration gradient profile. It is determined by the slope n of a plot of $\log M$ against \log time, where M is the amount of penetrant observed. The behaviour of these systems can be described by a single diffusion coefficient.

3. 1. 1. 2. Case II diffusion

In Case II diffusion, the other extreme, diffusion is very rapid compared with the relaxation processes. For this case, the short time dependence of the concentration is characterised by $n = 1$. It is determined by the slope n of a plot of $\log M$ against \log time, where M is the amount of penetrant observed. The behaviour of these systems can also be described by a single parameter; the constant velocity of an advancing front of liquid located at the boundary between swollen gel and glassy core.

3. 1. 1. 3. Case III or non - Fickian or anomalous diffusion

This occurs when the diffusion and relaxation rates are comparable. Two or more parameters are needed to describe this behaviour. n is between 0.5 and 1, or changes sigmoidally from one to the other. This system lies between Case I and Case II and accommodates all the cases that cannot be described by Case I and II.

Anomalous behaviour can be caused by changes in polymer structure on solubility and diffusional mobility or internal stresses.

Sometimes "dual-mode " sorption kinetics are employed to characterise penetrant diffusion in PVC polymers (Li et al. 1996 and 1996a, Chan et al. 1992, Okuno et al. 1995, Parker and Ranney 1994, Vergnaud 1994).

3. 1. 2. Dual - mode sorption

A full theoretical treatment of dual-mode sorption can be found in "Dual-mode sorption theory" by Vieth and co-workers (Vieth et al. 1991), and in "The mathematics of diffusion" by Crank (Crank 1994).

In the simplest case of dual mode sorption, there are two concurrent mechanisms of sorption : ordinary dissolution, and "hole-filling". Meares' investigations showed evidence that the glassy state contains a distribution of micro-voids frozen into the structure as a result of the cooling down of the polymer through its glass transition temperature (T_g). These "hole" or micro-voids are the result of restricted segmental rotations of the polymer chains. Chan and co - workers (Chan et al. 1992 and 1993) have shown there is a wide range of these micro-domains, or free-volume pockets in PVC, in which penetrant molecules tend to form clusters. Free-volume parameters for various solvents were estimated by Hong (Hong 1995) using viscosity-temperature data. Using these parameters in conjunction with the Vrentas - Duda free

volume theory, diffusion behaviour for several polymer / solvent systems were predicted.

For gas molecule sorption in glassy polymers, the sorption of mobile species can, be described by a linear law :

$$C_D = k_D p \quad (\text{eq. 3. 6.})$$

Where C_D = the concentration of dissolved molecules,
 k_D = Henry's law dissolution constant,
 p = the partial pressure of penetrant gas.

The second mode of sorption occurring by immobilisation of the species at a fixed number of sites within the polymer can be represented by a non-linear Langmuir expression :

$$C_H = \frac{C'_H b p}{1 + b p} \quad (\text{eq. 3. 7.})$$

Where C_H = the concentration of molecules "absorbed in microvoids",
 C'_H = the concentration in the holes at saturation,
 b = the hole affinity constant.

The total concentration of penetrant is simply equal to the sum of penetrant in the film :

$$C = C_D + C_H \quad (\text{eq. 3. 8.})$$

Therefore the sorption isotherm at equilibrium can be written as :

$$C = k_D p + \frac{C'_H b p}{1 + b p} \quad (\text{eq. 3. 9.})$$

(eq. 3. 9.) has been successfully used to study various penetrant-polymer systems (Haward 1973, Vieth et al. 1976, Okuno et al. 1995.).

In glassy polymers sorption of water is often accompanied by significant swelling of the polymer network, thus the concentration of available sites changes with the degree of sorption.

3. 2. WATER

The structure of the water molecule : it possesses two hydrogen bond acceptor sites, and two hydrogen bond donor sites, i.e. pure water contains as many hydrogen bonds as covalent bonds. Interactions of water molecules in liquid water has been widely studied. It was noted very early on, that the frequency of OH stretching vibration decreases with increasing strength of the hydrogen bond (Pimentel and McClellan 1960 and 1971).

In the study of water, two main streams of interpretation are generally used :

1. The continuum approach (Falk 1975, Schiffer and Hornig 1968, Curnutte and Bandekar 1972) ; this suggests the existence of a continuous network of H - bonded molecules where the distortion of H - bonds results in a continuous distribution of the H - bond distances, angles and energies.

2. The mixture approach in which water is treated as a pseudo - polymeric material composed of a mixture of "defect" and "non - defect" water molecules, or "hydrogen - bonded" and "non - hydrogen bonded" molecules, which interchange between them as a function of temperature. The mixture approach was first used by Cross et al in 1937 (Cross et al. 1937).

This is the most employed model in the recent literature (Walrafen 1972, Luck 1974, D'Arrigo et al. 1981, Green et al. 1981, Hare and Sorensen 1990 and 1992, Marechal 1991).

Nevertheless, the analysis of most vibrational bands of H₂O (and D₂O) remain difficult, due to the overlapping different vibrational bands, and because of the

intermolecular, as well as, intramolecular coupling of vibrations. The breaking and reforming of intramolecular H - bonds happen on a pico second time scale.

3. .2 . 2. Water in polymeric membranes

Much work has already been done in this field using many spectroscopic techniques such as NMR (Otting et al. 1991 and 1991a, Denisov and Halle 1996), FTIR and Raman (Marechal and Chamel 1996, Nguyen et al. 1991 and 1996, Falk 1980, Quezado et al. 1984, Luck et al. 1980, Bashir et al 1995, Murphy and Depinho 1995, Van Alsten and Coburn 1994, Crupi et al. 1996), neutron scattering (Settles and Doster 1996, Bryant 1996, Denisov and Halle 1996), light scattering (Tao 1993, Tao et al. 1989).

The main problem seems our ability to distinguish bound water from bulk water, and various techniques have been devised to circumvent this problem. Those include the use of selective probes (Otting et al. 1991, Denisov and Halle 1996), spectral contrast (Settles and Doster 1996, Bryant 1996, Giordano et al. 1993 and 1995, Van Alsten and Coburn 1994), and spectral subtraction (Marechal and Chamel 1996, Falk 1980, Quezabo 1984).

A very convenient tool for looking at water is FTIR - ATR spectroscopy ; it has many advantages (see chapter 2., 6, and 7.) such as high sensitivity to structural and conformational changes, no saturation problems due to its small sampling depth (Mirabella 1985, Pereira and Yarwood 1994) (in the order of 0.5 to 2.0 μm). FTIR - ATR is an *in - situ* technique, which permits both kinetic and structural data to be obtained simultaneously.

Recent work on the perturbation of water molecules close to an organic interface using this technique has been carried out on microemulsions (Christopher et al. 1992, Gonzalez - Blanco et al. 1997, Ononi and Santucci 1993), and polymers (Marechal and Chamel 1996, Nguyen et al. 1991 and 1996, Falk 1980, Quezabo et al. 1984, Luck et al. 1980, Scherer et al. 1985 and 1974, Maeda et al 1993 and 1995 and 1996).

Because of the unique structure of water, it is able to insert itself and form H - bonds in natural and synthetic polymers. Small amounts of absorbed water in polymers can induce important changes of their physical properties (Crist 1993), and it can also act as a plasticiser (Roff and Scott 1956).

Water in polymer matrices behaves quite differently from water in solution; this has been shown to be due to the fact that it is restricted into smaller spaces (Doster et al. 1986, Teixeira and Stanley 1980, Settles and Doster 1996, McBrierty et al. 1993, Otting et al. 1991).

The bandshape, frequency and intensity of water in polymers is different from bulk water, but can be treated the same way. The differences have been explained as due to difference in surrounding environment (Falk 1980, Scherer et al. 1985 and 1974, Maeda et al. 1993, 1995 and 1996, D'Aprano et al., 1992 and 1988, Moran et al. 1995), the water forming clusters (Scherer et al. 1985, Murphy and Depinho 1995, Van Alsten and Coburn 1994, Sutander et al. 1994 and 1995) and water orientation (Bashir et al. 1995).

FTIR - ATR spectroscopy was the technique we chose to use to determine the perturbation of water in uPVC and pPVC films. Our interpretation of the water band provides a combination between the "mixture approach" and the "continuum approach" as will be demonstrated in chapter 7.

3. 3. REFERENCES

Armstrong R.D., Horvai G., *Electrochimica Acta*, 1990, **35**, 1.

Balik C.M., Xu J.R., *J. of Appl. Polym. Sci.*, 1994, **52(7)**, 975.

Bashir Z., Church S.P., Waldron D., *Polymer*, 1995, **35**, 967.

Bouzon J., Vergnaud J.M., *Eur. Polym. J.*, 1991, **27(2)**, 115.

Bryant R.G., *Ann. Rev. Biophys. Biomol. Structures*, 1996, **25**, 29.

Cadmus E.E., Brophy J.F., *Kunststoffe*, 1982, **72(4)**, 233.

Chan A.D.C., Li X., Harrison D.J., *Anal. Chemi.*, 1992, **64(21)**, 2512.

Chan A.D.C., Harrison D.J., *Anal. Chem.*, 1993, **65**, 32.

Christopher D.J., Hills B.P., Belton P.S., Yarwood J., *J. Coll. Int. Sci.*, 1992, **152**, 465.

Cogan - Farinas C.K., Doh L., Venkatraman S., Potts R.O., *Macromolecules*, 1994, **27**, 5220.

Comyn J., *Polymer. Permeability*, Chapman and Hall, 1993.

Crank J., *The Mathematics of Diffusion*, second edition, Oxford publications, 1994.

Crist B. in *Materials Science and Technology*, volume 12, eds. : Thomac E.L., VCH, Weinheim , 1993, pp 444.

Cross P.C., Burnham J., Leighton P.A., *J. of the American Chem. Soc.*, 1937, **59**, 1134.

Crupi V., Jannelli M.P., Magazu S., Maisano G., Majolino D., Migliardo O., Ponterio R., *J. of Mol. Struct.*, 1996, **381**, 207.

Curnutte B., Bandekar J., *J. of Mol. Spec.*, 1972, **41**, 500.

D'Aprano A., Lizzio A., Turco Liveri V., Aliotta F., Vasi C., Bardez E., Donato D.I., Larrey B., Migliardo P., *Prog. Coll. Poly. Sci.*, 1992, **89**, 258.

D'Aprano A., Lizzio A., Turco Liveri V., Aliotta F., Vasi C., Bardez E., Donato D.I., Larrey B., Migliardo P., *Phys. Chem.*, 1988, **92**, 4436.

D'Arrigo G., Maisano G., Mallamace F., Migliardo P., Wanderlingh F., *J. of Chem. Phys.*, 1981, **75**, 4264.

Denisov V.P., Halle B., *Faraday Discuss.*, 1996, **103**, 227.

Doster W., Bachleitner A., Dunn R., Heibl M., Lücher E., *Biophys. J.*, 1986, **50**, 213.

Falk M., *Chem. and Phys. of Aqueous Gas Sol.*, [Proc. Symp.] Electrochem. Soc. Inc., Princeton, N-J, 1975, 19.

Falk M., *Can. J. Chem.*, 1980, **58**, 1495.

Fieldson G.T., Barbari T.A., *Polymer*, 1993, **34**(6), 1146.

Fieldson G. T., Barbari T. A., *AIChE J.*, 1995, **41**(4), 795.

Finch C.A., *Chemistry Technology of Water Soluble Polymers*, Plenum, New York, 1983, Chap. 17.

Giordano R., Teixeira J., Wanderlingh U., *J. of Mol. Struct.*, 1993, **296**, 271.

Giordano R., Teixeira J., Wanderlingh U., *Physica B*, 1995, **213**, 769.

Gonzalez - Blanco C., Rodriguez L.J., Velazquez M.M., *Langmuir*, 1997; **13**, 1938.

Gray A., Gilbert M., *Polymer*, 1975, **16**, 387.

Green J. L., Lacey A. R., Sceats M. G., *J. Phys. Chem.*, 1986, **90**, 3958.

Green J. L., Lacey A. R., Sceats M. G., *J. Phys. Chem.*, 1987, **91**, 1694.

Hajatdoost S., Yarwood J., *J. of Chem. Soc., Faraday Trans.*, 1997, **93**(8), 1613.

Hare D.E., Sorensen C.M., *J. of Chem. Phys.*, 1990, **93**, 25 and 6954, and 1992, **96**, 13.

Haward R.N., *The Physics of Glassy Polymers*, Applied Science Publisher LTD, London, 1973.

Hong S.U., *Ind. Eng. Chem. Res.*, 1995, **34**, 2536.

Hopfenberg H.B., Stannett V.T., Folk G.M., *Polym. Eng. and Sci.*, 1975, **15**(4), 261.

Klier J., Peppas N.A., *Polym. Bull.*, 1986, **16**, 359.

Krongauz V.V., Mooney W.F., Palmer J.W., Patricia J.J., *J. of Appl. Polym. Sci.*, 1995, **56**, 1077.

Lane D.M., McDonald P.J., *Polymer*, 1997, **38**(1), 2329.

Li Z., Li X., Petrovic S., Harrison D.J., *Anal. Chem.* 1996, **68**(10), 1717.

Li Z., Li X., Rothmaier M., Harrison D.J., *Anal. Chem.*, 1996a, **68**(10), 1728.

Luck W.A.P., in : *Structure of Water and Aqueous Solutions*, Verlag Chemie, Weinheim, 1974, pp247 - 284.

Luck W.A.P., Schiøberg G.D., Sieman U, *J. of Chem. Soc., Faraday Trans. 2*, 1980, **76**, 136.

Maeda Y., Tsukida N., Kitano H., Terada T., Yamanaka J., *J. of Phys. Chem.*, 1993, **97**, 3619.

Maeda Y., Tsukida N., Kitano H., Terada T., Yamanaka J., *Spectro Chimica Acta*, 1995, **51**, 2433.

Maeda Y., Tsukida N., Kitano H., Terada T., Yamanaka J., *Macromol. Chem. Phys.*, 1996, **197**, 1681.

Marechal Y., *J. of Chem. Phys.*, 1991, **95**, 5565.

Marechal Y., Chamel A., *J. of Phys. Chem.*, 1996, **100**, 8551 and *Faraday Discuss.*, 1996, **103**, 349.

McBrierty V.T., Coey J.M.D., Boyle N.G., *Chem. Phys. Lett.*, 1993, **86**, 16.

Mirabella F.M., *Appl. Spec. Rev.*, 1985, **21**, 45.

Moran P.D., Bowmaker G.A., Cooney R.P., Barlett J., Woofrey J.L., *Langmuir*, 1995, **11**, 738.

Murphy D., Depinho M.N., *J. of Membr. Sci.*, 1995, **106**, 245.

Nguyen Q.T., Byrd E., Lin C., *J. of Adhes. Sci. and Technol.*, 1991, **5**, 697.

Nguyen Q.T., Favre E., Ping Z.F., Neel J., *J. of Membr. Sci.*, 1996, **113**, 137.

Ogawa T., Nagata T., Hamada Y., *J. of Appl. Polym. Sci.*, 1993, **50**, 981.

Okuno H., Renzo K., Uragami T., *J. of Membr. Sci.*, 1995, **103**, 13.

Ononi G., Santucci A., *J. of Phys. Chem.*, 1993, **97**, 5430.

Otting G., Liepinsh E., Wuthrich K., *J. of the American Chem. Soc.*, 1991, **113**, 4363.

Otting G., Liepinsh E., Wuthrich K., *Science*, 1991a, **254**, 974.

Parker L.V., Ranney T.A., *Ground Water Monitoring and Remediation*, 1994, **14**(3), 139.

Peraira M.R., Yarwood J., *J. of Chem. Soc., Faraday Trans.*, 1996, **92**(15), 2731.

Peraira M.R., Yarwood J., *J. of Chem. Soc., Faraday Trans.*, 1996a, **92**(15), 2736.

Pereira M.R., Yarwood J., *J. of Polym. Sci. part B : Polym. Phys.*, 1994, **32**; 1881.

Pimentel G.C., McClellan A.L., *The Hydrogen Bond*, Freeman and co., San Francisco, 1960, pp83.

Pimentel G.C., McClellan A.L., *Ann. Rev. Phys. Chem.*, 1971, **22**, 347.

Quezado S., Kwak J.C.T., Falk M., *Can. J. Chem.*, 1984, **62**, 958.

Roff W.J., Scott J.R., in *Fibres, Films Plastics and Rubbers*, Butterworths and co., London, 1956.

Scherer J.R., Bailey G.F., Kird S., Young R., Malladi D.P., Bolton B, *J. of Phys. Chem.*, 1985, **89**, 312.

Scherer J.R., Go M.K., Kint S., *J. of Phys. Chem.*, 1974, **78**, 1304.

Schiffer J., Hornik D.F., *J. of Chem. Phys.*, 1968, **49**, 450.

Settles M., Doster W., *Faraday Discuss.*, 1996, **103**, 269.

Shailaja D., Yasseen M, *Polym. Int.*, 1993, **32**, 247 - 250.

Southern E., Thomas A.G., *ACS Symposium Series 127*, 1980, 375.

Storey R.F., Kenneth A., Cole M., Cole B., *Macromolecules*, 1991, **24**, 450.

Sutander P., Ahn D.J., Franses E.I., *Macromolecules*, 1994, **27**, 7316.

Sutander P., Ahn D.J., Franses E.I., *Thin Solid Films*, 1995, **263**, 134.

Tao N.J., in : *Water and Biological Macromolecules*, ed. : Westhof E., McMillan Press Ltd., London, 1993, pp266 - 292.

Tao N.J., Lindsay, S.M., Rupprecht A., *Biopolymers*, 1989, **28**, 1019.

Teixera J., Stanley H.E., *J. of Chem. Phys.*, 1980, **73**, 3404.

Van Alsten J.G., *Trip*, 1995, **3(8)**, 272.

Van Alsten JG, Coburn J.C., *Macromolecules*, 1994, **27**, 3476.

Vergnaud J.M., *Macromolecular Symposia*, 1994, **84**, 377.

Vergnaud J.M., *Liquid Transport Processes in Polymeric Materials : Modeling and Industrial Application*, Prentice - Hall, 1991.

Vieth W.R., *Diffusion in and through Polymers : Principles and Applications*, Oxford, New York, 1991.

Vieth W.R., Howell J.M., Hsieh H., *J. of Membr. Sci.*, 1976, **1**, 177 - 220.

Walrafen G.E., in : *Water a Comprehensive Treatise*, volume 1. eds. : Franks F., Plenum Press, New York, 1972, pp208 - 209.

Widmer H.M., *Anal. Meth. Instrum.*, 1993, **1**, 60.

CHAPTER 4. :
EXPERIMENTAL TECHNIQUES.

CONTENTS

CHAPTER 4. : EXPERIMENTAL TECHNIQUES	110
4. 1. SAMPLE PREPARATION	112
4. 1. 1. Materials.....	112
4. 1. 2. For ATR and Raman spectroscopy	114
4. 1. 3. For rotating disc experiment.....	116
4. 2. FTIR - ATR SPECTROSCOPY IN THE STUDY OF DIFFUSION	116
4. 2. 1. The method of sorption for the study of Fickian diffusion.....	116
4. 2. 2. Application of FTIR - ATR spectroscopy to the dual -mode sorption mode.	120
4. 2. 3. Acquisition of the infrared diffusion data	122
4. 3. RAMAN MICROSCOPY	125
4. 3. 1. The Renishaw Ramascope 2000	125
4. 3. 2. Raman mapping and depth profiling	127
4. 3. 2. 1. Raman mapping.....	127
4. 3. 2. 2. Raman depth profiling	130
4. 3. 2. 3. Raman imaging	131
4. 4. THE ROTATING DISC METHOD.....	131
4. 4. 1. Experimental set - up	132
4. 5. EXPERIMENTAL PROCEDURE (FOR EACH SAMPLE)	143
4. 6. REFERENCES.....	144

CHAPTER 4. : EXPERIMENTAL TECHNIQUES

4. 1. SAMPLE PREPARATION

4. 1. 1. Materials

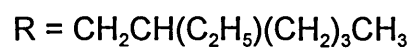
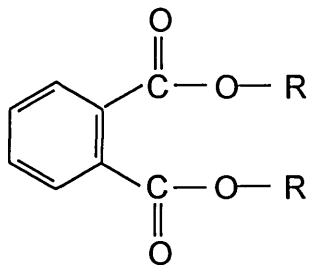
The various materials used for this work are :

The polymer :

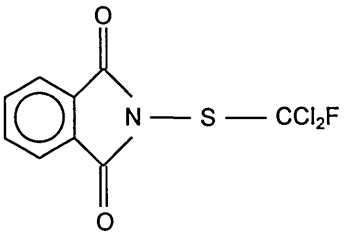
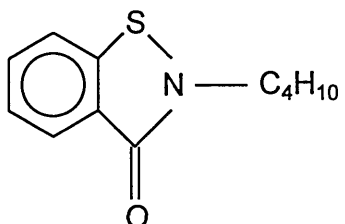


The plasticiser :

Diethylphthalate (DEP) :

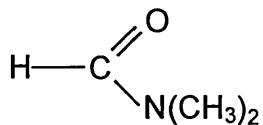


The biocides :

Name	Formula	Appearance
Fluorfolpet (N-dichlorofluoromethylthio phthalimide)		White powder
Vanquish (n-butyl-1,2-benzisothiazolin-3-one)		Red - orange liquid

The solvent :

Dimethylformamide



The PVC powder, the plasticiser DOP and the solvent DMF were obtained from Aldrich;

- Polyvinyl chloride, catalogue no. 18,262-1
- N, N-Dimethylformamide, catalogue no.27,054-7
- Dioctylphthalate, catalogue no. D20,115-4

The pure biocide compounds were supplied by Zeneca Specialties in Manchester.

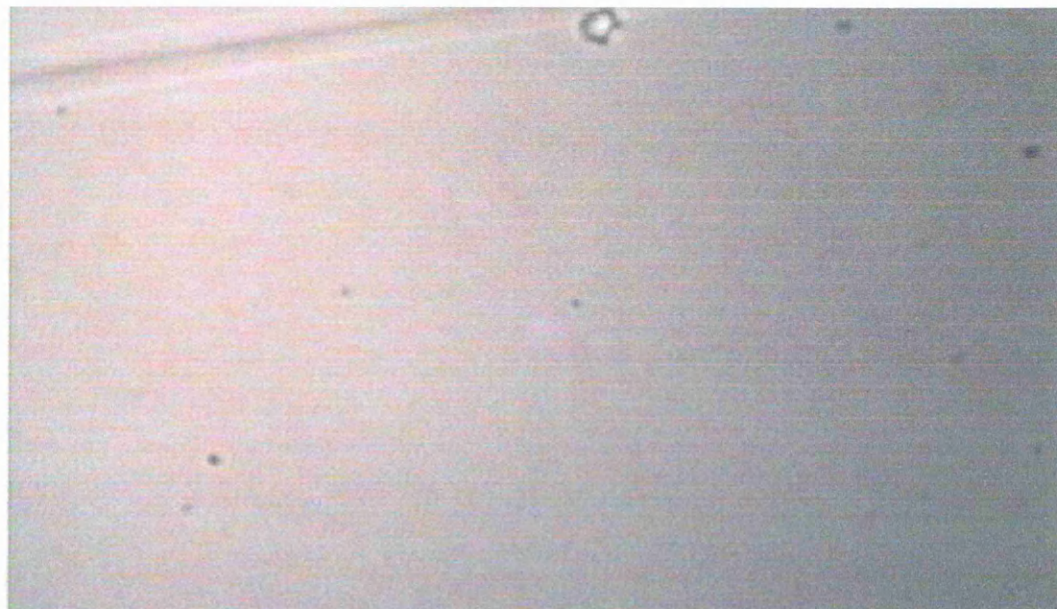
4. 1. 2. For ATR and Raman spectroscopy

The films were cast from solution onto a ZnSe ATR crystal. The reason for using the ATR crystal as substrate for both the ATR and the Raman experiment was because this allowed the sample to be analysed by both techniques under the same “film conditions”, and to use both techniques sequentially, i.e. the same film was analysed by two techniques.

The dimensions of the ATR crystal were 6 x 1 x 0.5 cm. The film was cast onto one of the larger faces of the crystal. The solutions were cast when warm (T = 40°C). The solvent was evaporated in the oven at 65°C for approximately 15 to 20 hours. The solutions used for casting were prepared by dissolving the PVC powder and other additives in DMF, first at room temperature, then the solutions were heated to 40°C for better dissolution of the materials. The solution was stirred constantly during dissolution.

The formulation of the samples has been quoted in %w/w throughout this thesis.

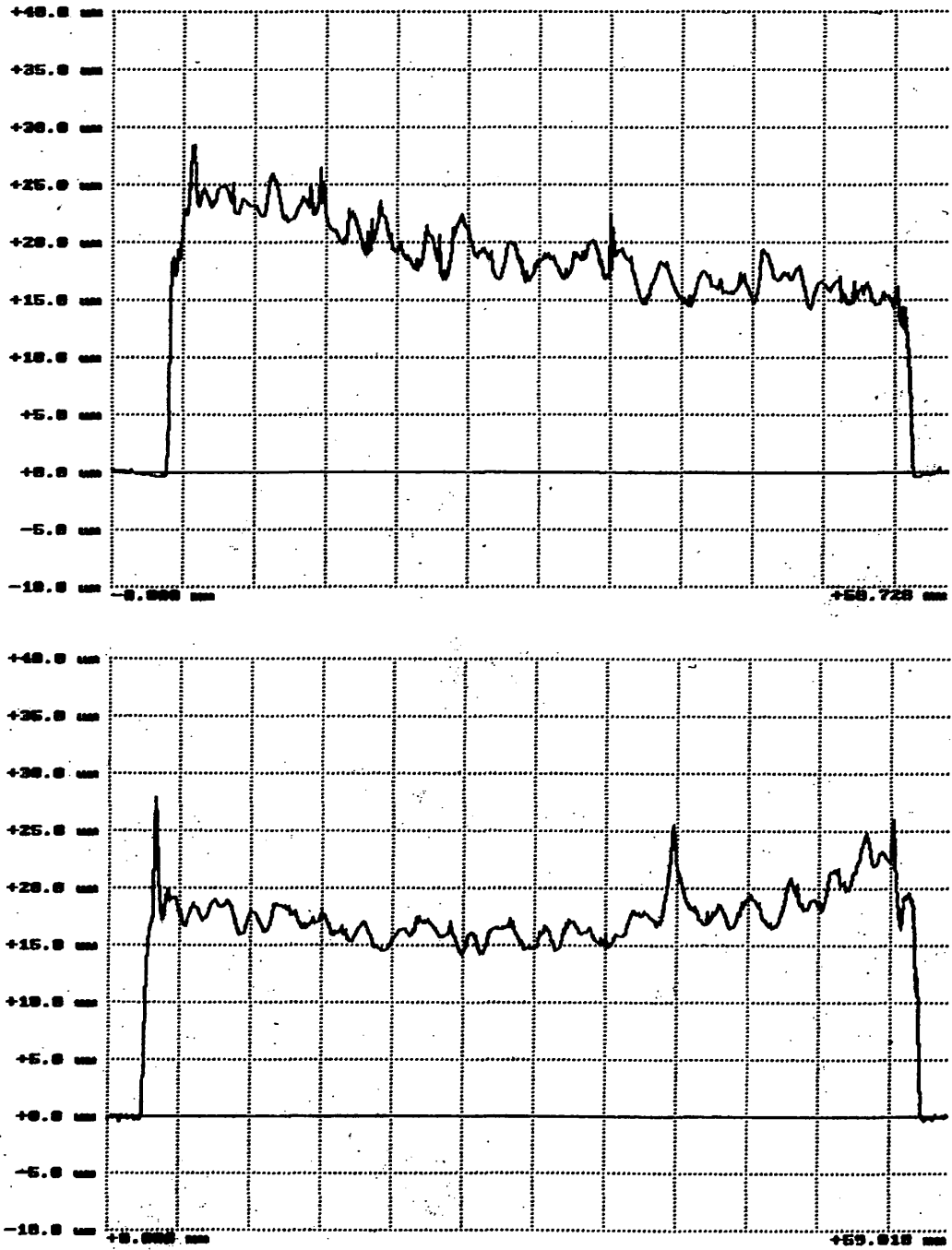
Figure 4. 1. Shows a typical optical micrograph from the surface of a film obtained from the above preparation method. It can be seen that the film shows no microvoids or defects. It was concluded that good blending of the plasticiser (and the biocide) with the polymer had taken place.



The thickness of the films was measured using either a mechanical surface profiling technique (i.e. a Talysurf), which has an accuracy of $0.2\mu\text{m}$, or an optical microscope, which has an accuracy of $1\mu\text{m}$. **Figure 4. 2.** shows a typical surface profile obtained by Talysurf.

The usual thickness of the film was about $15\mu\text{m}$.

Figure 4. 2. : Typical surface profiles obtained from Talysurf on 20% DOP / 5% fluorfolpet / PVC films.



4. 1. 3. For rotating disc experiment

The polymer films were prepared by casting from solution onto glass petri-dishes. The solvent was evaporated in the oven at 65°C for approximately 24 hours. The polymer films were then peeled off the dish and discs of diameter 2.5 cm were cut out, weighed, and the thickness measured using a micrometer. The usual thickness of the disc was about 150 μm.

4. 2. FTIR - ATR SPECTROSCOPY IN THE STUDY OF DIFFUSION

4. 2. 1. The method of sorption for the study of Fickian diffusion

The method of sorption kinetics is one of the most used experimental techniques for studying the diffusion of small molecules in polymers.

As stated previously, the equation for 1 - D molecular diffusion in a polymer can be described by Fick's second law :

$$\frac{\partial C}{\partial t} = D \left(\frac{\partial^2 C}{\partial x^2} \right) \quad (\text{eq. 4. 1.})$$

When a film of thickness 2 L is placed in an infinite bath of penetrant, with initial concentration zero, and the boundary conditions for a region $-L < x < L$ are as follows :

$$C = 0 \text{ at } t < 0 ; 0 \leq x \leq L,$$

$$C = 0 \text{ at } t \geq 0 ; x = L,$$

$$\left(\frac{\partial C}{\partial x} \right) = 0 \text{ at } t \geq 0 ; x = 0.$$

Where x = position in the film,

t = time.

Then the concentration C_t of the penetrant is given by :

$$\frac{C_t - C_0}{C_\infty - C_0} = 1 - \frac{4}{\pi} \sum_{n=0}^{\infty} \frac{(-1)^n}{2n+1} \exp\left[\frac{-D(2n+1)^2 \pi^2 t}{4L^2}\right] \cos\left[\frac{(2n+1)\pi x}{2L}\right] \quad (\text{eq. 4. 2.})$$

Where C_0 = the concentration at $t = 0$,

C_∞ = the concentration at equilibrium.

In sorption kinetics experiments the mass of sorbed penetrant is measured as a function of time. The integration of (eq. 4. 2.) over the thickness of the film, gives the equation for the mass of sorbed penetrant :

$$\frac{M_t}{M_\infty} = 1 - \sum_{n=0}^{\infty} \frac{8}{(2n+1)^2 \pi^2} \exp\left[\frac{-D(2n+1)^2 \pi^2 t}{4L^2}\right] \quad (\text{eq. 4. 3.})$$

Where M_t = the mass sorbed at time t ,

M_∞ = the mass sorbed at equilibrium.

(Eq. 4. 3.), describes Fickian sorption kinetics. It can be modified in order to interpret the FTIR-ATR experiment :

As shown in chapter 2., in the ATR experiment, the decaying electric field interacts with transition dipoles ($\partial\mu / \partial Q$) in the film. The decay of the field can be expressed as :

$$E = E_0 \exp(-\gamma z) \quad (\text{eq. 4. 4.})$$

Where E_0 = the electric field amplitude at the surface, and

$$\gamma = \frac{2n_2 \pi \sqrt{\sin^2 \theta - \left(\frac{n_1}{n_2}\right)^2}}{\lambda} \quad (\text{eq. 4. 5.})$$

Where n_2 = the refractive index of the ATR crystal,
 n_1 = the refractive index of the film.

If one assumes that only weak absorption occurs it is possible to combine the Beer - Lambert law with the evanescent field strength equation.

$$\frac{I}{I_0} = e^{-A} \approx (1 - A) \quad (\text{eq. 4. 6.})$$

or,

$$dI = -I_0 dA \quad (\text{eq. 4. 7.})$$

Where I = the intensity of incident light,
 I_0 = the intensity of transmitted light,
 A = the absorbance.

The relationship between the absorption of the electromagnetic waves and the quantity of absorbing material is expressed as :

$$dI = \alpha I dz = -\epsilon C I dz \quad (\text{eq. 4. 8.})$$

Where α = the absorption coefficient,
 ϵ = the molar extinction coefficient,
 I = light intensity at position z ,
 C = the concentration of absorbing group.

Substitution of (eq.4. 7.) in (eq.4. 8.) gives :

$$dA = \epsilon C \frac{I}{I_0} dz \quad (\text{eq. 4. 9.})$$

Integrating (eq. 4. 9.) gives :

$$A = \int_0^L \frac{\varepsilon C l}{l_0} dz \quad (\text{eq. 4. 10.})$$

N. B. :in the ATR configuration the penetrant enters the film only from one direction, L is the thickness of the film.

For multiple reflections :

$$A = \int_0^L N \varepsilon^* C E_0^2 \exp(-2\gamma z) dz \quad (\text{eq. 4. 11.})$$

Where $\varepsilon^* = \frac{\varepsilon}{l_0}$

Substitution of (eq. 4. 3.) into (eq. 4. 11.) and integration gives :

$$\frac{A_t - A_0}{A_\infty - A_0} = 1 - \frac{8\gamma}{\pi [1 - \exp(2L\gamma)]} \sum_{n=1}^{\infty} \frac{\left[\exp\left(\frac{-D(2n+1)^2 \pi^2 t}{4L^2}\right) \left[\frac{(2n+1)}{2L} \pi \exp(-\gamma 2L) + (-1)^n (2\gamma) \right] \right]}{(2n+1) \left[4\gamma^2 + \left(\frac{(2n+1)\pi}{2L} \right)^2 \right]} \quad (\text{eq. 4. 12.})$$

Where A_t = the absorbance at time t,

A_∞ = the absorbance at equilibrium,

A_0 = the absorbance at t=0.

(Eq. 4. 12.) describes the Fickian diffusion in an ATR experiment. But the diffusion of water into PVC follows a dual - mode sorption model, in which one species is totally mobile and the other only partially mobile.

4. 2. 2. Application of FTIR - ATR spectroscopy to the dual -mode sorption mode.

The equation for a 1 - D molecular diffusion can be described by Fick's second law ;

For the partially mobile molecules :

$$\frac{\partial C_1}{\partial t} = D_1 \left(\frac{\partial^2 C_1}{\partial z^2} \right) \quad (\text{eq. 4. 13.})$$

Where $C_{1(0)} = x_1 C_0$ and $C_{1(t=\infty)} = x_1 C_\infty$,

x_1 = the fraction of partially mobile molecules,

C_0 = the initial concentration,

C_∞ = the concentration at equilibrium,

D_1 = the diffusion coefficient of partially mobile molecules.

For the totally mobile molecules :

$$\frac{\partial C_2}{\partial t} = D_2 \left(\frac{\partial^2 C_2}{\partial z^2} \right) \quad (\text{eq. 4. 14.})$$

Where $C_{2(0)} = x_2 C_0$ and $C_{2(t=\infty)} = x_2 C_\infty$,

x_2 = the fraction of totally mobile molecules,

C_0 = the initial concentration,

C_∞ = the concentration at equilibrium,

D_2 = the diffusion coefficient of totally mobile molecules,

$x_1 + x_2 = 1$.

Therefore if the new boundary conditions are substituted into (eq. 4. 12.), we get :

For the first sorption mode :

$$\frac{A_1 - x_1 A_0}{x_1 (A_\infty - A_0)} = 1 - \frac{8\gamma}{\pi [1 - \exp(2L\gamma)]} \sum_{n=1}^{\infty} \left[\frac{\exp\left(\frac{-D_1(2n+1)^2 \pi^2 t}{4L^2}\right) \left[\frac{(2n+1)}{2L} \pi \exp(-\gamma 2L) + (-1)^n (2\gamma) \right]}{(2n+1) \left[4\gamma^2 + \left(\frac{(2n+1)\pi}{2L}\right)^2 \right]} \right]$$

(eq. 4. 15.)

For the second sorption mode :

$$\frac{A_2 - x_2 A_0}{x_2 (A_\infty - A_0)} = 1 - \frac{8\gamma}{\pi [1 - \exp(2L\gamma)]} \sum_{n=1}^{\infty} \left[\frac{\exp\left(\frac{-D_2(2n+1)^2 \pi^2 t}{4L^2}\right) \left[\frac{(2n+1)}{2L} \pi \exp(-\gamma 2L) + (-1)^n (2\gamma) \right]}{(2n+1) \left[4\gamma^2 + \left(\frac{(2n+1)\pi}{2L}\right)^2 \right]} \right]$$

(eq. 4. 16.)

Where A_1 = the absorbance of partially mobile molecules at time t,
 A_2 = the absorbance of totally mobile molecules at time t,

or,

$$A_1 = \left(1 - \sum D_1\right) x_1 (A_\infty - A_0) + x_1 A_0 \quad (\text{eq. 4. 17.})$$

$$A_2 = \left(1 - \sum D_2\right) x_2 (A_\infty - A_0) + x_2 A_0 \quad (\text{eq. 4. 18.})$$

Where

$$\sum D_x = \frac{8\gamma}{\pi [1 - \exp(2L\gamma)]} \sum_{n=1}^{\infty} \left[\frac{\exp\left(\frac{-D_x(2n+1)^2 \pi^2 t}{4L^2}\right) \left[\frac{(2n+1)}{2L} \pi \exp(-\gamma 2L) + (-1)^n (2\gamma) \right]}{(2n+1) \left[4\gamma^2 + \left(\frac{(2n+1)\pi}{2L}\right)^2 \right]} \right]$$

And x = 1 or x = 2.

The model for the dual -sorption diffusion mode in the ATR experiment can be obtained by adding (eq. 4. 17.) and (eq. 4. 18.) and substituting x_2 by $(1 - x_1)$:

$$\frac{A_t - A_0}{A_\infty - A_0} = (1 - \sum D_1)x_1 + (1 - \sum D_2)(1 - x_1) \quad (\text{eq. 4. 19.})$$

Where A_t = the total absorbance at time t.

The parameters D_1 and D_2 can be calculated using the Levenberg - Marquardt least squares fitting procedure. A program written in PASCAL by Dr. Marcia Pereira was used here.

4. 2. 3. Acquisition of the infrared diffusion data

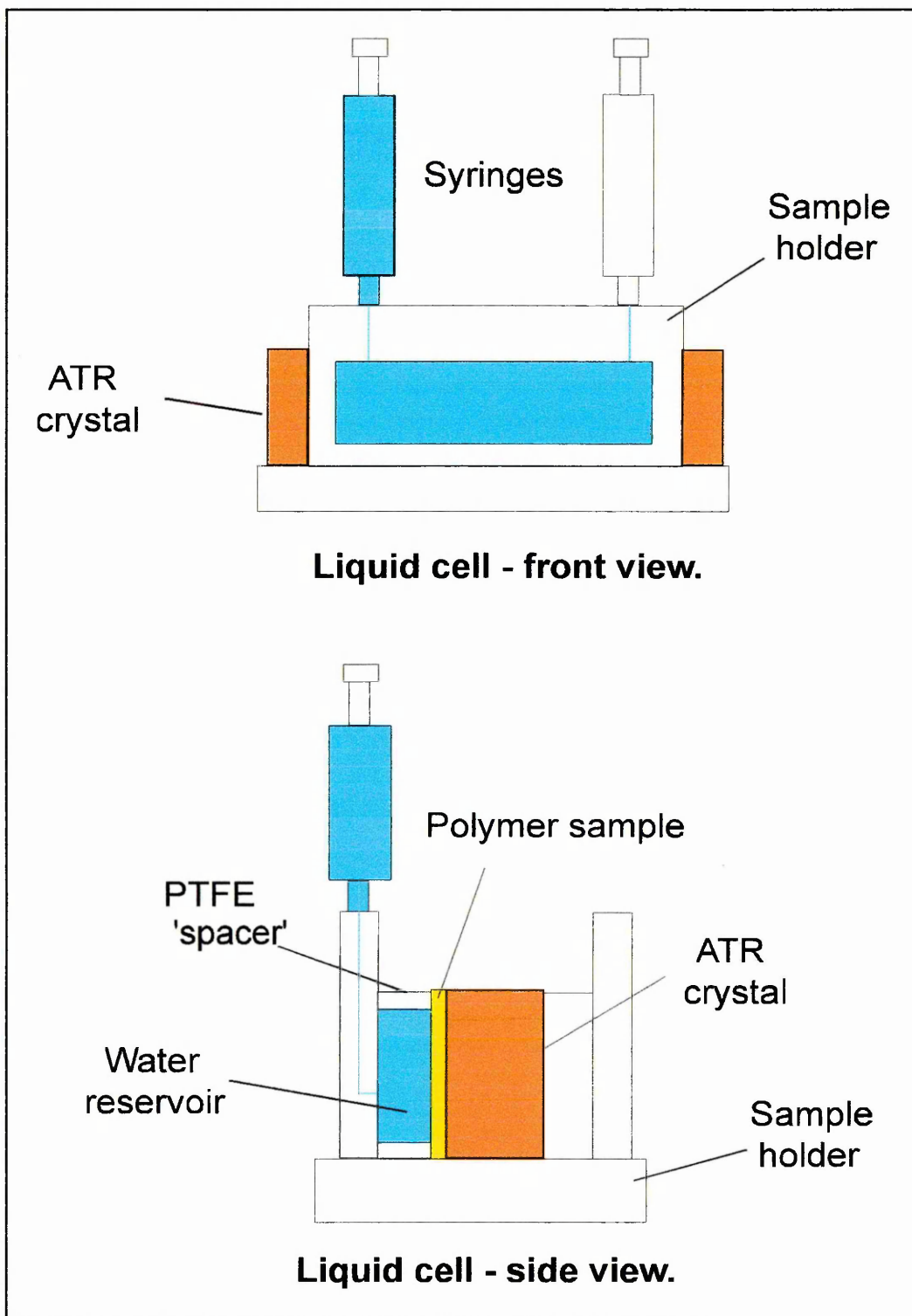
The experimental set - up used for the ATR - experiment is shown in **figure 4. 3.**

In the experiment, the PVC film was cast onto one side of the ZnSe - ATR crystal. The crystal was mounted into the liquid cell. PTFE "spacers" are added, one on each side of the prism, in order to create an effectively infinite reservoir of liquid, and the second one to protect the surface of the crystal from the metal of the cell. The cell was closed, so as to obtain an air tight system. The cell was then placed into the ATR accessory on the infrared instrument.

The infrared spectra were recorded using a FIRST or WINFIRST macro program, which records spectra as following :

- (i) a spectrum of the dry film was taken first, which served as background for the analysis of the data, then
- (ii) acquisition of a spectrum every minute for 30 minutes, then
- (iii) acquisition of a spectrum every 5 minutes for 5 hours.

Figure 4. 3. : ATR - FTIR experimental set - up.



The liquid (water) was introduced in the cell using syringes before step (ii).

The time needed to acquire a spectrum was about 42 seconds. Therefore the time quoted, corresponds to the start of the scan.

The instrumental parameters are :

Instrument = Matson Polaris FT IR spectrometer

Resolution = 4 cm^{-1}

Sample scans = 25

Iris = 25 %

Signal gain = 1

Mirror velocity = 40 cm^{-1}

Apodisation = triangular

The diffusion data were obtained by integrating the ν (OH) band of water between $2950 - 3700\text{ cm}^{-1}$, and a plot of these integrated intensities versus time yielded the diffusion curve.

Diffusion profiles of other species in the film can also be obtained providing they have detectable and distinguishable infrared bands. This is the case for fungicide fluorfolpet a component present in the formulation of the PVC film used for the experiments. Hence it is possible to follow the leaching of the fungicide into the water simultaneously to the water absorption phenomenon.

The swelling of the polymer matrix can also be monitored this way.

The leaching of fluorfolpet and the swelling of the PVC matrix will be discussed in details in chapters 6. and 8.

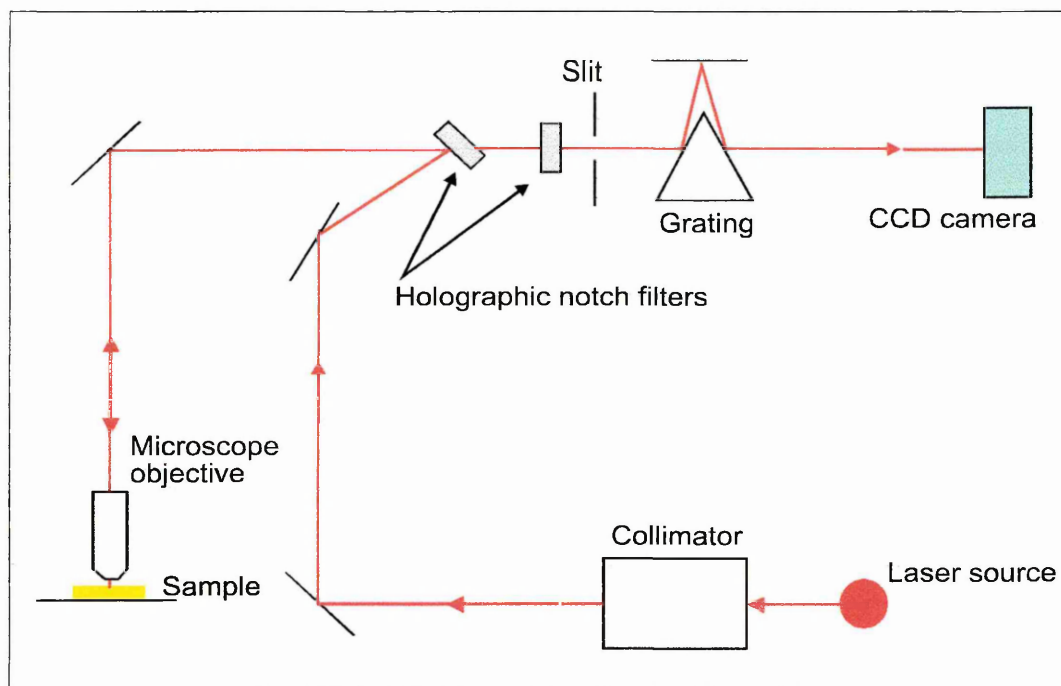
4. 3. RAMAN MICROSCOPY

The Raman microspectrometer used in this study was a Renishaw Ramascope 2000 system (Batchelder et al. 1991 and 1992, Williams et al. 1994 and 1994a.), with a 633 nm excitation laser. The instrument can operate in three different modes : Raman microprobe, Raman confocal mode and Raman imaging mode. The instrument is equipped with a computer-controlled stepping motor driven stage, whereby the instrument can be used to perform Raman mapping and Raman depth-profiling. Raman imaging (Gardiner and Bowden 1990, Govil et al. 1991, Traedo and Morris 1994, Barbillat et al. 1994, Evans et al. 1996), mapping (Evans et al. 1996, Gardiner and Bowden 1990) and depth - profiling (William et al. 1994, Tabaksbalt 1992, Tabaksblat et al. 1991, Hajatdoost and Yarwood 1996) have been applied to a variety of materials.

4. 3. 1. The Renishaw Ramascope 2000

Figure 4. 4. shows a schematic of the Renishaw Ramascope 2000 system, showing the path of the laser reaching the sample, and the path of the backscattered light to the detector.

Figure 4. 4. : A schematic of the Renishaw Ramascope 2000 system.



This system utilises the so - called back scattering configuration in which the scattered light is collected using the same objective as is used to focus the laser onto the sample.

The most important features of this system are :

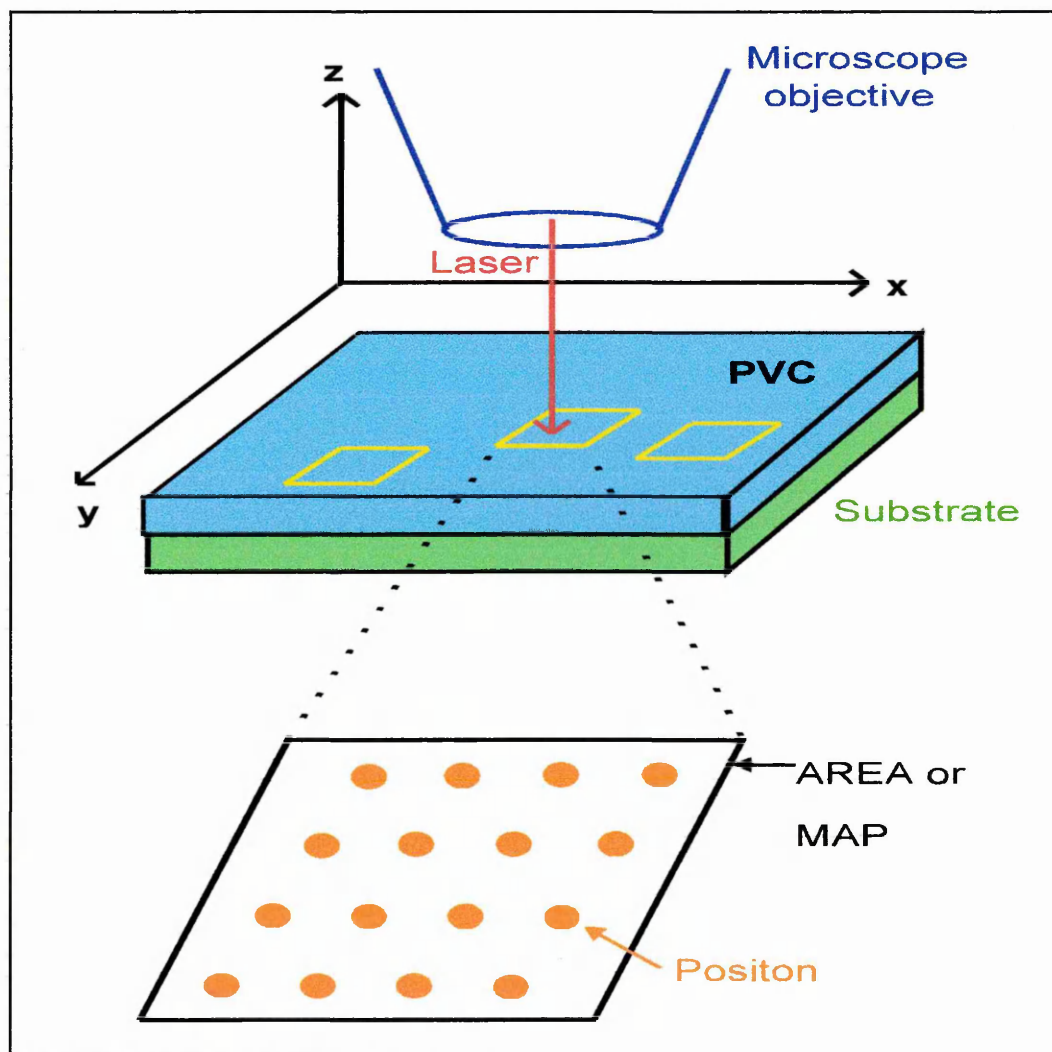
- the two holographic notch filters which remove the Rayleigh scatter. Without them we would not be able to see the Raman scattering,
- the adjustable slit, together with the CCD detector, which are used to obtain the confocal set - up,
- the plasma line rejection filters,
- the diffraction grating.

As shown on **Figure 4. 4.**, the laser beam enters the spectrometer through the back, is collimated, then reflected via mirrors onto the first holographic notch filter, then onto the microscope, and focused down onto the sample by the objective. The backscattered light travels back along the microscope column via the second notch filter through the slit, and is then reflected from the prism onto the diffraction grating, before reaching the CCD detector (Peltier - cooled multi - channel charged coupled device).

4. 3. 2. Raman mapping and depth profiling

4. 3. 2. 1. Raman mapping

Figure 4. 5. Shows how Raman microscopy is used to determine the distribution of small molecules in a polymer matrix.

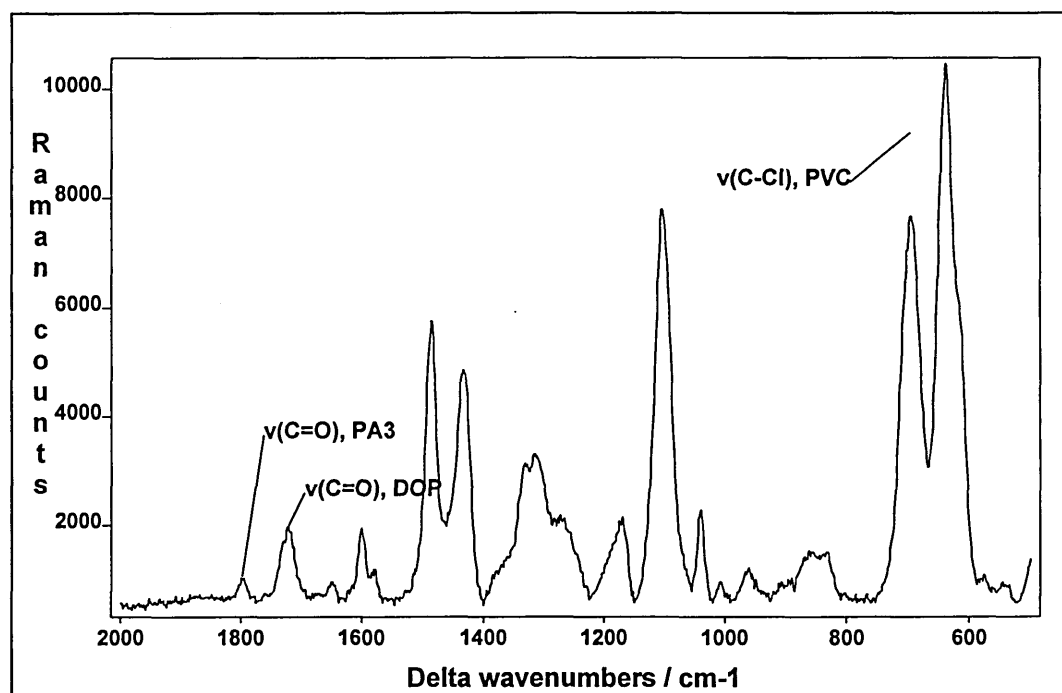


A microscope is used to focus on a particular area of the sample, and within this particular area, we are able to examine the Raman spectra of the film. By detecting the Raman spectra at several positions at regular intervals of the film,

we can assess the distribution of components within the xy directions. This can be done using the confocal set-up or working in the normal Raman microprobe mode.

Figure 4. 6. shows a typical spectrum of a PVC film (5% PA3 / 20% DOP / PVC). Three bands are marked on the spectrum, which correspond to the $\nu(\text{C}-\text{Cl})$ stretching vibration of PVC between $590 - 750 \text{ cm}^{-1}$, the $\nu(\text{C}=\text{O})$ stretching vibration of DOP at 1726 cm^{-1} , and the $\nu(\text{C}=\text{O})$ stretching vibration of fluorfolpet at 1786 cm^{-1} .

Figure 4. 6. : A typical spectrum of a PVC film (5% PA3 / 20% DOP / PVC).



Because every species has a particular Raman spectrum, the Raman spectrum of the mixture can be decomposed into the Raman spectra of its components. Identification of these bands is not always simple and may fail, due to overlapping of the bands in the mixture spectrum. However it is often possible to identify at least one band particular to each of the components (providing there are not too many components and that their respective Raman spectra are quite different).

In a pPVC film with formulation 5% fluorfolpet, 20% DOP, such bands were easily identified. The spectral data can be used to construct a map.

This is done by calculating the band area ratios PVC/DOP and PVC/PA3 following :

$$PVC / DOP = \frac{A_{(PVC)}}{A_{(DOP)}}$$

$$PVC / PA3 = \frac{A_{(PVC)}}{A_{(PA3)}}$$

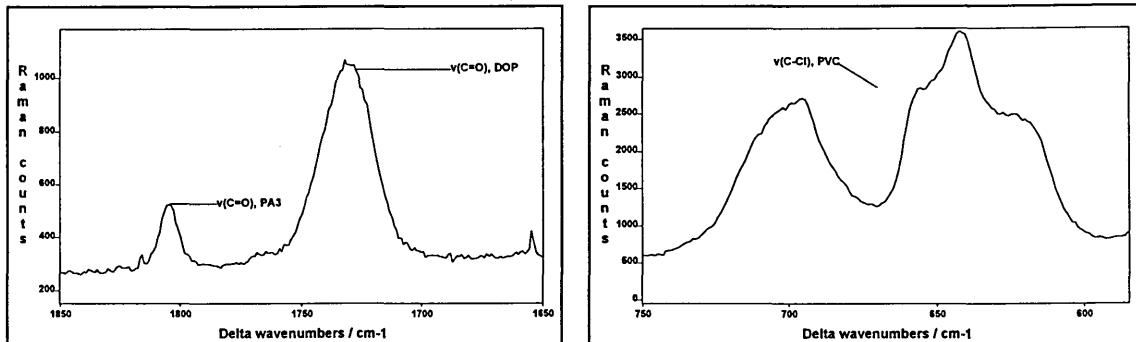
Where $A_{(PVC)}$ = the area under the $\nu(C-Cl)$ stretching vibration of PVC between 590 - 750 cm^{-1} ,

$A_{(DOP)}$ = the area under the $\nu(C=O)$ stretching vibration of DOP at 1726 cm^{-1} ,

$A_{(PA3)}$ = the area under the $\nu(C=O)$ stretching vibration of fluorfolpet at 1786 cm^{-1} .

This is shown in **Figure 4. 7.**

Figure 4. 7. : PVC, DOP and PA3 peak area.



These ratios were plotted against the position at which each individual spectrum was taken, thereby obtaining a molecular distribution map of the surface of the film for a particular component of the film.

A ratio of band area to the PVC band was used in order to obtain quantitative information about the distribution of the materials in the film, i.e. relative

concentration of materials, as indeed, absolute concentration values are very difficult to obtain in Raman (as explained in section 2. 2. 4.). Also errors due to the fluctuation of the laser power throughout the duration of the experiment are minimised, as well as, the errors due to the focusing of the laser as a consequence of the rapid decrease in intensity with distance from the focal object plane. (see *figure 2. 20.*).

4. 3. 2. 2. Raman depth profiling

In the same way as Raman mapping is performed on the xy plane, it is possible using confocal Raman microscopy to obtain spectra of sections of a film at various depth (along the z - axis).

The depth profiling experiment started by taking a spectrum of the surface of the film, and then collecting spectra every 2 μm step, moving down into the bulk of the film, until the surface of the crystal was reached.

The data was analysed in the same way as the Raman mapping data, and yielded a depth profile consisting of a plot of the band area ratio of PVC by the additive as a function of depth.

When the depth profile was obtained as a direct plot of the band area of the component against the depth, the resulting profile was a convolution of the confocal response of the instrument with the actual depth profile (see section 2. 2. 3.).

4. 3. 2. 3. Raman imaging

The Raman imaging mode produces a photograph like image of the sample using light scattered from a particular Raman peak.

Raman imaging basically involves the collection of spectral data from a series of spatial points on the sample, and explicitly uses two - dimensional detectors, CCD or diode array detectors. When both dimensions of the 2 - D array of sensitive elements of the CCD are being used for recording spatially dependent Raman intensities at a particular Raman peak, the distribution of the Raman intensity at a chosen fixed Raman band is obtained for a given sample area. This technique is called imaging (Markwort et al. 1995, Williams et al. 1994, Traedo and Morris 1993, Harris et al. 1994).

The incident laser beam is no longer collimated and no longer focused on a tiny spot on the sample by the microscope. But instead, the incident light is focused on a larger area of the sample and the entire area is analysed at once. Because only a specific bandpass is analysed in this mode, the imaging beam is passed through thin interference filters. These filters have a narrow bandpass and are used to isolate the light from a chosen Raman band that is characteristic of the material of interest. The light is then collected by the detector, which observes the entire field simultaneously.

Highly fluorescent specimens will generate problems in Raman imaging as the detector cannot distinguish fluorescence from Raman scattering. Distinct spectral features must exist, characteristic of one phase, well separated from the spectrum of the other components.

4. 4. THE ROTATING DISC METHOD

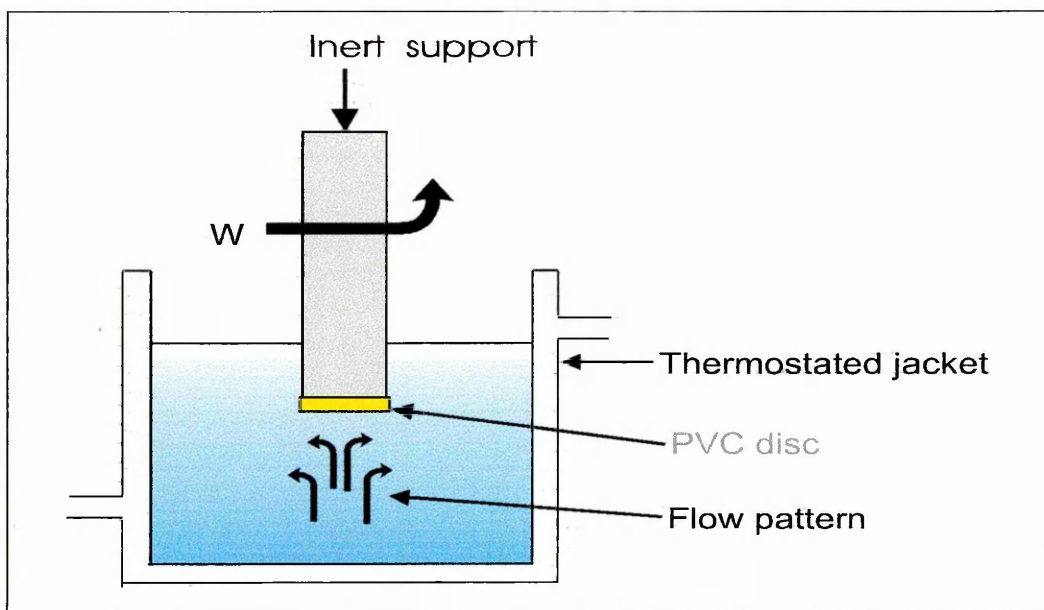
Although the leaching of small molecules from a polymer matrix can be followed using FTIR - ATR spectroscopy, the introduction of the rotating disc study method seeks to extend the studies using ATR spectroscopy.

The rotating disc (RD) experiment differs from the ATR experiment in that the RD method is a dynamic experiment, whereas the ATR, is a static experiment. The rotating disc method has been used routinely in the pharmaceutical industry to study controlled release of drugs from polymeric devices (Chien et al. 1975), and in electrochemistry (Bard and Faulkner 1980).

4. 4. 1. Experimental set - up

The solid film (of a diameter of 2.5 cm) is supported flush to the end of a shaft of inert material, which is rotated at fixed angular frequency (W / Hz) in a known volume of water. The rotation was controlled to a precision of 0.01 Hz, using a proportional feedback mechanism. The temperature of the water is controlled using a jacketed glass vessel in conjunction with a water bath. A schematic of the apparatus is shown on **figure 4. 8.**

Figure 4. 8. : A schematic of the rotating disc apparatus.



The rotating disc acts like a pump, causing the bulk solution to be brought up adjacent to the solid film, setting up a concentration gradient, drawing out the leachate from the film. A laminar flow of fluid exists, which creates a layer of

solution (adjacent to the solid surface) in which the concentration drops from a value characteristic of the surface region of the film to the values in the bulk solution.

The thickness of this layer can be calculated (Levich 1962) using :

$$\delta = 0.643 D^{1/3} \nu^{1/6} W^{1/2} \quad (\text{eq. 4. 20.})$$

Where δ = the thickness of the layer,
 D = the diffusion coefficient,
 ν = the kinetic viscosity of the solution,
 W = the angular frequency.

The flux of the leaching species from the film surface into the bulk solution is expressed as :

$$J = \frac{D(C_0 - C_b)}{\delta} \quad (\text{eq. 4. 21.})$$

Where C_0 = leachate concentration at the surface of the film,
 C_b = leachate concentration in the bulk solution,
 J = the flux.

The rotating disc apparatus was used at Zeneca Specialties in Manchester, under the supervision of Dr. D. Hodge and Dr. J. Booth. The apparatus was originally supplied by Oxford Electrodes.

The leaching experiment was started by sticking the sample disc to the shaft of inert material using low melting point wax, then the disc was rotated at the desired speed outside of the water. Time $t = 0$ corresponds to the immersion of the disc into the water. Leachate samples were taken in 3 cm³ aliquots at 15 minute intervals. The samples were then analysed using UV spectroscopy. In order to quantify the amount of fungicide present in the samples, a calibration

curve was first constructed for the fungicides. **Figures 4. 9.** and **4. 10.** show the UV a spectrum of aqueous solutions of fluorfolpet and vanquish.

The UV spectrometer used was a Perkin Elmer Lambda 2 spectrometer.

Figure 4. 9. : UV spectrum of an aqueous fluorfolpet solution (8 ppm).

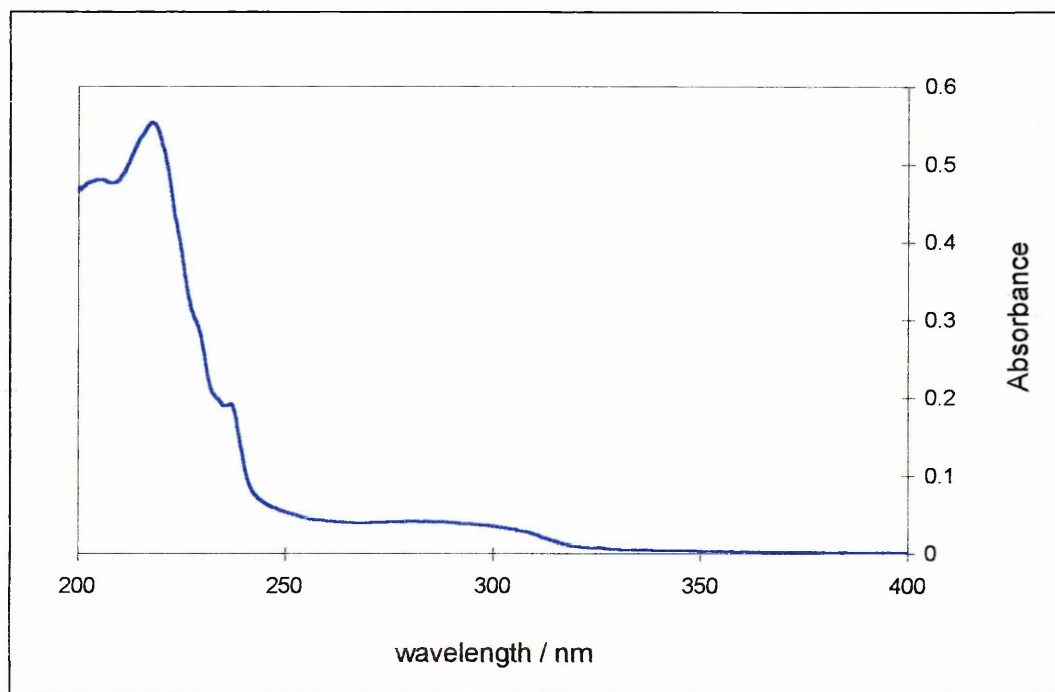
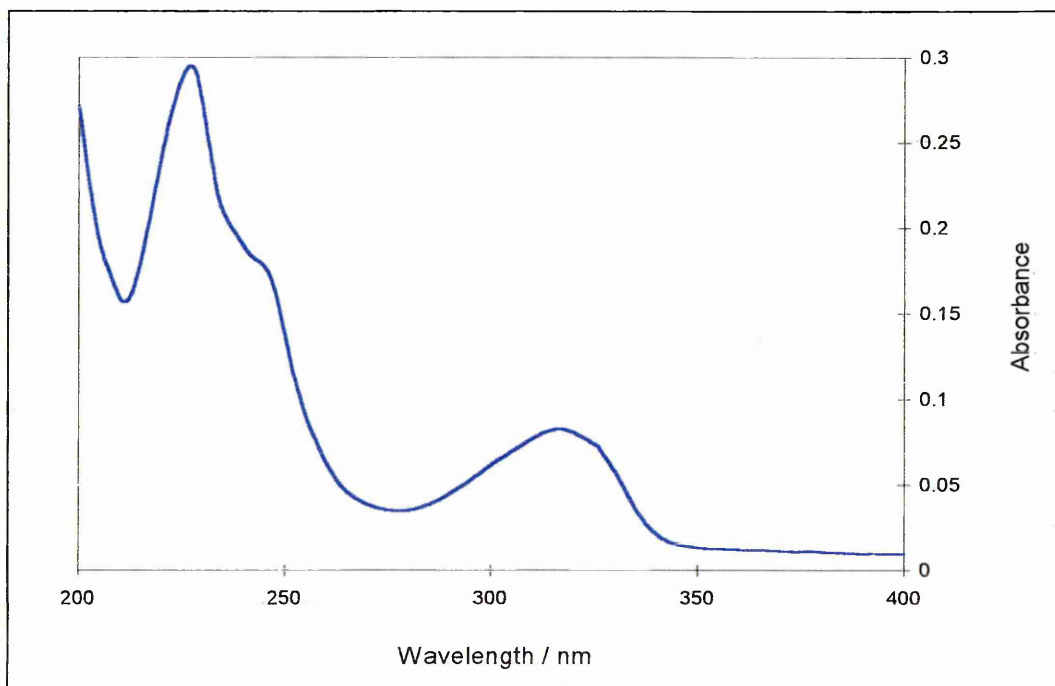


Figure 4. 10. : UV spectrum of an aqueous vanquish solution (6 ppm).



Tables 4. 1. and **4. 2.** show the absorbance values for the standard solutions used to construct the calibration curves for the fungicides fluorfolpet and vanquish respectively. And **figures 4. 11.** and **4. 12.** show the calibration curves obtained for fluorfolpet and vanquish respectively.

Table 4. 1. : results of UV analysis on fluorfolpet standard solutions.

Concentration (ppm)	Absorbance at 237 nm
0	0.000
1.5	0.028
3	0.055
4.5	0.083
6	0.112
7.5	0.138
9	0.165
10.5	0.193
12	0.219
15	0.274

Figure 4. 11. Calibration curve for fluorfolpet.

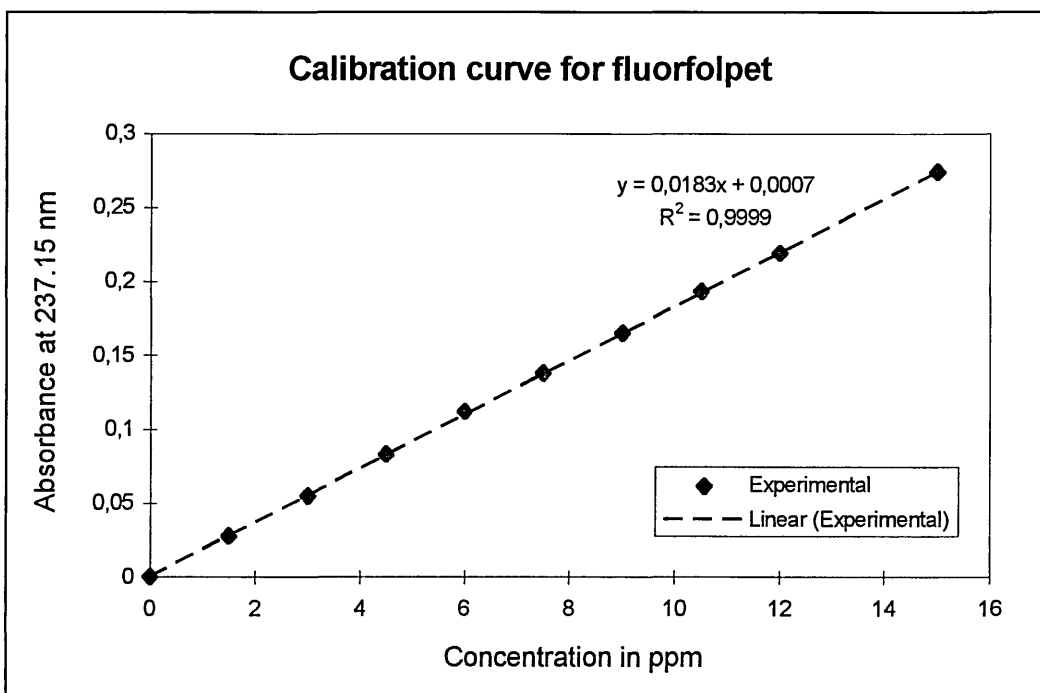
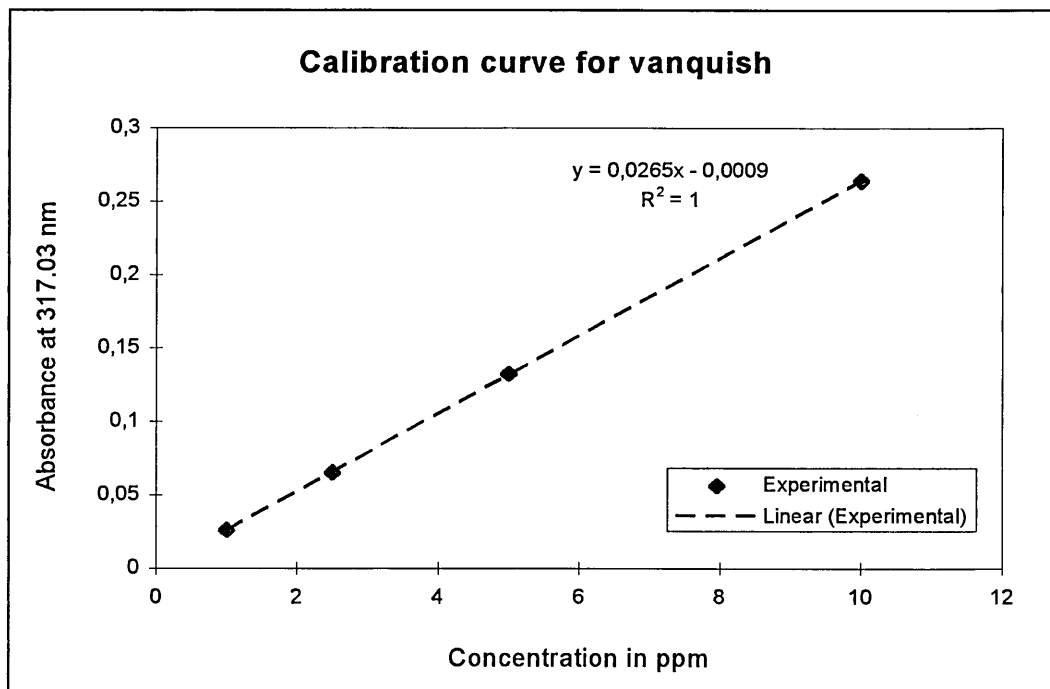


Table 4. 2. Results of UV analysis on vanquish standard solutions.

Concentration (ppm)	Absorbance at 317 nm
1	0.0257
2.5	0.065
5	0.1392
10	0.264

Figure 4. 12. Calibration curve for vanquish.



4. 4. 2. Theory

Preliminary work done on paint sample by J. Booth at Zeneca Specialties in Manchester revealed that the mass of biocide expelled is directly proportional to the square root of time, indicating a Fickian diffusion process.

Three diffusion scenarios can be envisaged :

1. The fungicide loading in the film (A) is less than its intrinsic solubility (C_s) in the polymer film, therefore the fungicide is molecularly dissolved in the polymer matrix.
2. The fungicide loading in the film (A) is bigger than its intrinsic solubility (C_s) in the polymer film, therefore resulting in two regions in the polymer :

(i) a zone on the surface of the film where the fungicide is dissolved in the polymer matrix,

(ii) a zone in the interior of the film where the fungicide is not dissolved in the polymer matrix.

3. The fungicide loading in the film (A) is similar to its intrinsic solubility (C_s) in the polymer matrix. This case will not be treated here, but the reader is referred to the work of Higuchi and Lee (Higuchi 1961 and 1963, Lee, 1980).

C_s can correspond to either the solubility of the diffusing (leaching) species in the matrix for non - porous substrates, or to the solubility of the diffusant in the permeating liquid within a solvent swollen porous matrix.

Conditions for the validity of the models :

- the diffusion coefficient is non - concentration dependent,
- there is no external mass - transfer resistance, i.e. zero solute concentration at solid - liquid interface,
- the rate of leaching of the solute into the liquid is limited only by the rate of solute within the film.

For the case $A < C_s$ (Crank 1978):

For a semi - infinite film :

Boundary conditions :

$t = 0, x > 0, C = A$ (uniform concentration throughout the film initially)

$t > 0, x = 0, C = 0$ (solute concentration at film surface is zero)

Where C is the concentration of leachate at position x within the film.

$$C = A \operatorname{erf} \frac{x}{2\sqrt{Dt}} \quad (\text{eq. 4. 22.})$$

Where A = the initial biocide loading in the sample (g/cm^3),

D = the diffusion coefficient of the biocide in the matrix (cm^2/s),

t = time (s).

Therefore,

$$D \left(\frac{\partial C}{\partial x} \right)_{x=0} = \frac{DA}{\sqrt{xDt}} \quad (\text{eq. 4. 23.})$$

Equation 4. 23. is the expression for the flux of leachate into the solution.

Integration of (eq. 4. 23.) gives :

$$M_t = 2A \sqrt{\frac{Dt}{\pi}} \quad (\text{eq. 4. 24.})$$

Where M_t = the amount of leachate which has left the polymer at time t.

or,

$$\frac{M_t}{M_\infty} = \frac{2}{\pi} \sqrt{\frac{Dt}{l^2}} \quad (\text{eq. 4. 25.})$$

Where M_∞ = the initial mass of solute,

l = the film thickness.

For a film of finite thickness :

Boundary conditions :

$t = 0, x > 0, C = A$ (uniform concentration throughout the film initially)

$t > 0, x = 0, C = 0$ (solute concentration at film surface is zero)

$x = 1, C = A$ (solute concentration at surface / interface is constant)

The total amount of leachate M_t which has left the matrix is found to be :

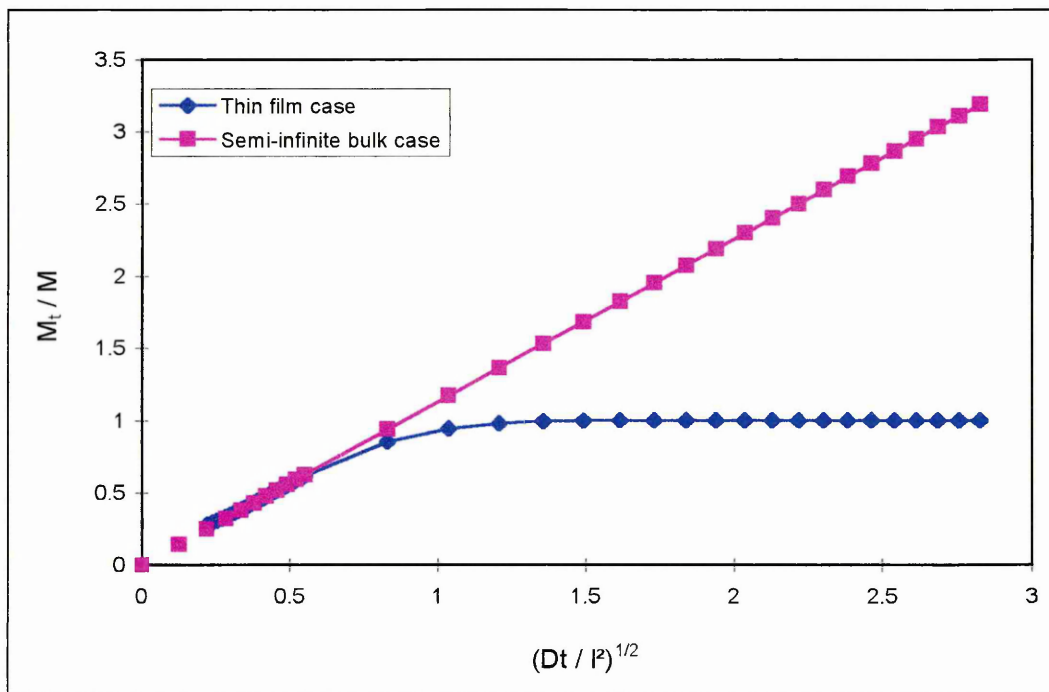
$$M_t = \frac{1}{2} Al \left\{ 1 - \frac{8}{\pi^2} \sum_{n=0}^{\infty} \frac{1}{(2n+1)^2} \exp \left[\frac{-D(2n+1)^2 \pi^2 t}{l^2} \right] \right\} \quad (\text{eq. 4. 26.})$$

or,

$$\frac{M_t}{M_{\infty}} = 1 - \sum_{n=0}^{\infty} \frac{8}{(2n+1)^2 \pi^2} \exp \left[\frac{-D(2n+1)^2 \pi^2 t}{4l^2} \right] \quad (\text{eq. 4. 27.})$$

(Eq. 4. 26.) is a solution to Fick's law, and reduces to 4. 23 at short times, which is shown in **figure 4. 13.**

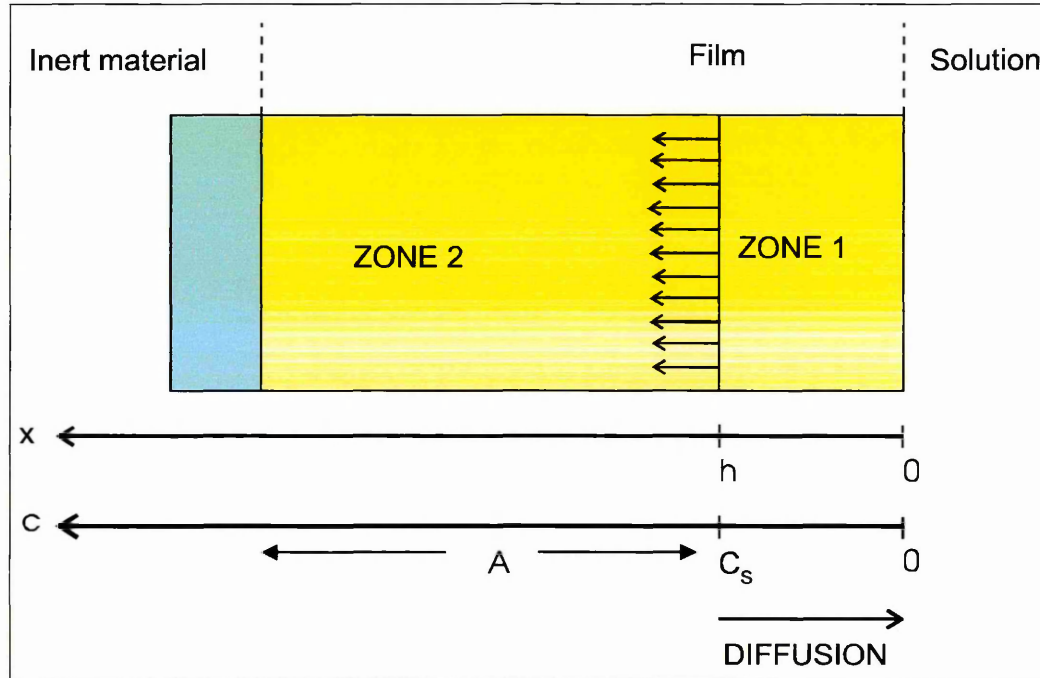
Figure 4. 13. : shows the plot of M_t/M_{∞} versus $(Dt/l^2)^{1/2}$ for the thin film and semi-infinite bulk case.



For the case $A > C_s$ (Higuchi 1961 and 1963) :

This results in two regions in the film as illustrated in **figure 4. 14.** :

Figure 4. 14. : shows a schematic of the concentration profile in the polymer films, as $A > C_s$.



(i) on the surface, the solute is dissolved in the polymer matrix. This region is defined by $0 < x < h$, and :

$$t = 0, x = 0, C = A$$

$$t > 0, x = h, C = C_s$$

$$x = 0, C = 0$$

(ii) on the interior, the solute is not dissolved in the polymer matrix. This region is defined by $x > h$ and :

$$t = 0, x = h, C = A$$

$$t > 0, x > h, C = A$$

As time progresses, the boundary between the two zones moves inward and reduces the size of the core containing the undissolved solute.

The transfer of solute from the interior (i.e. undissolved solute) to the surface (dissolved solute) is rapid compared to the diffusion within the surface.

Therefore according to Fick's law, with the boundary conditions

$$t = 0, x > 0, C = A$$

$$t > 0, x = 0, C = 0$$

$$\frac{\partial M_t}{\partial t} = D \frac{C_s}{h} \quad (\text{eq. 4. 27.})$$

or,

$$A \frac{\partial h}{\partial t} - \frac{1}{2} C_s \frac{\partial h}{\partial t} = D \frac{C_s}{h} \quad (\text{eq. 4. 28.})$$

This can be rearranged to give :

$$\frac{\partial h}{\partial t} \left(A - \frac{1}{2} C_s \right) = D \frac{C_s}{h} \quad (\text{eq. 4. 29.})$$

Integrating both sides gives :

$$t = \frac{h^2}{4C_s D} (2A - C_s) \quad (\text{eq. 4. 30.})$$

or,

$$h = 2 \sqrt{\frac{DtC_s}{2A - C_s}} \quad (\text{eq. 4. 31.})$$

We have (from (eq. 4. 26. and 4. 27) :

$$M_t = hA - \frac{hC_s}{2} \quad (\text{eq. 4. 32.})$$

Therefore substitution of (eq. 4. 31.) and (eq. 4. 32.) leads to :

$$M_t = \sqrt{Dt(2A - C_s)C_s} \quad (\text{eq. 4. 33.})$$

For a porous matrix, correction must be made to allow for the porosity of the matrix :

$$D_{\text{effective}} = \frac{\varepsilon D}{\tau} \quad (\text{eq. 4. 34.})$$

Where ε = the porosity of the solid,
 τ = the tortuosity of the solid.

Experimentally, the following assumption are made :

- PVC is a non - porous matrix,
- the effect of swelling is negligible.

And D can be calculated from (eq. 4. 24.).

4. 5. EXPERIMENTAL PROCEDURE (FOR EACH SAMPLE)

For each sample the following experimental procedure was followed :

- Raman mapping : data for three maps are recorded,
- Raman depth profiling : data for two or three depth profiles are recorded,
- FTIR-ATR experiment, during which the diffusion of water into the sample is monitored,
- FTIR-ATR experiment, during which the water is removed from the sample, by a flow of nitrogen in the cell,
- Raman mapping : the same areas as previously are again examined,
- Raman depth profiling : the same positions as previously are again examined,
- UV analysis on the diffusion water.

4. 6. REFERENCES

Barbillat J., Dhamelincourt P., Delaye M., DaSilva E., *J. of Raman Spec.*, 1994, **25**, 3.

Bard A. J., Faulkner R., *Electrochemical methods*, Willey, New York, 1980.

Batchelder D.N., Cheng C., Pitt G.D., *Adv. Mat.*, 1991, **3**, 566.

Batchelder D.N., Cheng C., Pitt G.D., *Measurments in Sci. and Tech.*, 1992, **3**, 561.

Chien Y. W., *J. of P:harma. Sci.*, 1974, **64**, 1776.

Crank J., *The Mathematics of Diffusion, second edition*, Oxford Science Publications, 1975.

Evans R., Kasteleiner T., Banga R., Hajatdoost S., Yarwood J., *J. of Raman Spec.*, 1996, **27**, 695.

Gardiner D.J., Bowden M, *Microscopy and Anal.*, 1990, **nov.**, 27.

Govil A., Pallister D.M., Chen L.H., Moris M.D., *Appl. Spec.*, 1991, **45**, 1604.

Govil A., Pallister D.M., Chen L.H., Moris M.D., *Appl. Spec.*, 1993, **47**, 75.

Hajatdoost S., Yarwood J., *Appl. Spec.*, 1996, **50(5)**, 558.

Harris T.D., Grober R.D., Trautman J.K., Betzig E., *Appl. Spec.*, 1994, **48(1)**, 14A.

Higuchi T., *J. of Pharma. Sci.*, 1961, **50(10)**, 874.

Higuchi T., *J. of Pharma. Sci.*, 1963, 52(12), 1145.

Lee P.I., *J. of Membr. Sci.*, 1980, 7, 255.

Levich V. G., in *Physiochemical Hydrodynamics*, Prentice-Hall, Englewood cliffs, 1962.

Markwort L., Kip B., DaSilva E., Roussel B., *Appl. Spec.*, 1995, 49(10), 1411.

Tabaksblat R., *Spec. Eur.*, 1992, 4(4), 22.

Tabaksblat R., Meier R.J., Kip B.J., *Appl. Spec.*, 1992, 46, 60.

Traedo P.J., Morris M.D., *Appl. Spec. Revs.*, 1994, 29(1), 1.

Williams K.J.P., Pitt G.D., Smith B.J.E., Whitley A., Batchelder D.N., Hayward I.P., *J. of Raman Spec.*, 1994, 25, 131.

Williams K.J.P., Pitt G.D., Batchelder D.N., Kip B.J., *Appl. Spec.*, 1994a, 48, 232.

CHAPTER 5. :
DETERMINATION OF THE DISTRIBUTION OF
FLUORFOLPET IN PLASTICISED PVC FILMS.

CONTENTS

CHAPTER 5.: DETERMINATION OF THE DISTRIBUTION OF FLUORFOLPET IN PLASTICISED PVC FILMS.	146
5. 1. INTRODUCTION.....	149
5. 2. RAMAN MAPPING.....	150
5. 2. 1. Method	150
a) Polyvinyl chloride	152
b) Dioctylphthalate	153
c) Fluorfolpet	154
d) Fluorfolpet / DOP / PVC.....	155
5. 2. 2. Quantitative analysis of the maps	157
5. 2. 3. Results and discussion	159
5. 2. 3. 1. Distribution of Dioctylphthalate on the surface of the film	159
5. 2. 3. 2. Redistribution (by leaching of fluorfolpet) of DOP on the surface of the film.....	160
5. 2. 3. 3. Distribution of fluorfolpet on the surface of the film	166
5. 2. 3. 4. Redistribution of fluorfolpet on the surface of the films due to leaching.....	169
5. 3. DEPTH PROFILING.....	175
5. 3. 1. Method	175
5. 3. 2. Quantitative analysis	175
5. 3. 3. Results and discussion	177
5. 3. 3. 1. Distribution of DOP as a function of depth	177
5. 3. 3. 2. Redistribution of DOP due to leaching (of PA3) in water	181
5. 3. 3. 3. Distribution of fluorfolpet as a function of depth	185

5. 3. 3. 4. Redistribution as a function of depth of fluorfolpet due
to leaching190

5. 4. CONCLUSION 195

5. 5. REFERENCES.....195

CHAPTER 5. : DETERMINATION OF THE DISTRIBUTION OF FLUORFOLPET IN PLASTICISED PVC FILMS

5. 1. INTRODUCTION

The efficiency of a biocide is, in part, limited by its active “surface” with regard to the damaging micro-organisms and hence the distribution of the biocidal molecules on the surface of the film. It is reasonable to assume that a uniform coverage will provide a better protection against degradation than a non-uniform or heterogeneous distribution, which would leave unprotected “patches”. Furthermore, a constant “feed” of biocide from the bulk of the material towards the surface would be of greater use than a surface layer, which might leave unprotected material, then very sensitive to degradation, once it has been consumed or simply washed off. This explains the interest shown here in determining the distribution of these molecules in plastic films. Our particular choice of biocide is fluorfolpet, and the polymer system chosen is dioctylphthalate / polyvinyl chloride.

In this chapter we present the results obtained on the distribution of fluorfolpet in plasticised PVC at different degrees of plasticisation. We also report the effect of water exposure on the distribution of both biocide and plasticiser, which we have termed the “redistribution”.

We will demonstrate that :

- (i) Raman microscopy is a very useful tool to study molecular distribution, in both the bulk and the surface;
- (ii) leaching of fluorfolpet can be measured quantitatively as well as qualitatively,
- (iii) leaching of fluorfolpet is proportional to the level of dioctylphthalate present in the film.

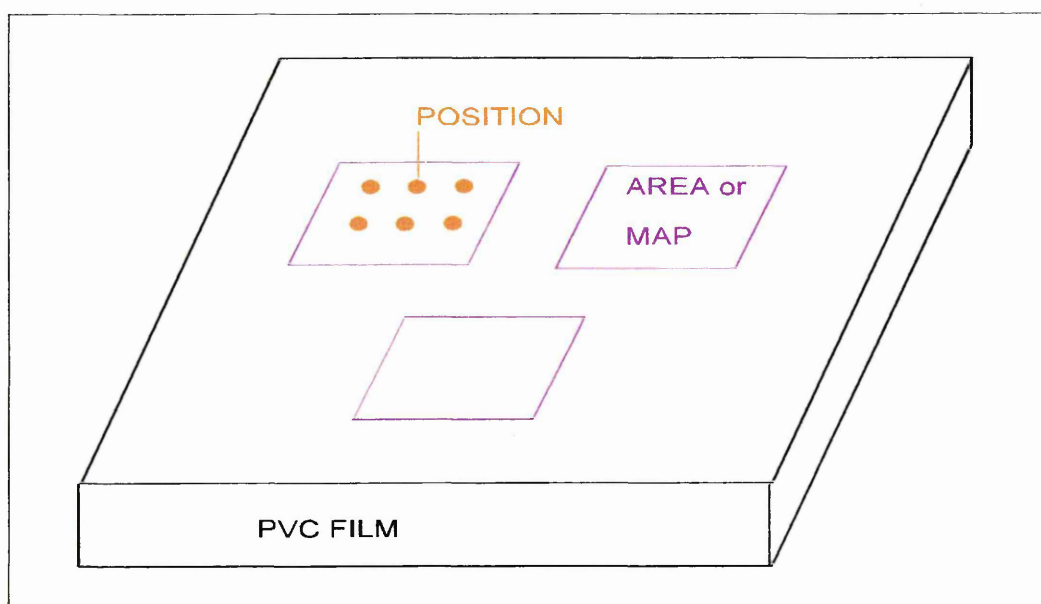
5. 2. RAMAN MAPPING

5. 2. 1. Method

The distribution of molecules on the surface is determined using Raman mapping. As explained in chapter 4., the construction of a map involves :

(i) the acquisition of a number of spectra, usually 49 per map, from a small area of the sample surface. The interval between each position at which the spectra are taken is 500 μm . (See **Figure 5. 1.**)

Figure 5. 1. A schematic of Raman mapping.



(ii) identification of component bands,

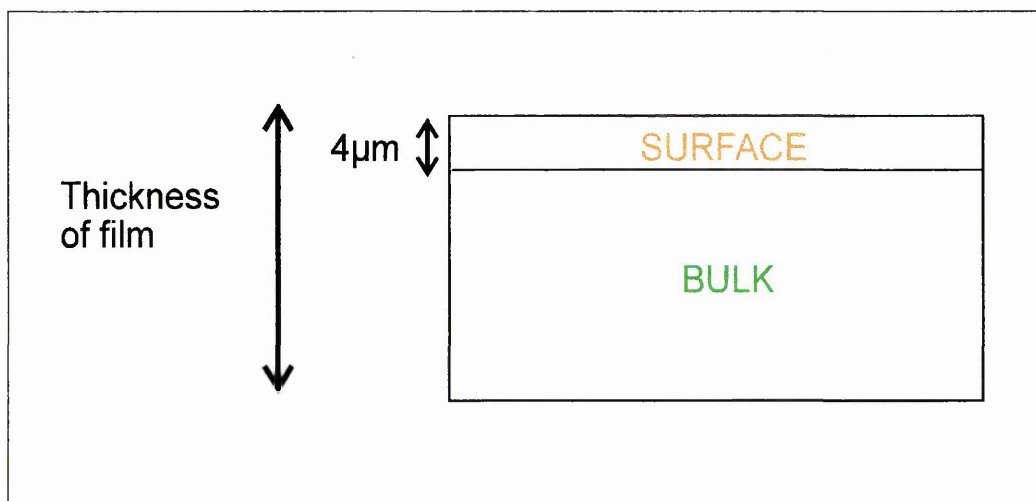
(iii) calculation of PVC/DOP and PVC/PA3 ratios, and construction of the map.

(i) Spectral acquisition :

The dimensions of an area analysed, are 3000 μm by 3000 μm , and the interval between each spectrum is 500 μm , i.e. 49 spectra are needed to construct a map. An exposure time of two times 20 seconds over the range 500-2000 cm^{-1} was used. The Raman micro-spectrometer was run in the normal mode utilising the x50 objective, therefore yielding a laser spot of 5 μm^2 , and depth resolution of 4 - 5 μm (see **figure 2. 20.**). Three different positions were mapped per sample.

Due to the spatial resolution obtained during Raman mapping, the terms surface and bulk are defined in **figure 5. 2.** :

Figure 5. 2. Definition of the terms “surface” and “bulk”.



(ii) Identification of component bands :

a) Polyvinyl chloride

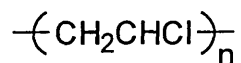
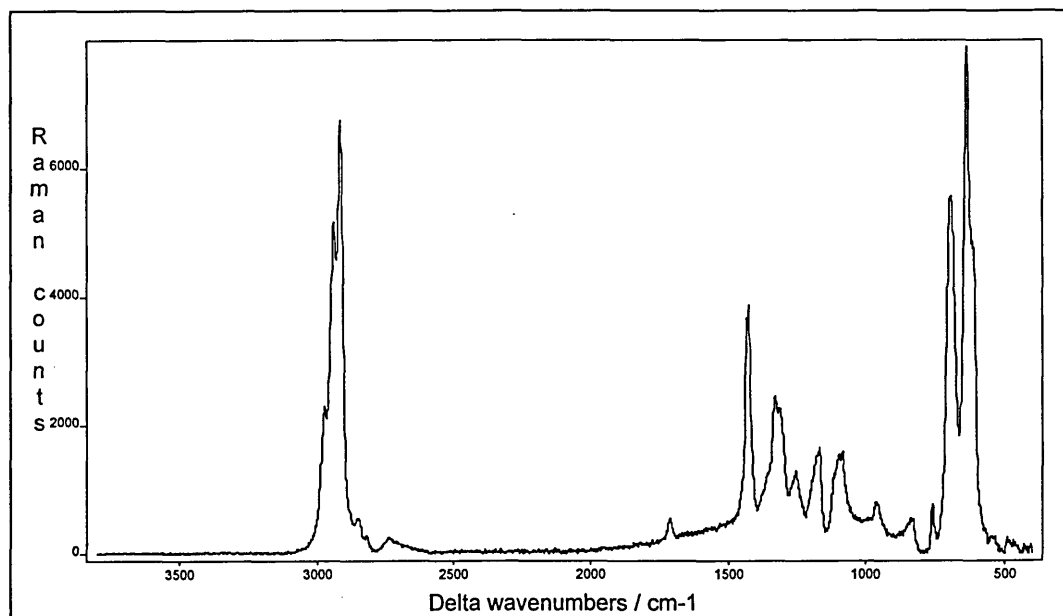


Figure 5.3. shows the spectrum of PVC obtained after a total exposure of $T = 5 \times 20$ sec.

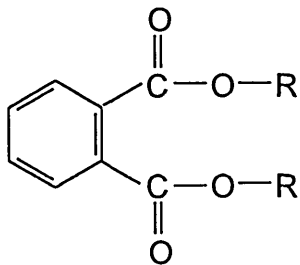
Figure 5. 3. Spectrum of PVC (T = 5 x 20 sec.).



Band assignment :

Wavenumbers (cm ⁻¹)	Assignment
567 - 750	C-Cl stretching mode
950	CH ₂ rocking mode
1090 - 1310	C-H stretching mode (from CH-Cl)
1414	CH ₂ bending mode
2800 - 3000	Aliphatic C-H stretching mode

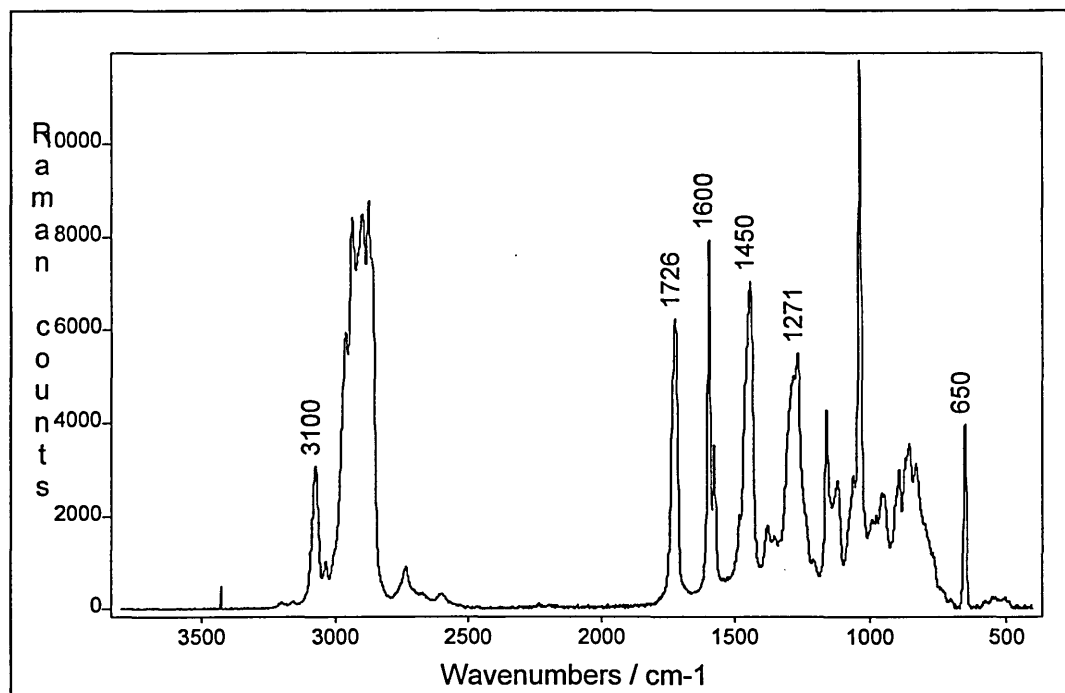
b) Dioctylphthalate



Where R = $\text{CH}_2\text{CH}(\text{C}_2\text{H}_5)(\text{CH}_2)_3\text{CH}_3$

Figure 5. 4. shows the spectrum of DOP. T = 50 sec.

Figure 5. 4. Spectrum of DOP (T = 50 sec.).



Band assignment :

Wavenumbers (cm^{-1})	Assignment
3100	Aromatic C-H stretching mode
3000 - 2900	Aliphatic C-H stretching mode
1726	Ester C=O stretching mode
1580 - 1600	Aromatic C=C stretching mode
1450	C-H bending mode (-CH ₂ -)
1271	Ester C-O stretching mode
650	Aromatic C-H bending mode

c) Fluorfolpet (PA3)

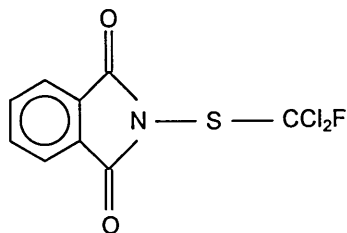
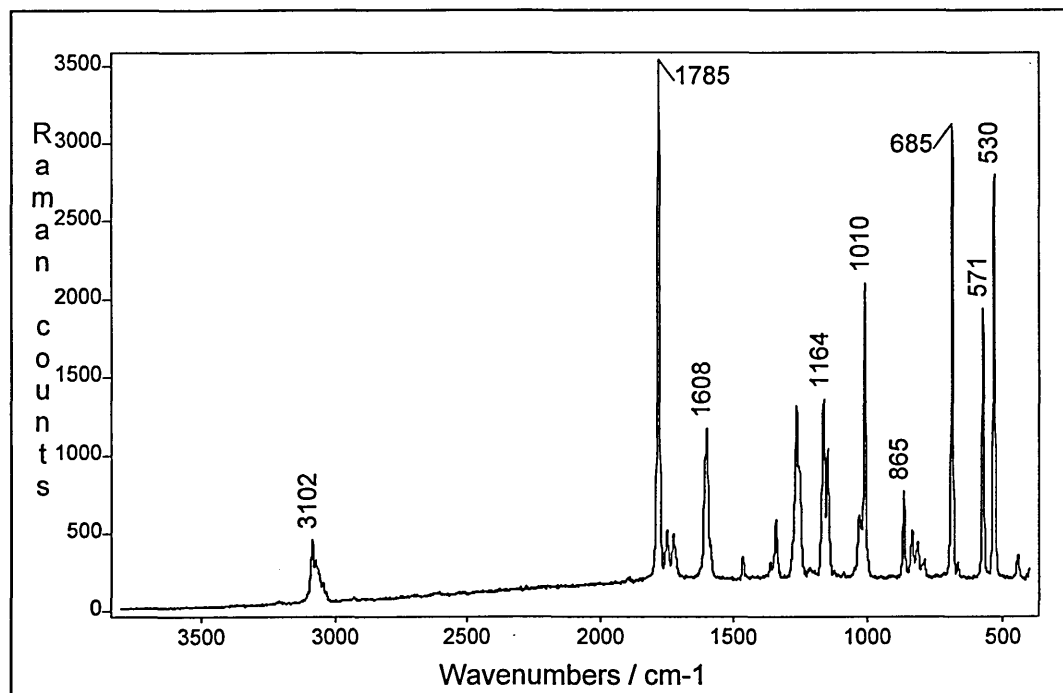


Figure 5. 5. shows the spectrum of fluorfolpet , T = 5 sec.

Figure 5. 5. Spectrum of fluorfolpet (T = 5 sec.).



Band assignment :

Wavenumbers (cm ⁻¹)	Assignment
3102	Aromatic C-H stretching mode
1785	C=O stretching mode
1608	Aromatic C=C stretching mode
1164	C-F stretching mode
1010	Aromatic ring vibration
865	S-N stretching mode
685	C-S stretching mode
530 - 571	C-Cl stretching mode

d) Fluorfolpet / DOP / PVC

Figure 5. 6. shows stacked spectra of PVC, DOP and fluorfolpet, and **figure 5. 7.** shows superimposed spectra of PVC, DOP and fluorfolpet, in the range 500 - 2000 cm^{-1} .

Figure 5. 6. Stacked spectra of PVC, DOP and fluorfolpet.

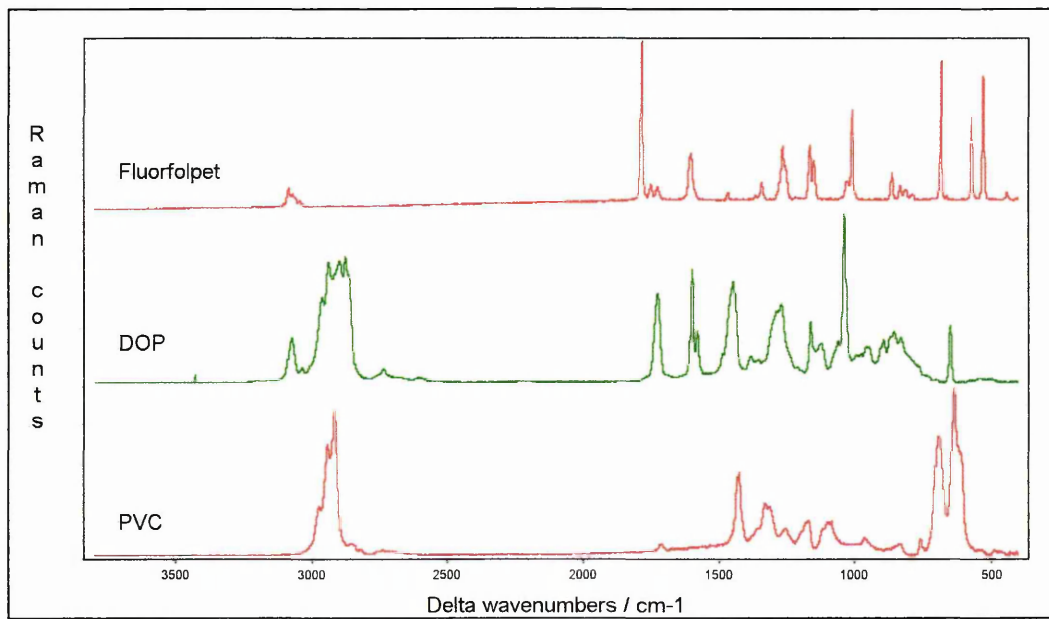
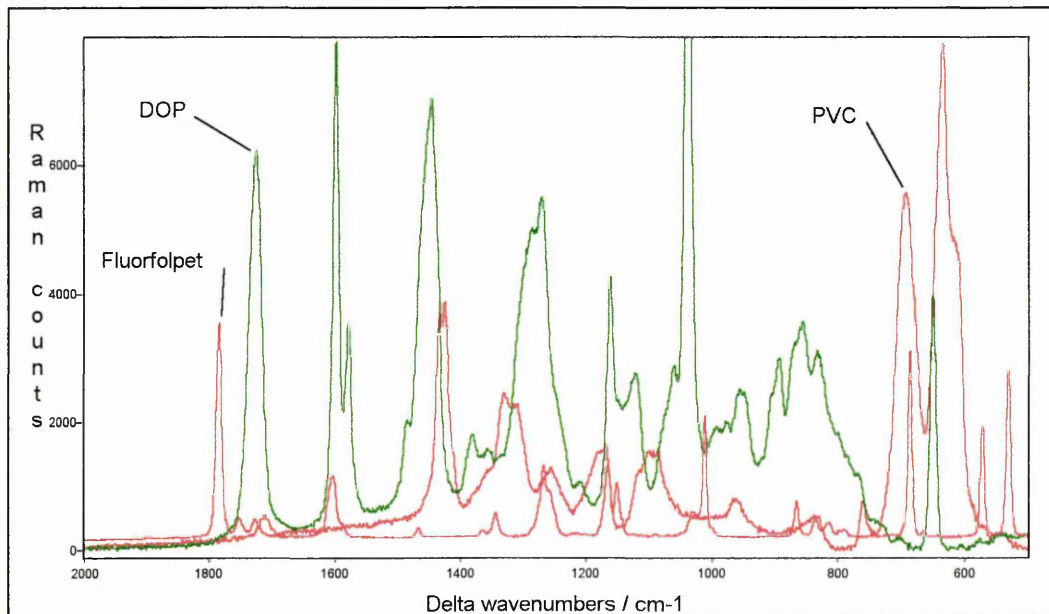


Figure 5. 7. Superimposed spectra of PVC, DOP and fluorfolpet.



Figures 5. 6. and 5. 7., clearly show that :

- Fluorfolpet can be identified by using the $\nu(\text{C}=\text{O})$ band at 1785 cm^{-1} , $\nu(\text{C}=\text{C})$ band at 1010 cm^{-1} , as well as $\nu(\text{C}-\text{Cl})$ band at $530 - 571\text{ cm}^{-1}$.
- The carbonyl $\nu(\text{C}=\text{O})$ band at 1726 cm^{-1} associated with DOP can be used to identify the plasticiser in a mixture.
- The $\nu(\text{C}-\text{Cl})$ band at $750 - 590\text{ cm}^{-1}$ can be used to identify PVC, although underlying bands of fluorfolpet and DOP are present. Due to the low percentage of fluorfolpet and DOP in the formulation, these bands will be totally dominated by the C-Cl stretching band of PVC, and not contribute significantly to the band intensity. Indeed, as it can be seen from **figure 5. 6. and 5. 7.** the band at 650 cm^{-1} of DOP and the 685 cm^{-1} band of PA3 have very similar intensities in the pure compound spectra. Furthermore, these latter two bands also have similar intensity to the two band at 550 and 530 cm^{-1} in the PA3 pure compound spectra. The latter two bands are present in the mixture spectrum (**figure 5. 8.**) as two very small bands (compared to the C-Cl bands of PVC). From this it is quite reasonable to conclude that the two DOP and fluorfolpet bands underneath the C-Cl band of PVC will not interfere in the calculation of the integrated intensity of the C-Cl stretching band.

Figure 5. 8. Spectrum of a PVC / 20% DOP / 5% PA3 film.

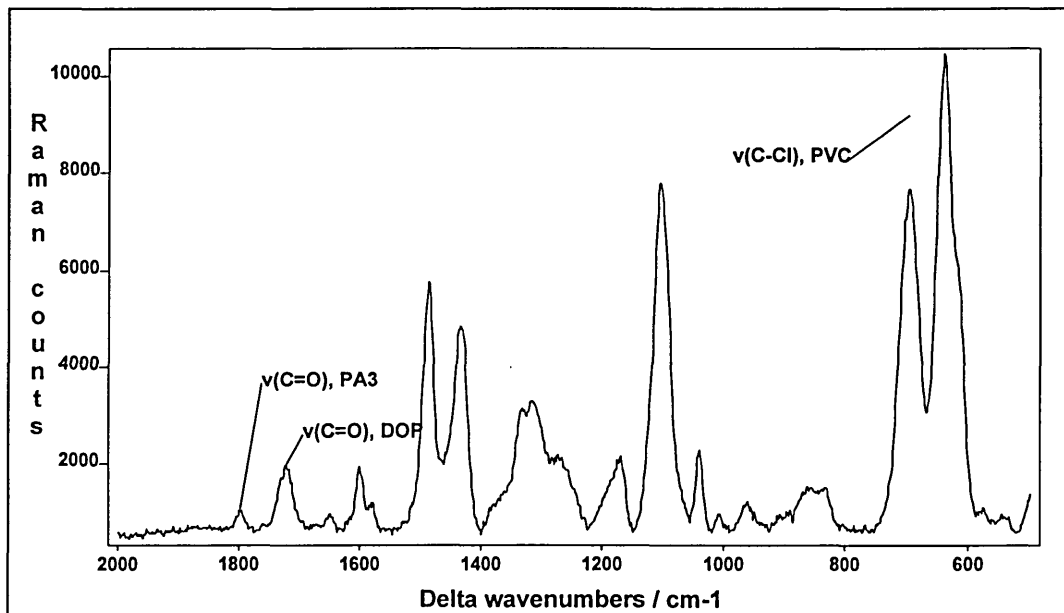


Figure 5. 8. shows the spectrum of a 20% DOP / 5% fluorfolpet / PVC film in the range $500 - 2000 \text{ cm}^{-1}$, $T = 2 \times 25 \text{ sec}$. **Figure 5. 8.** demonstrates the suitability of the bands identified above. Therefore the quantitative analysis was done using the following bands, $\nu(\text{C}=\text{O})$ at 1785 cm^{-1} for fluorfolpet, $\nu(\text{C}=\text{O})$ at 1726 cm^{-1} for DOP and $\nu(\text{C}-\text{Cl})$ between $590-750 \text{ cm}^{-1}$ for PVC.

(iii) Calculation of PVC/DOP and PVC/PA3 ratios, as demonstrated in chapter 4. **Figures 5. 9.** and **5. 10.** show typical maps obtained for the distribution of fluorfolpet and dioctylphthalate in a 20% DOP / 5% PA3 / PVC film.

5. 2. 2. Quantitative analysis of the maps

A quantitative analysis was achieved by calculating the mean and standard deviation of the PVC/DOP and PVC/PA3 ratios, thereby obtaining the overall level of component in the mapped area, and a measure of the heterogeneity of the distribution. A comparison between these values in the distribution maps and the values in the redistribution maps yields the loss of fluorfolpet (and / or DOP) from the film.

Comparing the average level of fluorfolpet and DOP from all three maps, allowed us to characterise the distribution of PA3 and DOP on a macroscopic level as well.

Calculation of the errors :

Error on the value of the PVC / PA3 and PVC / DOP ratios were obtained using the following approach : errors arise from the measurement of the band areas of the fluorfolpet, DOP and PVC bands. These errors were estimated by measuring the area of the same band repeatedly and the difference in the measurement of this area constitute the error obtained in the band area (expressed as %) which were 10%, 6% and 2% for PA3, DOP and PVC band areas respectively. The errors on the ratios PVC / PA3 and PVC / DOP therefore become 12% and 8% respectively.

(The errors quoted are mean values of the errors obtained from a full set of data.)

Figure 5. 9. A typical map obtained for the distribution of fluorfolpet in a 20% DOP / 5% PA3 / PVC film.

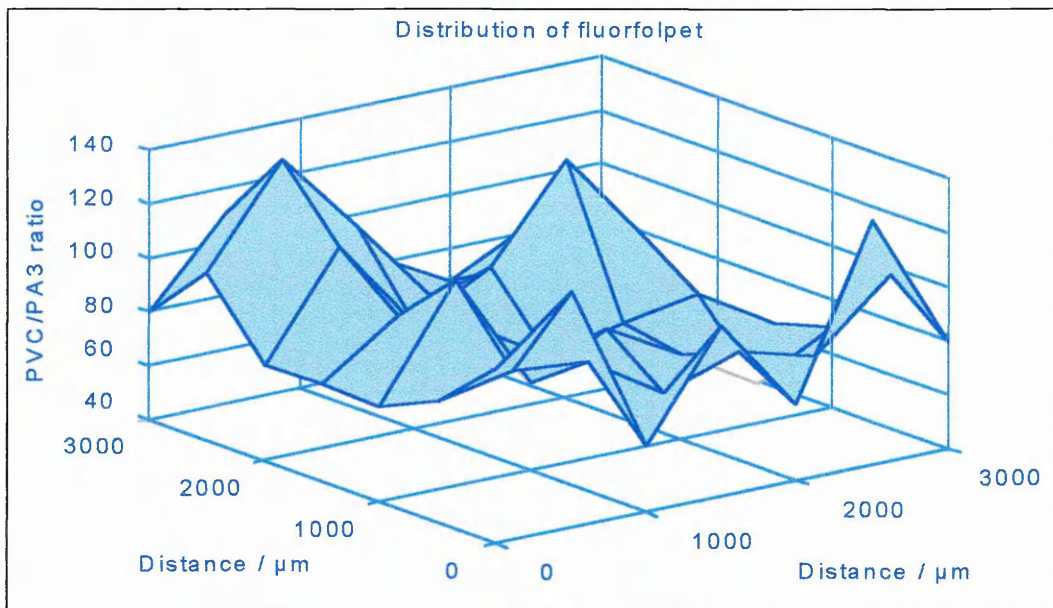
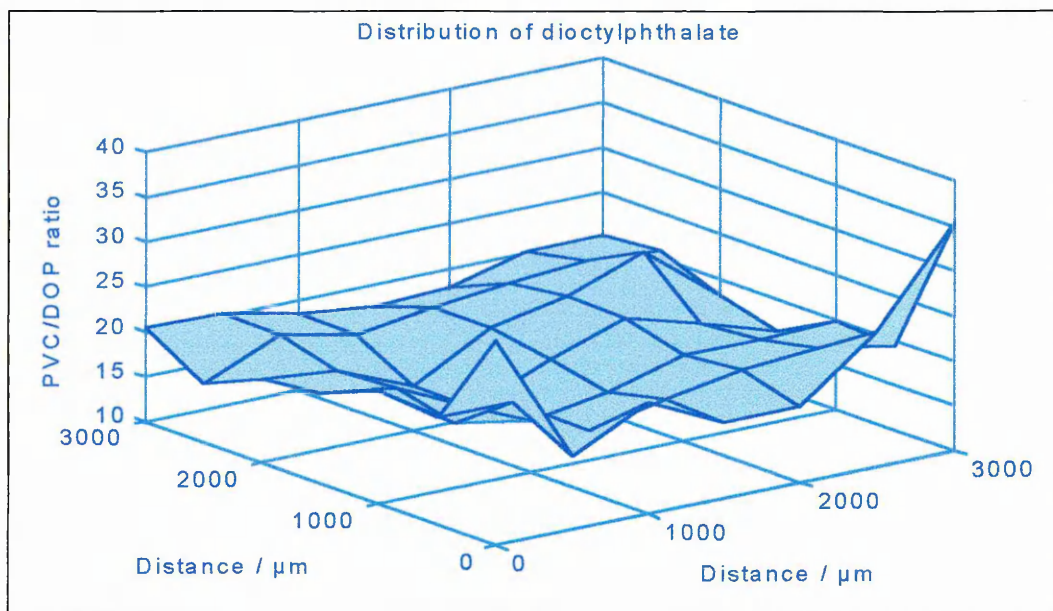


Figure 5. 10. A typical map obtained for the distribution of dioctylphthalate in a 20% DOP / 5% PA3 / PVC film.



5. 2. 3. Results and discussion

5 .2. 3. 1. Distribution of Dioctylphthalate on the surface of the film

Table 5. 1. (below) presents the mapping statistics for the distribution of dioctylphthalate as a function of DOP content.

Table 5. 1. Mapping statistics for the distribution of dioctylphthalate as a function of DOP content.

DOP (%)	MAP	PVC/DOP ratio	Mean value for PVC/DOP ratio
10	1	44 ± 16	44
	2	43 ± 13	
	3	46 ± 10	
10	1	50 ± 12	51
	2	47 ± 12	
	3	55 ± 20	
15	1	17 ± 3	18
	2	18 ± 3	
	3	19 ± 3	
15	1	20 ± 2	19
	2	19 ± 3	
	3	20 ± 2	
20	1	20 ± 4	19
	2	19 ± 2	
	3	20 ± 4	
25	1	13 ± 2	13
	2	13 ± 2	
	3	12 ± 1	
25	1	13 ± 1	13
	2	13 ± 2	
	3	13 ± 2	
25	1	14 ± 2	14
	2	14 ± 2	
	3	14 ± 2	
30	1	12 ± 1	12
	2	12 ± 1	
	3	11 ± 1	
30	1	11 ± 2	11
	2	11 ± 2	
	3	11 ± 1	

The variation of concentration of DOP within the confinement of a map (as shown by the values of the standard deviation from the mean PVC/DOP ratio value within each map) demonstrate the heterogeneity of the distribution of DOP on a microscopic level. Concentration differences between two positions up to 35% have been observed for films containing 10% dioctylphthalate. Generally the variation from one position to another (at 500 μm intervals) is much smaller, of the order of 15 to 25%.

On the other hand, comparison of the overall concentration of DOP of each of the three mapped areas, reveals only minor differences, of the order of 4%, showing no evidence of a significant fluctuation of DOP levels across the film.

Chalykh and Belokurova (Chalykh and Belokurova 1982) used electron microscopy to investigate plasticised PVC films. They found that when the plasticiser DOP was used, there was a transition from a one phase system to a two phase system at 20% plasticiser concentration, due to a lack of plasticiser solubility in the polymer at concentration higher than 20%. However the Raman experiments show no evidence of such a transition from a homogeneous to a heterogeneous system on the microscopic level at any DOP concentration.

5. 2. 3. 2. Redistribution (by leaching of fluorfolpet) of DOP on the surface of the film

Leaching was performed as described in section 2 chapter 4.

Table 5. 2. presents the mapping statistics for the redistribution of dioctylphthalate as a function of DOP content. The difference (in percentage) on the overall level of DOP in the films between before and after leaching of fluorfolpet is given in column 5.

Table 5 .2. Mapping statistics for the redistribution of dioctylphthalate as a function of DOP content.

DOP (%)	MAP	PVC/DOP ratio	Mean value for PVC/DOP ratio	Difference in DOP level (%)
10	1	53 ± 21	50	-12
	2	48 ± 20		
	3	48 ± 20		
10	1	45 ± 9	47	+8
	2	49 ± 12		
	3	48 ± 16		
15	1	18 ± 2	19	-5
	2	18 ± 2		
	3	20 ± 3		
15	1	20 ± 3	20	-5
	2	20 ± 3		
	3			
20	1	21 ± 3	20	-5
	2	20 ± 3		
	3	20 ± 5		
25	1	13 ± 2	13	0
	2	13 ± 2		
	3	13 ± 2		
25	1	14 ± 3	13	0
	2	13 ± 2		
	3	13 ± 2		
25	1	15 ± 2	15	-5
	2	15 ± 2		
	3	15 ± 2		
30 ^(a)	1	11 ± 1	10	+17
	2	10 ± 2		
	3			
30 ^(a)	1	12 ± 1	12	-5
	2	12 ± 1		
	3	12 ± 2		

^(a) fluorfolpet crystallised out.

Crystallisation out of fluorfolpet was noticed shortly after the leaching experiment, **figure 5. 11.** shows a micrograph of the film surface. As can be seen from the micrograph there are small transparent crystals imbedded in the polymer matrix. These crystal were identified, using confocal Raman, as fluorfolpet crystals. **Figure 5. 12.** shows a spectrum of one of the crystals (T = 2 x 200 s.).

Figure 5. 11. A micrograph of the film surface from a film containing 30% DOP.

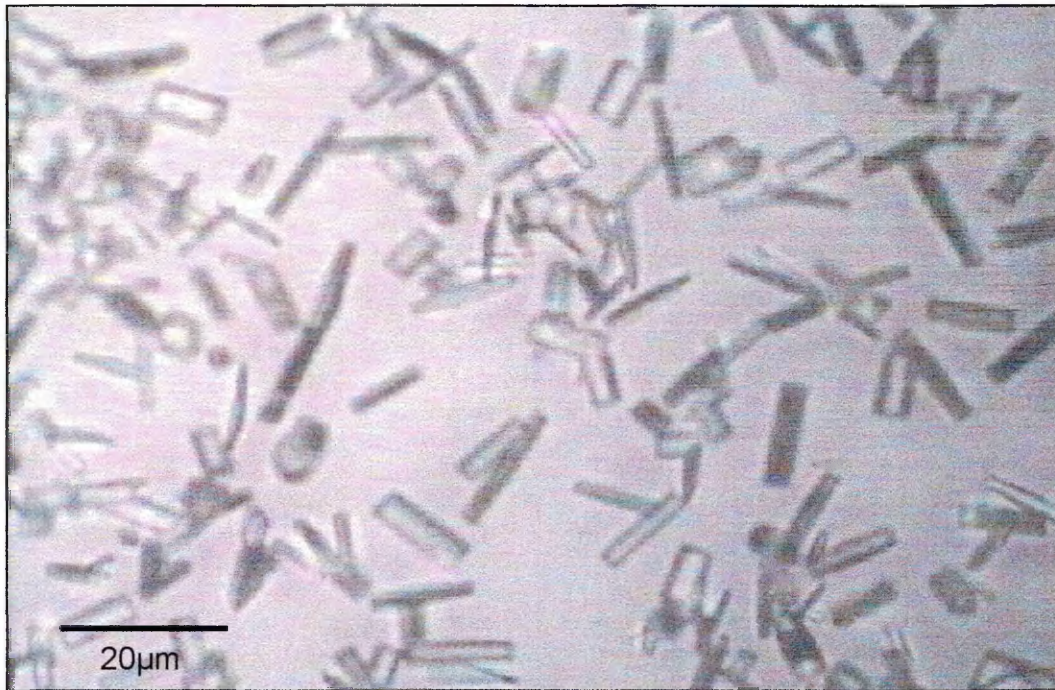
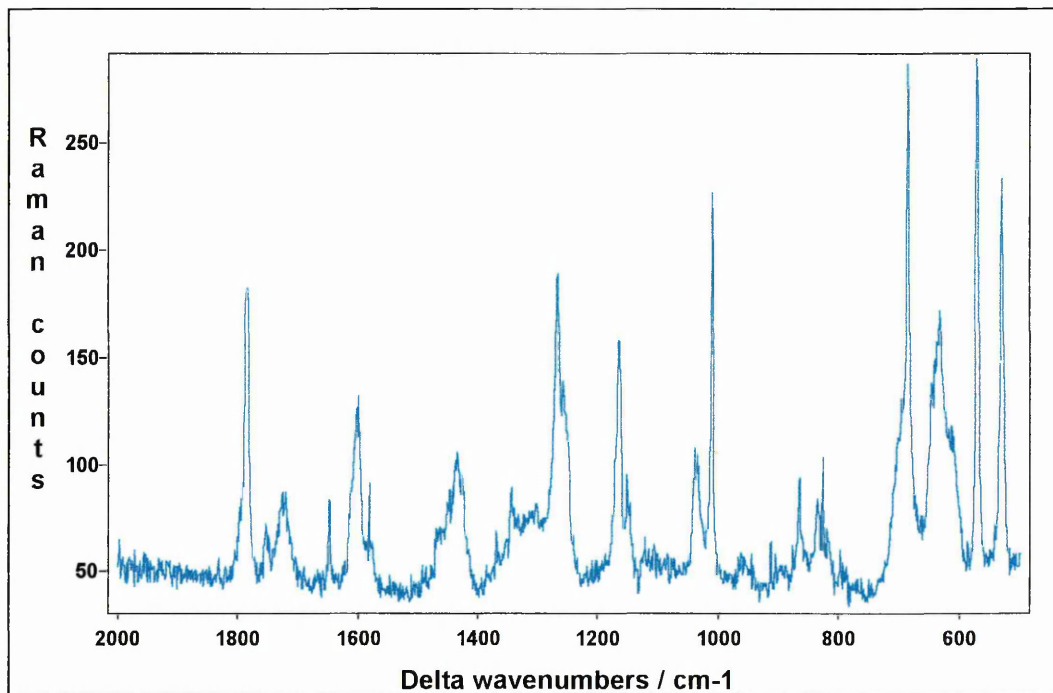


Figure 5. 12. A spectrum of a crystal embedded in a 30% DOP / 5% PA3 / PVC film ($T = 2 \times 200$ s.).



The same conclusions can be drawn from the results in the redistribution as in the distribution. They are that we can observe a heterogeneous distribution of the plasticiser on a μm scale, but there is no evidence of significant fluctuation of DOP levels across the film. (See **figures 5. 13. to 5. 18.**)

Figures 5. 13., 5. 14., 5. 15. show the plot of three distribution maps for DOP in a 20% DOP / 5% PA3 / PVC.

Figure 5. 13. Distribution map 1.

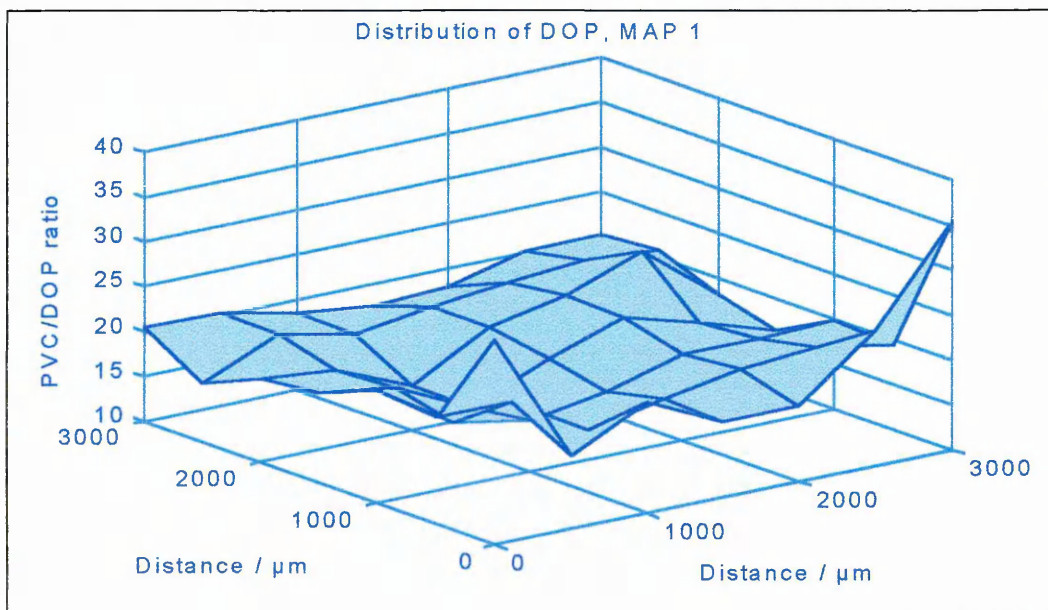


Figure 5. 14. Distribution map 2.

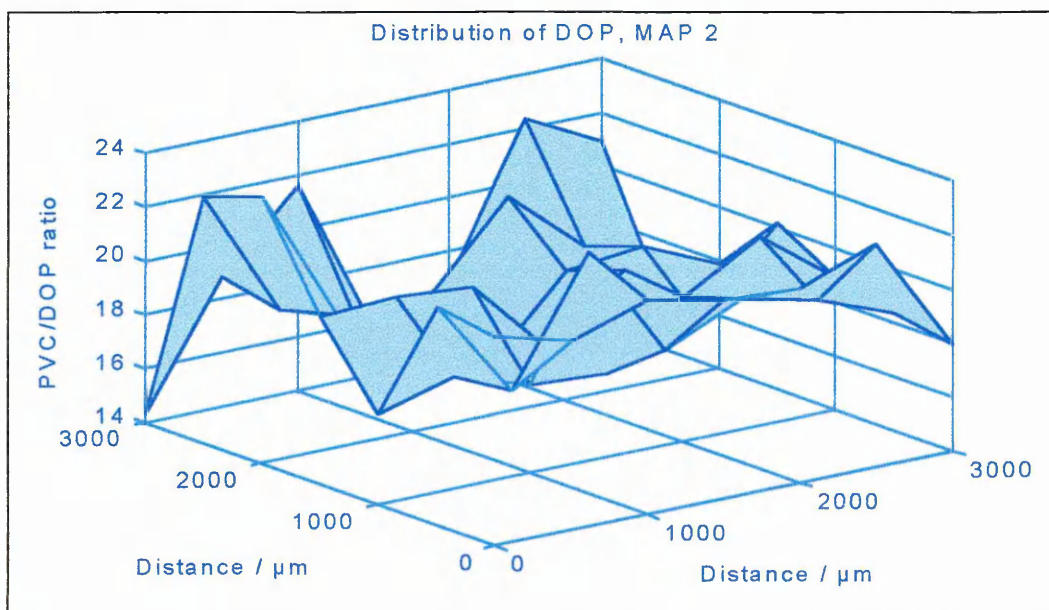
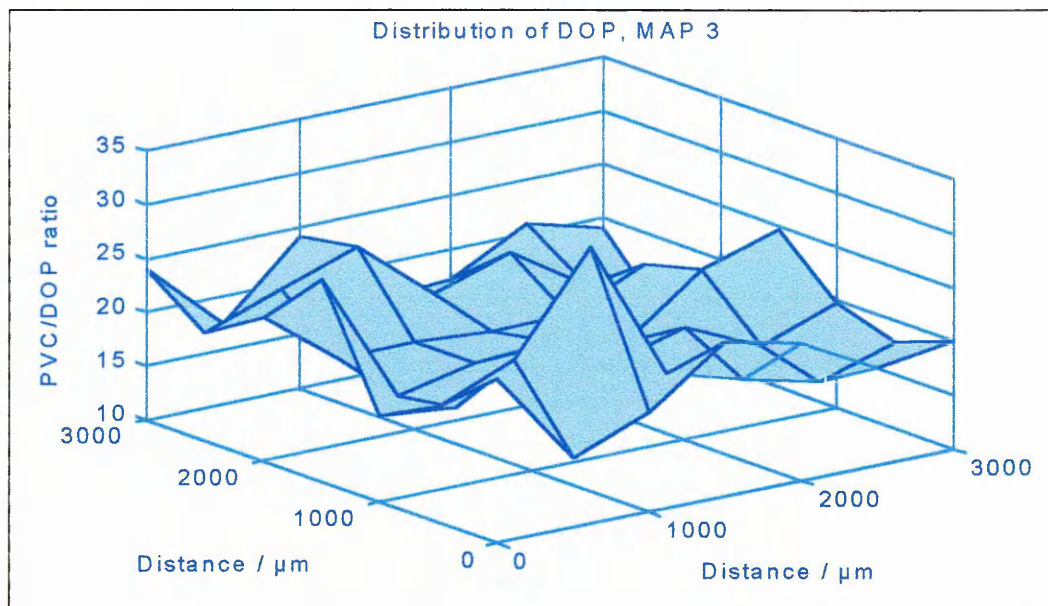


Figure 5. 15. Distribution map 3.



Values obtained for the difference of DOP concentration in the films between after and before the leaching experiment were very small, and within the experimental error. This strongly suggests that no DOP was lost during the period in which the films were in contact to water. (see **figures 5. 13. to 5. 18.**).

Plasticisers and other additives are well known to migrate from the films into the media the films are in contact with (Figge 1980, Messadi and Vergnaud 1982, Vergnaud 1994, Messadi and Gheid 1994, Messadi and Vergnaud 1997,). Murase and co-workers (Murase et al. 1994) and Fayad (Fayad et al. 1997) and co-workers found that plasticisers of which dioctylphthalate would leach into water when the plastic film was exposed to high temperature (~120°C), or left outdoors for long periods (25 days), or exposed to sunlight (UV) and water. Indeed degradation of PVC films is accompanied by leaching of plasticiser.

Other experiments by Messadi and Vergnaud (Messadi and Vergnaud 1982) also found that there were no transfers of DOP and liquid solutions of ethanol and water having less than 8% ethanol, i.e. no migration of DOP into pure water (these experiments were performed at 30°C). The latter experiments by Messadi and Vergnaud suggest that the driving force for migration is strongly related to solubility. As the amount of ethanol in the mixture decreases, so

does the leaching of DOP into the solution. DOP is quite soluble in ethanol, but insoluble in water.

Figures 5. 16., 5. 17., 5. 18. show the plot of three redistribution maps for DOP in a 20% DOP / 5% PA3 / PVC.

Figure 5. 16. Redistribution map 1.

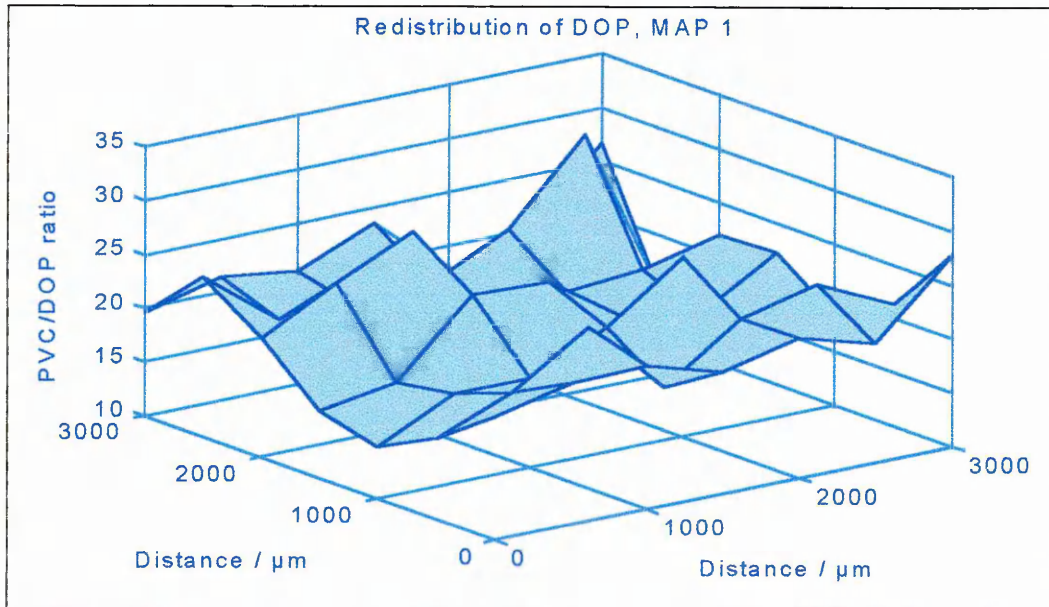


Figure 5. 17. Redistribution map 2.

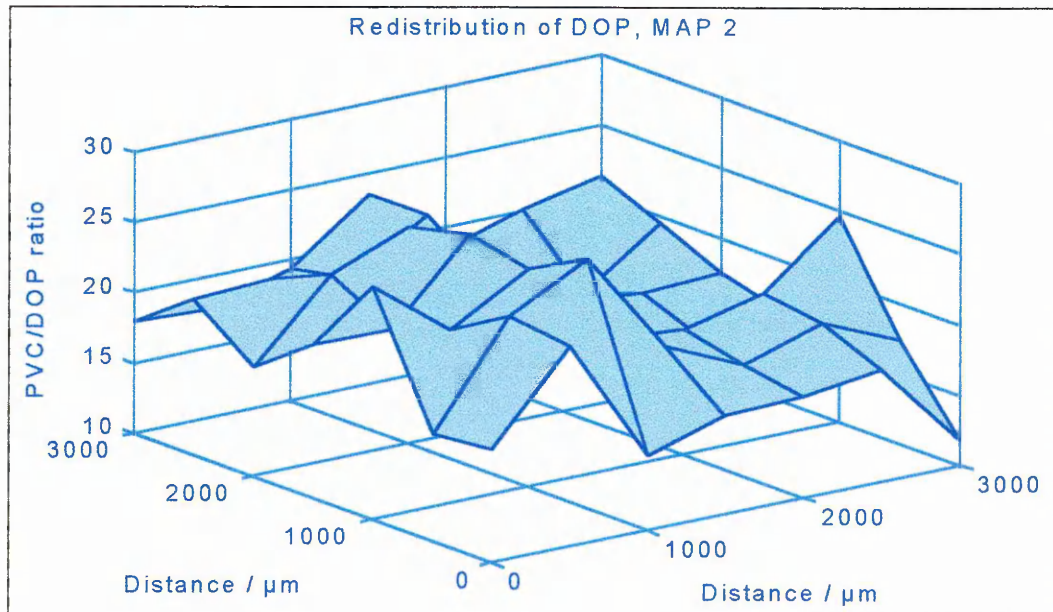
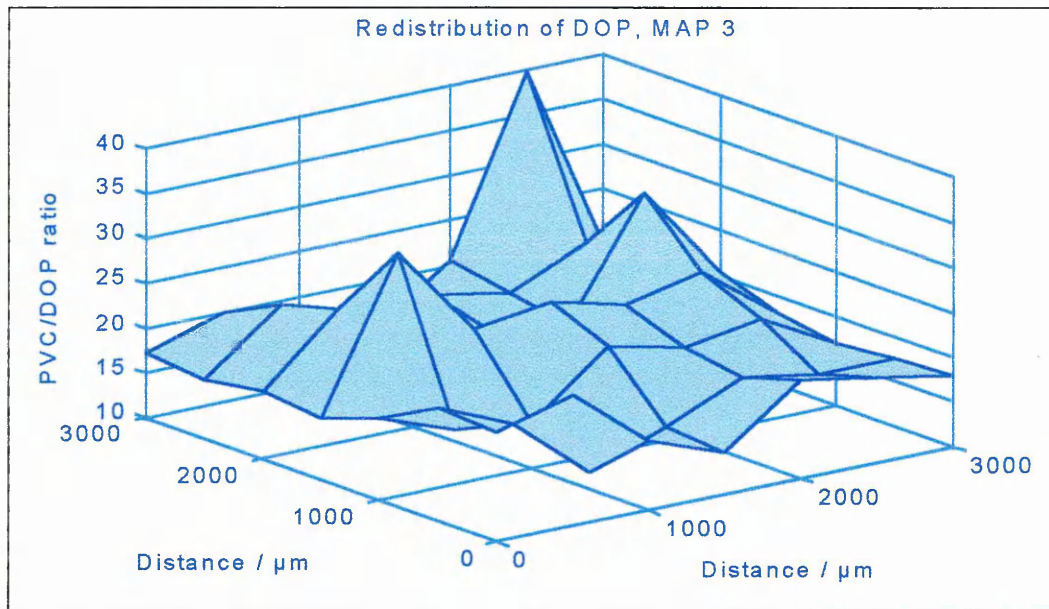


Figure 5. 18. Redistribution map 3.



5. 2. 3. 3. Distribution of fluorfolpet on the surface of the film

All the films examined contain the same amount of fluorfolpet (PA3) ; 5% in weight.

Table 5. 3. (below) presents the mapping statistics for the distribution of fluorfolpet as a function of DOP content.

As for DOP, the distribution of fluorfolpet inside the area mapped is heterogeneous, indeed the level of fluorfolpet varies between 20% and 35%(and occasionally 45%) from the mean values from point to point. It appears that the heterogeneity is not function of the plasticiser content.

It can also be seen that the standard deviations in individual maps are generally higher for the distribution of fluorfolpet than for the distribution of DOP. this is an indication of a more heterogeneous distribution of fluorfolpet molecules.

A comparison of the mean values of all three maps for any particular sample, on the other hand, indicates that the overall level of fluorfolpet throughout the whole sample only varies very slightly, about 2 - 5%, (with two exception, due to a slightly higher level of fluorfolpet in one of the maps). This denotes a constant level of fluorfolpet over the whole sample. This is also shown by **figures 5. 19 to 5. 21..**

Table 5. 3. Mapping statistics for the distribution of fluorfolpet as a function of DOP content.

DOP (%)	MAP	PVC/PA3 ratio	Mean value for PVC/PA3 ratio
10	1	64 ± 17	64
	2	62 ± 12	
	3	65 ± 13	
10	1	79 ± 26	70
	2	58 ± 13	
	3	74 ± 32	
15 ^(b)	1	217 ± 63	195
	2	212 ± 67	
	3	156 ± 49	
15 ^(b)	1	122 ± 46	121
	2	115 ± 41	
	3	127 ± 51	
20	1	86 ± 20	82
	2	77 ± 20	
	3	82 ± 17	
25	1	67 ± 24	65
	2	68 ± 19	
	3	61 ± 14	
25	1	56 ± 14	57
	2	57 ± 14	
	3	58 ± 11	
25 ^(b)	1	110 ± 48	107
	2	113 ± 30	
	3	97 ± 26	
30	1	21 ± 1	21
	2	22 ± 2	
	3	20 ± 2	
30	1	38 ± 7	38
	2	37 ± 7	
	3	40 ± 3	

^(b) much higher ratios were obtained possibly through the use of a different instrument to the other measurements.

Figures 5. 19., 5. 20. and 5. 21. show fluorfolpet distribution maps obtained for a 20% DOP / 5% PA3 / PVC film.

Figure 5. 19. Distribution map 1.

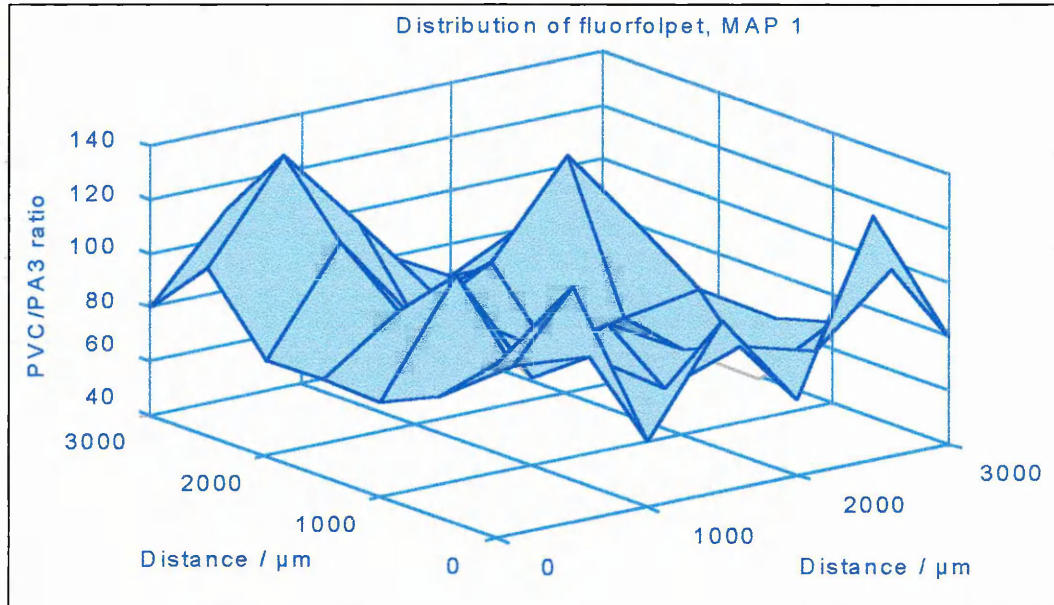


Figure 5. 20. Distribution map 2.

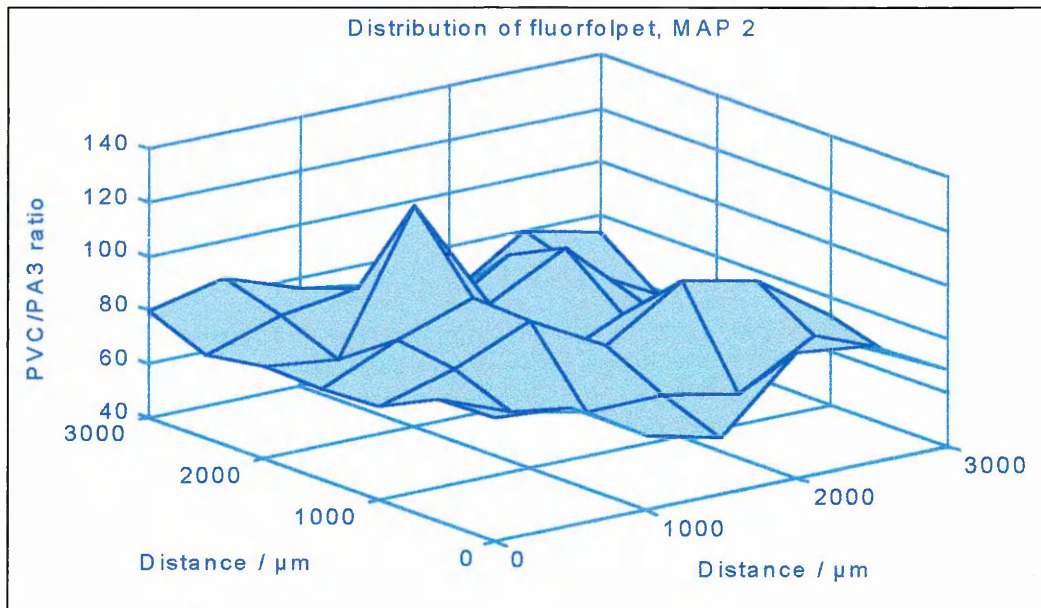
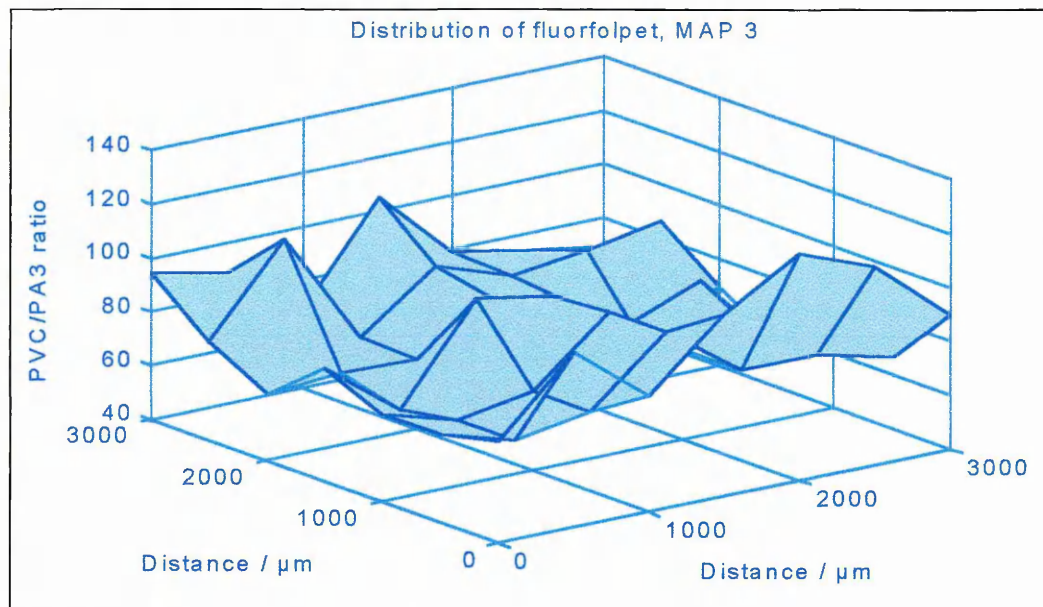


Figure 5. 21. Distribution map 3.



5. 2. 3. 4. Redistribution of fluorfolpet on the surface of the films due to leaching

Leaching was performed as described in section 2 chapter 4.

Table 5. 4. (below) presents the mapping statistics for the redistribution of fluorfolpet as a function of DOP content. The difference in overall level of fluorfolpet in the films between before and after leaching is given in column 5 in percentage.

Table 5. 4. Mapping statistics for the redistribution of fluorfolpet as a function of DOP content.

DOP (%)	MAP	PVC/PA3 ratio	Mean value for PVC/PA3 ratio	Difference in PA3 level (%)
10	1	71 ± 21	68	-6
	2	68 ± 17		
	3	64 ± 14		
10	1	71 ± 18	72	-3
	2	62 ± 15		
	3	82 ± 22		
15 ^(b)	1	248 ± 62	238	-18
	2	212 ± 61		
	3	253 ± 53		
15 ^(b)	1	150 ± 76	145	-16
	2	141 ± 51		
	3			
20	1	119 ± 57	108	-24
	2	108 ± 53		
	3	97 ± 26		
25	1	74 ± 16	84	-23
	2	93 ± 33		
	3	85 ± 21		
25	1	79 ± 18	73	-22
	2	71 ± 23		
	3	68 ± 18		
25 ^(b)	1	116 ± 40	119	-10
	2	135 ± 35		
	3	106 ± 26		
30 ^(a)	1	23 ± 3	24	-12.5
	2	25 ± 3		
	3			
30 ^(a)	1	42 ± 6	42	-10
	2	43 ± 6		
	3	42 ± 6		

A (-) sign denotes leaching of fluorfolpet from the film.

^(a) fluorfolpet crystallised out.

^(b) much higher ratios were obtained possibly through the use of a different instrument to the other measurements.

As shows by **table 5. 4.**, data confirm that we found as before :

- heterogeneous distribution on microscopic level,
- no significant fluctuation of fluorfolpet level across the film, (see **figures 5. 19. to 5. 24.**).

Figure 5. 22, 5. 23 and **5. 24** show fluorfolpet redistribution maps for a 20% DOP / 5% PA3 / PVC film.

Figure 5. 22. Fluorfolpet redistribution map 1.

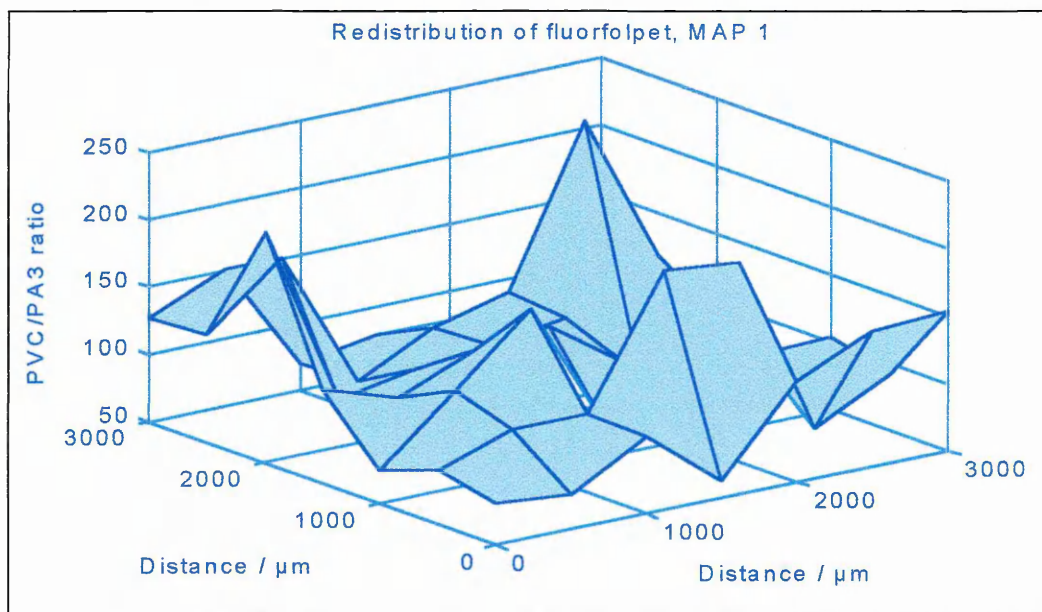


Figure 5. 23. Fluorfolpet redistribution map 2.

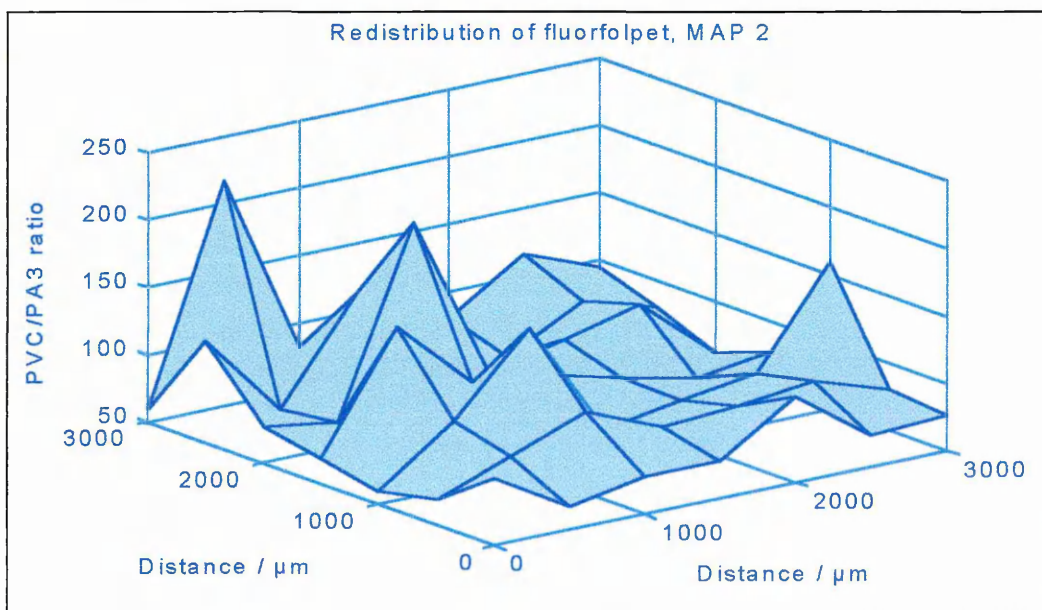
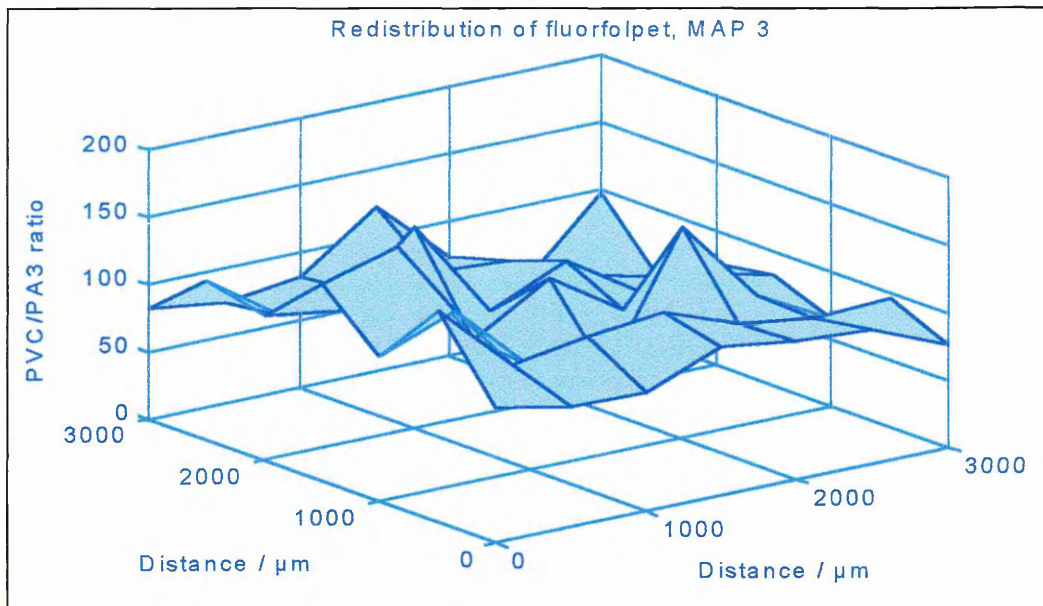
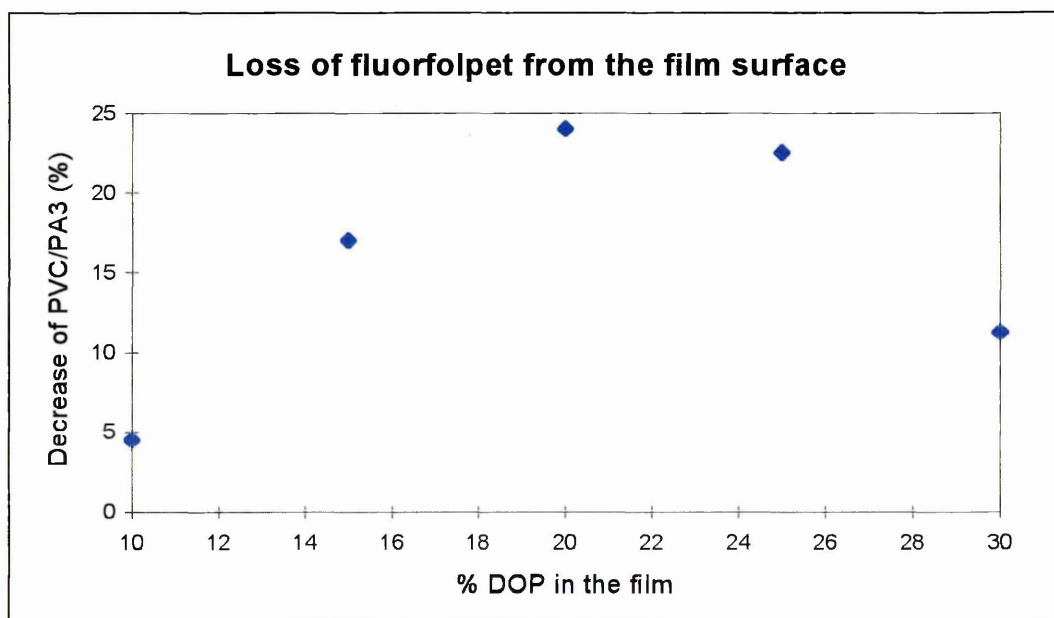


Figure 5. 24. Fluorfolpet redistribution map 3.



But more importantly, **table 5. 4.** shows a decrease in the overall concentration of fluorfolpet on the film surface. The proportion of fluorfolpet removed from the surface, is dependent upon the degree of plasticisation of the film, indeed the amount of fluorfolpet displaced from the surface of the film reaches a maximum for films containing 20% plasticiser. This is more clearly demonstrated in **figure 5. 25.**, which shows a plot of the percentage of fluorfolpet lost (from an initial loading of 5%) against plasticiser concentration.

Figure 5. 25. Loss of fluorfolpet from the film surface.



Vergnaud and Messadi (Vergnaud 1994, Messadi and Vergnaud 1997, Taverdet et al. 1982) postulate that when a plasticised poly (vinyl chloride) film is in contact with a liquid some matter transfer may take place, the liquid entering the polymer while the plasticiser or any other additive present in the formulation leaves the polymer. These two mass transfers are controlled by transient diffusion and are connected with each other. In chapter 6., we show that the diffusion rates of water entering the polymer as well as the water content of the film show an identical dependence on DOP concentration as the leaching detected by Raman mapping, thereby showing interdependence between leaching and solvent penetration. Therefore similarly to diffusion, leaching of fluorfolpet may be connected to mean free volume and chain mobility in the films. As the concentration of plasticiser in the film increases, the mean free volume increases accordingly (Borek and Osoba 1996a and 1996b), as does the chain mobility, as demonstrated by the decreasing Tg (see **table 5. 5.**).

Table 5. 5. Glass transition temperatures as a function of DOP content.

DOP (%)	Tg (°C)
10	32.6
15	22.5
20	12.3
25	1.8
30	-8.5

The degree of leaching of fluorfolpet from the film is most probably related to its solubility in water (15 ppm) in that, as more water penetrates the film, a larger amount of PA3 dissolves in the penetrant and leaches out. In chapter 6., we showed that the water content at equilibrium is strongly dependent upon the level of plasticiser in the film. Riquet and co-workers in their study of the diffusion of fatty and aqueous liquids into rigid PVC propose that penetrant diffusion activates the migration of the additives, by mobilising the small molecules which then rapidly diffuse out of the polymer material.

From the two additives in the films, only fluorfolpet leaches out of the film. This may be explained by their difference of solubility in water. Solubility values of fluorfolpet in water and DOP as well as DOP and other phthalate esters in

water are presented in **Table 5. 6.** It shows that fluorfolpet is only slightly soluble, but DOP is totally insoluble. We can see that fluorfolpet is more soluble in DOP than in water, but still leaching is occurring. At 5% of total weight concentration, the concentration of PA3 in the film exceeds largely its solubility value in DOP. Furthermore, at high concentration of DOP (30%), precipitation and agglomeration of fluorfolpet was observed, in one sample within 7 days from the sample preparation. This suggests that the fluorfolpet molecules in the film are not just dissolved in the plasticiser, but dispersed in the polymer matrix.

The decrease in fluorfolpet leaching at 25% DOP concentration and higher may be explained by one or all of the following :

- decrease in mean free volume brought about by the occupation of the free volume sites by a plasticiser excess,
- “antiplasticisation” of the films (antiplasticisation is discussed in some detail in chapter 6.),
- decreasing water content of the films.

Table 5. 6. Solubility of fluorfolpet and phthalate esters in water (Simonds et al. 1949,).

Compounds	Solubility in water	Solubility in DOP
Fluorfolpet	15 ppm	~2% by wt
Dimethylphthalate	0.43% by wt	-
Diethylphthalate	0.09% by wt	-
Dipropylphthalate	0.015% by wt	-
Dibutylphthalate	0.001% by wt	-
Diocetylphthalate	insoluble	-

5. 3. DEPTH PROFILING

5. 3. 1. Method

To obtain a depth profile of a given film the following steps are needed :

(i) the instrument was set in confocal mode, with the relevant parameters :

- using the x100 objective,
- choosing the size of the camera to match an area of 576 x 5 pixels,
- closing the instrument slit to 10 μm .

This results in a spatial resolution of about 2 μm , as demonstrated in chapter 2.

The power of the laser reaching the sample is 5 mW.

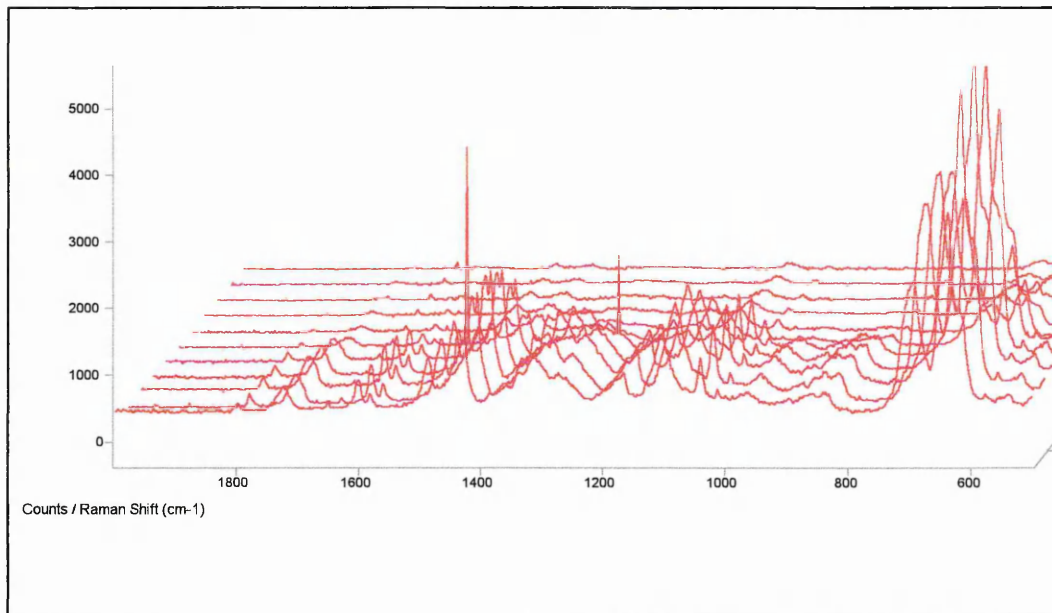
(ii) the depth profile was either started at the top or the bottom of the film, spectra were taken at intervals of 2 μm , over the range 500 - 2000 cm^{-1} , with a total exposure of 2 x 200 sec.

(iii) the ratios PVC/DOP and PVC/PA3 were calculated, in order to obtain the depth profile plot of PVC/DOP or PVC/PA3 versus distance in μm .

5. 3. 2. Quantitative analysis

Here again semi - quantitative analysis was achieved by calculating the mean and standard deviation of the PVC/DOP and PVC/PA3 ratios, thereby obtaining the overall level of component in the z direction.

Figure 5. 26. A typical depth-profile raw data set.

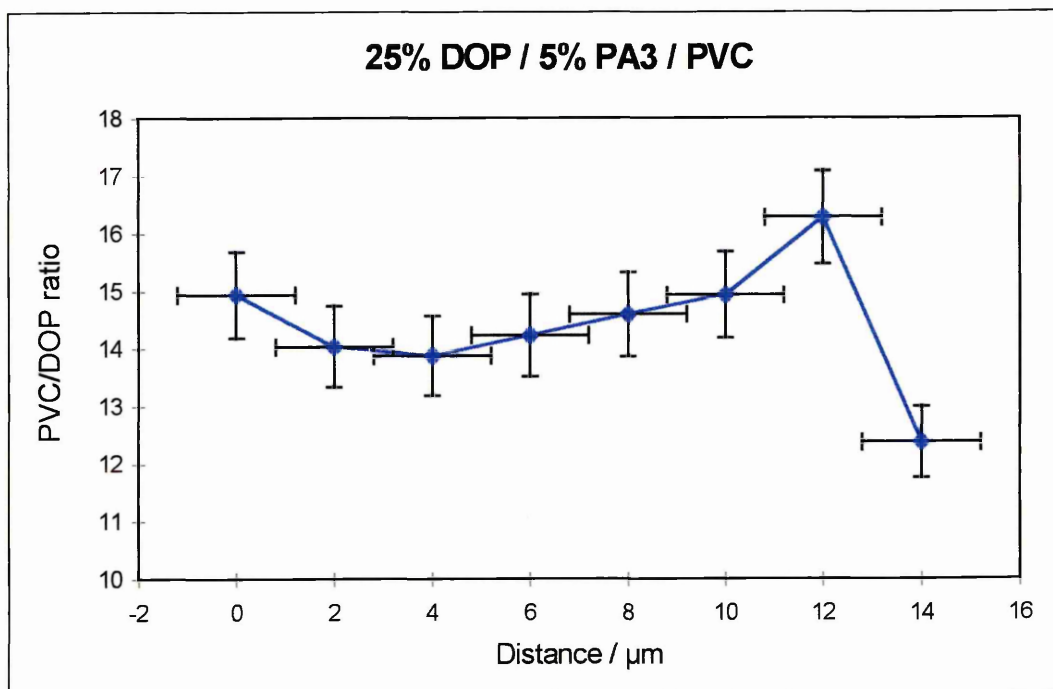


A depth profile also includes measurements of the concentration of DOP and fluorfolpet from the surface. Therefore the depth profile plots will also highlight any differences between the surface and the bulk of the film.

The intensity of the spectrum collected during a confocal experiment was much lower than the one collected with the instrument in non - confocal arrangement. This is due to the smaller amount of light collected. Furthermore the intensity of the spectrum decreased rapidly with increasing sample depth, giving rise to a decrease in S/N ratio (by about 50%), and an increase in the error of measuring the integrated intensity of the peaks (deteriorating with depth).

Figure 5. 27. shows a typical depth profile plot of the distribution of DOP showing the error bars. X error bars are derived from the volume sampled around the focus point, and Y error bars show an average of the estimated error due to integration measurement.

Figure 5.27. A typical depth profile.



5. 3. 3. Results and discussion

5. 3. 3. 1. Distribution of DOP as a function of depth

Table 5. 7. presents the depth profiling and mapping statistics for the distribution.

Table 5. 7. Depth profiling and mapping statistics for the distribution of DOP.

DOP (%)	PVC/DOP ratio from mapping	Mean value of PVC/DOP ratio from mapping	PVC/DOP ratio from depth profiling	Mean value of PVC/DOP ratio from depth profiling
10	44 ± 16 43 ± 13 46 ± 10	44	26 ± 8 32 ± 13 39 ± 8	32
10	50 ± 12 47 ± 12 55 ± 20	51	33 ± 5 35 ± 6	34
15	17 ± 3 18 ± 3 19 ± 3	18	22 ± 2	22
15	20 ± 2 19 ± 3 20 ± 2	19	22 ± 4	22
20	20 ± 4 19 ± 2 20 ± 4	19	23 ± 8 19 ± 12	21
25	13 ± 2 13 ± 2 12 ± 1	13	14 ± 1 14 ± 1	14
25	13 ± 1 13 ± 2 13 ± 2	13	15 ± 3 14 ± 2	14
25	14 ± 2 14 ± 2 14 ± 2	14	13 ± 1 16 ± 2	14
30	12 ± 1 12 ± 1 11 ± 1	12	13 ± 2 15 ± 3	14
30	11 ± 2 11 ± 2 11 ± 1	11	14 ± 1 15 ± 2	14

The standard deviation of the mean concentration of DOP within single depth profiles demonstrate the heterogeneous characteristic of the distribution of DOP in the bulk. The approximate standard deviation of a given set of data (*table 5. 7.*) may vary between 7 and 35 % (at intervals of 2 μm), but variations of more than 25 % are unusual.

The comparison of the overall concentration of DOP for each depth profile (represented by the mean value of PVC/DOP ratios per depth profile) shows that the level of DOP in the bulk is relatively invariant over the entire film.

By comparing the mean values of PVC/DOP ratios obtained from Raman mapping with the values obtained from depth profiling, it can be seen that the level of plasticiser in the bulk is marginally smaller than that on the surface of the films, except for the samples containing only 10% plasticiser. Indeed, this is also apparent from the depth profile plots in **figures 5. 28.** and **5. 29.**

Figure 5. 28. Depth profile plot of a film containing 10% DOP. 0 = film / crystal interface (B) and 12 = film / air interface (T).

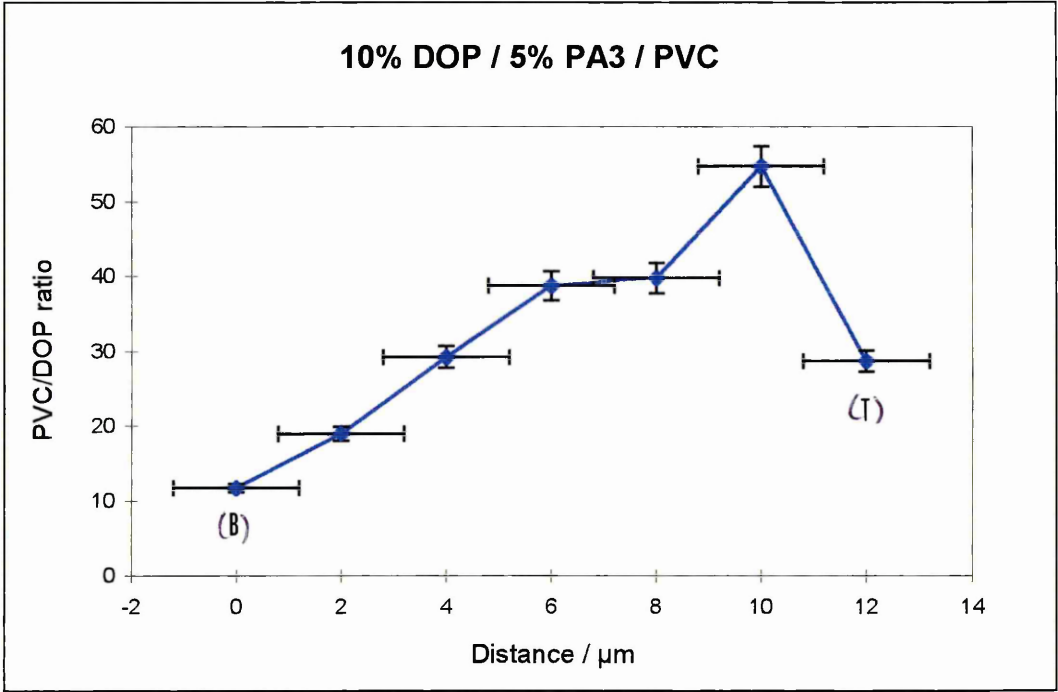


Figure 5. 29. Depth profile plot of a film containing 25% DOP. 0 = film / crystal interface (B) and 18 = film / air interface (T).

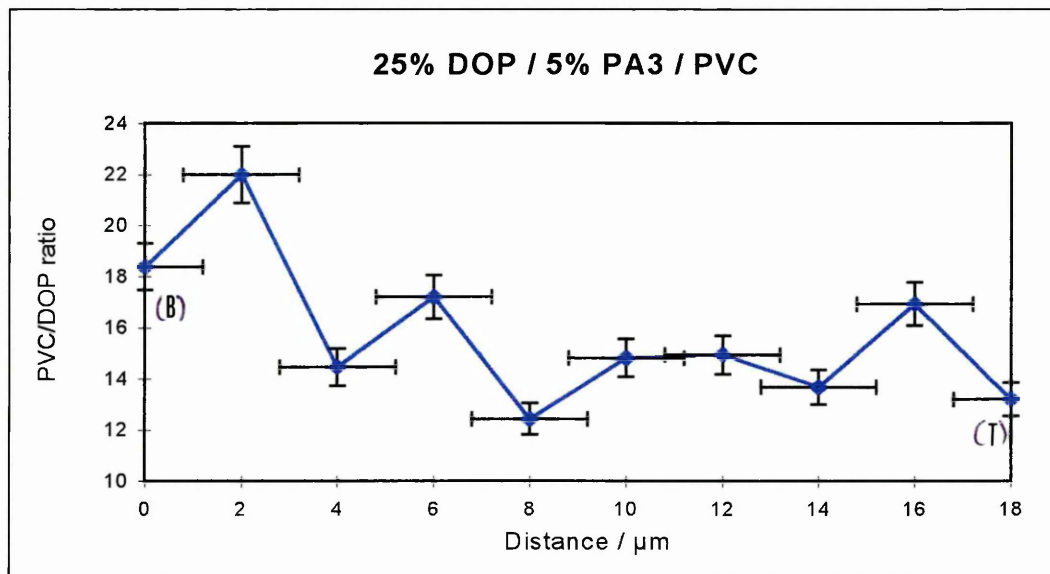
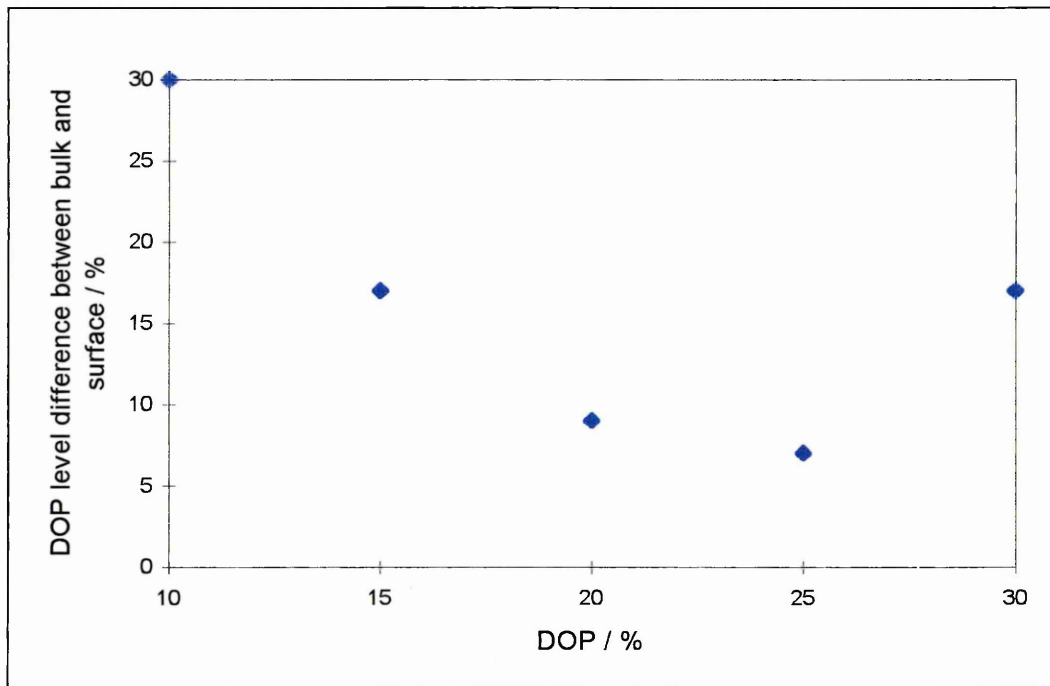


Figure 5. 30. Difference of DOP concentration between the bulk and the surface.



The difference of DOP concentration between the bulk and the surface increases as the plasticiser concentration increases to 25%, at 30% DOP in the film, it decreases again. **Figure 5. 30.** shows a plot of the difference in DOP concentration (expressed as percentage) between the bulk and the surface of

the film, as a function of total DOP concentration in the film. This shows there is an increase in the homogeneity of the film (between bulk and surface) as the plasticiser content increases to 25%, at which concentration the solubility limit or saturation of DOP in PVC is reached (Chalykh and Belokurova 1982).

5. 3. 3. 2. Redistribution of DOP due to leaching (of PA3) in water

Table 5. 8. shows the mean levels of DOP in the films (obtained from depth profiling) as a function of DOP concentration. Results before and after leaching are given.

Table 5. 8. Mean levels of DOP in the films as a function of DOP concentration.

DOP (%)	Level of DOP before leaching (as PVC/DOP ratios)	Level of DOP after leaching (as PVC/DOP ratios)
10	32	35
10	34	36
15	22	16
15	22	20
20	21	21
25	14	13
25	14	14
25	14	13
30	14	10
30	14	12

Table 5. 8. shows that the overall concentration of DOP has not changed upon redistribution. Indeed the PVC/DOP ratios remain unchanged within the experimental error, which confirms the results obtained by Raman mapping.

Table 5. 9. presents the depth profiling and mapping statistics for the redistribution (after leaching).

Table 5. 9. Depth profiling and mapping statistics for the redistribution (after leaching).

DOP (%)	PVC/DOP ratio from mapping	Mean value of PVC/DOP ratio from mapping	PVC/DOP ratio from depth profiling	Mean value of PVC/DOP ratio from depth profiling
10	53± 21 48 ± 20 48 ± 20	50	38 ± 3 33 ± 13	35
10	45 ± 9 48 ± 12 48 ± 16	47	34 ± 8 38 ± 7	36
15	12 ± 2 18 ± 2 20 ± 3	19	16 ± 3	16
15	20 ± 3 20 ± 3	20	20 ± 5	20
20	21 ± 3 20 ± 3 20 ± 5	20	25 ± 1 18 ± 3	21
25	13 ± 2 13 ± 2 13 ± 2	13	13 ± 2 13 ± 2	13
25	14 ± 3 13 ± 2 13 ± 2	13	15 ± 1 14 ± 2	14
25	15 ± 2 15 ± 2 15 ± 2	15	14 ± 2 11 ± 2	13
30	11 ± 1 10 ± 2	10	10 ± 2 11 ± 2	10.5
30	12 ± 1 12 ± 1 12 ± 2	12	13 ± 2 12 ± 2	12.5

The standard deviation of the mean concentration of DOP within single depth profiles demonstrate the heterogeneous characteristic of the distribution of DOP in the bulk after treatment with water. The approximate standard deviation of a given set of data (**table 5. 9.**) may vary between 2 and 45 % (at intervals of 2 µm), but variations of more than 25 % are unusual.

The comparison of the overall concentration of DOP for each depth profile (represented by the mean value of PVC/DOP ratios per depth profile) shows that the level of DOP in the bulk is relatively invariant over the entire film.

There is very little difference in DOP concentration (about 5 to 7% which is of the order of the estimated experimental error) between the bulk and the surface in the majority of the films (see **Figure 5. 31.**). Films containing 10% DOP still show a large difference between the bulk and the surface concentration, of the order of 25% ; the amount of plasticiser is higher in the bulk than on the surface (see **Figure 5. 32.**).

Figure 5. 31. Depth profile plot of a sample containing 25% DOP . 0 = film / air interface (T) and 18 = film / crystal interface (B).

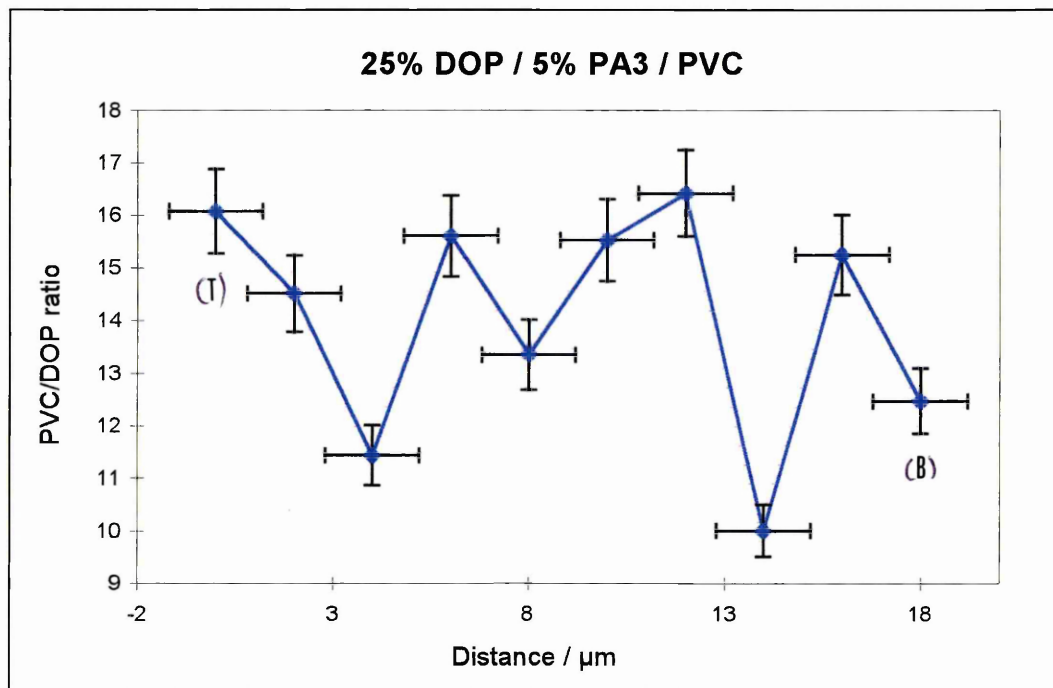
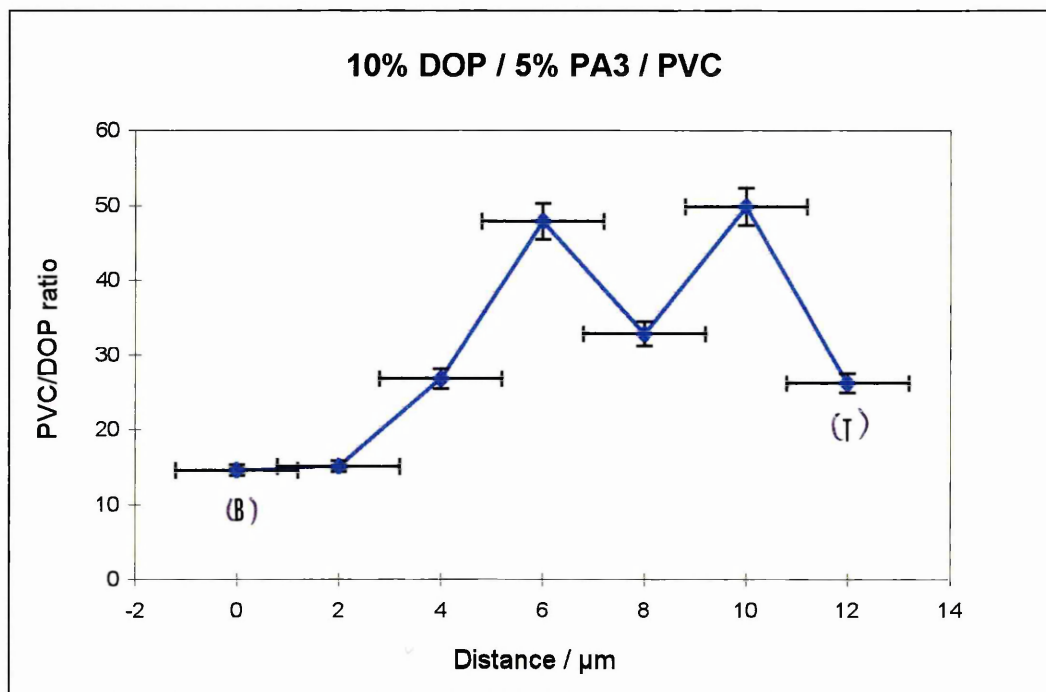


Figure 5. 32. Depth profile plot of a sample containing 10% DOP . 0 = film / crystal interface (B) and 12 = film / air interface (T).



For films containing more than 10% (in weight) DOP, we can see that a redistribution of the molecules has taken place during ingress and removal of water ; we observe a more homogeneous distribution of DOP between the surface and the bulk of the film. As water diffuses into the films and creates additional free volume and chain mobility by swelling and plasticisation of the polymer matrix, small molecules are able to move more freely inside the matrix. Also leaching of fluorofolpet from the films provides extra voids (or void space) for the plasticiser.

All the experiments were carried out at ambient temperature (20 - 26°C) and at 10% DOP concentration. The glass transition temperatures of these films is 32.6°C, and therefore the polymer was in the glassy state, whereas for the films containing 15% or more DOP, the glass transition temperature is below 22 °C. Flexibility and chain mobility is increased in the rubbery state compared to the glassy state, and therefore it is plausible to suggest that the heterogeneity of the distribution of DOP between the bulk and the surface is a consequence of the lack of mobility of the molecules in the polymeric matrix.

5. 3. 3. 3. Distribution of fluorfolpet as a function of depth

Table 5. 10. presents the depth profiling and mapping statistics for the distribution.

Table 5. 10. Depth profiling and mapping statistics for the distribution.

DOP (%)	PVC/PA3 ratio from mapping	Mean value of PVC/PA3 ratio from mapping	PVC/PA3 ratio from depth profiling	Mean value of PVC/PA3 ratio from depth profiling
10	64 ± 17 62 ± 12 65 ± 13	64	46 ± 18 53 ± 19 58 ± 8	52
10	79 ± 26 58 ± 13 74 ± 32	70	68 ± 14 63 ± 6	65
15 ^(b)	217 ± 63 212 ± 67 156 ± 49	195	259 ± 105	259
15 ^(b)	122 ± 46 115 ± 41 127 ± 51	121	143 ± 40	143
20	86 ± 20 77 ± 20 82 ± 17	82	86 ± 43 72 ± 50	79
25	67 ± 24 68 ± 19 61 ± 14	65	70 ± 11 56 ± 23	63
25	56 ± 14 57 ± 14 58 ± 11	57	54 ± 13 71 ± 10	62
25	110 ± 48 113 ± 30 97 ± 26	107	90 ± 50 99 ± 30	94
30 ^(a)	21 ± 1 22 ± 2 20 ± 2	21	18 ± 4 28 ± 8	23
30 ^(a)	38 ± 7 37 ± 7 40 ± 3	38	45 ± 14 41 ± 3	43

^(a) fluorfolpet crystallised out.

^(b) much higher ratios were obtained possibly through the use of a different instrument to the other measurements.

The standard deviation of the mean concentration of fluorfolpet within single depth profiles demonstrates the heterogeneous characteristic of the distribution of the biocide in the bulk. The level of fluorfolpet may vary between 4 and 60 % at intervals of 500 μm , but a typical variation from position to position is of the order of 20 %.

The comparison of the overall concentration of fluorfolpet per sample (represented by the mean value of PVC/DOP ratios per depth profile) shows that the level of PA3 in the bulk is similar over the entire film. This high-lights the homogeneous characteristic of the macroscopic distribution of fluorfolpet in PVC.

Comparison between the average DOP level on the surface and in the bulk (i.e. between mapping and depth profiling) yields two types of films :

- (i) when DOP concentration is lower than or equal to 15% , then there is a difference of about 15% in the biocide loading between the surface region and the bulk of the film; at 10% DOP loading there is more PA3 in the bulk than on the surface, whereas at 15% DOP loading, the opposite is true (see **Figure 5. 33.** and **5. 34.**)
- (ii) when DOP concentration is higher than or equal to 20%, when there is no noticeable difference between the level of fluorfolpet in the bulk and on the surface, i.e. no segregation between the two region.

Depth profiles plots may show a slightly higher concentration of PA3 near the bottom of the film, as can be seen in **figure 5. 35.** in a film containing 20% DOP.

Figure 5. 33. Depth profile plot of a film containing 10% DOP. 0 = film / crystal interface (B) and 12 = film / air interface (T).

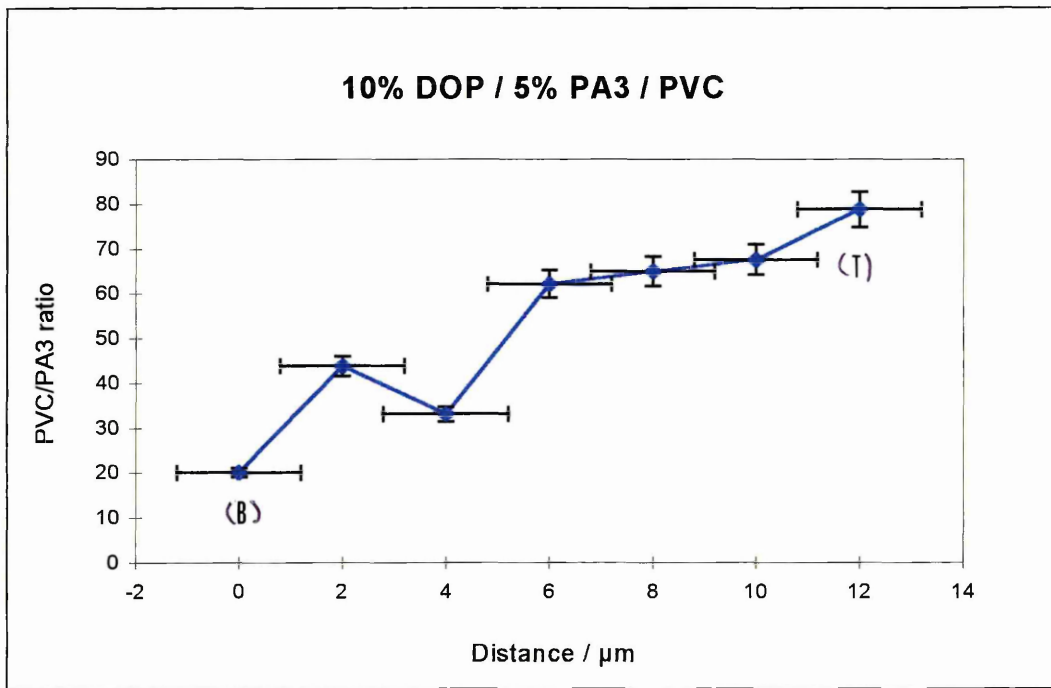


Figure 5. 34. Depth profile plot of a film containing 10% DOP. 0 = film / crystal interface (B) and 12 = film / air interface (T).

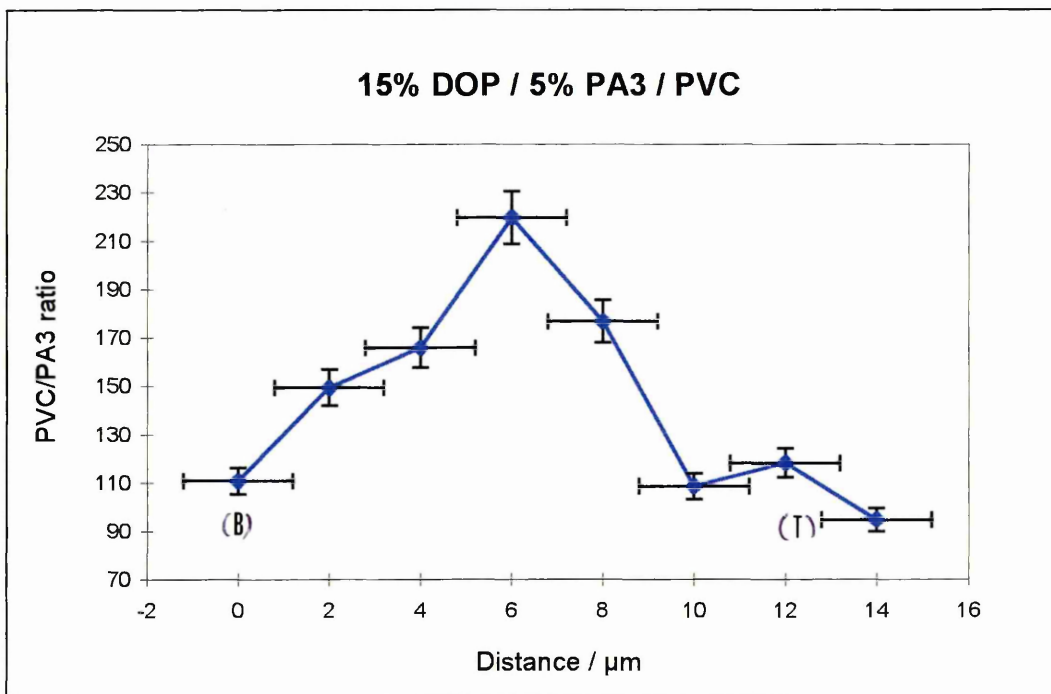
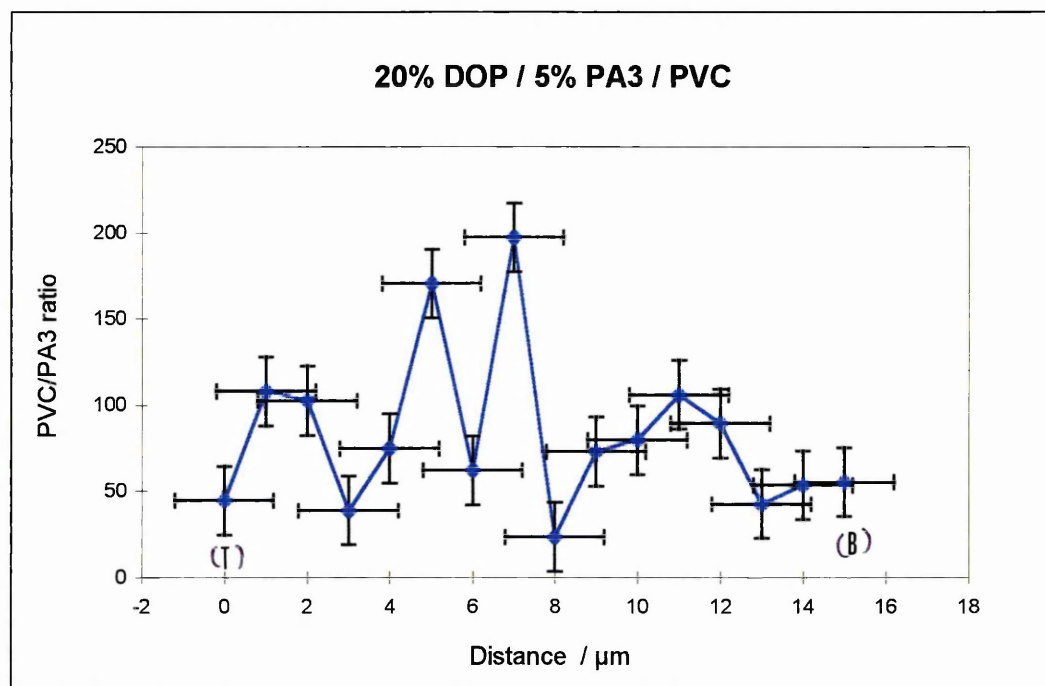


Figure 5. 35. Depth profile plot of a film 20% DOP. 0 = film / air interface (T) and 15 = film / crystal interface (B).



The difference in distribution of fluorfolpet between films containing 10 and 15% DOP, and the ones containing 20, 25 and 30% DOP may be explained by the increase of PA3 solubility in the polymer matrix as the T_g is lowered and more free volume introduced, or by the difference in state the polymer matrix is in ; glassy or rubbery. In the glassy polymer the ratio of crystalline to amorphous ratio is larger than in the rubbery polymer. Plasticisation and diffusion are phenomenon taking place in the amorphous region only (Tabb and Koenig 1975, Tsou and Geil 1972). Amorphous regions surround crystalline regions (Theodorou and Jasse 1983), therefore the higher the crystallinity the bigger the heterogeneity.

5. 3. 3. 4. Redistribution as a function of depth of fluorfolpet due to leaching

Leaching is performed according to the method described in section 2 chapter 4.

Table 5. 11. shows the mean levels of fluorfolpet in the films (obtained from depth profiling) as a function of DOP concentration. Results before, after and the difference in overall level between the two are given.

Table 5. 11. Mean levels of fluorfolpet in the films (after and before leaching).

DOP (%)	Level of PA3 before leaching (as PVC/PA3 ratio)	Level of PA3 after leaching (as PVC/PA3 ratio)	Difference in PA3 level between before and after (%)
10	52 ± 5	49 ± 10	+6
10	65 ± 2	64 ± 10	+2
15	143 ± 40	146 ± 37	-2
20	79 ± 7	104 ± 2	-24
25	63 ± 7	72 ± 14	-14
25	62 ± 8	65 ± 4	-4
30	43 ± 2	43 ± 2	-1

Table 5. 11. shows that fluorfolpet was removed from the films containing 20 and 25% DOP, but at 10, 15 and 30% DOP content the experiment does not allow us to conclude that leaching has occurred ; variations obtained were smaller than the estimated experimental error. The positive difference in PA3 content after the leaching at 10% DOP concentration suggests that redistribution but not leaching (or uptake, which is impossible) has occurred.

Figure 5. 36. shows a plot of percentage fluorfolpet leached versus DOP concentration in the film.

This confirms the results obtained from mapping. A more in depth study of the individual profiles is needed to determine if leaching is a surface or bulk phenomenon.

Figure 5. 36. A plot of percentage fluorfolpet leached versus DOP concentration in the film.

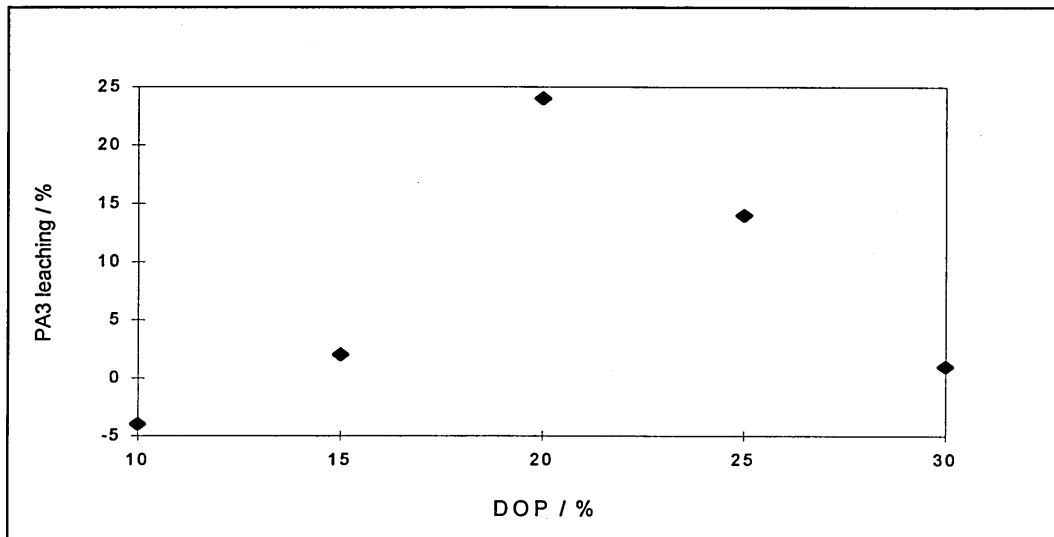


Table 5. 12. presents the depth profiling and mapping statistics for the redistribution of fluorfolpet.

DOP (%)	PVC/PA3 ratio from mapping	Mean value of PVC/PA3 ratio from mapping	PVC/PA3 ratio from depth profiling	Mean value of PVC/PA3 ratio from depth profiling
10	71 ± 21 68 ± 17 64 ± 14	68	49 ± 13	49
10	71 ± 18 62 ± 15 82 ± 22	72	54 ± 9 74 ± 18	64
15 ^(b)	150 ± 76 141 ± 51	145	146 ± 37	146
20	119 ± 57 108 ± 53 97 ± 26	108	106 ± 35 103 ± 46	104
25	74 ± 16 93 ± 33 85 ± 21	84	72 ± 14	72
25	79 ± 18 71 ± 23 68 ± 18	73	69 ± 22 61 ± 10	65
30 ^(a)	23 ± 3 25 ± 3	24	45 ± 5 5 ± 1	-
30 ^(a)	42 ± 6 43 ± 6 42 ± 6	42	45 ± 13 42 ± 9	43

^(a) fluorfolpet crystallised out.

^(b) much higher ratios were obtained possibly through the use of a different instrument to the other measurements.

As before treatment of the film with water, it can be seen that we have a heterogeneous microscopic distribution, and a fairly homogeneous macroscopic distribution of the fluorfolpet in the films, independently of their concentration in DOP.

When comparing the average amount of fluorfolpet present in the bulk and on the surface (i.e. PVC/PA3 ratios from depth profiling and mapping), see **table 5. 12.** and **figure 5 .39.**, one can see at once that the concentration of fluorfolpet is higher in the bulk than on the surface. **Figures 5. 37.** and **5. 38.** show two depth profile plots of 10 and 25% plasticised films. These plots show that the region from which the fluorfolpet was removed is the surface region, but also that this region may extend slightly from what was defined as surface in **figure 5. 2.** It is also apparent from the profiles that the amount of fluorfolpet removed decreases with depth. We can therefore conclude that leaching first happens on the surface at the film / liquid interface, and progressively either the PA3 molecules move towards the surface, or are directly removed from lower depths in the film. These finding are in total agreement with Murase and co-workers (Murase et al. 1993) on the migration of plasticiser from heat degraded PVC films.

Figure 5. 37. Depth profile plot of a film containing 10 % DOP. 0 = film / crystal interface (B) and 8 = film / air interface (T).

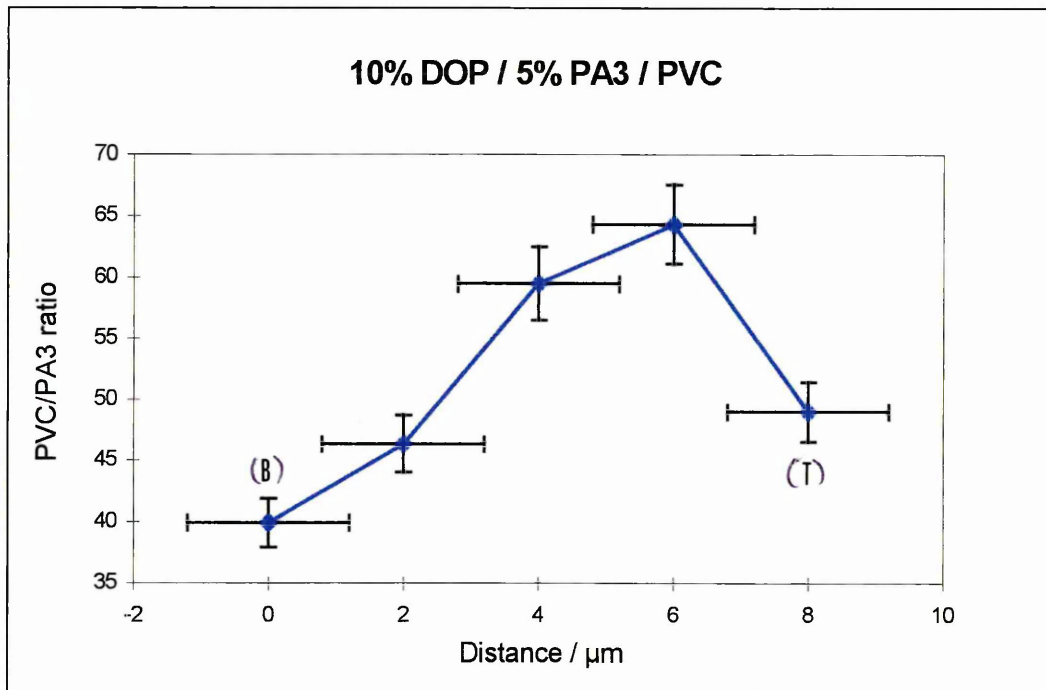
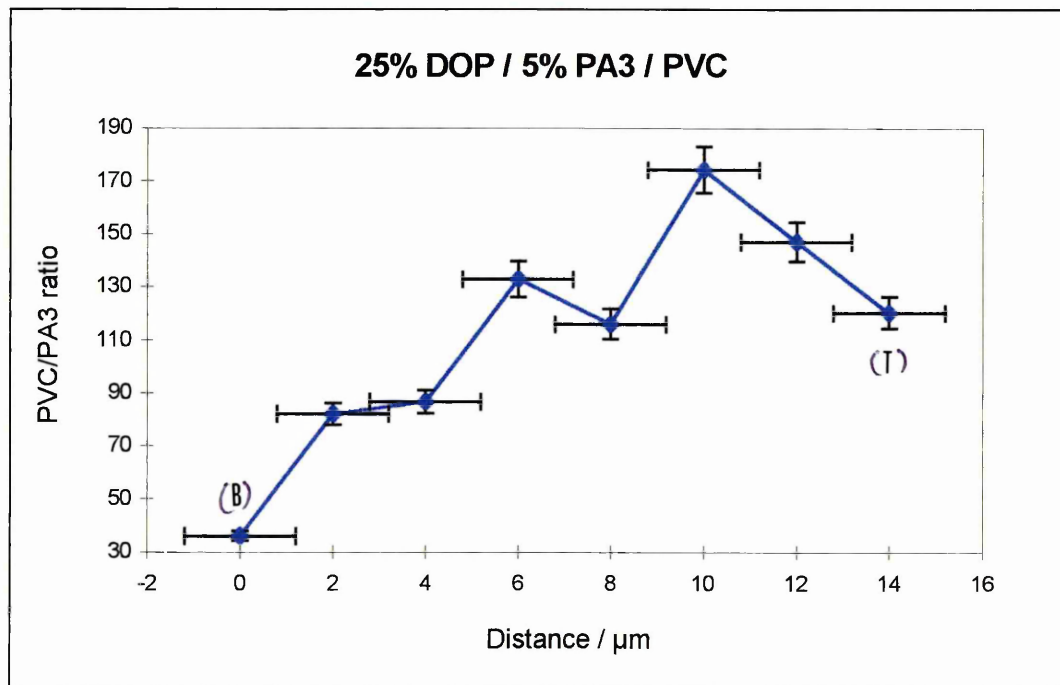
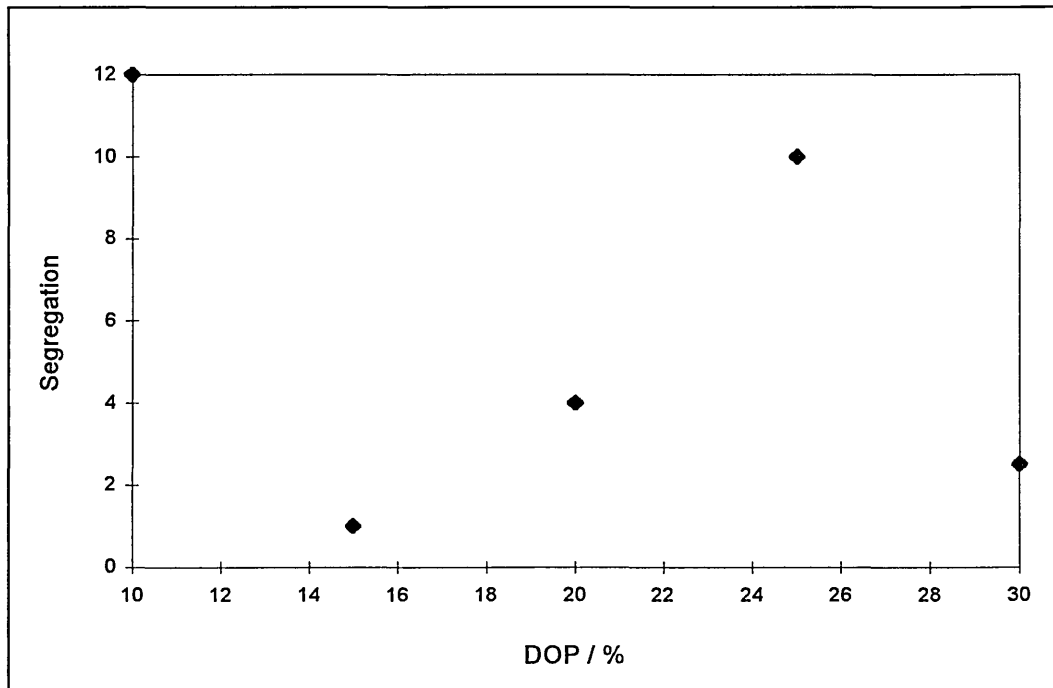


Figure 5. 38. Depth profile plot of a film containing 25 % DOP. 0 = film / crystal interface (B) and 14 = film / air interface (T).



Samples with 15% DOP show a quite different behaviour one from the other ; one sample shows an important segregation between the bulk and the surface, whereas the other one demonstrates no significant difference in concentration throughout the film. At 15% DOP concentration the films have a Tg of 22.5°C. Therefore, depending on the ambient temperature on the day of the experiment, the film might have been in the glassy or rubbery state. By comparison with films containing 10% DOP, it is clear that the film showing a high concentration difference between the bulk and the surface, was in the glassy state when the experiment was performed.

Figure 5. 39. shows the segregation between the surface and the bulk of the films due to leaching of the fluorfolpet molecules. Segregation is expressed as the difference in percentage of the overall level of fluorfolpet from mapping and depth profiling.



Segregation is high around 20 and 25% and low at 30% DOP concentration. Segregation is more important at concentrations at which leaching is more important, showing that leaching is more rapid than the migration of fluorfolpet inside the film (Murase et al. 1993).

5. 4. CONCLUSION

The results shown in this chapter have demonstrated the potential of Raman depth profiling and especially Raman mapping as a tool for the study of molecular distribution and leaching. The following information on the distribution and leaching of DOP and fluorfolpet has been drawn from the above results :

- The distribution of both dioctylphthalate and fluorfolpet were found to be heterogeneous on a microscopic level, but homogeneous on a macroscopic scale. This was true for both the bulk and the surface, and before and after leaching of fluorfolpet.
- There was segregation of the DOP distribution (i.e. concentration) between the bulk and the surface of the film before leaching of fluorfolpet, followed by a redistribution of the molecules after leaching of fluorfolpet molecules. No segregation between the distribution of DOP in the bulk and on the surface was noticed after leaching.
- No segregation between bulk and surface distribution was noticed for fluorfolpet before leaching.
- The redistribution of fluorfolpet molecules in the films (from mapping and depth profiling) showed that leaching is strongly dependent upon the plasticiser concentration or amount of water penetrating the film. It was demonstrated that leaching could be a consequence of :
 - (i) excess number of fluorfolpet molecules in the film,
 - (ii) solubility of fluorfolpet in water,
 - (iii) chain mobility and free volume parameters of the film. Indeed leaching was more important in those films where chain mobility and free volume were the highest.
- Leaching yielded strong differences of fluorfolpet concentration between the bulk and the surface of the sample, the surface showing a much weaker concentration of PA3. This clearly demonstrated that leaching occurred from the surface, i.e. from the film/solvent interface.

5. 5. REFERENCES

Borek J., Osoba W., *J. of Radioanal. and Nuclear Chem.*, 1996a, **211**(1), 61.

Borek J., Osoba W., *J. of Polym. Sci.*, 1996b, **34**(11), 1903.

Chalyk A. E., Belokurova A. P., *Izvestiya vysshikh uchebnykh zavedenii khimiya i khimicheskaya tekhnologiya*, 1982, **25**(5), 607.

Fayad N. M., Sheikheldin S. Y., Al-Malack H., El-Mubarak A. H., Khaja N., *J. of Env. Sci. and Health part A - Env. Sci. and Eng.*, 1997, **32**(4), 1065.

Figge K., *Prog. in Polym. Sci.*, 1980, **6**, 187.

Messadi D., Gheid A. E. H., *Eur. Polym. J.*, 1994, **30**(2), 167.

Messadi D., Vergnaud J. M., *J. of Appl. Polym. Sci.*, 1982, **27**, 3945.

Messadi D., Vergnaud J. M., *Eur. Polym. J.*, 1997, **33**(7), 1167.

Murase A., Sugiura M., Araga T., *Polym. Degrad. and Stability*, 1994, **43**, 415.

Riquet A. M., Sandray V., Akermann O., Feigenbaum A., *Science des Aliments*, 1991, **11**, 341.

Simonds, Weith, Bigelow, *Handbook of Plastics*, Norstrand, second edition, 1949.

Tabb T. L., Koenig J. L., *Macromolecules*, 1975, **8**, 929.

Taverdet J. M., Hivert M., Vergnaud J. M., *Abstract of Papers from the American Chem. Soc.*, 1982, 184, P8-orpl.

Tsou P. K., Geil P. H., *J. of Int. Polym. Mat.*, 1972, **1**, 223.

Vergnaud J. M., *Macromol. Symp.*, 1994, **84**, 377.

CHAPTER 6. :
HYDRATION AND DEHYDRATION OF
PLASTICISED PVC FILMS.

CONTENTS

CHAPTER 6. : HYDRATION AND DEHYDRATION OF PLASTICISED PVC FILMS.....	197
6. 1. INTRODUCTION.....	199
6. 2. HYDRATION OF PLASTICISED PVC FILMS.....	200
6. 2. 1. Determination of the diffusion coefficients using the dual - mode sorption model.....	202
Diffusion coefficients :	204
Equilibrium water content of PVC films	208
Swelling of the matrix	211
6. 2. 2. Determination of the diffusion coefficients using sorption kinetics, and Fick's second law	215
6. 2. 3. Conclusions.....	221
6. 3. DEHYDRATION OF PLASTICISED PVC FILMS.....	224
Diffusion rates	226
Shrinking of the polymer matrix.....	228
Conclusion	231
6. 4. REFERENCES.....	232

CHAPTER 6. : HYDRATION AND DEHYDRATION OF PLASTICISED PVC FILMS.

6. 1. INTRODUCTION

Although the diffusion of organic solvents and vapours into rigid and plasticised PVC films (Okuno et al. 1995a and 1995b, Park and Bontoux 1993, Berens 1989, Jenke 1993, Coughlin et al. 1991, Messadi et al. 1991, Perry et al. 1991 and 1994, Valtier et al. 1995, Ercken et al. 1995, Berens and Hopfenberg 1982, Taverdet et al. 1982, Cherry and Yue 1986) has been widely studied, as has the diffusion of foodstuff related liquids (Badeka and Kontominas 1996, Fayad et al. 1997, Hammarling et al. 1988, Goulas et al. 1998 and 1995, Petersen and Breindahl 1998, Riquet et al. 1991, Messadi and Gheid 1994, Vergnaud 1996, Kalaouzis and Demertzis 1993), much less attention has been given to the sorption and desorption of liquid water into PVC films (Marian et al. 1970, Armstrong et al. 1990, Stauffer et al. 1981, Bouzon and Vergnaud 1991, Li et al. 1996a and 1996b, Kalaouzis and Demertzis 1993, Messadi and Gheid 1994, Chan et al. 1992). Transport of water vapour (Okuno et al. 1995b and 1993, Shailaja and Yaseen 1993) in plasticised PVC matrixes also received only a small amount of attention.

But many PVC applications involve contact of the polymer with water, as for example shower curtains or water bottles, water distribution systems, food wrappings, ion - selective membranes, etc. Therefore, an investigation of the hydration and dehydration of PVC systems by FTIR - ATR spectroscopy was conducted, and results of the investigation are presented in this chapter.

Two categories of samples were examined :

- DOP / PVC films,
- DOP / fluorfolpet (PA3) / PVC films.

All samples were prepared following the method given in chapter 4. These are the same samples which were used to explore the distribution and redistribution of fluorfolpet and DOP in PVC films by Raman microscopy.

6. 2. HYDRATION OF PLASTICISED PVC FILMS

Details of the FTIR - ATR experimental set-up can be found in chapter 4. The uptake of water by the film was monitored using the (O-H) stretching band of water between 2950 and 3700 cm^{-1} . As water diffuses into the film the $\nu(\text{O-H})$ stretching band grows, as can be seen in **figure 6. 1.**

By comparing the spectra of water as it diffuses into the polymer (see **figure 6. 2.**), it is obvious that (a) the shape of the water spectrum in the 3000 to 3600 cm^{-1} region varies as a function of time. The shoulder at 3200 cm^{-1} grows more quickly than the main band at 3400 cm^{-1} ; (b) there is a slight shift of the band position, with time, towards the lower wavenumbers, indicating a strengthening of the water hydrogen bond network. The electronic perturbation of water molecules absorbed in PVC films is discussed further in chapter 7.

Figure 6. 1. and **6. 2.** show the infrared spectra for water diffusing into a 20% DOP / 5% PA3 / PVC polymer film as a function of time.

Figure 6. 1. Infrared spectra for water diffusing into a 20% DOP / 5% PA3 / PVC film (overlaid).

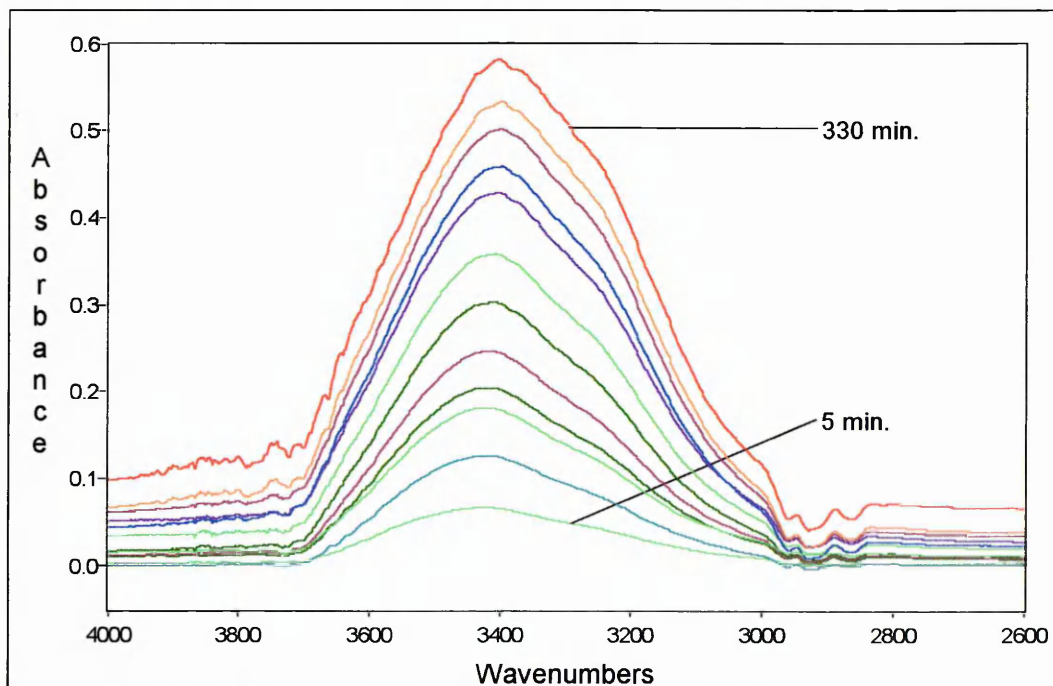
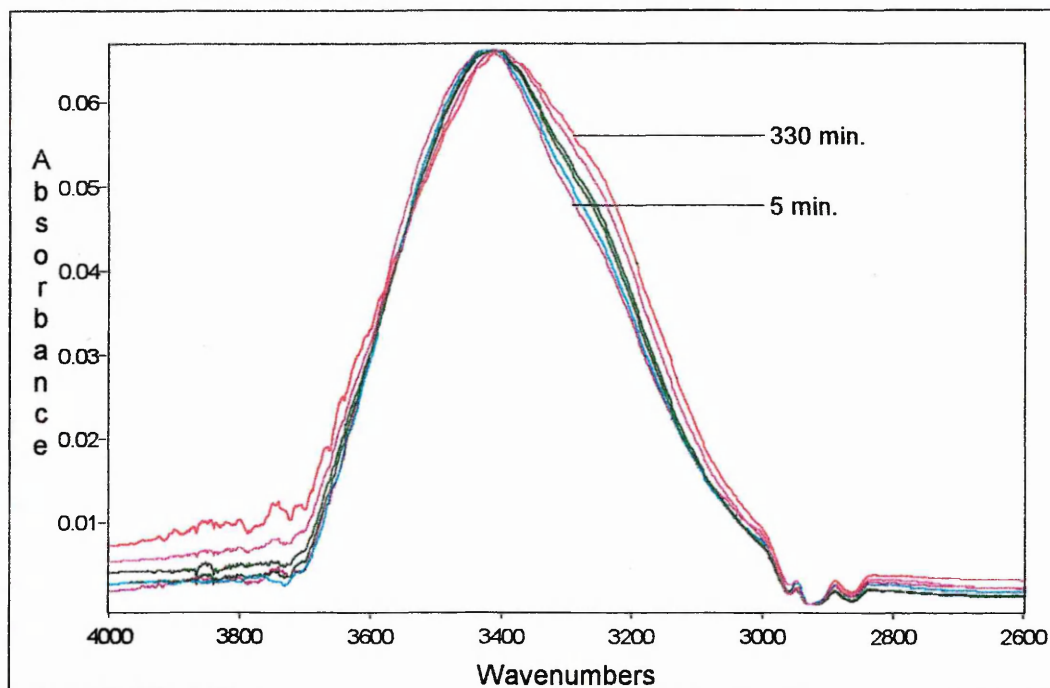
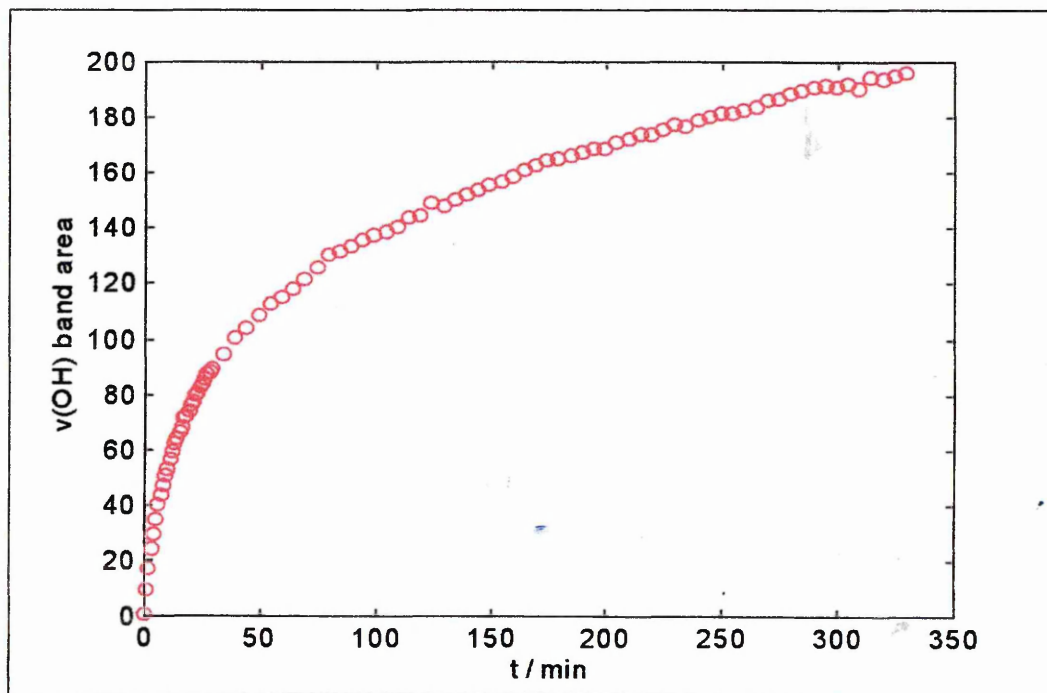


Figure 6. 2. Infrared spectra for water diffusing into a 20% DOP / 5% PA3 / PVC film (superimposed).



The plot of the integrated area under the $\nu(\text{OH})$ stretching band of water versus time yields the diffusion curve (**Figure 6. 3.**).

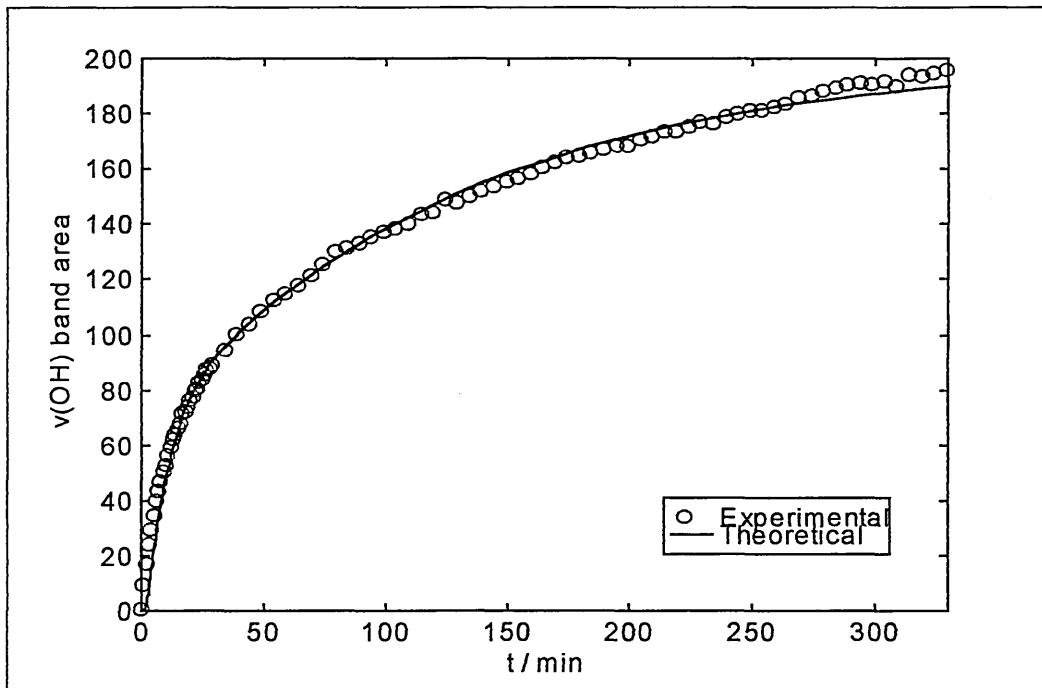
Figure 6. 3. A plot of the diffusion curve of water into a 20% DOP / 5% PA3 / PVC film.



6. 2. 1. Determination of the diffusion coefficients using the dual - mode sorption model

Okuno and co-workers and Li, Chan and co-workers (Okuno et al. 1995a and 1995b, Li et al. 1996a and 1996b, Chan et al. 1992) previously found that the absorption of water (liquid or vapour) into PVC is well described by the dual-mode sorption model. A dual-mode sorption model was therefore used to determine the diffusion coefficients D_1 and D_2 of water diffusing into the PVC samples. Descriptions of the model are given in chapter 3. and chapter 4., along with the mathematical treatment. The fitting procedure yields a theoretical diffusion curve that is described by the following parameters; a diffusion coefficient, D , a constant k_d , $k_d \times D$ gives the second diffusion coefficient, and X_1 the fraction of partially mobile molecules of water in the system (see **figure 6. 4.**).

Figure 6. 4. Shows the results obtained by a typical fitting procedure on the diffusion of water into a 20% / 5% PA3 / PVC film.



(NB : Equilibrium was not reached after 330 min., but it was shown by Sammon (Sammon 1997) that the result of the fitting procedure was not influenced by the sorption equilibrium not being reached.)

Tables 6. 1. and **6. 2.** present the values of the diffusion coefficients obtained using this method for the diffusion of water into DOP / PVC and DOP / fluorfolpet / PVC films respectively as a function of DOP concentration. (The concentration of fluorfolpet in the DOP / fluorfolpet / PVC films is always of 5%^{w/w}).

Table 6. 1. Diffusion coefficients for water into DOP / PVC films.

SAMPLE NO	% DOP	Tg (°C)	D ₁ (cm ² /s)	D ₂ (cm ² /s)
29	0	63.6	2.2e-8	2.6e-9
53	0	63.6	2.84e-8	2.51e-9
56	0	63.6	2.09e-8	3.30e-9
38	10	43.2	1.59 e-8	9.03e-10
58	15	36.5	4.16e-8	3.63e-9
59	15	36.5	2.54e-8	2.36e-9
28	20	20.4	9.7e-8	4.6e-9
60	25	18.2	8.62e-8	8.09e-9
61	25	18.2	6.35e-8	6.48e-9
33	30	-2.3	4.59e-8	3.25e-9
57	30	-2.3	9.12e-8	8.59e-9

Table 6. 2. Diffusion coefficients for water into DOP / 5% fluorfolpet / PVC films.

SAMPLE NO	% DOP	Tg (°C)	D ₁ (cm ² /s)	D ₂ (cm ² /s)
39	10	32.8	5.05e-8	2.95e-9
40	10	32.8	3.91e-8	3.87e-9
41	10	32.8	5.54e-8	3.69e-9
52	15	22.5	3.92e-8	3.25e-9
54	15	22.5	4.88e-8	3.82e-9
21	20	12.3	1.19e-7	8.7e-9
22	20	12.3	1.93e-7	1.42e-8
24	20	12.3	1.30e-7	9.3e-9
25	20	12.3	1.87e-7	1.55e-8
50	25	1.8	5.10e-8	4.42e-9
51	25	1.8	6.37e-8	6.00e-9
27	30	-8.5	1.11e-7	8.9e-9
35	30	-8.5	9.24e-8	8.45e-9
47	30	-8.5	2.32e-8	2.05e-8

Diffusion coefficients :

Figures 6. 5. and 6. 6. show a plot of diffusion coefficients against DOP concentration and Tg for DOP / PVC and DOP / PA3 / PVC films.

Table 6. 3. lists glass transition temperatures of the polymers obtained from DSC measurements (Perkin Elmer DS7). The measurements are courtesy of Paul Rainsford (Zeneca Specialties, Manchester).

Figure 6. 5. A plot of diffusion coefficients against DOP concentration and Tg for DOP / PVC films.

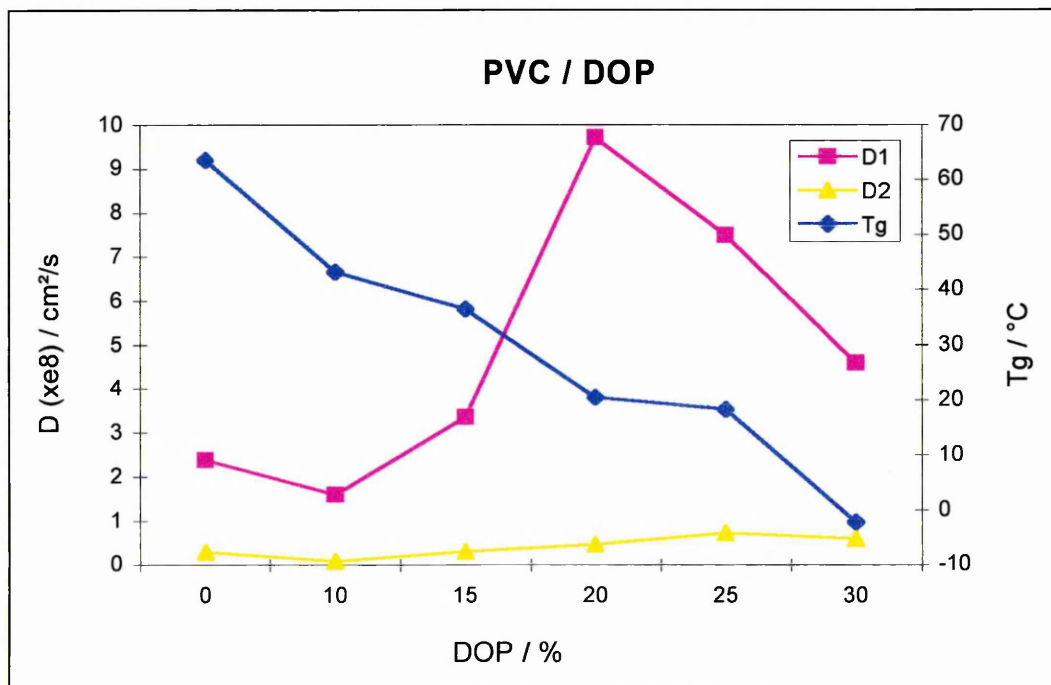
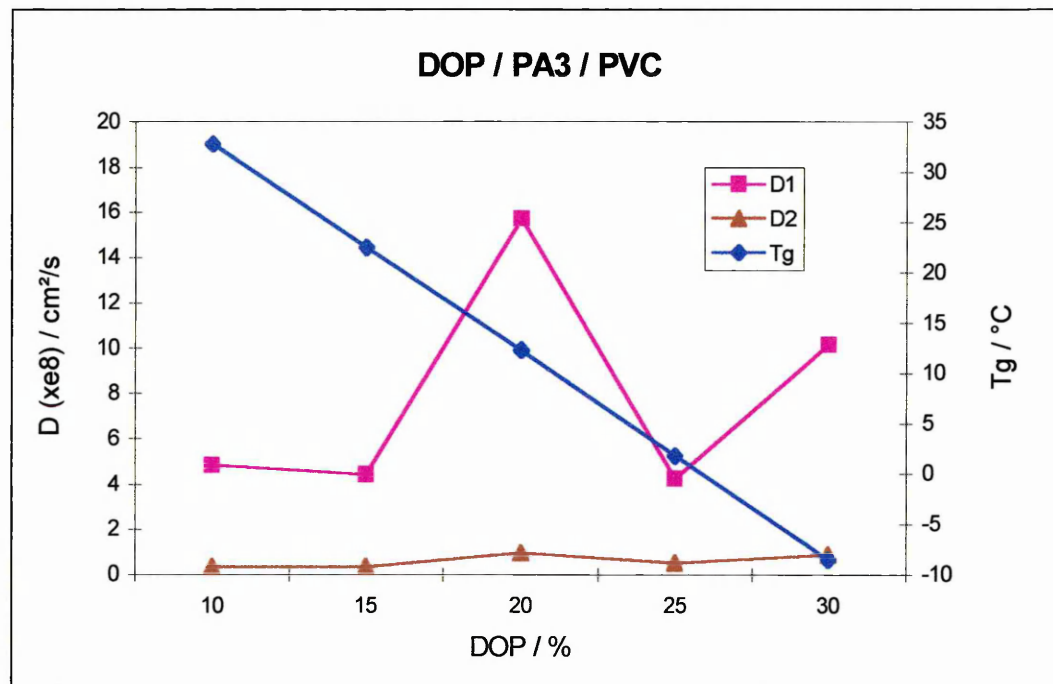


Table 6. 3. Glass transition temperatures of the polymers.

DOP (%)	Tg (°C), in DOP / PVC films	Tg (°C), in DOP / PA3 / PVC
0	63.6	-
10	43.2	32.6
15	36.5	22.5
20	20.5	12.3
25	18.2	1.8
30	-2.3	-8.5

Figure 6. 6. A plot of diffusion coefficients against DOP concentration and Tg for DOP / PA3 / PVC films.



As can be seen from **tables 6. 1.** and **6. 2.**, the rate of diffusion of water into pPVC films is dependent upon the amount of plasticiser in the film. Taverdet and co-workers (Taverdet et al. 1982) also found that the diffusion coefficients of alkanes (n-heptane, n-nonane) into pPVC were dependent on the plasticiser concentration. The rate of diffusion reaches a maximum at 20% DOP content, in both cases DOP / PVC and DOP / PA3 / PVC films. (See **figures 6. 5.** and **6. 6.**).

The presence of plasticiser in the PVC membranes lowers the Tg of the membrane (see **table 6. 3.**) ; the chain mobility is enhanced, and leads to an increase in the free volume, which can be measured using PAS (Positron Annihilation Spectroscopy) (Jean 1993, Borek and Osoba 1996a , 1996b). Borek and Osoba showed that the amount of free volume increases linearly as the concentration of dioctylphthalate increases. Hence permeation rates should increase with increasing level of plasticiser (0 - 30% in wt), as observed by Shailaja and Yaseen (Shailaja and Yaseen 1993) for the permeation of water vapour through PVC membranes.

However, others have shown in their studies on the diffusion of di-n-alkylphthalates in PVC (Griffiths et al. 1984) that for higher alkyl group phthalates, the free volume increases up to medium concentrations and then decreases. Therefore we expect a similar effect for the rate of sorption of water by PVC matrixes, as indeed is shown by our results.

For pPVC films plasticised with PDEA (a dibutyl ester of polyethylene glycol adipate) and PPA (a dibutyl ester of polypropylene glycol adipate), Chalykh and Belokurova observed an increase in diffusion rates of water followed by a decrease in diffusion rate with increasing plasticiser concentration (Chalykh and Belokurova 1982). The maximum diffusion rates were detected at 29% and 38 % plasticiser content respectively (see **table 6. 4.**). However in the case of DOP they only observed a decrease in the slope of a plot of D versus DOP concentration starting at 20% DOP concentration. Chalykh and Belokurova attributed these changes of behaviour with plasticiser content to a transition from homogeneous mixture of polymer and plasticiser to a heterogeneous mixture. Results from Raman mapping and depth profiling do not show any evidence of this.

Elwell and Pethrick as well as Borek and Osoba (Elwell and Pethrick 1990, Borek and Osoba 1996a) have described a similar phenomenon of reduction of the mean free volume in polymer matrixes, although not for PVC plasticised with dioctylphthalate, and for lower plasticiser content (~ 5%). This is the so called “anti-plasticisation” effect.

Anti-plasticisation is characterised by (Anderson et al. 1995) :

- the Tg of the polymer and its “free volume” decrease, at the same time,
- the polymer becomes stiffer and more brittle as plasticiser concentration increases (modulus and tensile strength increase significantly),
- small quantities of plasticiser are involved,
- transport properties are affected (Maeda and Paul 1987).

Anti-plasticisation is thought to result from one or more of the following :

- a decrease in free volume upon addition of small volume of the plasticiser, allowing the chains to arrange in a more ordered densely packed state or

more simply the plasticiser fills the excess volume (Vrentas et al. 1988, Maeda and Paul 1987),

- Suppression of the secondary relaxation transitions at the temperature of interest (Roy et al. 1987),
- polymer - diluent interactions which create steric hindrance and decrease segmental mobility of the polymer (Roy et al. 1987, Liu et al. 1990).

Previously published data (see **table 6. 4.**), show that the rate of diffusion of water lies between 10^{-8} cm²/s for non plasticised PVC and 10^{-6} cm²/s for highly plasticised PVC films in the initial stage of sorption, and is of the order of 10^{-9} cm²/s for the second stage of sorption. Our results fit well within these boundaries.

Table 6. 4. Previously published diffusion data by other workers.

Solvent	Plasticiser	Plasticiser content (% wt)	Diffusion coefficients (cm ² /s)	T (°C)	Authors
Water vapour	0		D _D = 2.75e-8 D _H = 6.51e-9	40	Okuno et al. 1995
Ethanol vapour	0		D _D = 1.37e-9 D _H = 4.99e-10	40	Okuno et al. 1995
Desorption of liquid water	DOA	66	D _i = (1-3) e-6 D ₂ = 10 ⁻⁹ - 10 ⁻⁸	22	Chan et al. 1992
Liquid water	DOA	66	D _i = 3±0.3 e-6 D ₂ = (1-6) e-9	-	Li et al. 1996
Water vapour	PNS	16 29 38 44	4.02e-8 2.80e-8 2.26e-8 2.56e-8	25	Chalykh and Belokurova 1982
Water vapour	PDEA	23 29 38	11.3e-8 13.5e-8 12.6e-8	25	Chalykh and Belokurova 1982
Water vapour	PPA	29 38 44	20.7e-8 32.2e-8 24.6e-8	25	Chalykh and Belokurova 1982
Water vapour	PAS	29 33 38	3.31e-8 6.61e-8 6.90e-8	25	Chalykh and Belokurova 1982

D_D, D_H, D_i, and D₂ refer to D due to concentration gradients in Henry mode and Langmuir mode, D initial and in the second stage respectively.

DOA = Dioctyl adipate, PNS = Polyneopentyl glycol succinate, PAS = Dibutyl ester of polyethylene glycol adipate sebacenate.

Equilibrium water content of PVC films

PVC discs (2 cm diameter) not containing any fluorfolpet were immersed in distilled water, and weighed at regular intervals to record the gain in weight of the discs due to sorption of water into the polymer matrix. **Table 6. 5.** shows the water uptake of the films at equilibrium. They represent a direct measurement of solubility.

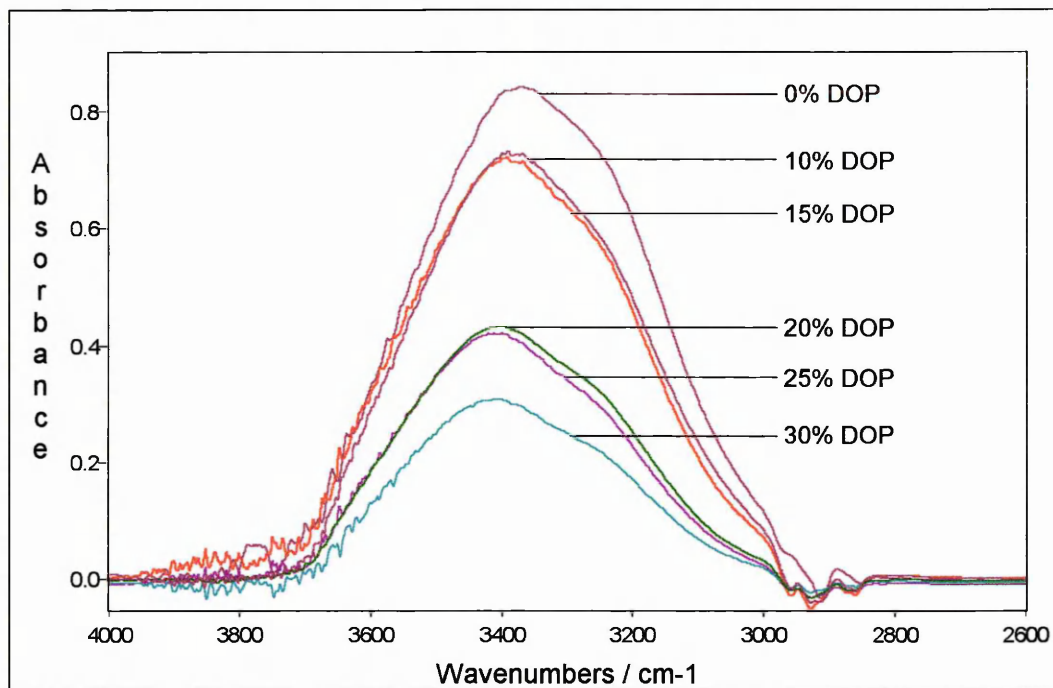
Table 6. 5. Water uptake of pPVC films at equilibrium.

DOP (%)	Water uptake (%)
0	0.9 ± 0.2
20	0.35 ± 0.01
30	0.28 ± 0.02

This shows that the amount of water penetrating the films decreases with increase of plasticiser content. This is also shown by the infrared spectra of the films at equilibrium in **figure 6. 7.**, which shows the $\nu(\text{O-H})$ stretching band of water between 3000 and 3700 cm^{-1} at various DOP concentrations. This could be due to :

- polymer - diluent interactions or diluent - plasticiser interactions, creating site exclusion, and thereby preventing sorption of water,
- decrease in solubility of water in the polymer as the plasticiser concentration increases,
- less available mean free volume in the polymer matrix with increase of DOP content. As diffusion rates initially go up, this can be ruled out.

Figure 6. 7. The $\nu(\text{O-H})$ stretching band of water between 3000 and 3700 cm^{-1} at various DOP concentrations.



Similar although slightly higher values were obtained by Chan and co - worker (Chan et al. 1992), who estimated the apparent equilibrium water content at 0.6 % for 66% DOA (dioctyladipate) plasticised PVC membranes. These values are comparable to those obtained by Berens (Berens 1989) for similar molecules in rigid PVC (see **table 6. 6**).

Table 6. 6. Equilibrium solvent content for rigid PVC films (from Berens).

Compound	Equilibrium gain (%wt)
Methanol	~ 1
Ethanol	~ 0.1
Isopropanol	~ 0.5

For the films containing fluorfolpet however, the amount of water in the polymer matrix increases with plasticiser content, and reaches a maximum at 25% DOP concentration (see **figure 6. 8.** and **figure 6. 9.**).

Figure 6. 8. The infrared spectra of the $\nu(\text{O-H})$ stretching region of water at equilibrium for PVC / DOP / PA3 films.

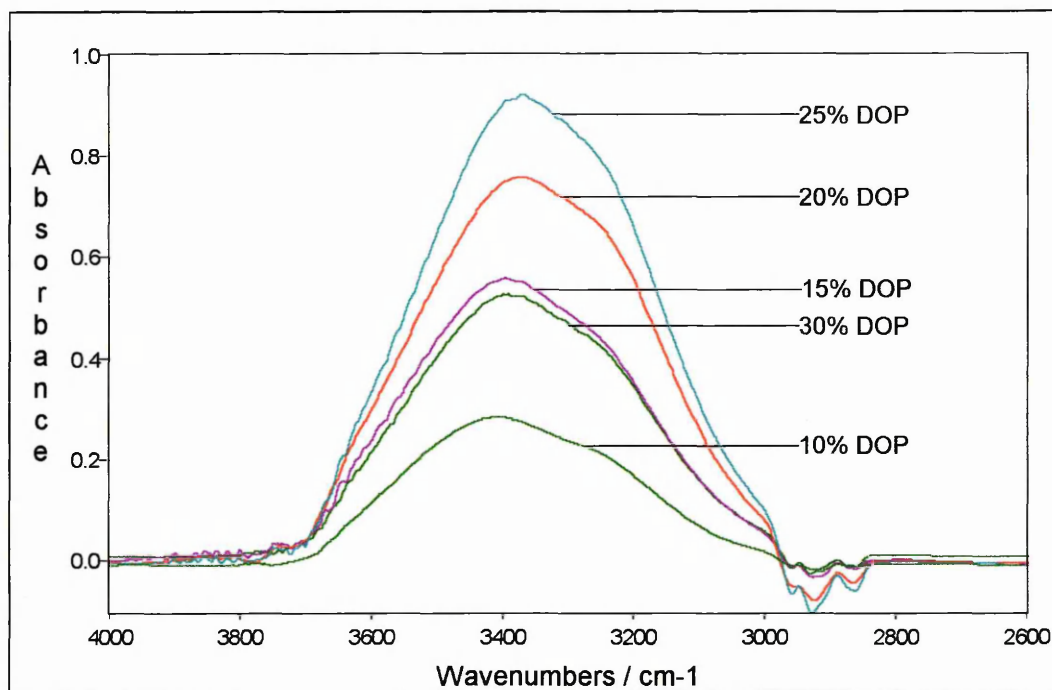
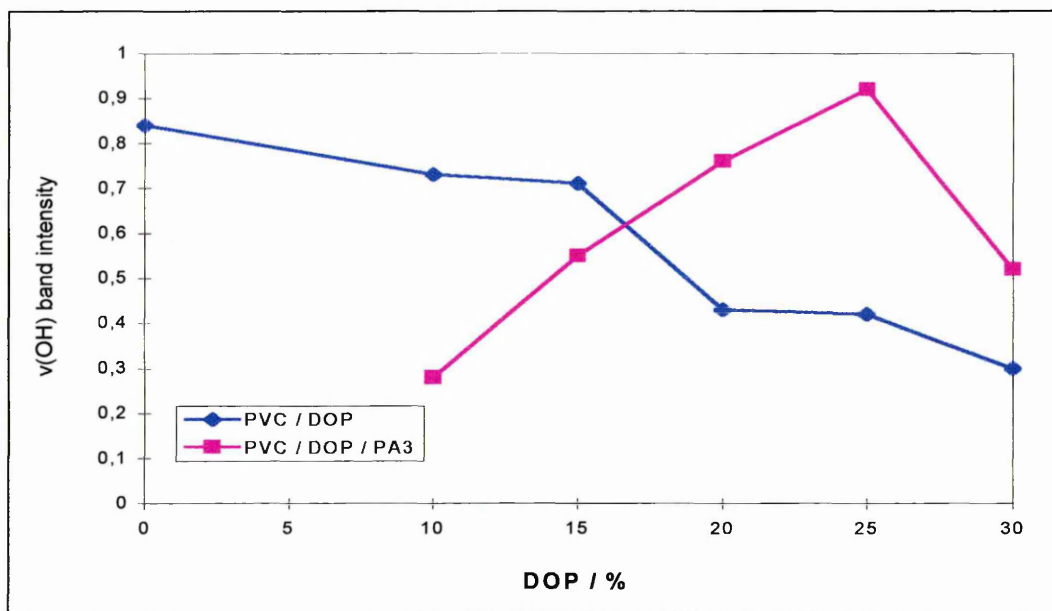


Figure 6. 9. A plot of band intensity against DOP concentration for PVC / DOP films and PVC / DOP / PA3 films.



The profiles of equilibrium water content and diffusion coefficient (see **figure 6. 6.**) are very similar. We already know that in a normal situation, as the plasticiser concentration increases, free volume increases and chain mobility

increases. Furthermore, as well as the plasticiser dioctylphthalate, the polymer matrix contains water, which is well known for its plasticisation effect, increasing the size of the free volume cavities of the polymer by swelling (swelling is discussed further later in this chapter) and providing a lubrication effect that promotes chain mobility and disrupts hydrogen-bonding (Hodge et al. 1995, De'Nève and Shanahan 1993).

The difference in sorption between the two types of films, indicates the significant effect of adding fluorfolpet on the properties of the film, by possibly :

- creating additional free volume,
- adding new interactions between plasticiser - biocide, biocide - polymer and biocide - water molecules, thereby reducing the number of interactions between the plasticiser or polymer molecules and water, thereby reducing the steric hindrance caused by it, allowing for more water to diffuse into the film,
- increasing chain mobility, indeed, **table 6. 3.** clearly shows that Tg is lower for films containing (only 5%) fluorfolpet.

The decrease of equilibrium water content and diffusion coefficient around 20, 25% DOP concentration may be explained by an overall decrease of free volume due to sites being occupied by the additional DOP molecules.

Swelling of the matrix

FTIR - ATR spectroscopy can be used to determine swelling in a polymer matrix, by following the intensity loss of $\nu(\text{C-H})$ bands as water diffuses into the film. This method was used by Balik and Xu (Balik and Xu 1994) to simultaneously study the diffusion of water, swelling and calcium carbonate removal in a latex paint ; the values for swelling using this method were in relatively good agreement with values obtained from microscopy, although slightly higher.

We applied a similar method to measure swelling of the PVC matrix during water sorption. The CH_2 rocking band at 950 cm^{-1} was used. **Figure 6. 10.** shows the (CH_2) rocking band at $t = 0$ and $t = 330 \text{ min.}$, and the difference spectrum for a DOP / PVC film, thereby establishing swelling has occurred.

Figure 6. 11. shows the swelling profile obtained by plotting the integration of the area under the (CH₂) band against time.

Figure 6. 10. The (CH₂) rocking band at $t = 0$ and $t = 330$ min., and the difference spectrum for a DOP / PVC film.

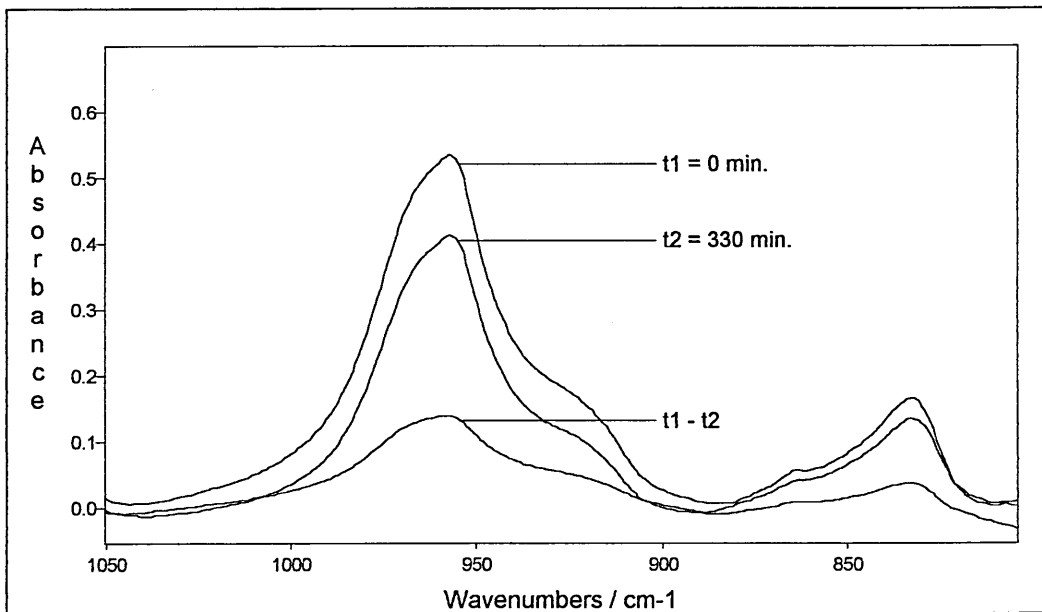
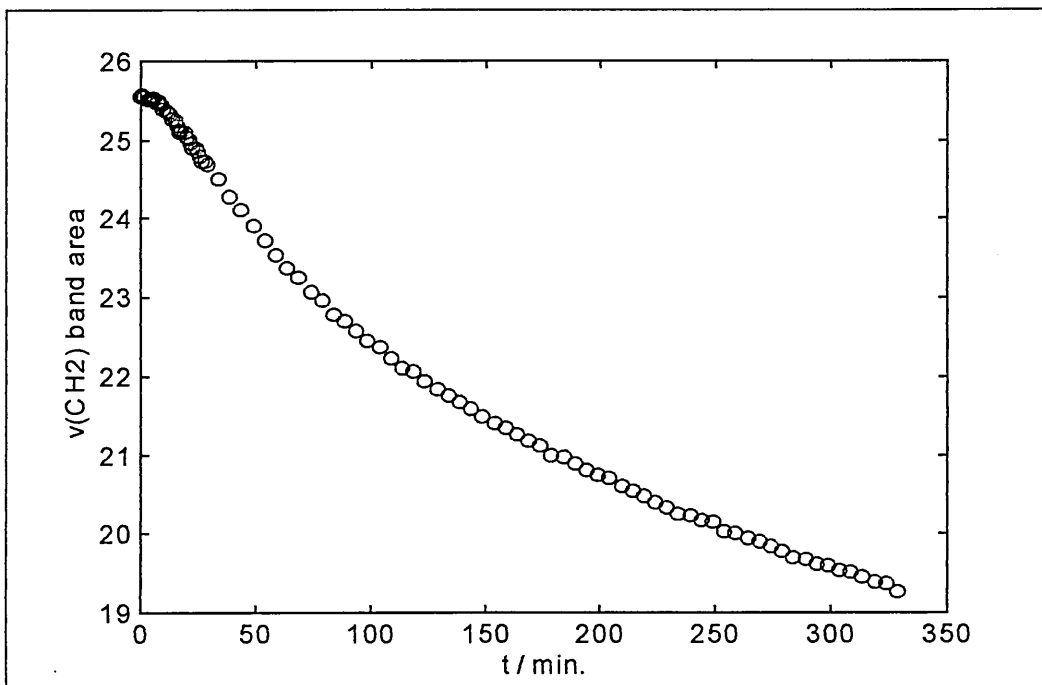


Figure 6. 11. The swelling profile obtained by plotting the integrated area under the (CH₂) band against time.



The percentage swelling of the matrix is obtained by comparing the area of the band in the dry film and at equilibrium water content. **Tables 6. 7.** and **6. 8.** present the percentage swelling obtained for PVC / DOP and PVC / DOP / PA3 films respectively, and **figure 6. 12.** shows a plot of swelling against DOP concentration for PVC / DOP and PVC / DOP / PA3 films.

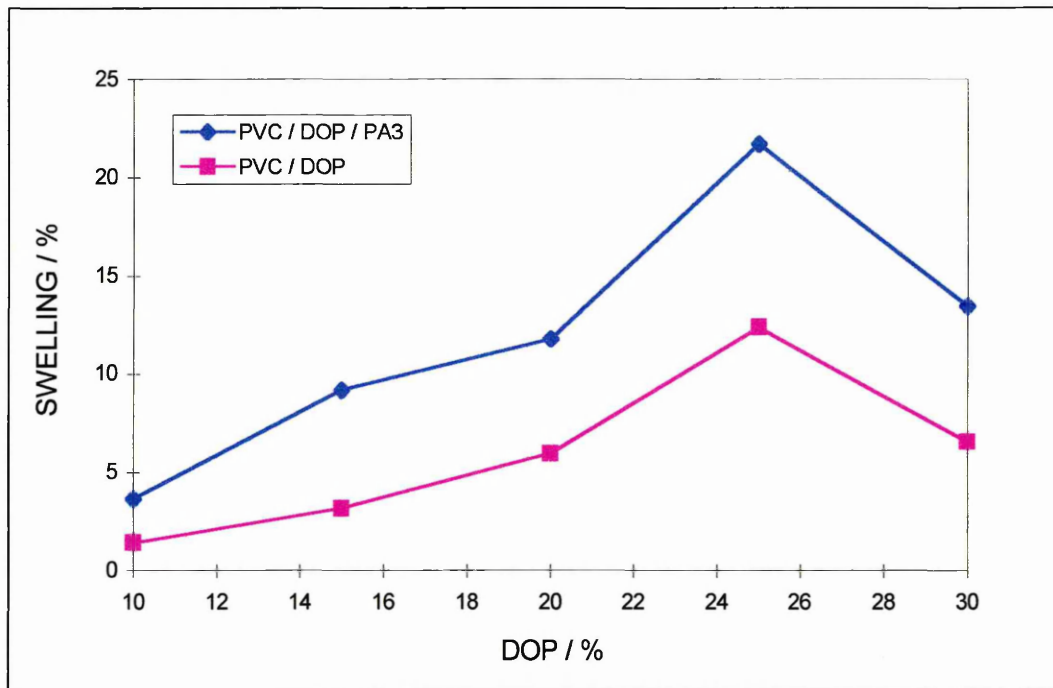
Table 6. 7. Percentage swelling of PVC / DOP films at equilibrium.

SAMPLE NO	DOP (%)	SWELLING (%)
29	0	19.86
53	0	15.14
56	0	26.62
38	10	1.42
58	15	3.17
59	15	14.5
28	20	5.97
60	25	17.85
61	25	6.92
33	30	2.20
57	30	10.92

Table 6. 8. Percentage swelling of PVC / DOP / PA3 films at equilibrium.

SAMPLE NO	DOP (%)	SWELLING (%)
39	10	2.03
40	10	6.56
41	10	2.32
52	15	8.18
54	15	10.20
21	20	13.64
22	20	13.65
24	20	8.22
25	20	11.74
50	25	25.13
51	25	18.29
27	30	10.58
33	30	20.55
57	30	9.25

Figure 6. 12. Plot of swelling against DOP concentration for PVC / DOP and PVC / DOP / PA3 films.



Swelling is more important in the films containing fluorfolpet, but the swelling versus DOP concentration pattern is similar in both cases. Swelling increases with plasticiser content to reach a maximum at 25% DOP concentration and then decreases.

Swelling induces an increase of free volume (Domjan et al. 1996) and mobility of the polymer chains.

Comparison of the diffusion coefficients (see **figure 6. 5.** and **6. 6.**) and swelling, show that their evolution with DOP is very similar, demonstrating the dependence of diffusion rate upon swelling.

Xiao and co - workers (Xiao et al. 1997) measured the extent of swelling of a PVC matrix for benzene, dichloromethane and trichloroethylene, showing that the degree of swelling is dependent upon the type of penetrant used.

6. 2. 2. Determination of the diffusion coefficients using sorption kinetics, and Fick's second law

The sorption of water into PVC involves two concurrent modes of diffusion, which can be modelled by dual-sorption kinetics. The dual-mode sorption model assumes the two diffusion modes involved to be Fickian. Therefore, a different approach was used to try and determine the two types of diffusion modes involved in the sorption of water by PVC.

As seen in chapter 3., the mass of sorbed molecules, at short time can be written as :

$$\frac{M_t}{M_\infty} = \frac{2}{L} \left(\frac{D}{\pi} \right)^{1/2} t^{1/2}$$

where M_t = mass sorbed at time t ,

M_∞ = mass sorbed at equilibrium,

L = thickness of the film,

D = diffusion coefficient.

And, the mass sorbed at longer time can be written as :

$$\ln \left(1 - \frac{M_t}{M_\infty} \right) = \ln \left(\frac{8}{\pi^2} \right) - \frac{D\pi^2 t}{4L^2}$$

This equation can be modified to describe the FTIR - ATR experiment as discussed by Fieldson and Barbari (Fieldson and Barbari 1992) to give :

At short times :

$$\frac{A_t}{A_\infty} = \frac{2}{L} \left(\frac{D}{\pi} \right)^{1/2} t^{1/2} \quad (\text{eq. 6. 1.})$$

At long times :

$$\ln\left(1 - \frac{A_t}{A_\infty}\right) = \ln\left(\frac{4}{\pi}\right) - \frac{D\pi^2 t}{4L^2} \quad (\text{eq. 6. 2.})$$

Using (eq. 6. 1.) and (eq. 6. 2.), one can determine the diffusion coefficients by plotting (A_t/A_∞) versus $t^{1/2}$ for early times and $\ln(1-A_t/A_\infty)$ versus t for long times.

Figure 6. 13A. and **6. 13B.** show the plots of (A_t/A_∞) versus $t^{1/2}$ for PVC / DOP and PVC / DOP / PA3 films respectively. **Figure 6. 14A.** and **6. 14b.** show the plots of $\ln(1-A_t/A_\infty)$ versus t for PVC / DOP and PVC / DOP / PA3 films respectively.

(NB : A_∞ is displayed as A on the graphs.)

Figure 6. 13A. Plot of (A_t/A_∞) versus $t^{1/2}$ for PVC / DOP.

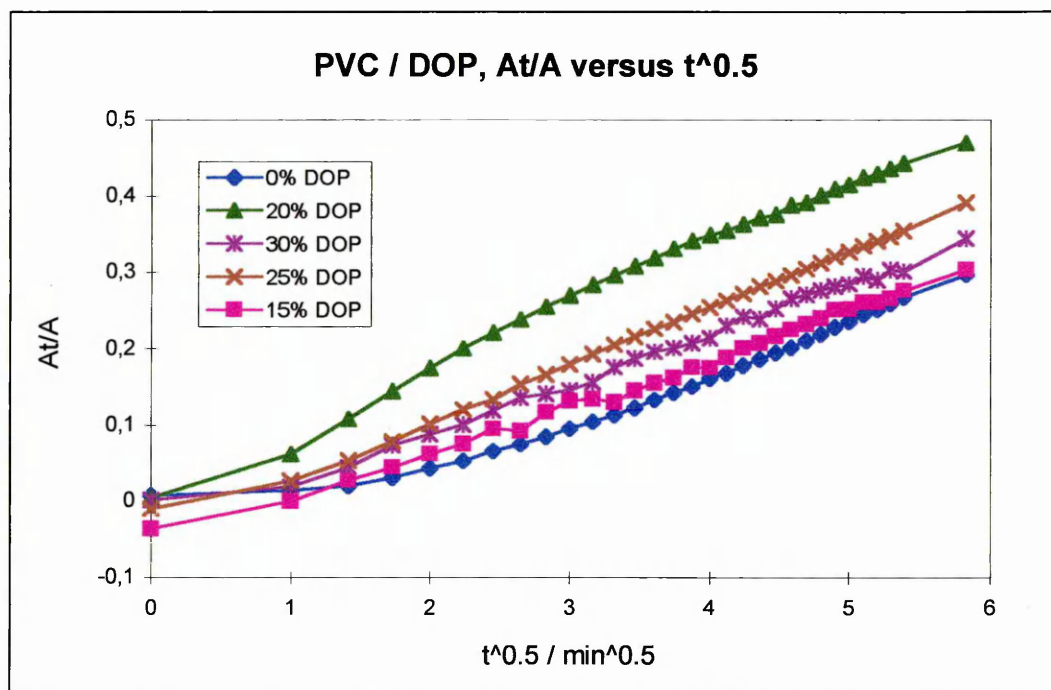


Figure 6. 13B. Plot of (A_t/A_∞) versus $t^{1/2}$ for PVC / DOP / PA3.

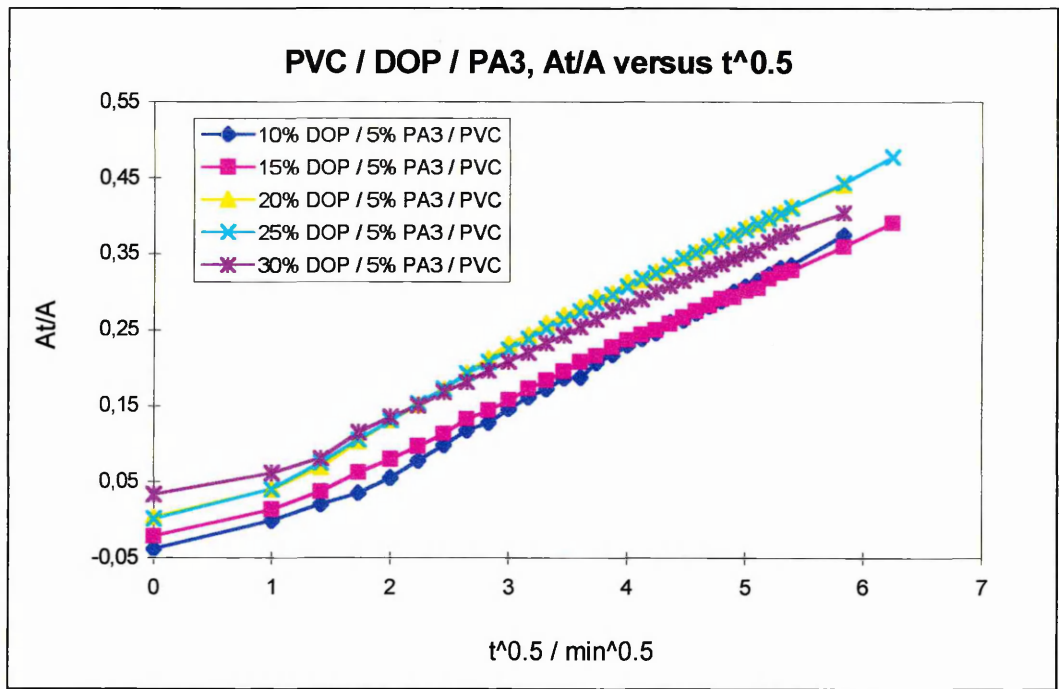


Figure 6. 14A. Plot of $\ln(1-A_t/A_\infty)$ versus t for PVC / DOP.

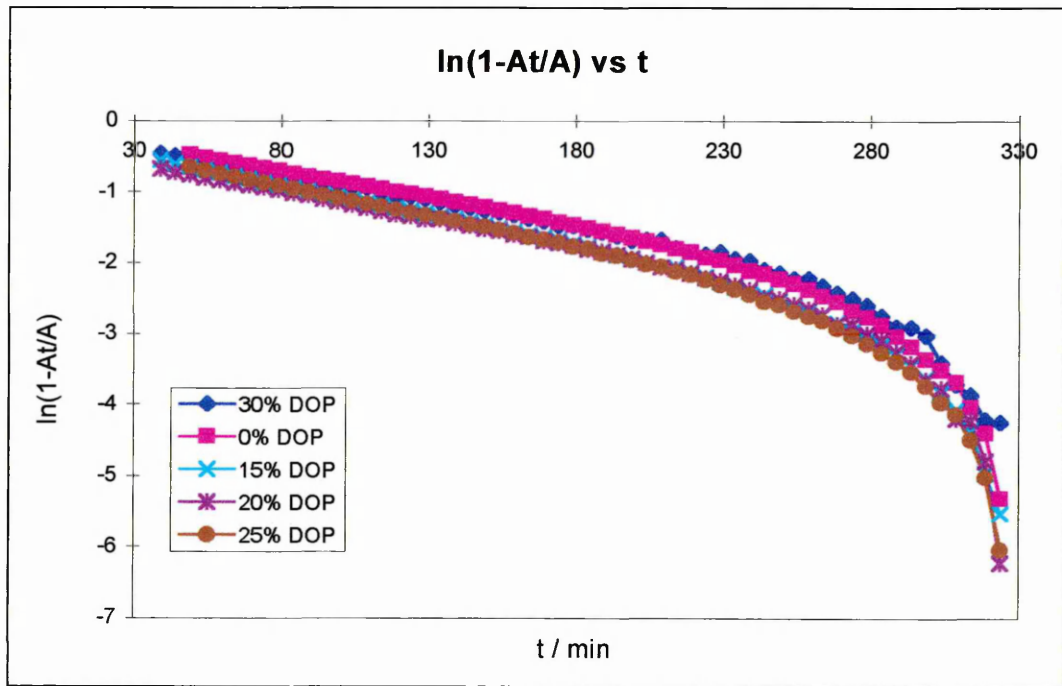
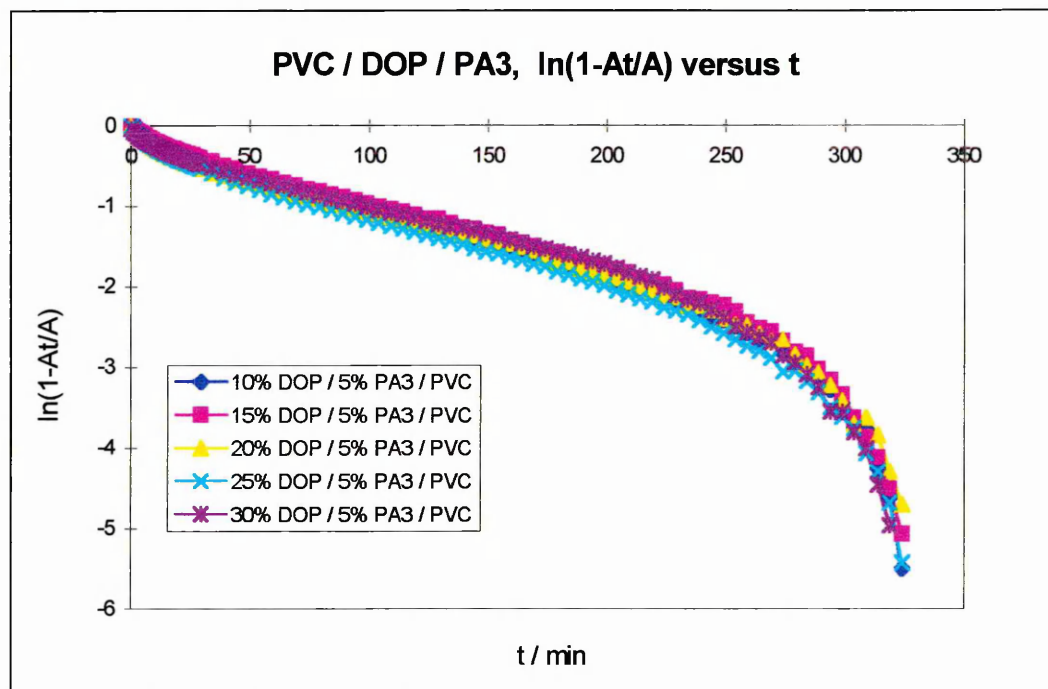


Figure 6.14B. Plot of $\ln(1-A_t/A_\infty)$ versus t for PVC / DOP / PA3.



A_t/A_∞ versus $t^{1/2}$ plots (figures 6.13.) :

- For pure PVC films, the plot of (A_t/A_∞) against $t^{1/2}$ is a concave curve, showing no linear part, which is more characteristic of a case II sorption mode (Fieldson and Barbari 1995).
- As the percentage of DOP in the film increases to 15, 25 and 30%, the plot (A_t/A_∞) against square root of time displays more Fickian like characteristics, i.e. a straight line (the very early curvature of the plot is due to the nature of the ATR experiment).
- At 20% DOP concentration the plot exhibits more of a convex curvature, more characteristic of the anomalous diffusion (i.e. the dual - mode sorption) mode.

Therefore we can conclude, that the diffusion process depends upon the amount of plasticiser present in the film (i.e. the degree of plasticisation). The addition of plasticiser results in the sorption process becoming more Fickian (except in the case of 20% DOP content). The addition of plasticiser to a glassy polymer improves its tensile strength and confers the polymer some rubber like properties. Rubbery polymers such as PET are well known to follow

a Fickian sorption process (Schloter and Furan 1992, Southern and Thomas 1980, Sammon 1997). Therefore, as the PVC polymer becomes more and more rubbery with addition of DOP, the diffusion mode is expected to become more and more Fickian. Furthermore, Berens (Berens 1989) shows that as the activity of the solvent changes, the sorption mode also changes. As the activity of TCE diminishes, the sorption of TCE into rigid PVC films tends toward Fickian behaviour. We have shown in section 6. 2. 1., that as the DOP concentration is increased, the sorption capability (i.e. water uptake at equilibrium) changes substantially. This could well induce a change in the diffusion mode.

$\ln(1-A_t/A_\infty)$ versus t plots (figures 6. 14.) :

These plots show that at all DOP concentrations, the mode of diffusion of water into the films at later times is Fickian like. Indeed, we observe, as predicted (Fieldson and Barbari 1993), a curve composed of two parts :

- (i) a linear part, expected for a Fickian diffusion behaviour,
- (ii) a curved part, as the equilibrium water content is reached.

The diffusion coefficients were calculated using the linear part of the curves, and are summarised in **table 6. 9.** and **figure 6. 15.**, and **table 6. 10.** and **figure 6. 16.**

Table 6. 9. Diffusion coefficients of water diffusing in PVC / DOP films. D_E and D_L represent the diffusion coefficients at early times and late times respectively.

SAMPLE NO	DOP (%)	D_E (cm ² /s)	D_L (cm ² /s)
29	0	3.57e-9	3.48e-9
53	0	5.24e-9	4.67e-9
56	0	8.66e-9	5.08e-9
38	10	6.33e-9	4.32e-9
58	15	6.11e-9	6.19e-9
59	15	3.61e-9	2.79e-9
28	20	1.18e-8	7.11e-9
60	25	1.21e-8	1.11e-8
61	25	1.00e-8	7.84e-9
33	30	3.47e-9	5.48e-9
57	30	1.25e-8	1.10e-8

Figure 6. 15. Plot of mean diffusion coefficients against DOP concentration.

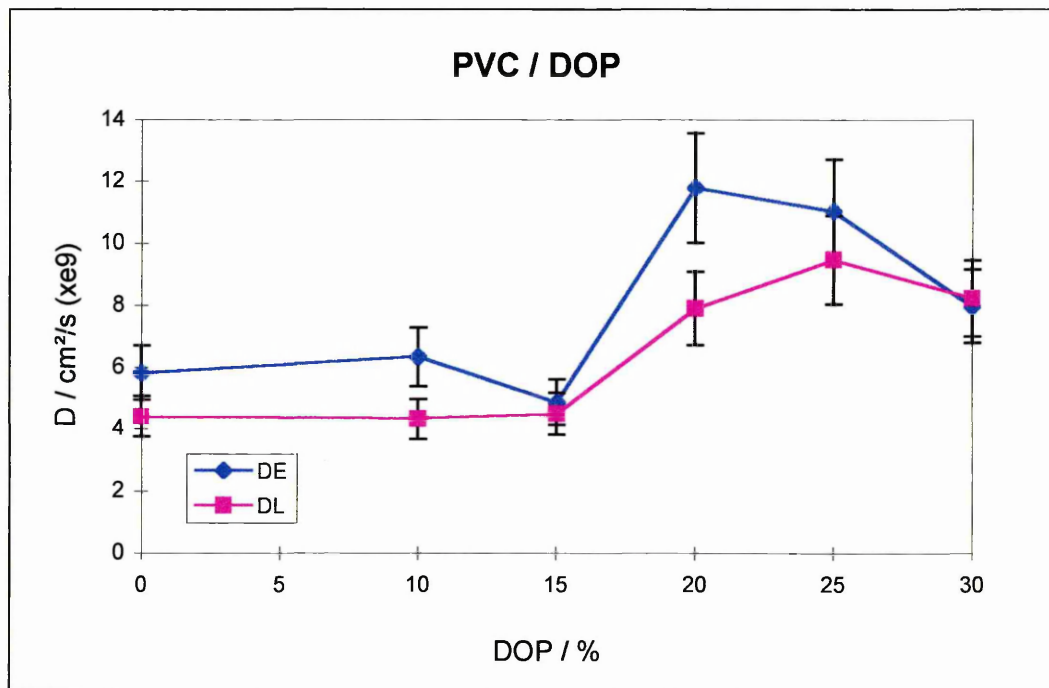
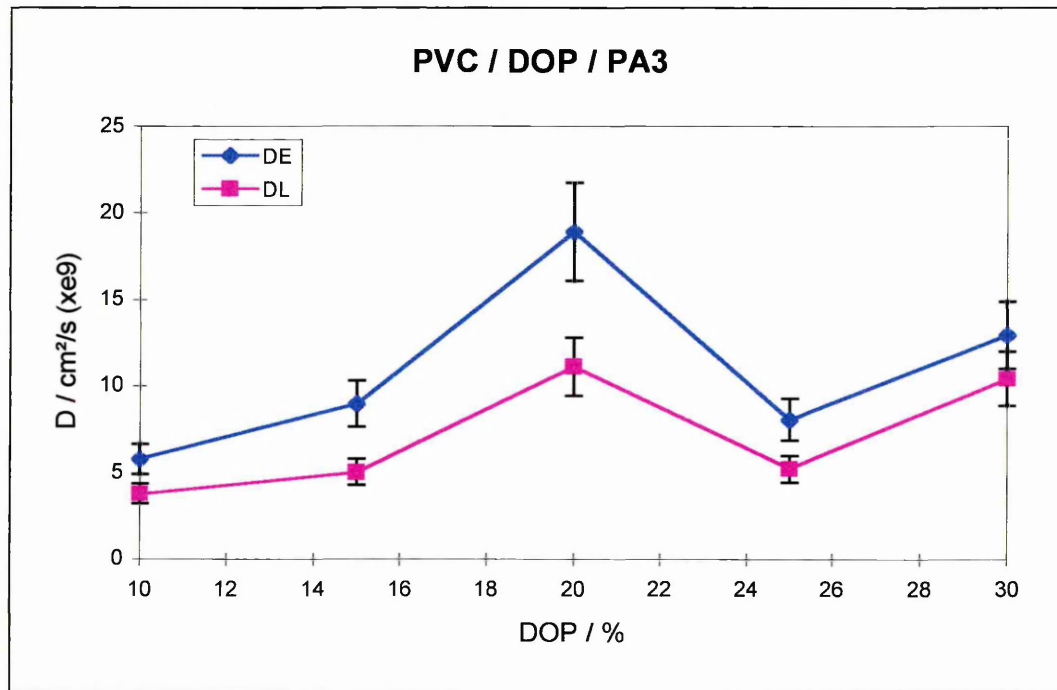


Table 6. 10. Diffusion coefficients of water diffusing in PVC / DOP / PA3 films. D_E and D_L represent the diffusion coefficients at early times and late times respectively.

SAMPLE NO	DOP (%)	D_E (cm²/s)	D_L (cm²/s)
39	10	2.68e-9	2.67e-9
40	10	8.88e-9	5.62e-9
41	10	6.55e-9	3.12e-9
52	15	6.06e-9	4.55e-9
54	15	1.19e-8	5.48e-9
21	20	4.87e-8	2.81e-8
22	20	1.90e-8	1.31e-8
24	20	1.88e-8	8.90e-9
25	20	3.91e-8	1.57e-8
50	25	5.44e-9	3.93e-9
51	25	1.07e-8	6.51e-9
27	30	1.16e-8	8.32e-9
33	30	1.43e-8	7.48e-9
47	30	3.49e-8	2.01e-8

Figure 6. 16. plot of mean diffusion coefficients against DOP concentration.



D_E (diffusion coefficient at early times) and D_L (diffusion coefficient at late times) are of the same order as D_1 and D_2 (calculated from dual mode fitting), and follow the same trends ; diffusion rates increase with increasing DOP concentration to reach a maximum at 20% DOP, to then decrease at 25% and 30% DOP content.

D_L values are generally lower than D_E values, indicating that the second stage of diffusion is slower, but the difference between D_E and D_L is much smaller than between D_1 and D_2 .

6. 2. 3. Conclusions

- The diffusion of water into PVC is a two stage process, the first one being more rapid than the second stage. Both stages appear to be pseudo Fickian in the films studied. The dual-mode model therefore fits the data reasonably well.

- Diffusion rates and swelling profiles are similar for both formulations ; they show a non-monotonic evolution with plasticiser concentration, and a maximum at 20 - 25% DOP concentration, showing that diffusion rates are determined by the swelling.
- Diffusion rates are independent of water content in the film.
- Diffusion rates are higher in the films containing fluorfolpet.
- Swelling is also higher in the films containing fluorfolpet.
- Glass transitions are lower for films containing fluorfolpet.
- Sorption of water from the two types of films is very different. PVC / DOP films show a net decrease of water content at equilibrium as the concentration of DOP increases, whereas PVC / DOP / PA3 films, show that water content depends on swelling of the film, i.e. it exhibits the same evolution with plasticiser concentration as swelling or indeed diffusion coefficients.

Diffusion rates are governed by some or all of the following factors :

- the chain mobility,
- the free volume in the polymer,
- the number of sites available for bonding of water molecules,
- the solubility of water and DOP in the polymer matrix.

Above T_g molecular structure of the polymer is dynamic ; as the concentration of DOP is increased, the T_g value is lowered, and chain mobility increases. Furthermore, frequent local conformational transitions can create transient pockets or voids, which are then available for the penetrant to move into the polymer matrix. But changes in T_g alone cannot account for the behaviour of the diffusion coefficient at DOP concentrations of 25% and 30%. We would expect a constant increase with DOP content increase, unlike our results have shown. When fluorfolpet is introduced in the formulation, the T_g is lowered further, suggesting that the fluorfolpet molecules increase further the chain mobility, and possibly the mean free volume in the matrix.

Free volume increases considerably as water swells the PVC matrix. Swelling is more important for films containing the biocide. It was shown that swelling increased with DOP content (for both PVC / DOP and PVC / DOP / PA3 films)

to reach a maximum at 20-25% DOP content. At concentrations higher than this, swelling decreases. As the plasticiser concentration becomes higher than 25%, the swelling, diffusion rates and water sorption diminish considerably. There can be a variety of causes responsible for this phenomenon :

- (i) "antiplasticisation",
- (ii) less available free volume in the polymer as plasticiser concentration increases, because the excess free volume is filled by the plasticiser. Indeed, Chalykh and Belokurova observed a phase transition from a one-phase to a two-phase system around 30% (for PDEA, PAS, PPA and PNS) and 20% (for DOP) plasticiser concentration, using electron microscopy (Chalykh and Belokurova 1982). The two-phase system consists of (i) plasticiser dissolved in PVC and (ii) plasticiser on its own. This transition is attributed to reaching the solubility limit of the plasticiser in the polymer.

This shows the dependence of diffusion rates upon free volume.

As free volume and indeed swelling increases the water content at equilibrium is expected to do so too. It was shown that also this was the case for films containing fluorfolpet but, it was not the case for PVC / DOP films. The water content at equilibrium decreases substantially as the DOP and swelling, hence mean free volume increase ; although there is ample free volume in the film, the water does not penetrate into the film. There may be two explanations for this phenomenon :

- (i) The flow of water molecules is hindered by interactions between the PVC-DOP, or H₂O-DOP and H₂O-PVC molecules. But, swelling would then also be affected in the same way as water sorption. This is not the case.
- (ii) The numbers of sites for absorption of water molecules, in the polymer are decreasing as DOP concentration increases, because they are being occupied by the DOP molecules. Indeed, addition of a small amount of PA3 molecules may increase the number of sites available, and therefore explain the different behaviour of water sorption in films containing fluorfolpet.

This demonstrates the dependence of water sorption capacity on the number of sites rather than free volume in the film. This also strongly suggest interactions between water and the PVC and the fluorfolpet molecules through the chlorine groups.

6. 3. DEHYDRATION OF PLASTICISED PVC FILMS

By blowing nitrogen gas through the ATR liquid cell, at a pressure of 0.5 bars, one can remove the water from the film, and follow the desorption process.

The desorption of water by the film was monitored using $\nu(\text{O-H})$ stretching band of water between 2950 and 3700 cm^{-1} . As the water is removed from the film, the absorbance of the $\nu(\text{O-H})$ stretching band decreases, as can be seen in **figure 6. 17.**, and the desorption curve was obtained by plotting the integrated area under the $\nu(\text{OH})$ stretching band against time (see **figure 6. 18.**)

Figures 6. 17A. and **6. 17B.** show the infrared spectra for water diffusing out of a 25% DOP / 5% PA3 / PVC polymer film as a function of time (stacked and overlaid) obtained by ratioing the spectra of the wet polymer against the spectrum of the dry polymer.

Figures 6. 17. show that as the water is removed from the film, (a) the shape of the water spectrum in the 3000 to 3600 cm^{-1} region varies as a function of time, the shoulder at 3200 cm^{-1} shrinking more quickly than the main band at 3500 cm^{-1} ; (b) there is a slight shift of the band position, with time, towards the higher wavenumbers, indicating a weakening of the hydrogen bond network of the water in the film. This will be discussed further in chapter 7.

Figure 6. 17A. Infrared spectra for water diffusing out of a 25% DOP / 5% PA3 / PVC film (overlaid).

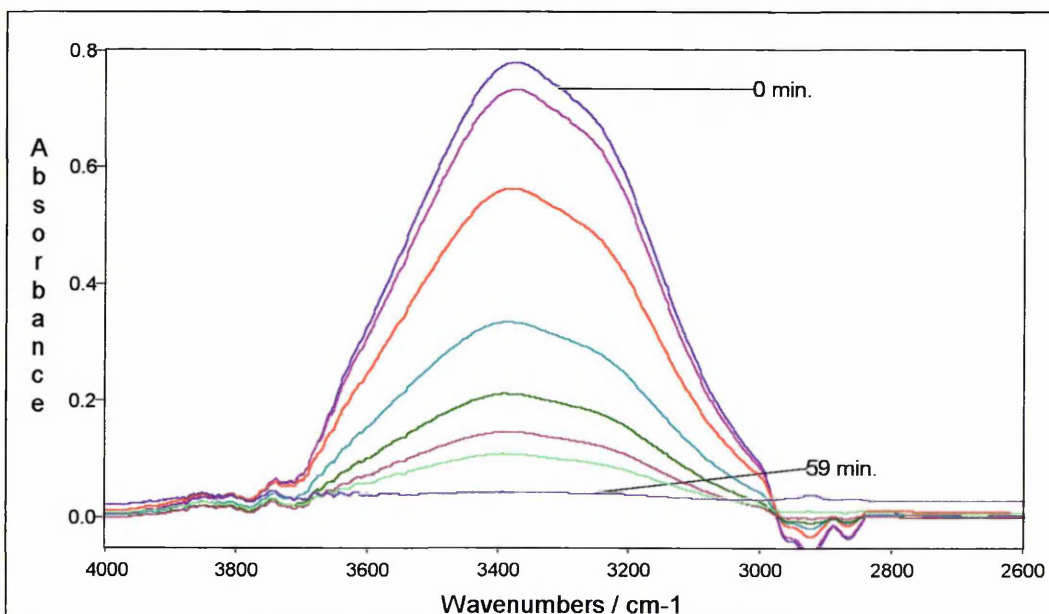


Figure 6. 17B. Infrared spectra for water diffusing out of a 25% DOP / 5% PA3 / PVC film (superimposed).

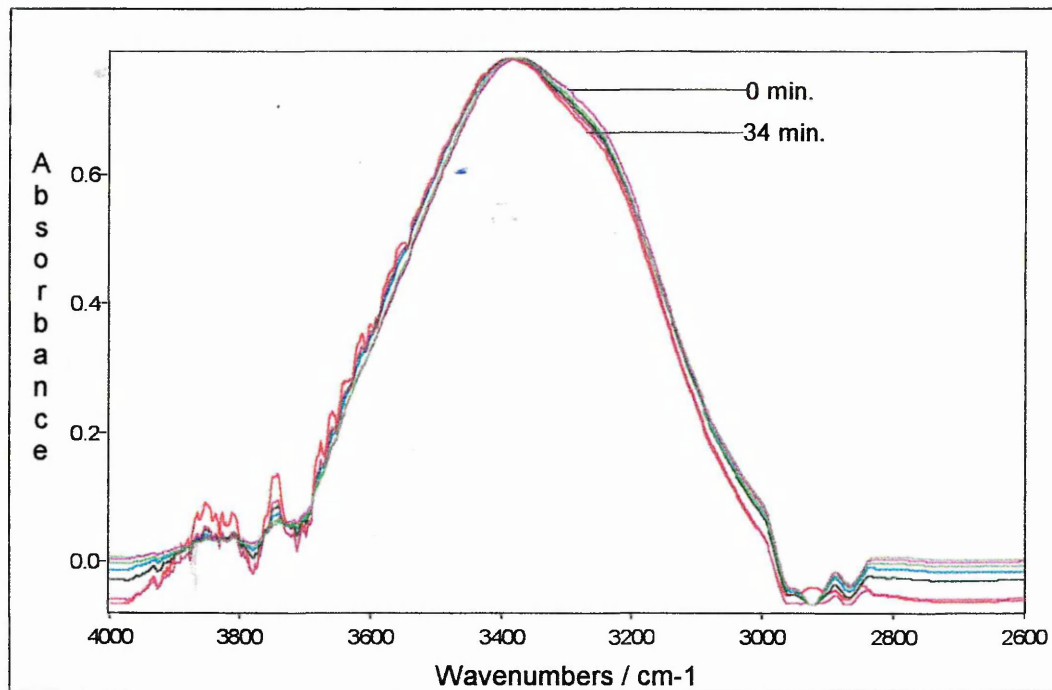
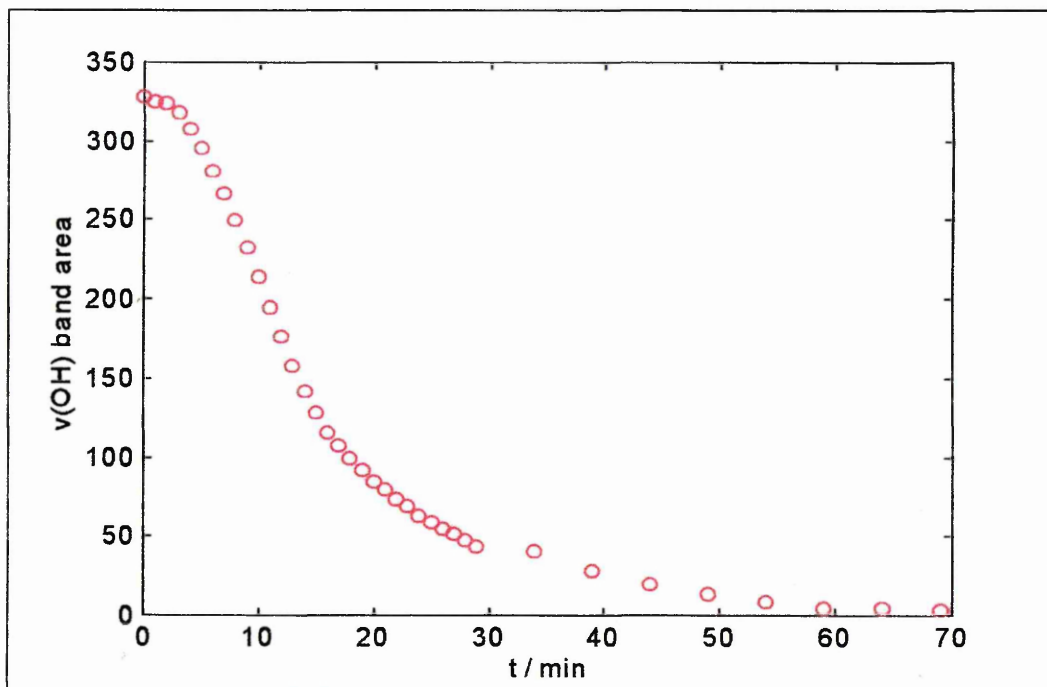


Figure 6. 18. A typical dehydration curve.



Diffusion rates

In order to determine the type of diffusion involved and the dynamics, of the desorption, the data was plotted as (A_t/A_∞) versus $t^{1/2}$ and (eq. 6. 1.) was used to determine the diffusion coefficient. The diffusion coefficients thereby obtained are presented in **tables 6. 11.** and **6. 12.** A similar equation was used by Chan and co - worker (Chan et al. 1992) to determine the rate of desorption of water from PVC-based ion - selective electrode membranes.

Figures 6. 19A. and **6. 19B.** show the plots of (A_t/A_∞) versus $t^{1/2}$ for PVC / DOP and PVC / DOP / PA3 films respectively.

(NB : A_∞ is written as A on the graphs)

Figure 6. 19A. Plot of (A_t/A_∞) versus $t^{1/2}$ for PVC / DOP films.

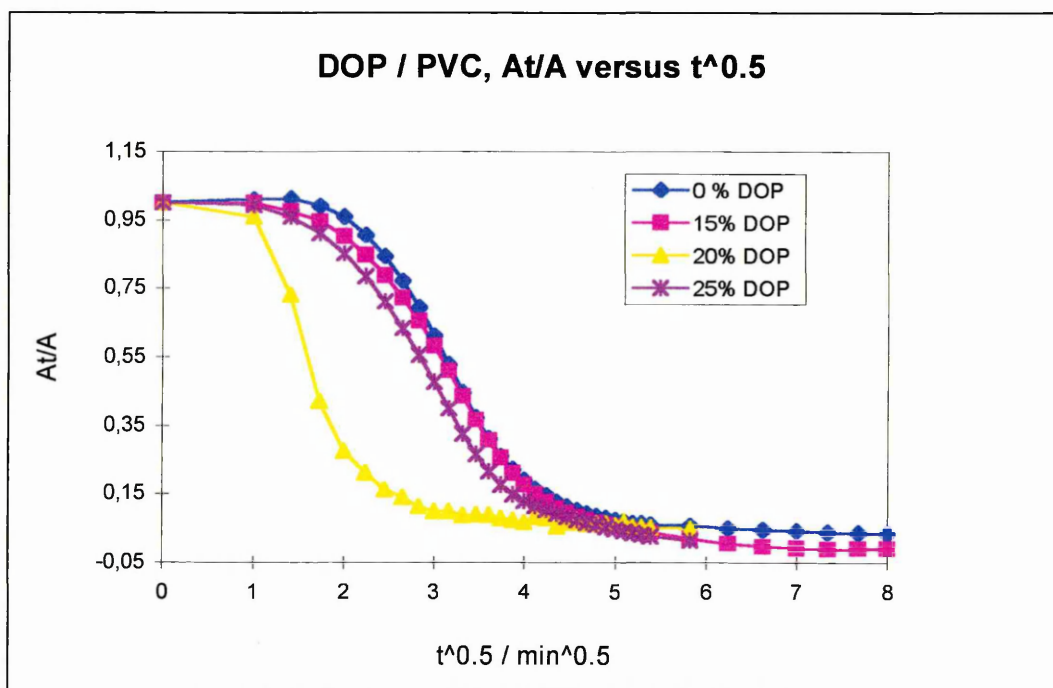


Figure 6. 19B. Plot of (A/A_∞) versus $t^{1/2}$ for PVC / DOP / PA3 films.

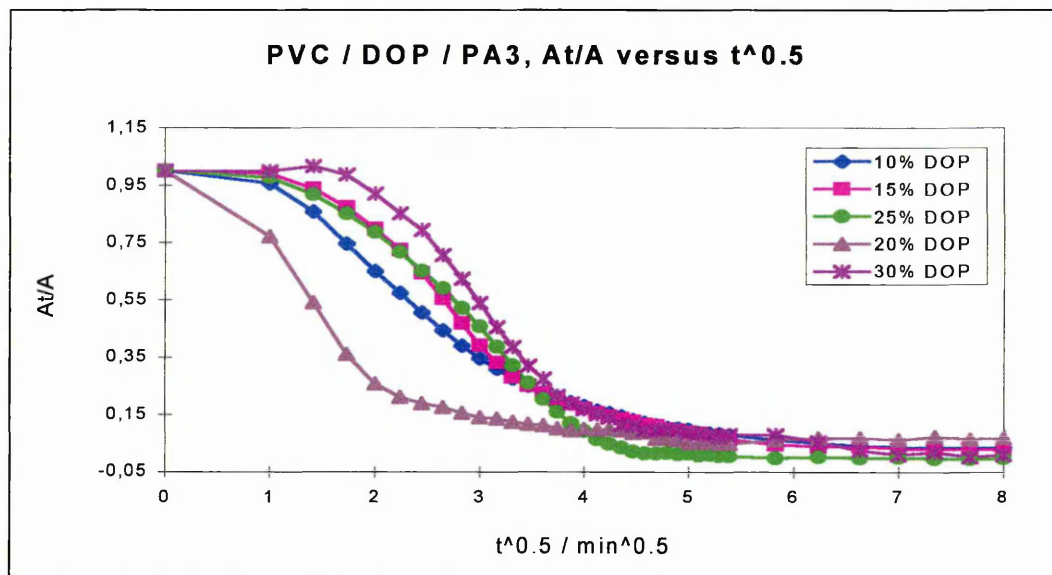


Table 6. 11. Diffusion coefficients for the diffusion of water out of PVC / DOP films.

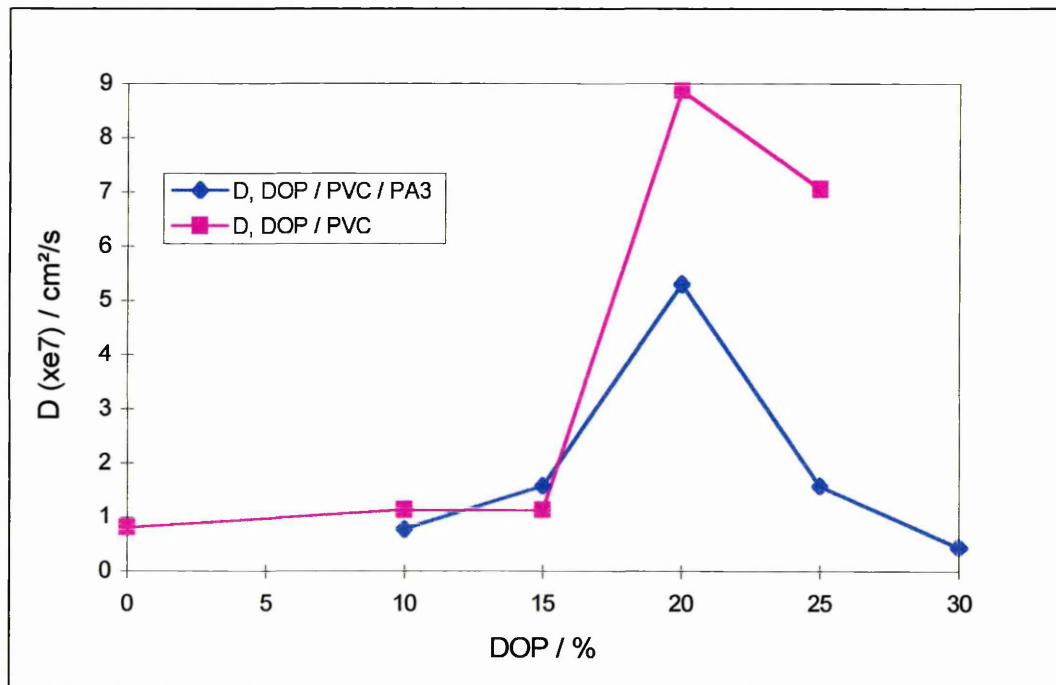
SAMPLE NO	DOP (%)	D (cm ² /s)
29	0	1.40e-7
53	0	6.26e-8
56	0	4.10e-8
38	10	1.14e-7
59	15	1.13e-7
28	20	8.87e-7
60	25	1.09e-6
61	25	3.2e-7

Table 6. 12. Diffusion coefficients for the diffusion of water out of PVC / DOP / PA3 films.

SAMPLE NO	DOP (%)	D (cm ² /s)
39	10	9.25e-8
40	10	1.33e-7
41	10	2.37e-8
52	15	2.16e-7
54	15	9.90e-8
24	20	6.21e-7
25	20	4.41e-7
50	25	1.05e-7
51	25	2.10e-7
27	30	4.38e-8
35	30	7.63e-7
47	30	8.18e-7

The desorption of water from PVC films is a very rapid process compared to the uptake, even though the nitrogen flow was very little (0.5 bars pressure). The desorption process appears to follow the anomalous diffusion mode. At 20% DOP content the desorption is much quicker than at any other plasticiser concentration, as demonstrated by **figure 6. 20.**

Figure 6. 20. Plot of the diffusion coefficients against DOP concentration for the removal of water from PVC films.



The desorption rates follow the same trends as the sorption rates :

- Diffusion rates are higher in the films containing fluorfolpet.
- Diffusion rates reach a maximum at 20% DOP concentration.

Shrinking of the polymer matrix

As the water retreats the swelling decreases and the films shrink, as can be seen in **figure 6. 21.** showing the film shrinking profile of a DOP / PVC film.

Table 6. 13. and **6. 14.** and **figure 6. 22.** show the shrinking of the film in percentage as a function of DOP concentration. The shrinking percentage is slightly higher than the swelling percentage ; showing that the films are dryer at the end of the water removal experiment than when the water uptake experiment started. This is probably due to some finite amount of water vapour

in the film from the atmosphere. The shrinking profile of the films with DOP concentration is similar to the diffusion rate profile.

Figure 6. 21. A typical shrinking profile for a PVC matrix.

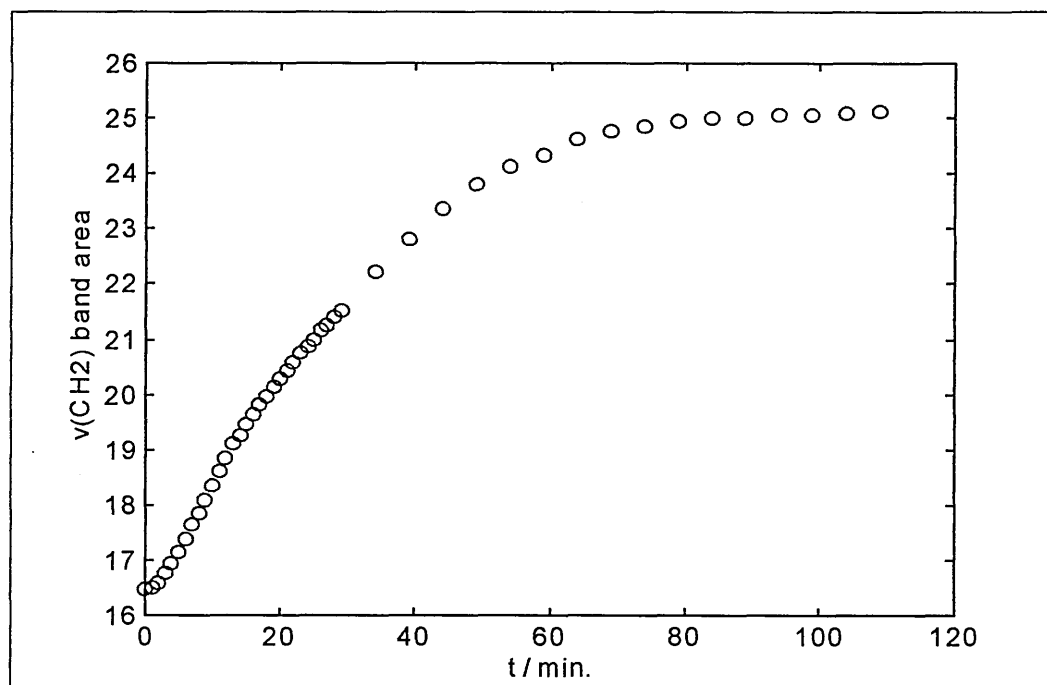


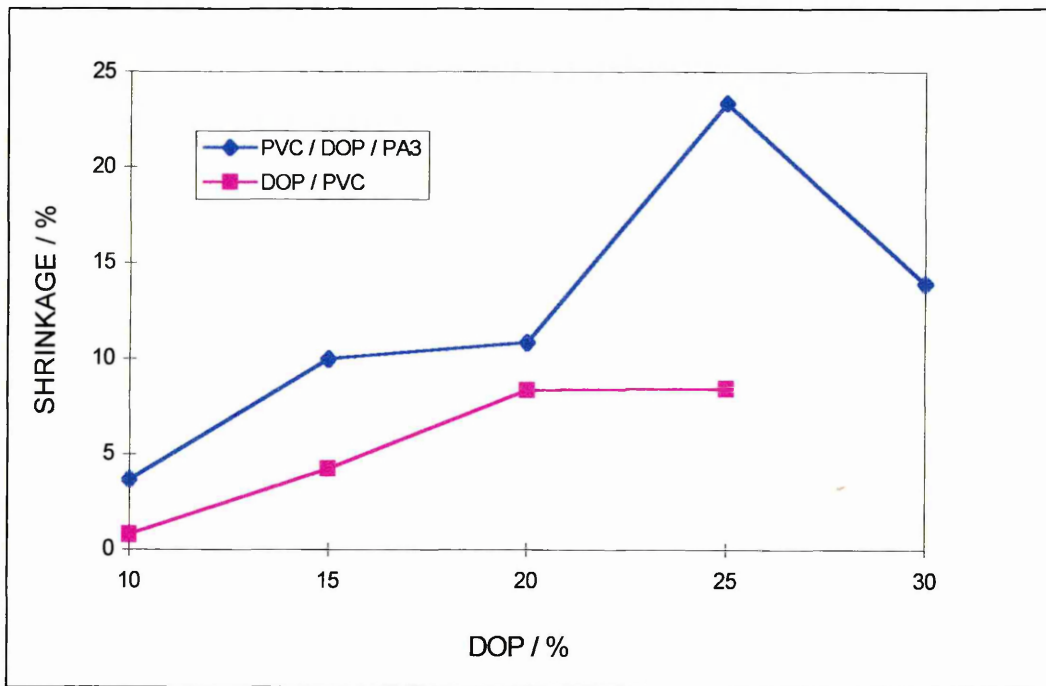
Table 6. 13. Shrinking of the PVC / DOP films during removal of water from the films.

SAMPLE NO	DOP (%)	SHRINKING (%)
29	0	26.25
53	0	19.65
56	0	24.91
38	10	0.77
59	15	4.21
28	20	8.34
60	25	8.42
61	25	19.55

Figure 6. 14. Shrinking of the PVC / DOP / PA3 films during removal of water from the films.

SAMPLE NO	DOP (%)	SHRINKAGE (%)
39	10	2.17
40	10	6.40
41	10	2.37
52	15	8.79
54	15	11.11
24	20	7.94
25	20	13.74
50	25	27.04
51	25	19.73
27	30	12.88
35	30	17.01
47	30	11.85

Figure 6. 22. Plot of the shrinking of the film in percentage as a function of DOP concentration.



Conclusion

The desorption process shows similar characteristics to the water uptake ;

- the diffusion coefficients behave in the same way with respect to the DOP concentration and type of film,
- the shrinking profiles are similar to the swelling profile.

The rates of diffusion are faster due to the fact that the removal is “forced”.

Although the mode of diffusion is different, removal of water from PVC film appears to follow the anomalous diffusion mode. It is reasonable to suggest that the sorption and desorption dynamics are controlled by the same factors.

6. 4. REFERENCES

Anderson S. L., Grulke E. A., DeLassus P. T., Smith P. B., Kocher C. W., Landes B. G., *Macromolecules*, 1995, **28**, 2944.

Armstrong R. D., Handyside T. M., Johnson B. W., *Corros. Sci.*, 1990, **30**, 569.

Badeka A. B., Kontominas M. G., *Zeitschrift fur Lebensmittel - Untersuchung und - Forschung*, 1996, **202(4)**, 313.

Balik C. M., Xu J. R., *J. of Appl. Polym. Sci.*, 1994, **52(7)**, 975.

Berens A. R., *J. of Appl. Polym. Sci.*, 1989, **37(4)**, 901.

Berens A. R., Hopfenberg H. B., *J. of Membr. Sci.*, 1982, **10(2-3)**, 283.

Borek J., Osoba W., *J. of Radioanal. and Nuclear Chem.*, 1996a, **211(1)**, 61.

Borek J., Osoba W., *J. of Polym. Sci.*, 1996b, **34(11)**, 1903.

Bouzon J., Vergnaud J. M., *Eur. Polym. J.*, 1991, **27(2)**, 115.

Chalykh A. E., Belokurova A. P., *Izvestiya vysshikh uchebnykh zavedenii khimiya i khimicheskaya tekhnologiya*, 1982, **25(5)**, 607.

Chan A. D. C., Li X., Harrison D. J., *Anal. Chem.*, 1992, **64(21)**, 2512.

Cherry B. M., Yue C. Y., *J. of Mat. Sci. Lett.*, 1986, **5(9)**, 852.

Coughlin C. S., Mauritz K. A., Storey R. F., *Macromolecules*, 1991, **24(7)**, 1526.

De'Nève B., Shanahan M. E. R., *Polymer*, 1993, **34(24)**, 5099.

Domjan A., Ivan B., Suvegh K., Vertes A., *J. of Radioanal. and Nuclear Chem.*, 1996, **211**(1), 219.

Elwell R. J., Pethrick R. A., *Eur. Polym. J.*, 1990, **26**, 853.

Ercken M., Adriaensens P., Vanderzande D., Gelan J., *Macromolecules*, 1995, **28**(25), 8541.

Fieldson G. T., Barbari T. A., *Polymer*, 1993, **34**(6), 1146.

Fieldson G. T., Barbari T. A., *AIChE J.*, 1995, **41**(4), 795.

Fayad N. M., Sheikheldin S. Y., AlMalack M. H., ElMubarack A. H., Khaja N., *J. of Environ. Sci. and Health, part A - Environ. Sci. and Eng. and Toxic and Hazard. Subs. Control*, 1997, **32**(4), 1065.

Goulas A. E., Kokkinos A., Kontominas M. G., *Zeitschrift fur Lebensmittel - Untersuchung und - Forschung*, 1995, **201**(1), 74.

Goulas A. E., Riganakos K. A., Ehlermann D. A. E., Demertzis P. G., Kontominas M. G., *J. of Food Protection*, 1998, **61**(6), 720.

Griffiths P. F. J., Krikor K., Park G. S., *Polymer Additives*, ed. J. E. Krests, Plenum Press, New York, USA, 1984, p. 249.

Hammarling L., Gustavsson H., Svensson K., Karlsson S., Oskarsson A., *Food Additives and Contaminants*, 1988, **15**(2), 203.

Hodge R. M., Bastow T. J., Edward G. H., Simon G.P., Hill A. J., *Macromolecules*, 1996, **29**, 8137.

Jean Y. C., *NATO Advanced Research Workshop*, 1993, **July 16 -17**, 563.

Jenke D. R., *J. of Pharma. Sci.*, 1993, **82**(6), 617.

Kalaouzis P. J., Demertzis P. G., *Polym. Int.*, 1993, **32**(2), 125.

Li Z., Li X. Z., Petrovic S., Harrison D. J., *Anal. Chem.*, 1996a, **68**(10), 1017.

Li Z., Li X. Z., Rothmaier M., Harrison D. J., *Anal. Chem.*, 1996b, **68**(10), 1726.

Liu Y., Roy A. K., Jones A. A., Inglefield P. T., Ogden P., *Macromolecules*, 1990, **23**, 968.

Maeda Y., Paul D. R., *J. of Polym. Sci., part B : Polym. Phys.*, 1987, **25**, 1005.

Marian S., Jagur - Grozinski J., Kedem O., Vodis D., *Biophys. J.*, 1970, **10**, 901.

Messadi D., Fertikh N., Gheid A. E. H., *Eur. Polym. J.*, 1991, **27**(11), 1187.

Messadi D., Gheid A. E. H., *Eur. Polym. J.*, 1994, **30**(2), 167.

Okuno H., Nishida T., Uragami T., *J. of Polym. Sci., part B, Polym. Phys.*, 1995a, **33**(2), 299.

Okuno H., Nishimoto H., Miyata T., Uragami T., *Makromol. Chem. - Macromol. Chem. and Phys.*, 1993, **194**(3), 927.

Okuno H., Renzo K., Uragami T., *J. of Membr. Sci.*, 1995b, **103**(1-2), 31.

Park J. K., Bontoux L., *J. of Appl. Polym. Sci.*, 1993, **47**(5), 771.

Perry K. L., McDonald P. J., Clough A. S., *Magnetic Resonance Imaging.*, 1991, **12**(2), 217.

Perry K. L., McDonald P. J., Randall E. W., Zick K., *Polymer*, 1994, **35**(13), 2744.

Petersen J. H., Breindahl T., *Food Additives and Contaminants*, 1998, **15**(5), 600.

Riquet A. M., Sandray V., Akermann O., Feigendaum A., *Science des Aliments*, 1991, **11**(2), 341.

Roy A. K., Inglefield P. T., Shibata J. H., Jones A. A., *Macromolecules*, 1987, **20**, 1434.

Sammon C., *Vibrational spectroscopic studies of diffusion and degradation processes in poly(ethylene terephthalate)*, PhD Thesis, 1998.

Schlöter N. E., Furan P. Y., *Vib. Spec.*, 1992, **3**, 147 and *Polymer*, **33**(16), 3323.

Shailaja D., Yaseen M., *Polym. Int.*, 1993, **32**(3), 247.

Southern E., Thomas A. G., *ACS Symposium Series 127*, 1980, 375.

Stauffer G. L., Kleinberg M. L., Rogers K. R., Latiolais C. J., *American Journal of Hospital Pharmacy*, 1981, **38**(7), 998.

Taverdet J. M., Hivert M., Vergnaud J. M., *Abstracts of Papers of the American Chemical Society*, 1982, **184**(sep), 8 -orpl.

Valtier M., Tekely P., Kiene L., Canet D., *Macromolecules*, 1995, **28**(12), 4075.

Vernaud J. M., *J. of Polym. Eng.*, 1996, **15**(1-2), 57.

Vrentas J. S., Ling H. C., Duda J. L., *Macromolecules*, 1988, **21**, 1470.

CHAPTER 7. :
FTIR-ATR STUDIES OF THE PERTURBATION OF
WATER MOLECULES IN A POLY(VINYL
CHLORIDE) MEMBRANE.

CONTENTS

CHAPTER 7. : FTIR-ATR STUDIES OF THE PERTURBATION OF WATER MOLECULES IN A POLY(VINYL CHLORIDE) MEMBRANE.	237
7. 1. INTRODUCTION.....	239
7. 2. METHOD.....	240
7. 2. 1. ATR measurements	240
7. 2. 2. Band fitting procedure	241
7. 2. 3. Quantitative measurement of the perturbation	246
7. 3. RESULTS AND DISCUSSIONS	248
7. 3. 1. Changes in band shape	248
7. 3. 2. Changes in band position.....	252
7. 3. 3. Changes in intensity.....	258
7. 4. REFERENCES.....	262

CHAPTER 7. : FTIR-ATR STUDIES OF THE PERTURBATION OF WATER MOLECULES IN A POLY(VINYL CHLORIDE) MEMBRANE.

7. 1. INTRODUCTION

It has been known for a long time, that polymer-surface bound water is (i) different from bulk water (Bellissent-Funnel et al. 1992, Doster et al. 1986, Teixeira et al. 1980, Toa 1993, Settles and Doster 1996, Bryant 1996, Otting et al. 1991, McBrierty et al. 1982, Giordano et Al. 1993 and 1995), (ii) important for the behaviour of such surfaces in many applications such as protein dynamics (Pethig 1992, Kauzmann 1959) , food preparation (Sartor and Johari 1996, Belton 1991) and transport phenomena across membranes (Li et al. 1996a and 1996b, Chan et al. 1992, Pereira and Yarwood 1996, Hajatdoost 1997).

One exciting approach to the characterisation of such perturbed water is to use the FTIR-ATR technique. It has considerable potential in the area for several reasons :

- the spectra are free from saturation artefacts, a major problem when studying water by infrared spectroscopy (Marechal and Chamel 1996a and 1996b),
- the sampling depth is dependent on controllable parameters (Mirabella 1985, Pereira and Yarwood 1994),
- *in-situ* monitoring of diffusion processes is possible (Van Alsten 1995, Jabbari and Peppas 1994 and 1995, Schlotter and Furlan 1992, Fieldson and Barbari 1993, Pereira and Yarwood 1996, Hajatdoost and Yarwood 1997, Balik and Xu 1994 and 1988),
- subtraction techniques available (as described in chapter 3.).

In this chapter, we explore the electronic perturbation of the water molecules caused by sorption into the PVC matrix. Liquid water was treated as though it was composed of a mixture of water molecules experiencing different strengths (weak and strong) and types ($\text{H}_2\text{O}-\text{H}_2\text{O}$, $\text{H}_2\text{O}-\text{DOP}$, $\text{H}_2\text{O}-\text{PVC}$ or $\text{H}_2\text{O}-\text{fluorfolpet}$) of hydrogen bonds. The most recent work on liquid water has been found to be consistent with a two state model (Walrafen et al. 1972, D'Arrigo et al. 1981, Ratcliffe and Irish 1982, Marechal 1991, 1993a and 1993b, and 1994, Libnau et al. 1994 and 1995, Hare and Sorensen 1990 and 1992, Marechal and Chamel 1996) ; two types of hydrogen bonded water, strongly and weakly bonded, or "defect" and "non-defect" water molecules. The band shape, frequency and intensity of water $\nu(\text{OH})$ band in the 3000 to 3700 cm^{-1} region is sensitive to changes in the water molecule environment (Marechal and Chamel 1996, Nguyen et al. 1991, Falk 1980, Van Alsten and Coburn 1994). The O-H stretching band of water at 3000 - 3700 cm^{-1} is due to intermolecular and intramolecular ($\nu_s(\text{OH})$ and $\nu_{as}(\text{OH})$) O-H oscillator coupling.

We chose to study the $\nu(\text{OH})$ stretching band of water, and not the bending mode, due to overlap between the $\nu(\text{C}=\text{O})$ stretching bands of fluorfolpet and DOP with the bending mode of water in the 1650 cm^{-1} region. Deconvolution is therefore difficult.

7. 2. METHOD

7. 2. 1. ATR measurements

All measurements were carried out in a liquid-holding ATR cell at ambient temperature. The data were taken as a function of time in connection with water diffusion measurement, as described in chapter 4. Materials and sample preparation are also described in chapter 4.

7.2.2. Band fitting procedure

A detailed analysis of the spectra was achieved by fitting the overall band profile of water in the polymer and pure water in the way shown in **figures 7. 1. and 7. 2.** Details of the component band parameters are shown in **table 7. 1.** Band decomposition was achieved using the curve fitting routine from the Grams-32 software. All the parameters, except the band shape which was fixed at 50% Gaussian / 50% Lorentzian, were allowed to vary upon iteration (see chapter 2.). The statistical parameters defined in the software manual were used as guide to “best fit”.

Figure 7. 1. Shows the band fitting results for water in pure PVC and plasticised PVC (pPVC) at equilibrium. (A) pure PVC, (B) 20% DOP / PVC, (C) 30% DOP / PVC.

Figure 7. 1. (A) Pure PVC.

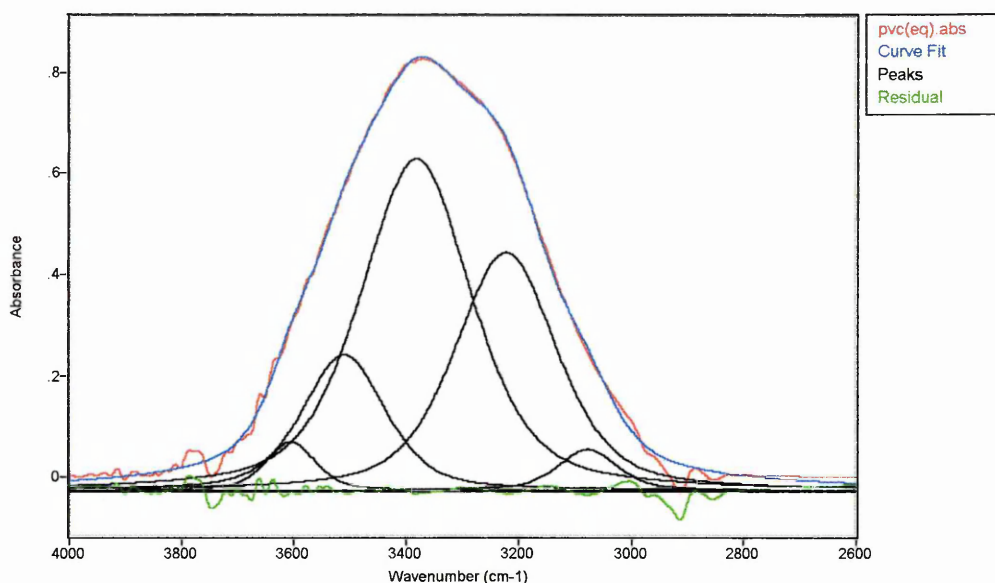


Figure 7. 1. (B) 20% DOP / PVC.

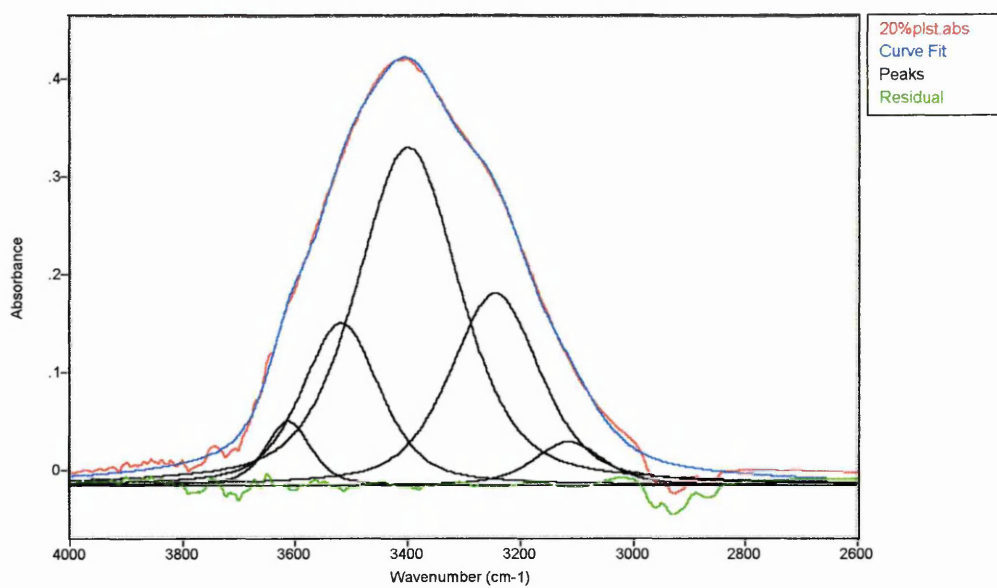


Figure 7. 1. (C) 30% DOP / PVC.

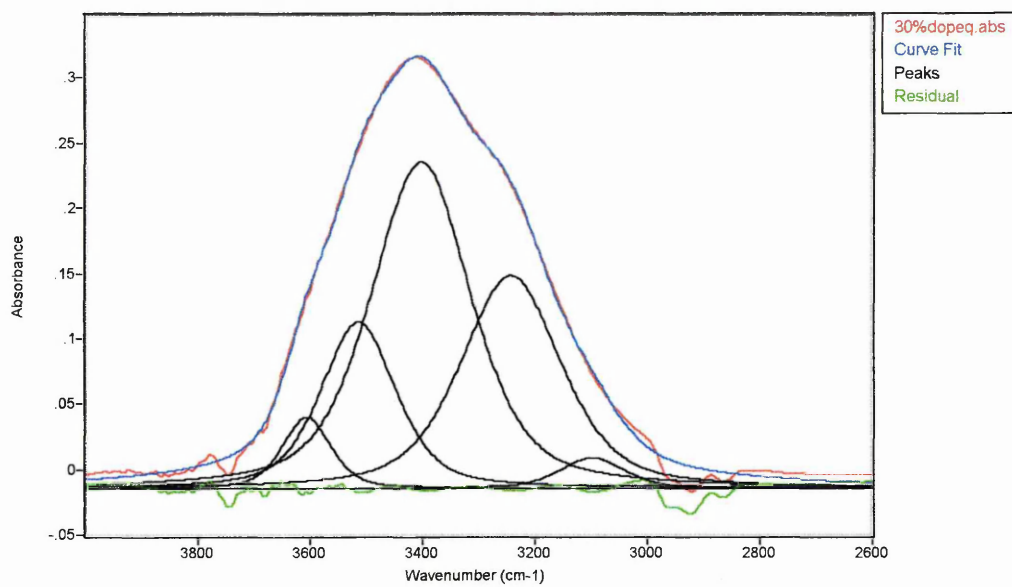


Figure 7. 2. Shows the band fitting results for pure water et 25°C.

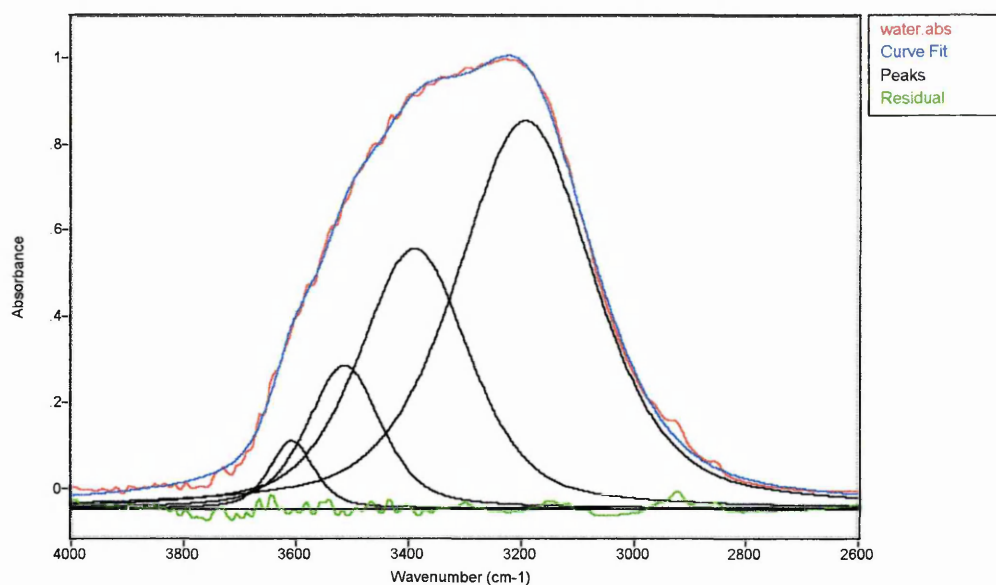


Table 7. 1. Shows the component band parameters for water in PVC as a function of addition of DOP and pure water, including the P factor of (eq. 7. 4.).

Position (cm ⁻¹)	Width (cm ⁻¹)	Area (cm ⁻¹)	Relative %	$\epsilon \times 10^{-8}$ (cm/mol)	P
PVC (0.95%)					
3604	93	12	3.8	3.07	16
3514	148	42	13.3	3.14	17
3393	211	138	43.7	3.88	21
3233	223	124	39.2	1.90	10
20% DOP / PVC (0.35%)					
3612	95	8	4.4	5.56	29
3518	164	34	18.8	6.90	36
3399	215	92	50.8	7.02	37
3244	189	47	26.0	1.96	10
30% DOP / PVC (0.28%)					
3606	103	7	5.0	6.04	32
3514	158	25	18.0	6.31	33
3402	211	65	45.8	6.16	33
3242	210	42	30.2	2.17	11
WATER					
3607	94	19	3.3		
3514	155	65	11.3		
3390	232	173	30.1		
3192	290	317	55.3		

The number of bands and relative positions for starting the band fitting routine were obtained through Fourier deconvolution of the $\nu(\text{OH})$ stretching band, as shown in **figure 7. 3.** Deconvolution parameters were as follows :

- W (full width at half height) = 150.00 cm^{-1}
- k (enhancement factor) = 1.5
- Fraction Lorentzian = 0.5
- Apodisation function = triangle

Also, in fitting our data for the pure water profile, we get very similar frequencies and relative intensities to those obtained by Libnau and co-workers (Libnau et al. 1995 and 1994).

Figure 7. 3. Shows the deconvoluted spectra of water in PVC. (A) pure PVC, (B) 20% DOP / PVC, (C) 30% DOP / PVC.

Figure 7. 3. (A) Pure PVC.

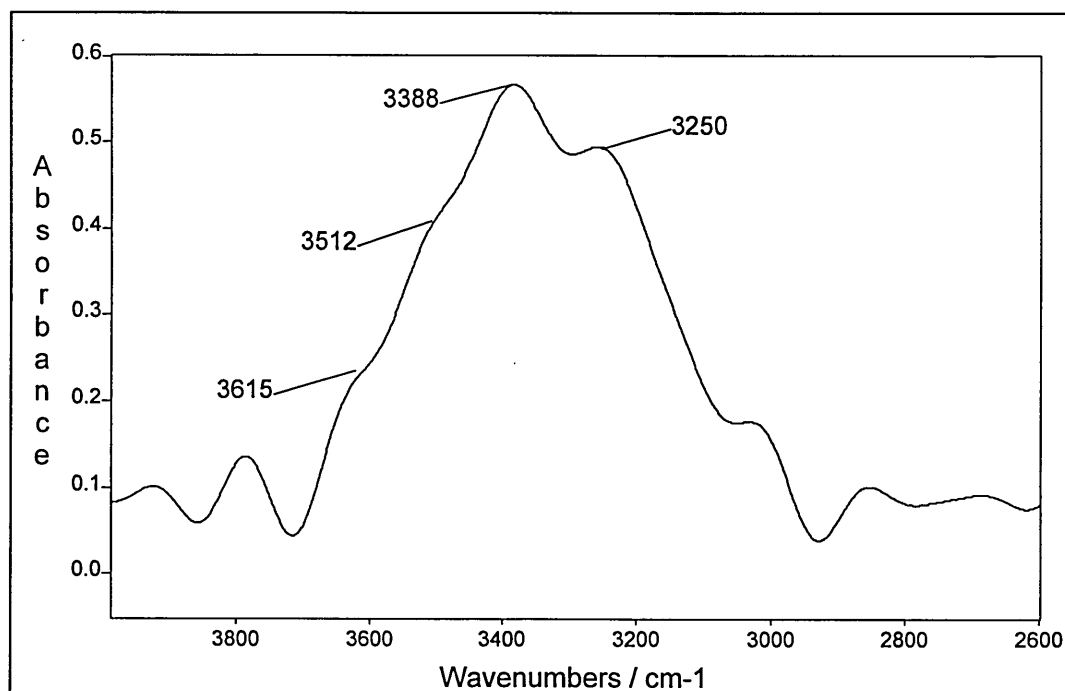


Figure 7. 3. (B) 20% DOP / PVC.

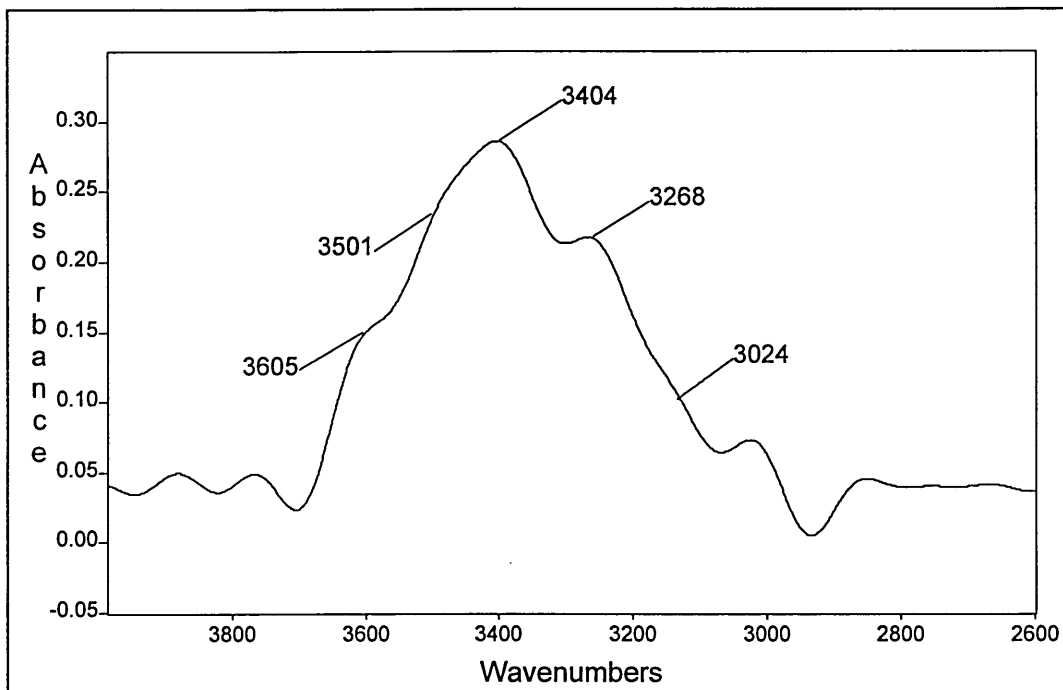
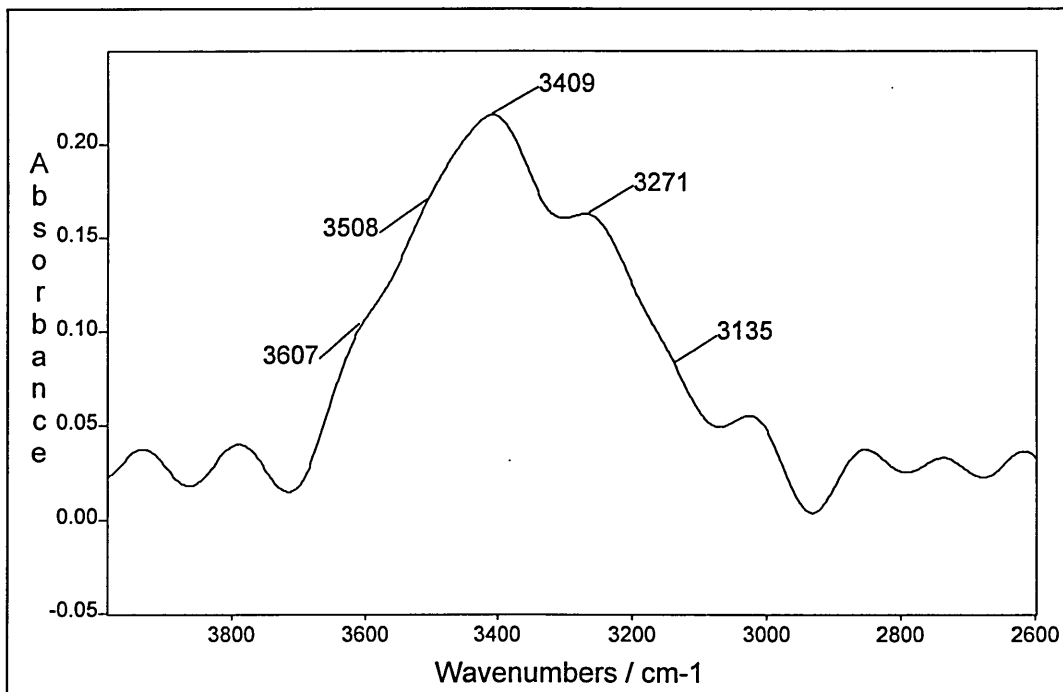


Figure 7. 3. (C) 30% DOP / PVC.

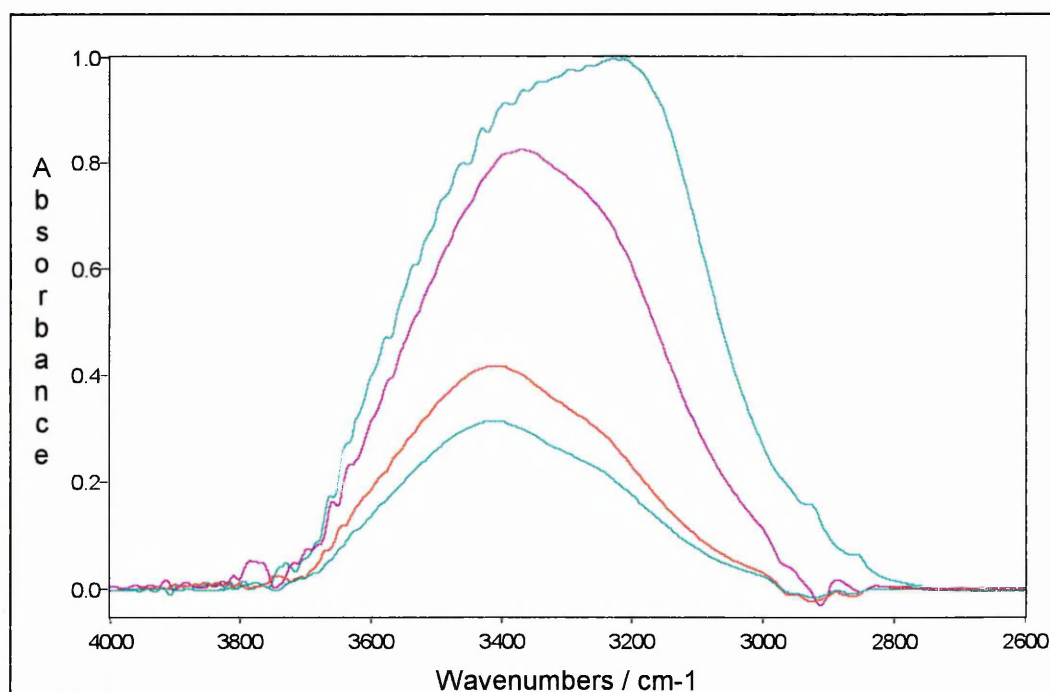


7. 2. 3. Quantitative measurement of the perturbation

As can be seen in **table 7. 1.**, the water uptake of pure PVC and pPVC films at equilibrium is very small (< 1%). However, the intensities of the overall $\nu(\text{OH})$ stretching band or indeed the component bands of water in the polymer compared to that of pure water (see **figure 7. 4.**) are much larger than expected. This emphasises that, in infrared spectroscopy there are likely to be changes of extinction coefficient when water molecules engage in or are released from their hydrogen bonding environment.

The extinction coefficient for pure water at 3360 cm^{-1} is $\epsilon_w = 18.830 \times 10^6 \text{ cm/mol}$ (Fringeli 1996).

Figure 7. 4. The spectra of water in PVC and pure water.



For an ATR experiment the absorbance of a particular band at wavenumber ν is given by :

$$\text{abs} = \log\left(\frac{I_0}{I}\right)_{\nu} = \epsilon_{\nu} c d_e \quad (\text{eq. 7. 1.})$$

Where ε = extinction coefficient,
 c = concentration,
 d_e = effective path length.

The corresponding integrated band intensity is expressed as :

$$B = \int \varepsilon_{\nu} d\nu = \text{area} / cd_e \quad (\text{eq. 7. 2.})$$

Because ε and B crucially depend on the molecular environment or perturbation (Marechal and Chamel 1996, Christopher et al. 1992, Falk 1975), comparison of B values for component bands of water in the polymer with those of pure water will therefore give a measure of that perturbation :

$$P = \frac{B_p}{B_w} \quad (\text{eq. 7. 3.})$$

Where P = some measure of the oscillator perturbation due to sorption in the polymer,
 B_p = apparent integrated intensities of the component bands of water in the polymer,
 B_w = apparent integrated intensities of the component bands of water in pure water.

Therefore the expression of P becomes :

$$P = \frac{B_p}{B_w} = \left(\frac{C_w}{C_p} \right) \left(\frac{d_w}{d_p} \right) \frac{\text{area}^p}{\text{area}^w} \quad (\text{eq. 7. 4.})$$

Where C_w = concentration of pure water (55 mol/l),
 C_p = concentration of water in the polymer,
 d_w = path length in pure water (0.7604),
 d_e = path length in polymer / water system (1.2955).

d_w and d_e were calculated using (eq. 2.) and (eq. 2.).

Example of calculation of P for pure PVC (band at 3604 cm^{-1}) :

$C_p = 1.25\text{ mol/l}$,

$\text{area}^p = 11.651$,

$\text{area}^w = 18.906$.

$$P = \left(\frac{55}{1.25} \right) \left(\frac{0.7604}{1.2955} \right) \frac{11.651}{18.906} = 15.915 \cong 16$$

Important assumptions must be made when using the method :

- (i) our spectra contain only intensity from water in the polymer matrix,
- (ii) a homogeneous distribution of water molecules occurs among the sites,
- (iii) changes of B are due only to network "perturbation" and / or interactions with polymer,
- (iv) there is a one to one correspondence of the component bands of pure water with those of water in the polymer.

7. 3. RESULTS AND DISCUSSIONS

7. 3. 1. Changes in band shape

Changes in band shape with time :

Independently from the formulation of the PVC films (i.e. non-plasticised, plasticised or plasticised and containing fluorfolpet), the shape of the water spectrum in the $3000 - 3700\text{ cm}^{-1}$ region varies as a function of time. The shoulder at 3200 cm^{-1} grows more quickly than the main band at 3400 cm^{-1} (see **figure 7. 5.**). The 3700 to 3400 cm^{-1} region is attributed to weak hydrogen bonding of the water molecules. Therefore as water diffuse into the film there is a strengthening of the water hydrogen bonded network.

Figure 7. 5. shows the infrared spectra for water diffusing into a PVC film as a function of time. (A) for pure PVC, (B) for a 25% DOP / PVC film, and (C) for a 20% DOP / 5% fluorfolpet / PVC film.

Figure 7. 5 (A). The infrared spectra for water diffusing into a PVC film.

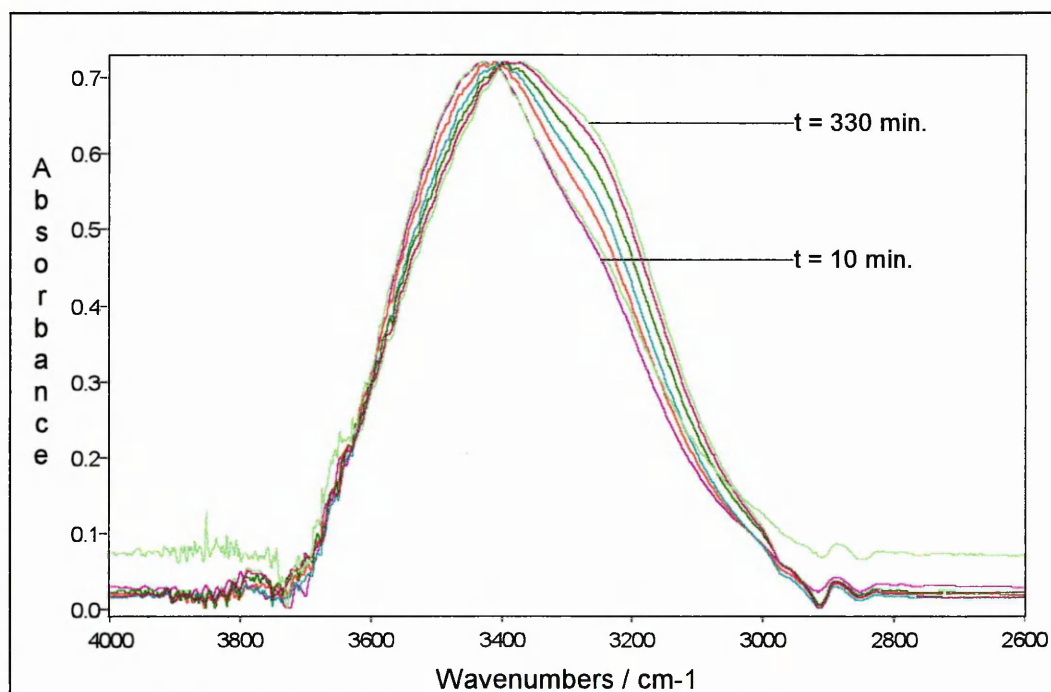


Figure 7. 5 (B). The infrared spectra for water diffusing into a 25% DOP / PVC film.

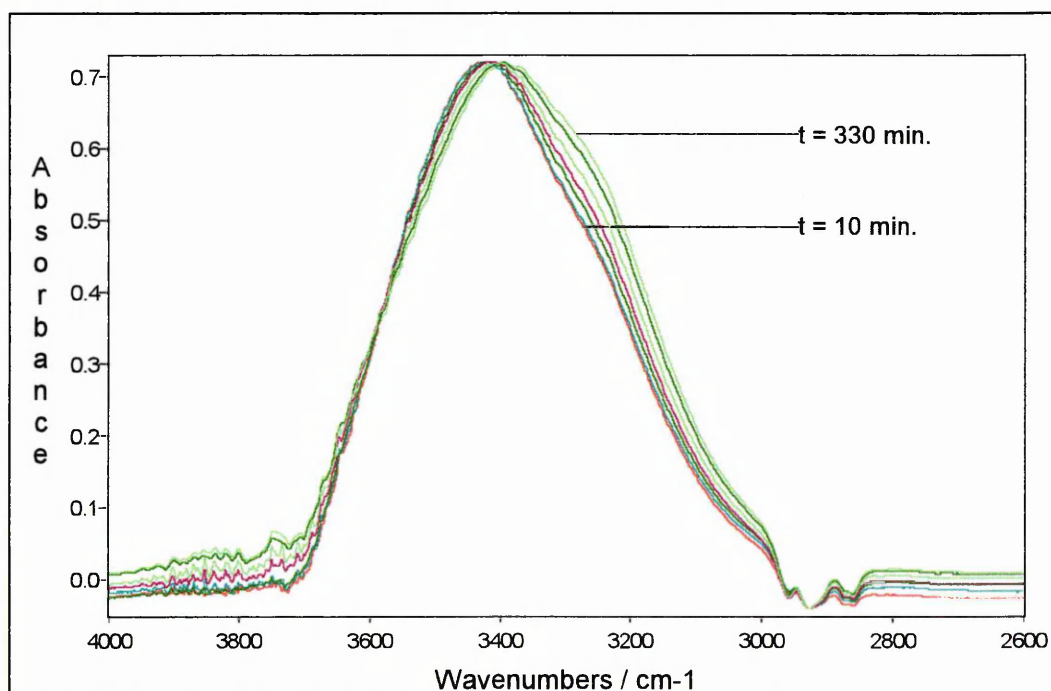
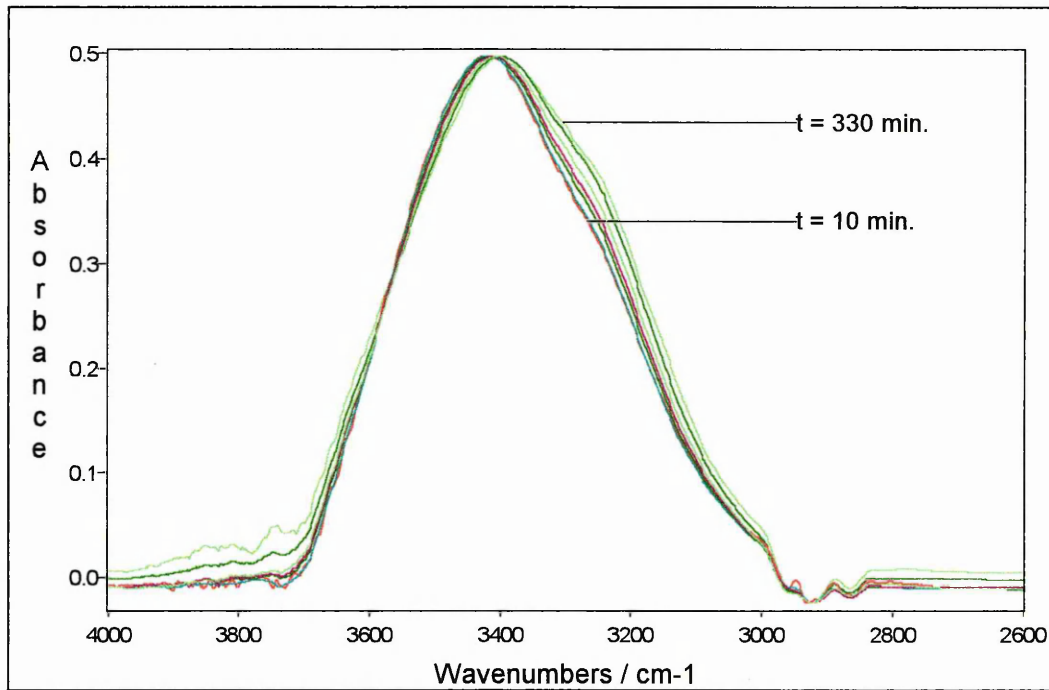


Figure 7. 5 (C). The infrared spectra for water diffusing into a 25% DOP / 5% fluorfolpet / PVC film.



Changes in band shape with DOP concentration (at equilibrium water content) :

The shape of the water spectrum in the 3000 to 3700 cm⁻¹ region varies with DOP concentration in the film.

For DOP / PVC films, it can be seen that as the dioctylphthalate concentration increases, the shoulder at 3200 cm⁻¹ shrinks, indicating a weakening of the hydrogen bonded network (see **figure 7. 6.**).

For DOP / PVC / fluorfolpet films, it can be seen that the hydrogen bond network weakens as follows : 20 ~ 25% < 15 ~ 30% < 10% DOP concentration (see **figure 7. 7.**).

Figure 7. 6. The infrared spectra of water in pPVC films, at equilibrium.

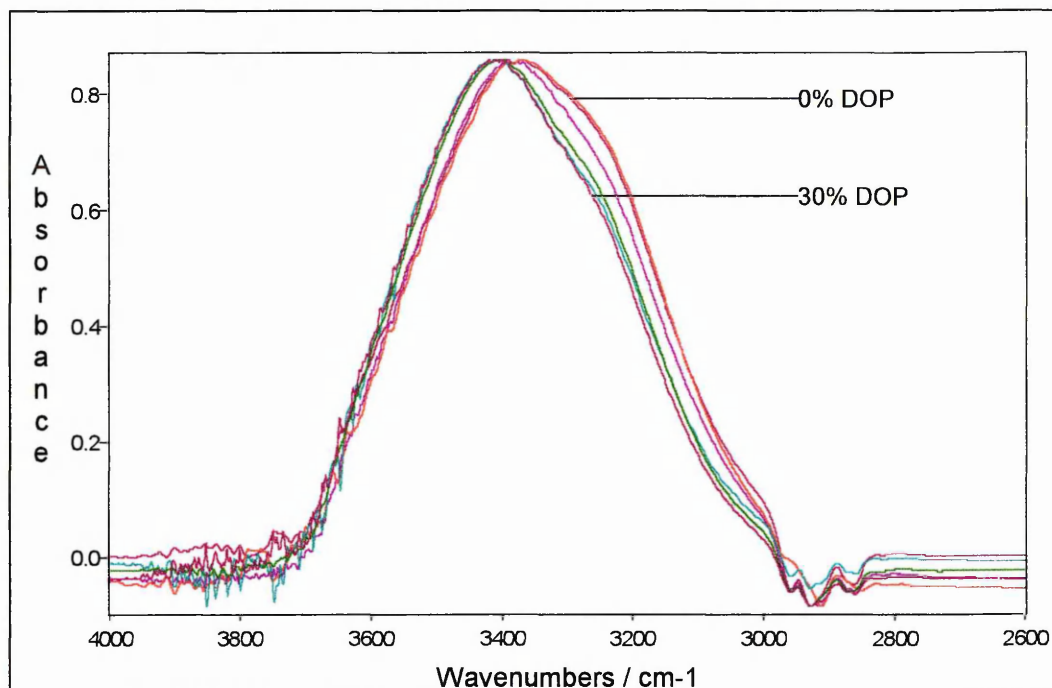
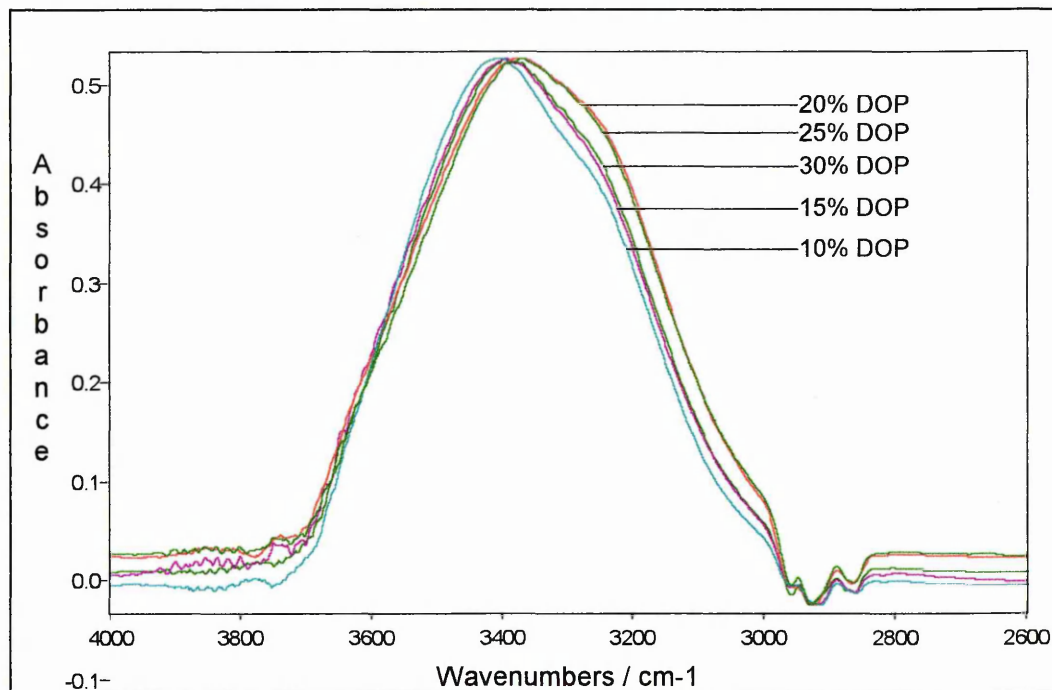


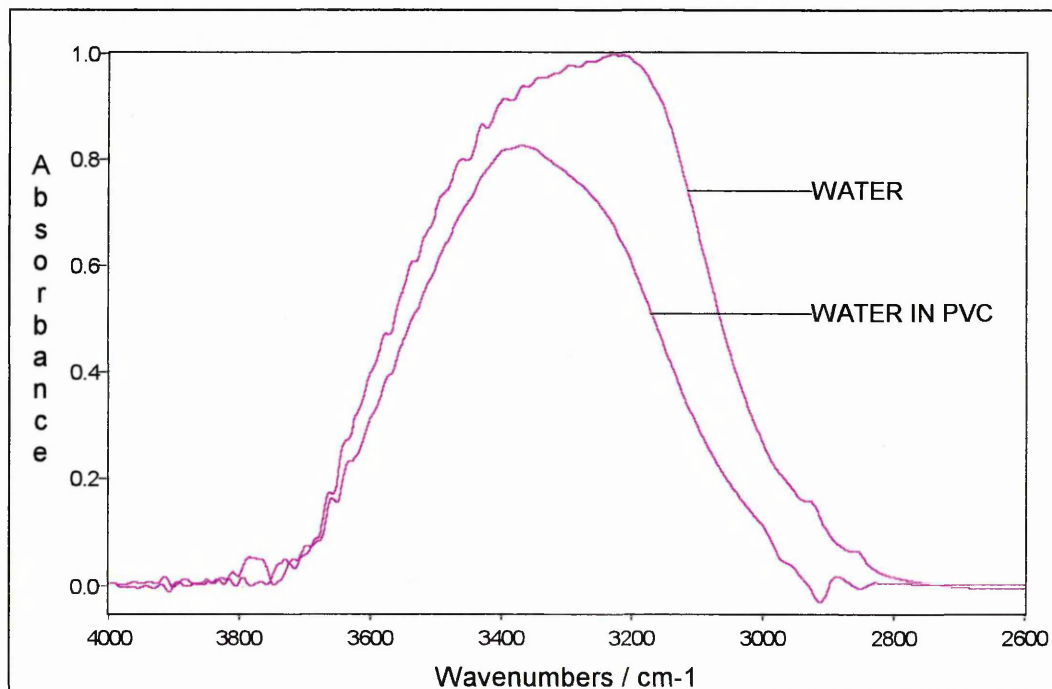
Figure 7. 7. The infrared spectra of water in pPVC films containing the additive fluorfolpet (5% in wt), at equilibrium.



Furthermore, the shape of the water spectrum in the polymer is quite different from that of pure water obtained under the same conditions in the same cell (**figure 7. 8.**). The relative decrease of the water band at lowest wavenumbers

for the polymer compared to that of water reflects the breaking of the strong hydrogen bonded water network and the greater importance of more weakly bound water species at wavenumbers near 3380 - 3530 cm^{-1} .

Figure 7. 8. The infrared spectrum of water in pure PVC (0.84 abs units) compared with pure water (0.99) spectrum, at equilibrium.



7. 3. 2. Changes in band position

Changes in band position with time :

Figure 7. 5. Clearly shows that there is a slight shift of the band position, with time, towards the lower wavenumbers, indicating a strengthening of the water hydrogen bonded network. This is true for pure PVC, pPVC and pPVC containing fluorfolpet.

Figure 7. 9. Shows the changes of frequency with time for the four bands of water in a 20% DOP / 5% fluorfolpet / PVC film. (A) "free" water, (B) "weakly hydrogen bonded" water, (C) "moderately hydrogen bonded" water, (D) "strongly hydrogen bonded" water.

As the behaviour with time of the overall band position (and band shape) of the $\nu(\text{OH})$ band of water in pure PVC, pPVC and pPVC containing fluorfolpet is identical, it is reasonable to suggest that the behaviour of the component bands will be the same for both film types (with or without fluorfolpet).

Figure 7. 9. (A) Changes of frequency with time of the “free” water component band of water in PVC.

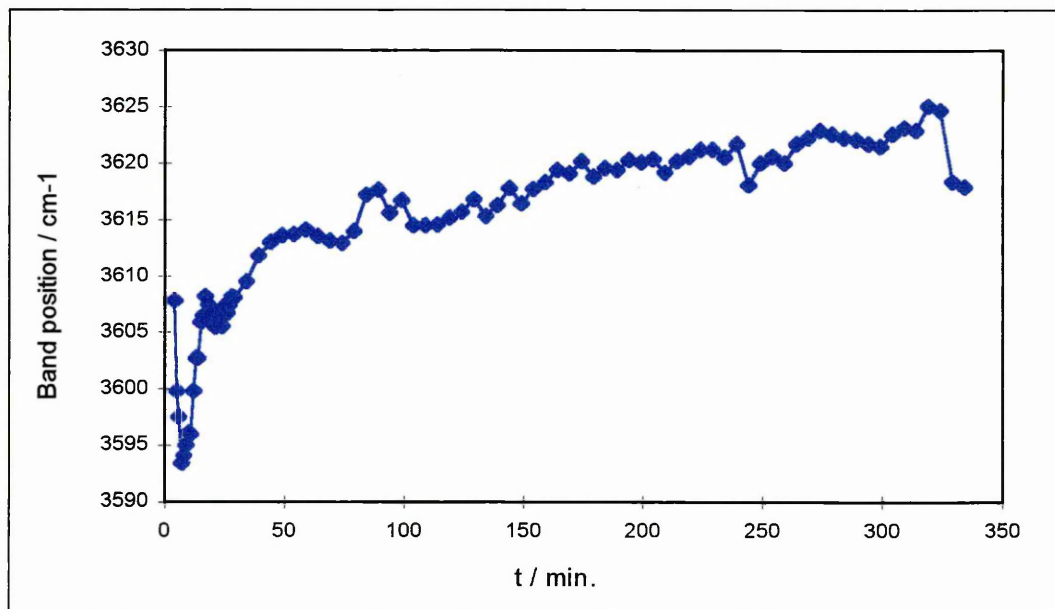


Figure 7. 9. (B) Changes of frequency with time of the “weakly hydrogen bonded” water component band of water in PVC.

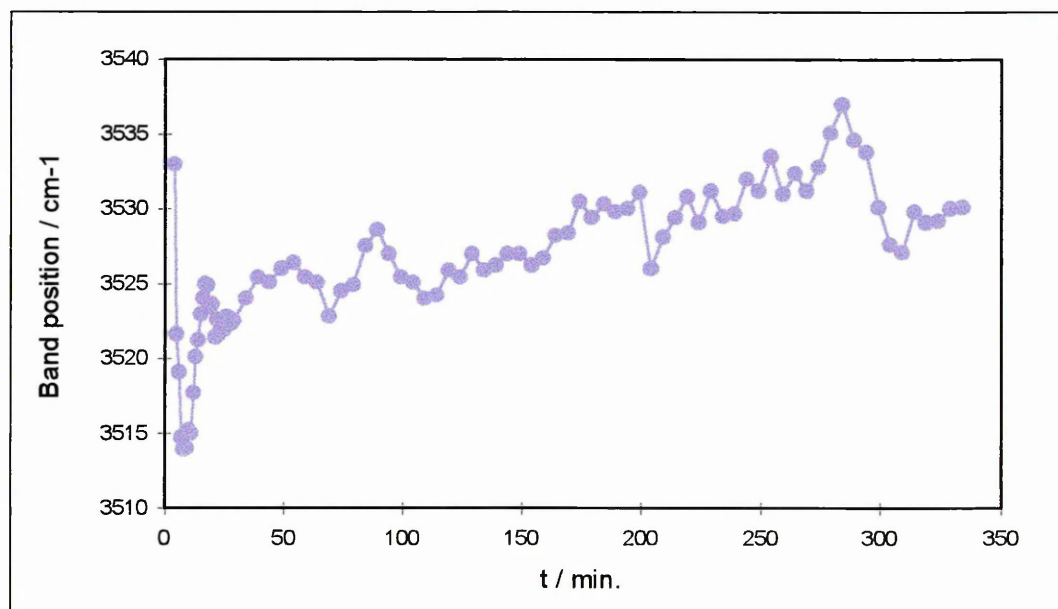


Figure 7. 9. (C) Changes of frequency with time of the “moderately hydrogen bonded” water component band of water in PVC.

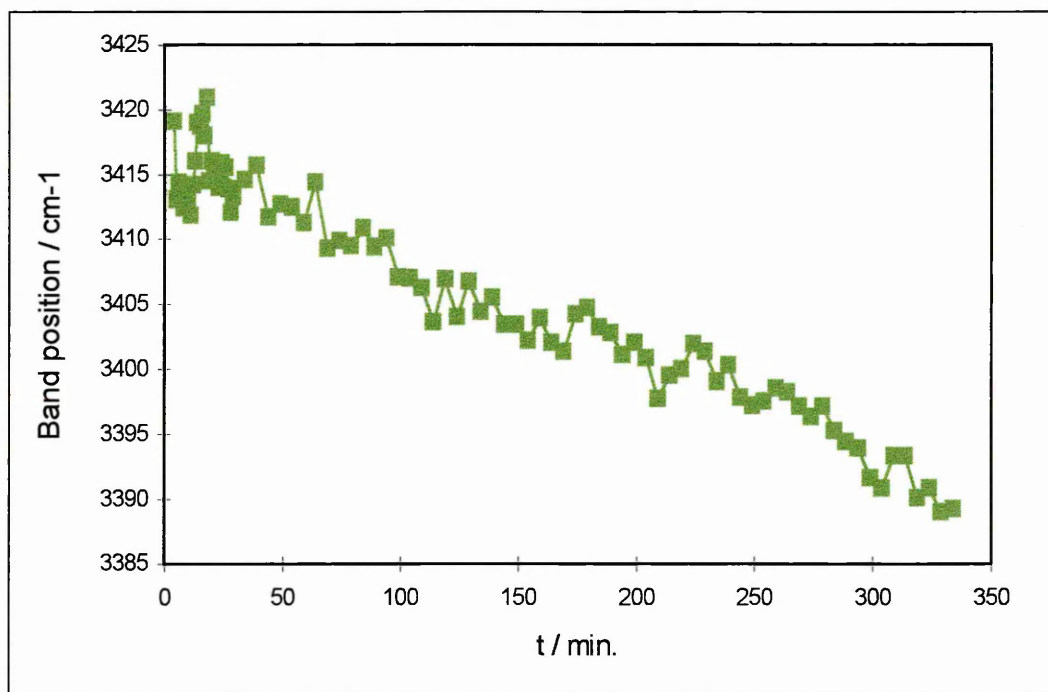
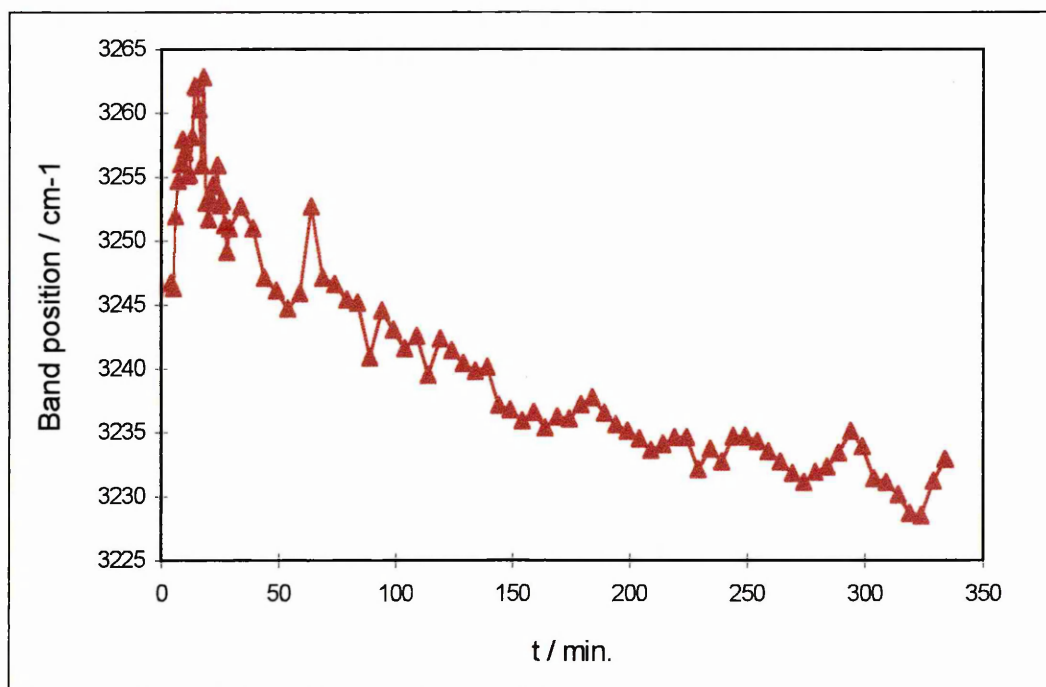


Figure 7. 9. (D) Changes of frequency with time of the “strongly hydrogen bonded” water component band of water in PVC.



Two out of the four bands also show a general shift to low wavenumbers when water dissolves in the polymer, in accordance with the overall band profile shift with time. The remaining other two bands show a shift in the opposite direction, towards high wavenumbers.

At the very early times (first 10 to 15 minutes), all the component bands shift towards lower wavenumbers, and two of them shift to lower wavenumbers than the corresponding band in pure water, implying that, when water first dissolves in the polymer, the interactions resulting (probably between water and the polymer or the plasticiser) are stronger compared with the corresponding interactions in liquid water. In all cases, as the amount of water in the polymer increases, the component bands shift to higher wavenumbers, reflecting the movement back towards the water environment to be found in liquid water, but always less strongly hydrogen bonded than in the full water network.

This suggest that at low concentration of water, the network is broken and the water molecules are arranged in small clusters within the polymer microstructure. As the amount of water increases in the polymer, the cluster size also increases, as expected.

Changes in band positions with DOP concentration :

The changes in band position with change in DOP concentration and addition of fluorfolpet to the film, confirm the observations obtained from the change in shape of the $\nu(\text{OH})$ stretching band of water in the polymers.

For PVC / DOP films : it can be seen that the bands shift towards higher wavenumbers as the percentage of DOP in the PVC films increases, i.e. towards weakening of the hydrogen bond network (see **figure 7. 6.**).

For PVC / DOP / PA3 : **figure 7. 7.** Shows that the position of the band shifts to increasing wavenumbers in the following order of DOP concentration on the film : 20 ~ 25% < 15 ~ 30% < 10%. This very much shows how the strength of the hydrogen network is related to the amount of water sorbed by the polymer. Indeed, the changes in hydrogen bonding strength in the polymer with DOP concentration reflects the sorption profiles obtained for both types of films in chapter 6. (**figure 6. 9.**). The lower the water content, the weaker the hydrogen network and vice versa.

Furthermore, comparison between the spectrum of pure water and water in PVC, shows that there is a considerable shift of the band position towards higher wavenumbers, i.e. weaker hydrogen bonding, for water in PVC (see **figure 7. 8.**). It has been generally found (Falk 1980, Quezado et al. 1984, Luck 1980, Scherer et al. 1985 and 1974, Maeda et al. 1993, 1995 and 1996, Bashir et al. 1995, Murphy and Depihno 1995, Van Alsten and Coburn 1994, Sutander et al. 1994 and 1995, Kusanagi and Yukawa 1994, Crupi et al. 1996), for a wide range of polymers, that water dissolved in an organic medium (either an organic solvent or polymer matrix) is, on average, more weakly hydrogen bonded than water molecules in the pure water network. This is probably due to the breaking of the water network to produce smaller clusters and the (weaker) hydrogen bonding of water molecules to the polymer chemical groups.

By examining the water spectrum as a function of time for desorption, more information on the question of the state of water in PVC can be obtained. **Figures 7.10.** and **7. 11.** both show the spectrum of water in the 3000 to 3700 cm^{-1} range for desorption, as a function of time. **Figure 7. 10.** shows the water band obtained by ratioing the spectrum of the dry film, in other words, the spectra show the state of water which is still in the polymer. It can be seen that there is a distinct band shift to low wavenumbers as water is gradually removed by the desorption process. This means that water in the polymer at longer time is, on average, more strongly hydrogen bonded. It therefore follows that the water molecules removed first are the more weakly hydrogen bonded molecules. This can also be seen from **figure 7. 11.**, which shows the spectra of water obtained by ratioing against the spectrum of the film saturated with water. These spectra show the difference between the water spectrum at equilibrium and that at any particular point in the desorption. In effect, this procedure gives an indirect measure of the water which has been removed. The profiles show a large main peak at 3400 cm^{-1} with only a small shoulder at 3200 cm^{-1} , therefore showing that the water which has "left" the polymer is relatively weakly hydrogen bonded compared with that which has remained in the film. It also shows a slight shift towards lower wavenumbers, demonstrating that the water being removed is gradually more hydrogen bonded.

Figure 7. 10. The spectra of water in PVC for desorption, ratioed against spectrum of dry film.

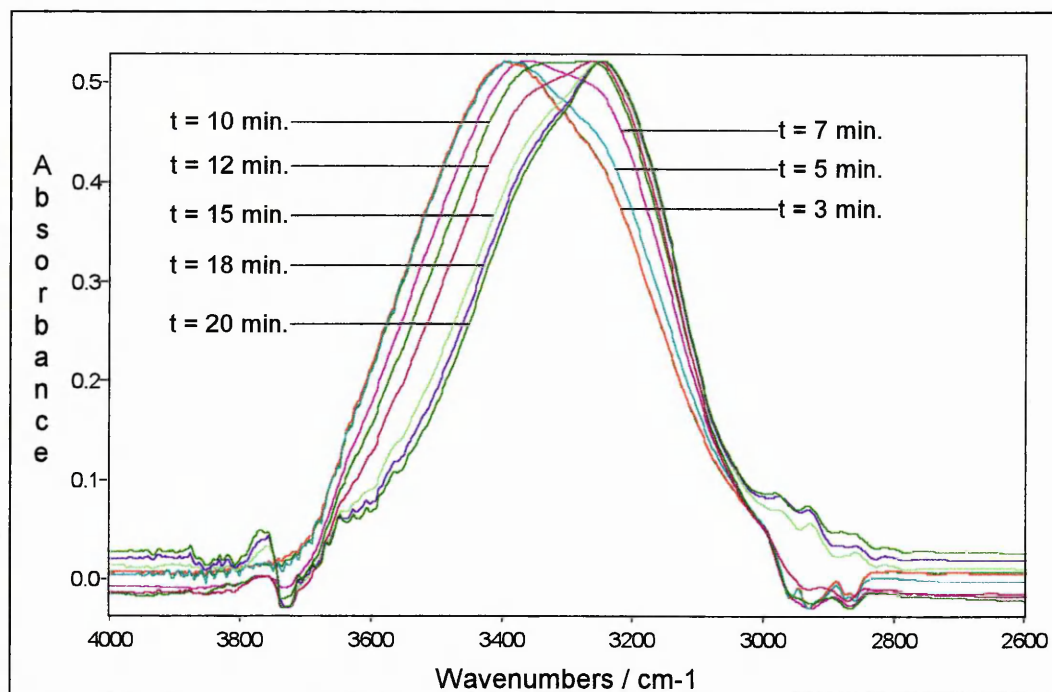
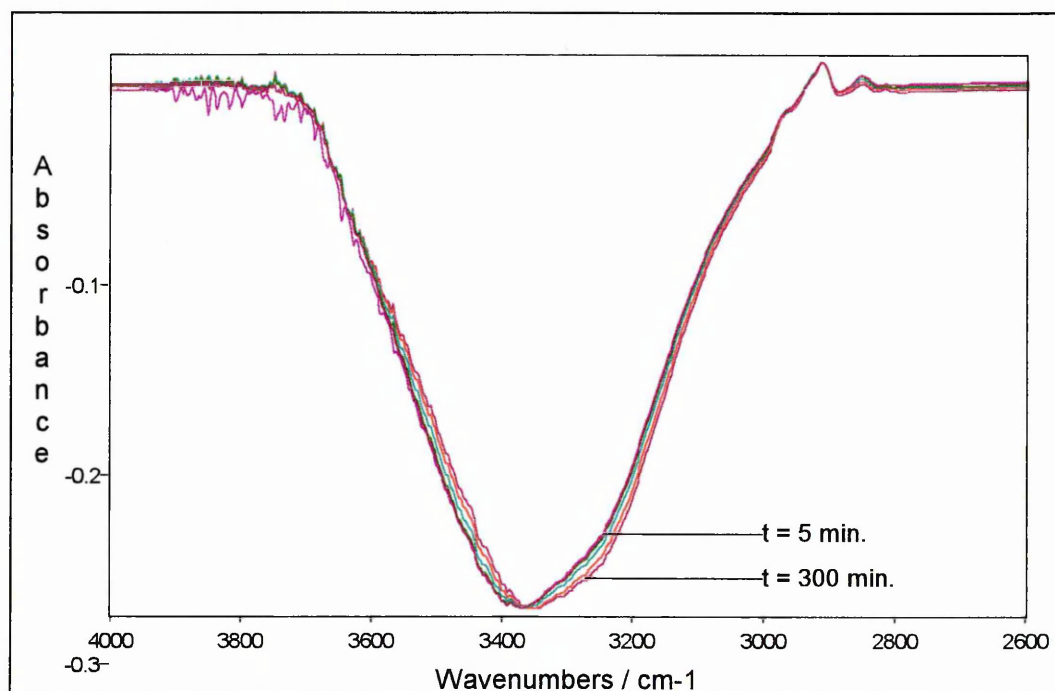


Figure 7. 11. The spectra of water in PVC for desorption, ratioed against spectrum of water saturated film.



7. 3. 3. Changes in intensity

Changes in intensity with time :

Most of the component bands (see **figure 7. 12.**) increase in intensity with time, as expected, since the water diffuses into the polymer during the experiment.

Figure 7. 12. shows the changes of intensity with time for the four bands of water in PVC. (A) “free” water, (B) “weakly hydrogen bonded” water, (C) “moderately hydrogen bonded” water, (D) “strongly hydrogen bonded” water.

Figure 7. 12. (A) Changes of intensity with time of the “free” water component band of water in PVC.

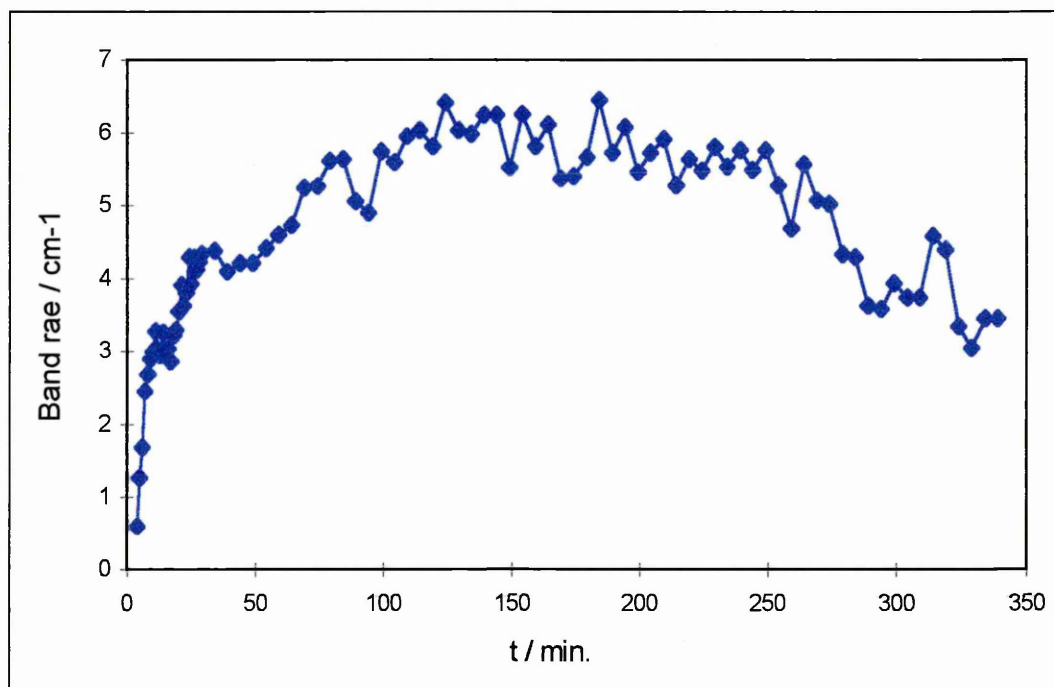


Figure 7. 12. (B) Changes of intensity with time of the “weakly hydrogen bonded” water component band of water in PVC.

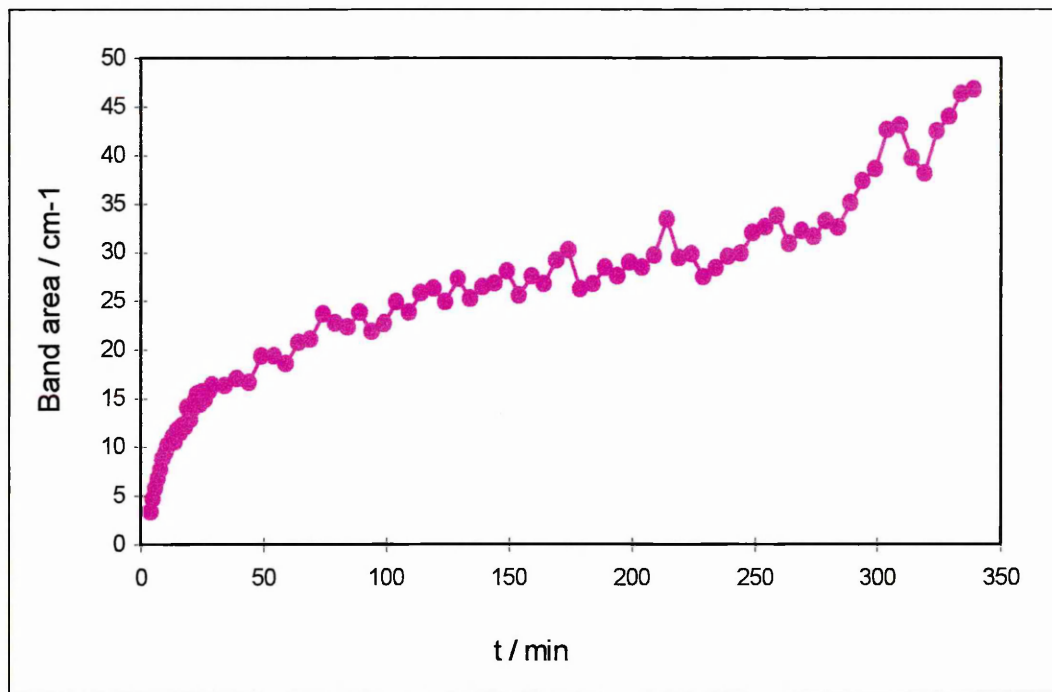


Figure 7. 12. (C) Changes of intensity with time of the “moderately hydrogen bonded” water component band of water in PVC.

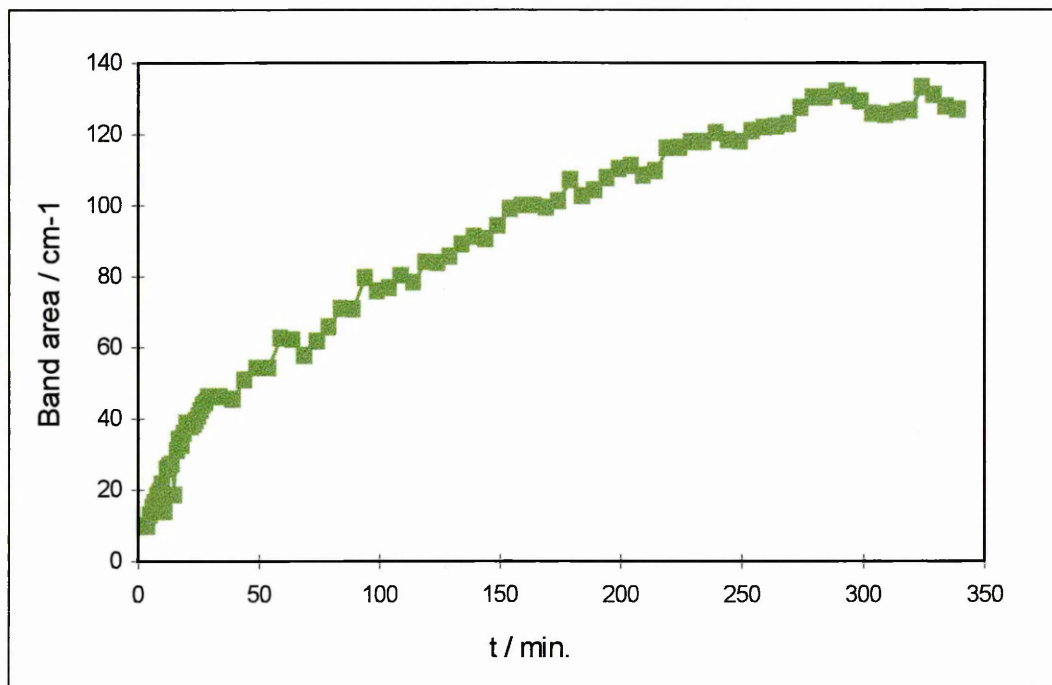
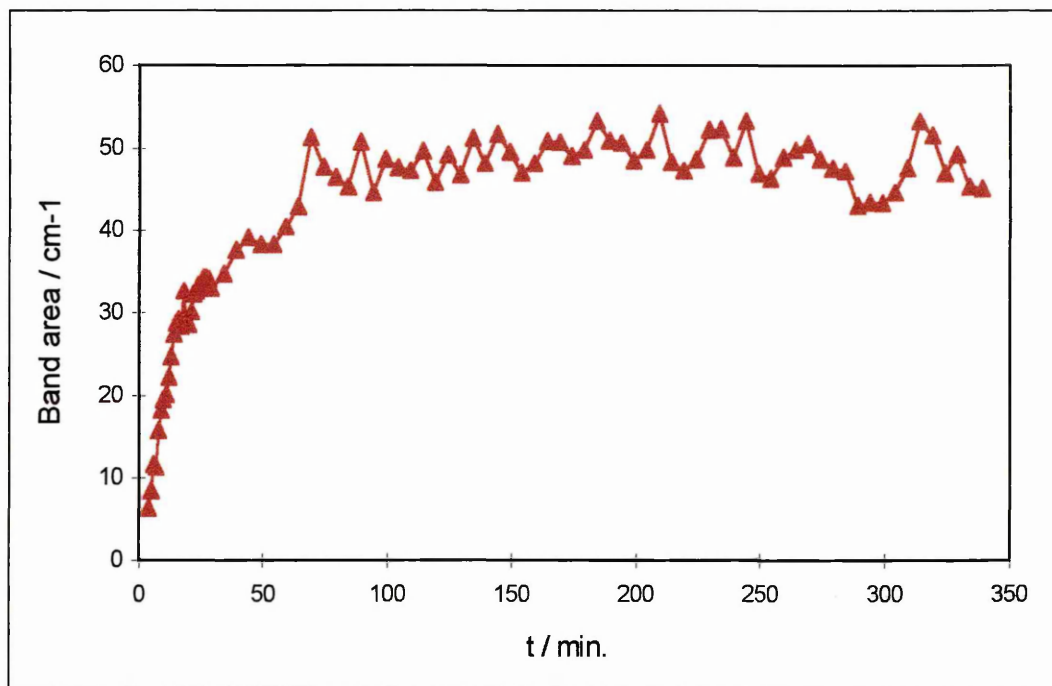


Figure 7. 12. (D) Changes of intensity with time of the “strongly hydrogen bonded” water component band of water in PVC.



Changes in intensity with DOP concentration :

The changes of extinction coefficients when molecules engage in or are released from their hydrogen bonding environment can be quantified by calculating the P factor (as described in section 7. 2 .3.). The values of P are given in **table 7. 1.**

The following types of behaviour can be observed from **table 7. 1. :**

- The component band at lowest wavenumbers (i.e. 3190 cm^{-1} for pure water, and 3240 cm^{-1} for water in PVC) is relatively less important for water in the polymer compared to pure water, reflecting the breaking up of the strongly hydrogen bonded water network and the greater importance of the more weakly bound water species at higher wavenumbers. The alteration of the lower frequency distribution of water $\nu(\text{OH})$ band in the polymer is attributed to (i) interactions of water with chemical groups on the polymer (Cl groups from PVC, ester groups from dioctylphthalate), (ii) formation of “clusters” of water molecules in voids, Chan and co-workers and Li and co-workers (Chan et al. 1992, Li et al. 1996a and 1996b) show evidence of the formation of water droplets throughout the PVC membrane as water diffuses into the film.

- P factors of the order of 10 - 37 are generally obtained. These are the result of a severe intensity enhancement (due to an increase of transition moment ($\partial\mu/\partial q$)) when water is sorbed into the polymer, and the water network of pure water broken, as demonstrated by lower P values for lower wavenumber bands. A similar effect was observed by Devlin and co-worker (Devlin 1990, Hernandez et al. 1998) in the water bending region. They recently demonstrated the dependence of the bending mode frequency on the extent of the hydrogen bonding for the ice-forming water. They showed that as the strength of the hydrogen network increases (i.e. as the bonding of the water molecules approaches that of the ice interior), the infrared band intensity of the bending mode decreases.
- The relative proportions of “moderately hydrogen-bonded” water and “strongly hydrogen-bonded” water changes in the polymer ; there are less “strongly hydrogen-bonded” water molecules and more “moderately hydrogen-bonded” water molecules compared to pure water (P is higher for “moderately hydrogen-bonded” than for “strongly hydrogen-bonded”), i.e. the hydrogen bonded network is weakened in the polymer.
- The P values are dramatically affected by whether or not DOP is added as a plasticiser :
 - (i) the equilibrium water content of pure PVC is considerably higher than that of plasticised PVC material. This is most probably due to saturation of the films. At higher DOP content, less sites are available for binding of water molecules (as discussed in chapter 6.).
 - (ii) the proportion of free water (at 3610 cm^{-1}) in pPVC is higher than that in uPVC, suggesting that DOP is more “hydrophobic” than PVC.

7. 4. REFERENCES

Balik C. M., Xu J. R., *J. of Appl. Polym. Sci.*, 1994, **52**, 975.

Balik C. M., Xu J. R., *Appl. Spec.*, 1988, **42**, 1543.

Bashir Z., Church S. P., Waldron D., *Polymer*, 1995, **35**, 967.

Bellissent-Funnel M. C., Teixeira J., Bradley K. F., Crespi H. L., Chen S. H., *J. of Phys. (Paris)*, 1992, **2**, 955.

Bellissent-Funnel M. C., Teixeira J., Bradley K. F., Crespi H. L., Chen S. H., *Physica B*, 1992, **180 - 181**, 740.

Belton P. S., *The Physical State of Water in Foods*, in *Food Freezing, Today and Tomorrow*, ed. Bold W. B., Springer -Verlag, Berlin, 1991.

Bryant R. G., *Ann. Rev. Biophys. Biomol. Struct.*, 1996, **25**, 29.

Chan A. D. C., Li X., Harrison D. J., *Anal. Chem.*, 1992, (21), 2512.

Christopher D. J., Hills B. P., Belton P. S., Yarwood J. *J. of Colloid Interface Sci.*, 1992, **152**, 465.

Crupi V., Jannelli M. P., Magazu S., Maisano G., Majolino D., Migliardo P., Ponterio R., *J. of Mol. Struct.*, 1996, **381**, 207.

D'Arrigo G., Mansano G., Mallamace F., Migliardo P., Wanderlingh F., *J. of Chem. Phys.*, 1981, **75**, 4264.

Devlin J. P., *J. Mol. Struct.*, 1990, **224**, 33.

Doster W., Bachleitner A., Dunau R., Hiebl M., Lüscher E., *Biophys. J.*, 1986, **50**, 213.

Falk M., *Can. J. of Chem.*, 1980, **58**, 1495.

Falk M., *Chem. Phys.: Aqueous Gas Solutions [Proc. Symp.]*; Electrochemical Society : Princeton, N. J., 1975.

Fieldson G. T., Barbari T. A., *Polymer*, 1993, **34**, 1146.

Fringeli U. P., in *Internal Reflection Spectroscopy : Theory and Applications*, ed. Mirabella F. M. Jr., Marcel Dekker Inc., New York, 1993.

Giordano R., Teixeira J., Wanderlingh U., *J. of Mol. Struct.*, 1993, **296**, 271.

Giordano R., Teixeira J., Wanderlingh U., *Physica B*, 1995, **213**, 769.

Hajatdoost S., Yarwood J., *J. of Chem. Soc., Faraday Trans.*, 1997, **93(8)**, 1613.

Hare D. E., Sorensen C. M., *J. of Chem. Phys.*, 1990, **93**, 6954, and 1992, **96**, 13.

Hernandez J., Uras N., Devlin P., *J. of Chem. Phys.*, 1998, **108(11)**, 4525.

Jabbari E., Peppas N. A., *J. of Mat. Sci.*, 1994, **29**, 3969.

Jabbari E., Peppas N. A., *Macromolecules*, 1995, **28**, 6229.

Kauzmann W., *Adv. Protein. Chem.*, 1959, **14**, 1.

Kusanagi H., Yukawa S., *Polymer*, 1994, **35**, 5637.

Li Z., Li X., Petrovic S., Harrison D. J., *Anal. Chem.*, 1996a, **68**(10), 1717.

Li Z., Li X., Rothmaier M., Harrison D. J., *Anal. Chem.*, 1996b, **68**(10), 1726.

Libnau F. O., Christy A. A., Kvalheim O. M., *Appl. Spec.*, 1995, **49**, 1431.

Libnau F. O., Kvalheim O. M., Christy A. A., Toft, *J. of Vib. Spec.*, 1994, **7**, 243.

Luck W. A. P., Schioberg G. D., Sieman U., *J. of the Chem. Soc., Faraday Trans. 2*, 1980, **76**, 136.

Maeda Y., Tsukida N., Kinato H., Terada T., Yamanaka J., *J. of Phys. Chem.*, 1993, **97**, 3619.

Maeda Y., Tsukida N., Kinato H., Terada T., Yamanaka J., *Spectrochimica Acta*, 1995, **51**, 2433.

Maeda Y., Tsukida N., Kinato H., Terada T., Yamanaka J., *Macromol. Chem. Phys.*, 1996, **197**, 1681.

Marechal Y., *J. of Phys. Chem.*, 1993a, **97**, 2846.

Marechal Y., *J. of Mol. Struct.*, 1994, **322**, 105.

Marechal Y., *J. of Chem. Phys.*, 1991, **95**, 5565.

Marechal Y., *J. of Phys. II*, 1993b, **3**, 557.

Marechal Y., Chamel A., *J. of Phys. Chem.*, 1996a, **100**, 8551.

Marechal Y., Chamel A., *Faraday Discuss.*, 1996b, **103**, 349.

McBrierty V. J., Coey J. M. D., Boyle N. G., *Chem. Phys. Lett.*, 1982, **86**, 16.

Mirabella F. M., *Appl. Spec. Rev.*, 1985, **35**, 5637.

Murphy D., Depinho M. N., *J. of Membr. Sci.*, 1995, **106**, 245.

Nguyen Q. T., Byrd E., Lin C., *J. of Adhes. Sci. and Techn.*, 1991, **5**, 697.

Otting G., Liepinsh E., Wuthrich K., *J. of the American Chem. Soc.*, 1991, **113**, 4363.

Otting G., Liepinsh E., Wuthrich K., *Science*, 1991, **254**, 974.

Pereira M. R., Yarwood J., *J. of Polym. Sci., part B, Polym. Phys.*, 1994, **32**, 1881.

Pereira M. R., Yarwood J., *J. of Chem. Soc., Faraday Trans.*, 1996, **92(15)**, 2731, and 2737 .

Pethig R., *Ann. Rev. Phys. Chem.*, 1992, **43**, 177.

Quezado S., Kwak J. C. T., Falk M., *Can. J. Chem.*, 1984, **62**, 958.

Ratcliffe C. I., Irish D. E., *J. of Phys. Chem.*, 1982, **86**, 4897.

Sartor G., Johari G. P., *J. of Phys. Chem.*, 1996, **100**, 1045.

Scherer J. R., Bailey G. F., Kird S., Young R., Malladi D. P., Bolton B., *J. of Phys. Chem.*, 1985, **89**, 312.

Scherer J. R., Go M. K., Kint S., *J. of Phys. Chem.*, 1974, **78**, 1304.

Schlotter N., Furlan P. V., *Polymer*, 1992, **33**, 3332.

Settles M., Doster W., *Faraday Discuss.*, 1996, **103**, 269.

Sutender P., Ahn D. J., Franses E. I., *Macromolecules*, 1994, **27**, 7316.

Sutender P., Ahn D. J., Franses E. I., *Thin Solid Films*, 1995, **263**, 134.

Tao N. J., in *Water and Biological Macromolecules*, ed. Westhof E., MacMillan Press Ltd, London, 1993, Chapter 9, pp 266 - 292.

Teixera J., Stanley H. E., *J. of Chem. Phys.*, 1980, **73**, 3404.

Van Alsten J. G., *Trends in Polym. Sci.*, 1995, **3**, 272.

Van Alsten J. G., Coburn J. C., *Macromolecules*, 1994, **27**, 3752 (3476).

Walrafen G. E., in *Water, A comprehensive Treatrise*, Plenum, New York, ed. Franks F., 1972.

Walrafen G. E., Fischer M. RM, Hakmatadi M. S., Yang W. H., *J. of Chem. and Phys.*, 1986, **85**, 6964, and 6970.

Walrafen G. E., Fischer M. RM, Hakmatadi M. S., Yang W. H., *J. of Phys. Chem.*, 1993, **97**, 5430.

CHAPTER 8. :
LEACHING STUDIES OF FLUORFOLPET.

CONTENTS

CHAPTER 8. : LEACHING STUDIES OF FLUORFOLPET.	267
8. 1. INTRODUCTION.....	269
8. 2. EXPERIMENTAL	270
8. 2. 1. FTIR-ATR spectroscopy.....	270
8. 2. 2. Rotating disc method	274
8. 3. RESULTS AND DISCUSSION.....	276
8. 3 .1. FTIR-ATR results	276
8. 3. 2. Rotating disc method	281
8. 4. SUMMARY AND CONCLUSIONS	289
8. 5. REFERENCES.....	290

CHAPTER 8. : LEACHING STUDIES OF FLUORFOLPET

8. 1. INTRODUCTION

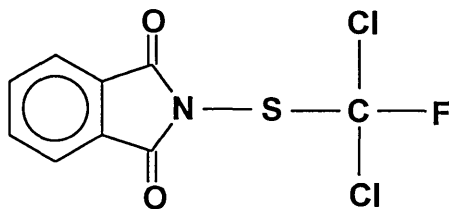
Considerable research interest has been shown in recent years in the phenomena and mechanisms underlying the transport of residual monomers and additives from polymeric materials into surrounding fluids and solids, because of the potential environmental hazard and toxicity of these additives (Sadiki et al. 1996, Papaspyrides and Papakonstantinou 1996, Fayad et al. 1997, Lakshmi and Jayakrishnan 1998, Kondyli et al. 1992). The additives most often studied are plasticisers. For PVC, usually the migration of DOP (dioctylphthalate) from the polymer film into organic solvent (Messadi et al. 1991, Messadi and Vergnaud 1997, Berens and Hopfenberg 1982, Taverdet et al. 1982) or fat simulant liquids (Kondyli et al 1992, Messadi and Gheid 1994, Riquet et al. 1991) is studied. Very little work has been done on the migration of other additives such as fillers (Balik and Xu 1994) or biocides. Biocide diffusion out of the processed vinyl products determines to a great extent the useful lifetime of the functional article.

Leaching of fluorfolpet was studied using Raman microscopy (see chapter 5.), FTIR-ATR spectroscopy and the rotating disc method. In this chapter results from ATR and the rotating disc (RD) method will be presented and discussed. The latter method was used to measure the diffusion coefficient of biocidal molecules migrating inside the films. This method has been used previously by Booth and co-workers (Zeneca Specialties Manchester) and has given satisfactory results in measuring the leaching rates of various biocides from paint films.

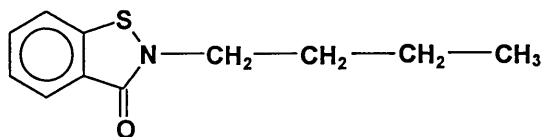
8. 2. EXPERIMENTAL

The leaching of two biocides was studied. These were fluorfolpet and vanquish.

fluorfolpet :



vanquish :



The polymer samples were prepared as described in chapter 4.

8. 2. 1. FTIR-ATR spectroscopy

Using ATR spectroscopy, it is possible to obtain the diffusion profiles not only of water in the polymer film, but also other species, providing they have detectable and distinguishable infrared bands. This is the case for the fungicide, fluorfolpet. Hence it is possible to follow the leaching of the fungicide into water and simultaneously monitor the water absorption phenomenon. This was done by following the decrease of the band at 805 -880 cm⁻¹ with time. As water diffuses into the polymer, the biocide band at 805 - 880 cm⁻¹ decreases in intensity ((see **figures 8. 1.** and **8. 2.**). A leaching profile of the fluorfolpet molecules with time was obtained by plotting the band area at 805 - 880 cm⁻¹ against time (see **figure 8. 3.**).

Figure 8. 1. The infrared spectrum of a film with composition 5% fluorfolpet / 20% DOP / PVC, in the range 500 - 2000 cm^{-1} .

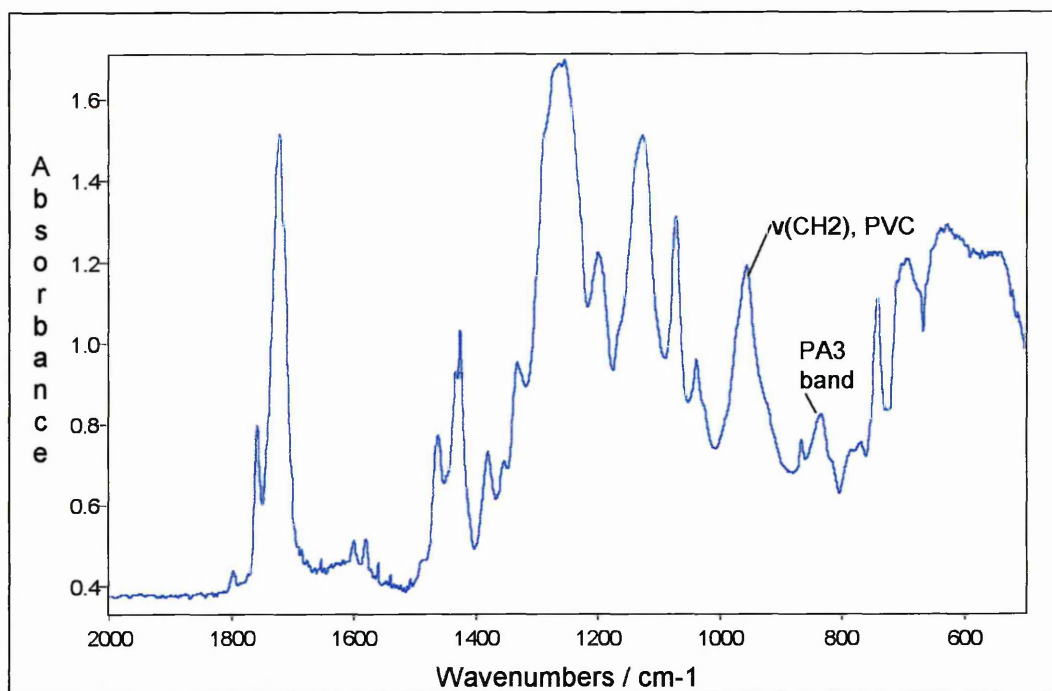


Figure 8. 2. The biocide band at 805 - 880 cm^{-1} at $t = 0$ and $t = 330$ min. and the difference spectrum, thereby establishing decrease of PA3 band.

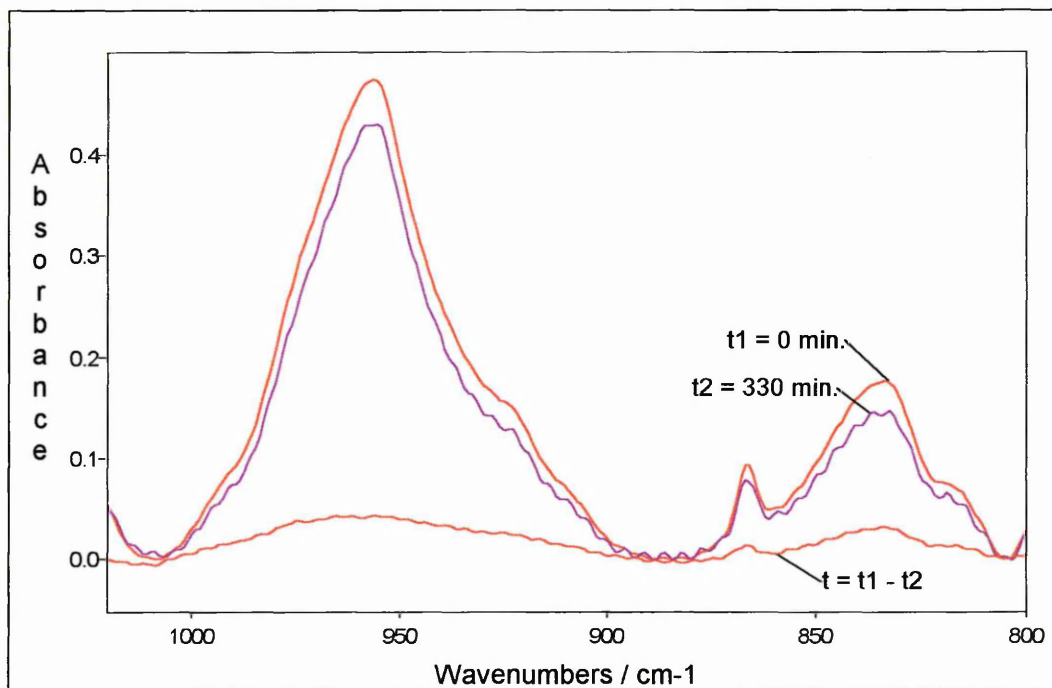
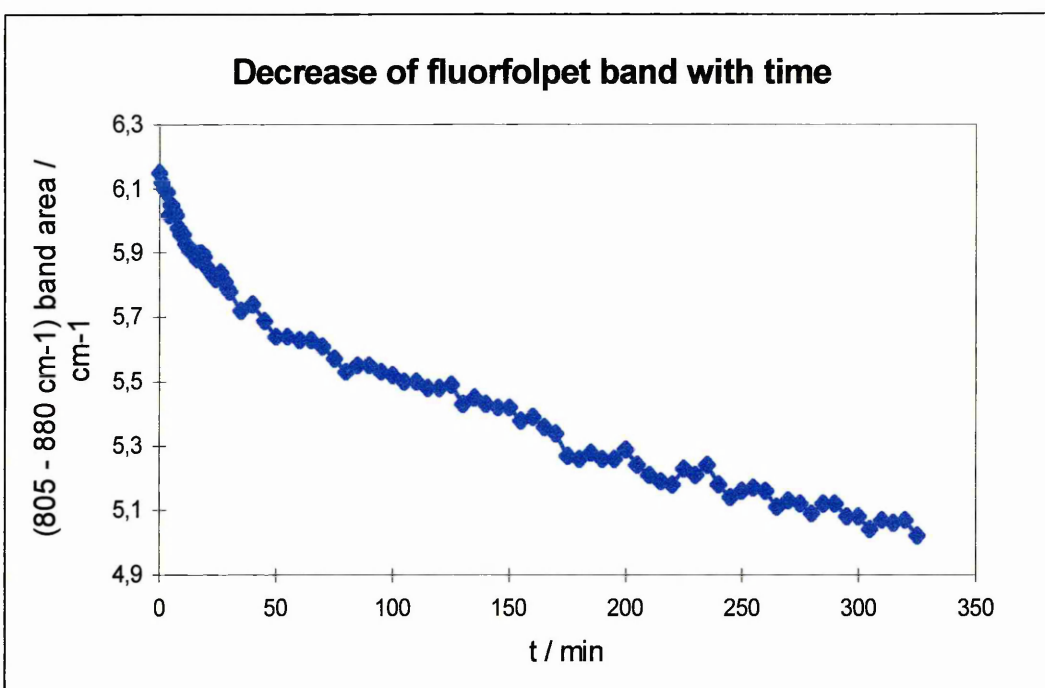


Figure 8. 3. The leaching profile of fluorfolpet from a 5% PA3/ 20% DOP / PVC film.



The diffusion of water into the polymer clearly induces swelling of the polymer film. That swelling can be followed, by monitoring the decrease of the band at 1010 - 885 cm^{-1} due to PVC, as described in chapter 6. The swelling of the polymer is also partly responsible for the decrease of the band at 880-805 cm^{-1} from fluorfolpet. Therefore by subtracting the swelling percentage from the overall decrease in fluorfolpet, one obtains a measurement of the loss of biocide (in %) from the film by leaching, i.e. % PA3 decrease - % swelling = effective % PA3 decrease. This figure can also be estimated by analysing the diffusion water, using UV-Vis spectroscopy. Fluorfolpet shows two peaks at 218.6 nm and 237.5 nm, and vanquish shows one band at 317.0 nm which can be used for UV analysis (see **figures 8. 4.** and **8. 5.**).

Figure 8. 4. A spectrum of an aqueous vanquish solution of concentration 8 ppm.

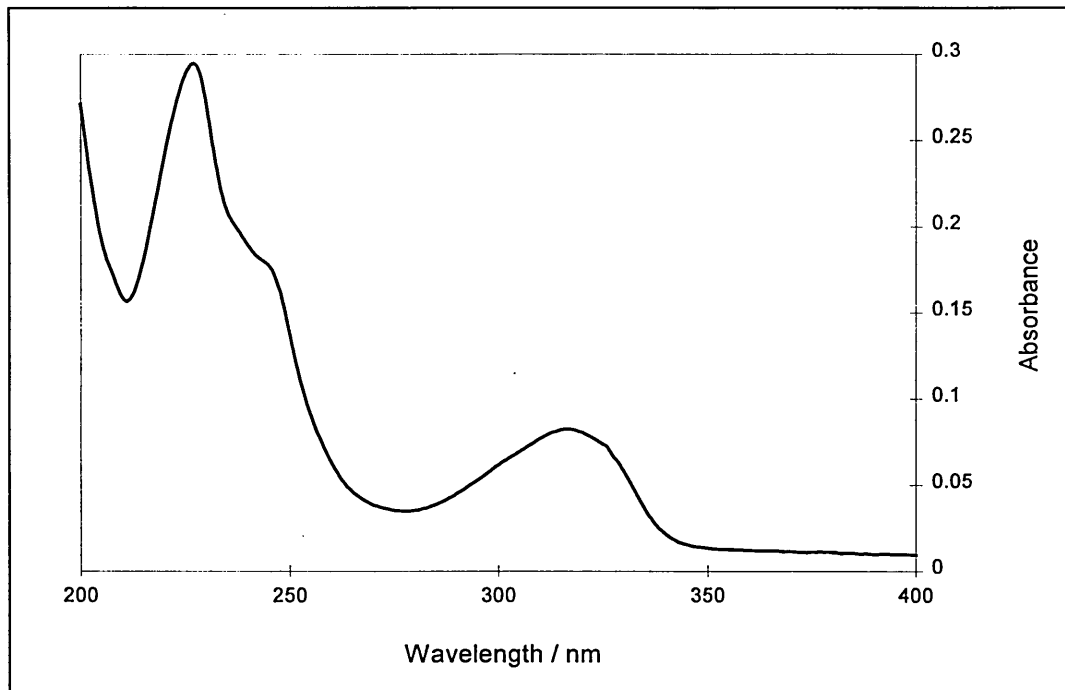
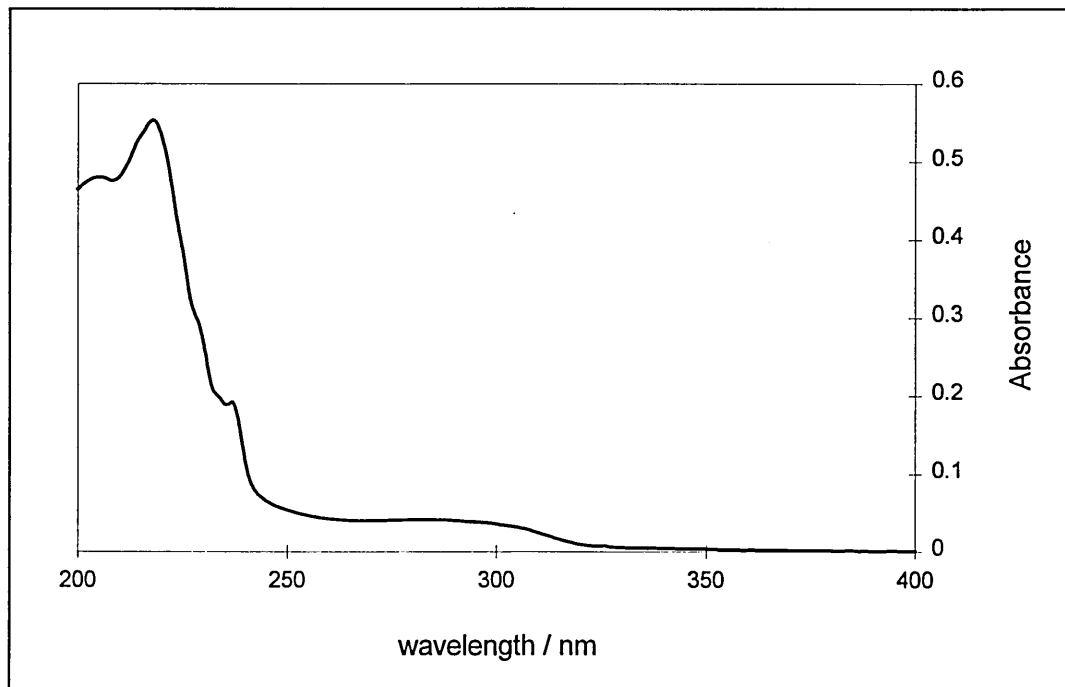


Figure 8. 5. A spectrum of an aqueous fluorfolpet solution of concentration 6 ppm.



8. 2. 2. Rotating disc method

Unlike the ATR experiment, which is a static experiment, the rotating disc method is a dynamic process. Under the experimental conditions (described in chapter 4.) and because the mass transport of the biocide from the surface into bulk solution is fast compared with the rate at which the biocide reaches the surface from the interior of the film, the leaching behaviour observed simply reflects migration of the leachate within the film. Leaching profiles were generated by measuring the concentration of leached biocide in bulk solution, by UV, as a function of time. In order to do this, calibration curves needed to be constructed.

Figure 8. 6. The calibration curve for vanquish.

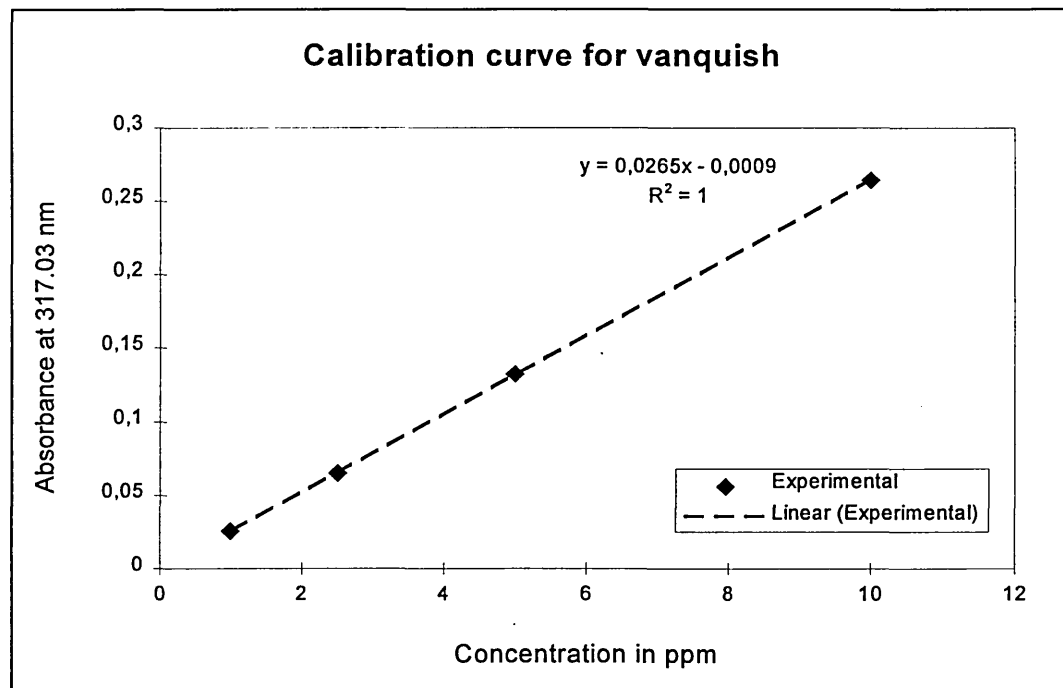
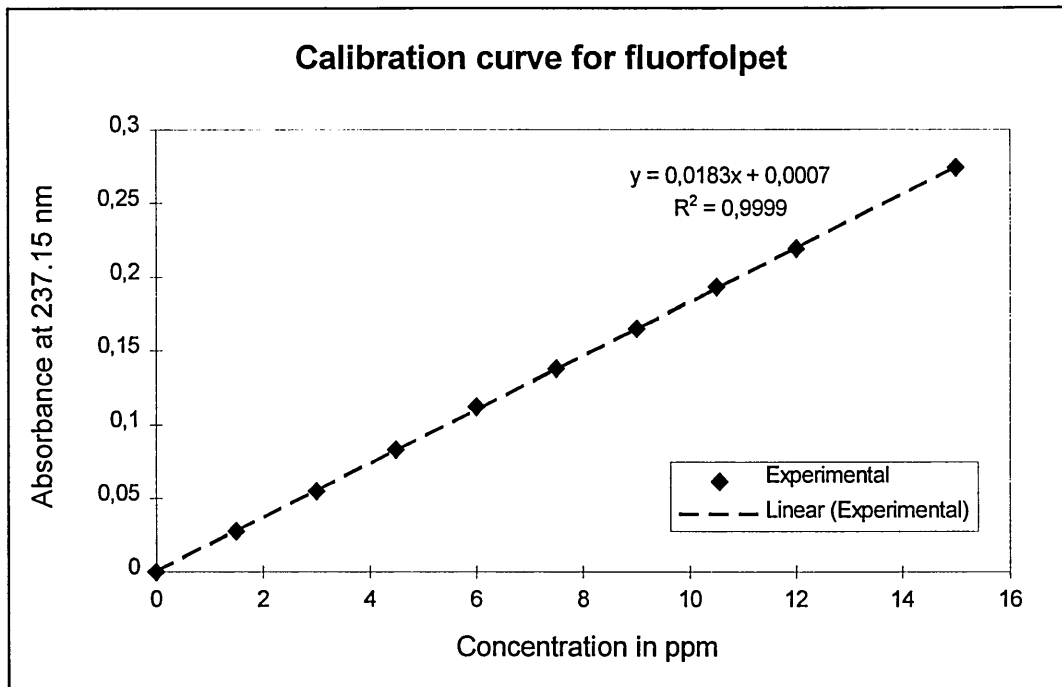


Figure 8. 7. The calibration curve for fluorfolpet.



The diffusion coefficient was obtained using equation (eq 4. 24) (see chapter 4.) :

$$M_t = 2A(Dt / \pi)^{1/2} \quad (\text{eq. 4. 24.})$$

Where

M_t = amount of biocide released after time t (g/cm²),

A = initial loading of biocide in the film (g/cm³),

D = diffusion coefficient of the leaching species within the film (cm²/s).

8. 3. RESULTS AND DISCUSSION

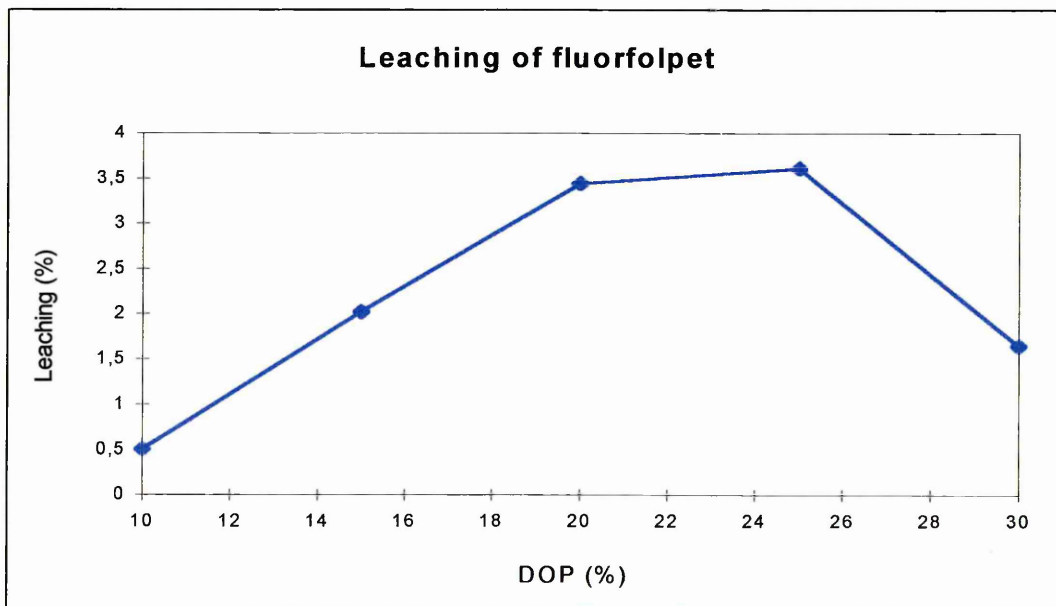
8. 3 .1. FTIR-ATR results

Table 8. 1. Shows the results obtained using the data collected during the water sorption experiments (11 different samples). All samples initially containing 5% fluorfolpet.

Effective PA3% =%PA3 decrease - %swelling.

DOP (%)	PA3 decrease (%)	Swelling (%)	Effective PA3 decrease (%)
10	2.05	2.03	0.02
10	6.91	6.56	0.35
10	2.98	2.32	0.66
15	10.20	8.18	2.02
20	18.37	13.64	4.73
20	15.80	13.65	2.15
20	8.56	8.22	0.34
20	12.50	11.74	0.76
25	28.75	25.14	3.61
30	12.57	10.58	1.99
30	21.2	19.9	1.3

Figure 8. 8. Shows a plot of the percentage fluorfolpet lost (from the initial 5%) by leaching against plasticiser concentration.



The amount of fluorfolpet leached from the film appears to be dependent on the concentration of DOP in the film (see **table 8. 1.** and **figure 8. 8.**). There is a non-monotonic change of the amount of fluorfolpet leached out with an increase of DOP concentration in the films. The profile of percentage fluorfolpet leached versus concentration reached a maximum around 25% DOP content, confirming the results obtained from Raman mapping (chapter 5.).

The table below (**table 8. 2.**) shows the results obtained from the examination of the diffusion waters, from each experiment, using UV spectroscopy. The UV spectra are shown on **figure 8. 9.**.

Table 8. 2. Shows the results of the UV spectroscopy analysis on the diffusion waters of 14 different experiments.

DOP (%)	Amount of PA3 in the water (mg) (x10e3)	Amount of PA3 leached (%)	Concentration of PA3 in the water (ppm)
10	-	-	-
10	-	-	-
10	-	-	-
15	9.58	0.68	4.79
15	12.82	0.91	6.41
20	13.75	0.97	9.17
20	16.30	1.15	10.87
20	19.60	1.38	13.70
20	11.60	0.82	7.73
25	17.67	1.25	8.83
25	13.00	0.92	6.50
25	14.92	1.05	7.41
30	13.96	0.99	6.98
30	7.90	0.56	7.90

(-) means we were not able to detect the presence of any fluorfolpet in the water.

Figure 8. 9. Shows UV spectra obtained from the ATR diffusion waters.

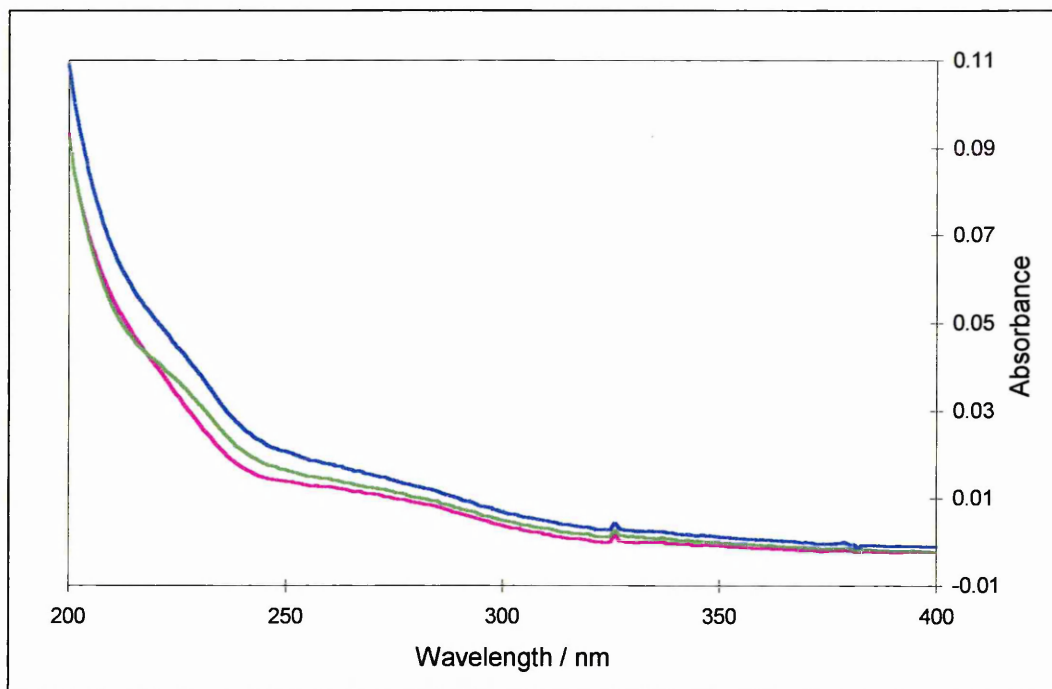
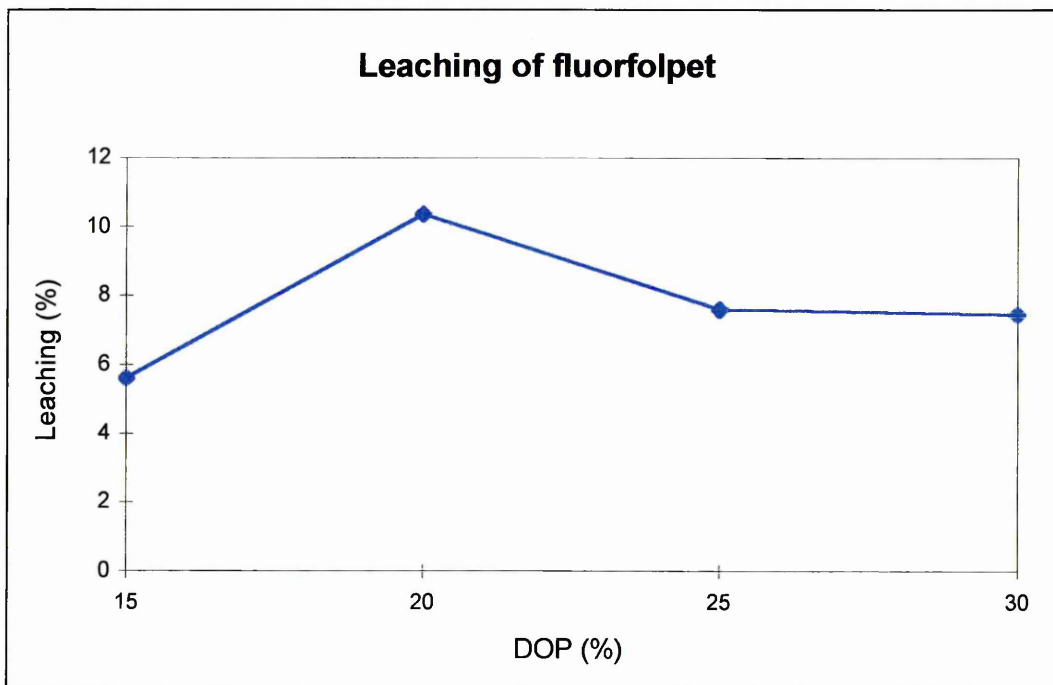


Figure 8. 10. Shows a plot of leaching (in %) against DOP concentration as obtained from UV measurements on diffusion waters.



The comparison between the results obtained from FTIR-ATR and the results from UV spectroscopy show a discrepancy : the leaching values from infrared

spectroscopy are much higher than the ones obtained from UV analysis. This could be due to either or both of the following :

- a) The effective penetration depth of the evanescent wave in the ATR experiment is very small (a few μm) (see chapter 2.), which means that only about 10% of the sample (starting at the crystal/film interface) is probed. Therefore the decrease of fluorfolpet resulting from the decrease in band area is the result from fluorfolpet molecules moving out of the sampling area and not necessarily out of the film. This provides definite evidence of migration of the fluorfolpet molecules from the bulk of the film towards the surface exposed to water.
- b) Analysis of the water requires manual removal from the cell (prior to drying of the film with gas N_2), i.e. a small quantity of water would always be trapped in the cell, and impossible to remove.

It is much more likely to be a) than b).

As can be seen from **table 8. 2.** the amount of fluorfolpet leached is lower than its solubility in water, i.e. the water was not saturated. It follows that the leaching process is not limited by the solubility of the leachate in the solvent.

Table 8. 2. and **figures 8. 8.** and **8. 10.** clearly demonstrate the dependence of leaching upon the concentration of DOP in the films. As the concentration of DOP in the film increases, so does the ratio of DOP to fluorfolpet molecules, whereas the ratio of PVC to PA3 decreases. **Table 8. 3.** shows the PVC/PA3 and DOP/PA3 ratios as DOP concentration in the films increases. If the fluorfolpet molecules were simply dissolved in the DOP, then as the DOP concentration increases, the dissolution capacity of the polymer should increase. The solubility for fluorfolpet in DOP is much larger than that in water, so leaching should decrease with increase of DOP content. This is clearly not the case. This suggests that the fluorfolpet molecules are actually dispersed in the polymer matrix itself. Furthermore, this shows that the solubility of the leaching species in the polymer matrix may influence the amount of additive leaving the matrix, but not completely determine the phenomenon. A

monotonic increase of the leaching with increase of DOP concentration would be expected if only one effect were relevant.

Table 8. 3. Shows the proportion of fluorfolpet with respect to PVC and DOP concentrations of the films.

DOP(%)	DOP / PA3 ratio	PVC (%)	PVC/PA3 ratio
10	2	85	17
15	3	80	16
20	4	75	15
25	5	70	14
30	6	65	13

As seen in previous chapters (chapter 5. and 6.), the amount of DOP in the films is responsible for the degree of chain mobility and free volume in the film, and therefore the amount of water sorbed in the films during diffusion. The amount of fluorfolpet leaching from the film seems to be directly related to the amount of water sorbed into the film, indeed the more water penetrates the film, the more fluorfolpet is removed (see *table 8. 4.*). This suggests that the fluorfolpet molecules are dissolved by the water, or in other words, made more mobile. This would be consistent with the theory of Riquet and co-workers (Riquet et al. 1991), who propose that penetrant diffusion activates the migration of the additives in the films, by mobilising the small molecules which then diffuse rapidly out of the polymer.

Table 8 .4. Shows the water content of the films at equilibrium (expressed as $\nu(\text{OH})$ band intensity in absorbance units) and the percentage fluorfolpet leached out with reference to DOP content.

DOP (%)	Water content at equilibrium	Leaching (%) from UV	Leaching (%) from ATR
10	0.28	0	0.34
15	0.55	0.795	2.02
20	0.76	1.080	3.44
25	0.92	1.073	3.61
30	0.52	0.775	1.29

The decrease in leaching at concentration of DOP higher than to 20% is most probably due to a decrease in the mean free volume in the polymer, brought about by the occupation of the voids by an excess of plasticiser, resulting in a net decrease of the water sorption capability of the matrix.

8. 3. 2. Rotating disc method

The leaching dynamics of two biocides, fluorfolpet and vanquish were studied. The concentrations of the biocides as well as that of DOP were varied.

By plotting the amount of biocide leached against time, the diffusion curve of the biocide was obtained, as shown by *figures 8. 11.* and *8. 12.* for the leaching of fluorfolpet from a 5% PA3 / 30% DOP / PVC disc and for the leaching of vanquish from a 5% BIT / 30% DOP / PVC film.

Figure 8. 11. The leaching profile of fluorfolpet from a 5% PA3 / 30% DOP / PVC film.

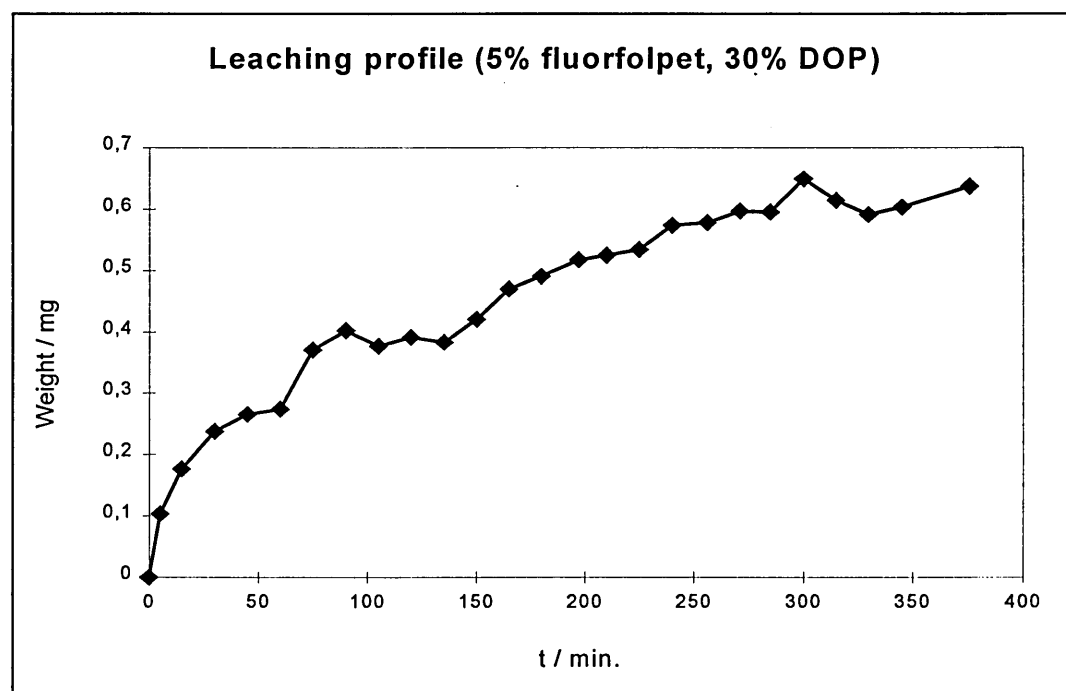
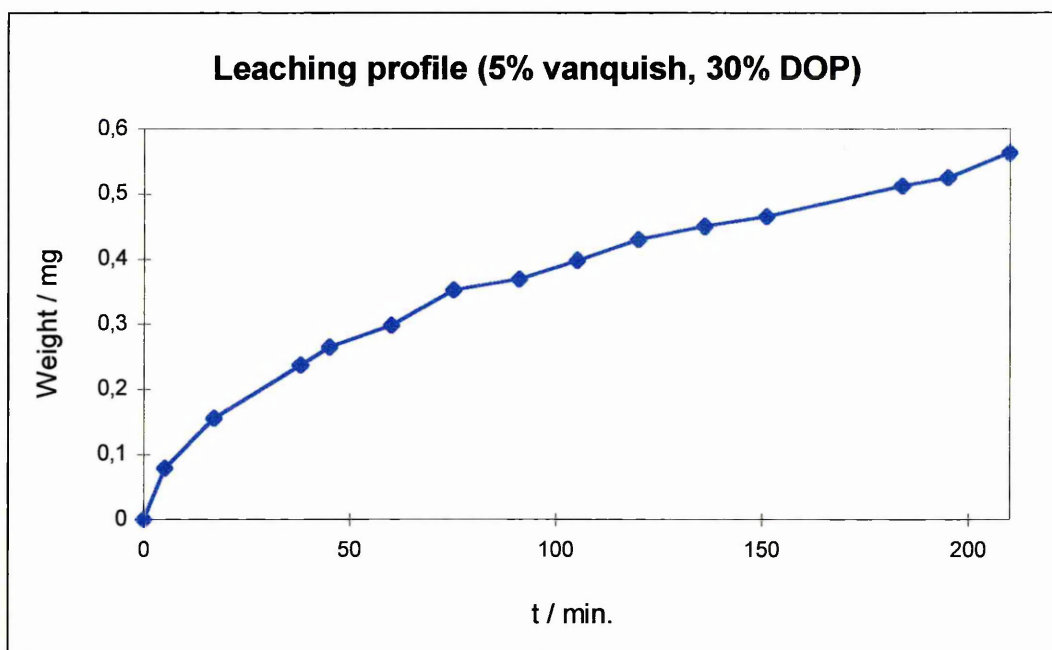


Figure 8. 12. The leaching profile of vanquish from a 5% BIT / 30% DOP / PVC film.



The diffusion coefficients were calculated from the slope of the plots M_t vs $t^{1/2}$ (see **figure 8. 13.**) and are displayed in **tables 8. 5.** and **8. 6.** for fluorfolpet and vanquish respectively.

Figure 8. 13. Plot of M_t vs $t^{1/2}$ for the leaching of vanquish from 5% BIT / 30% DOP / PVC film.

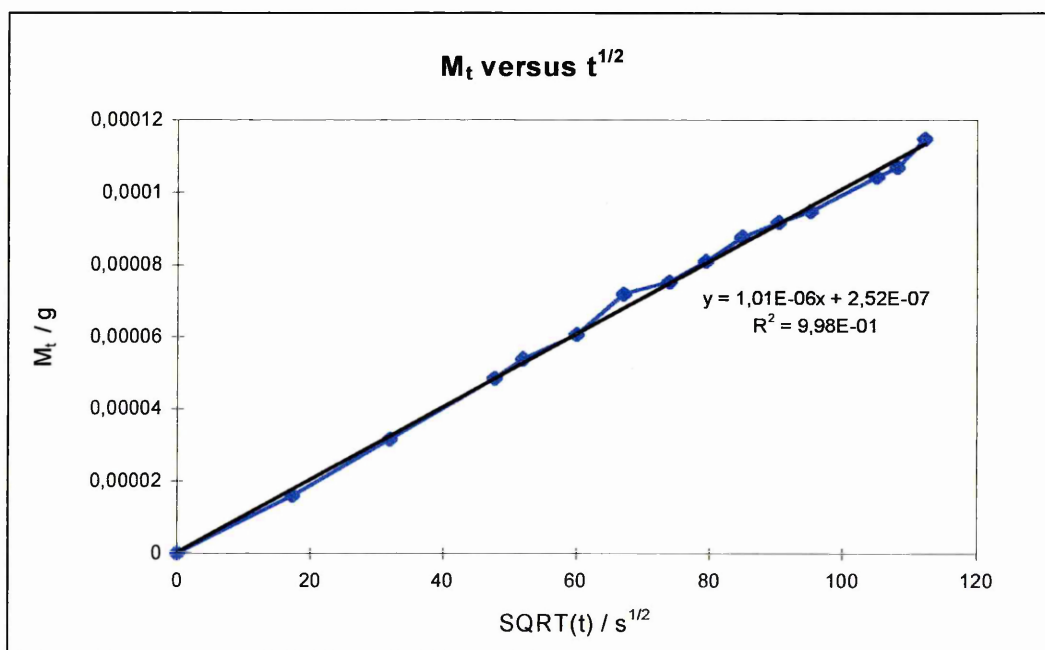


Table 8. 5. Shows the diffusion coefficients for the migration of fluorfolpet in plasticised PVC films. The diffusion coefficients were calculated from the plots M_t versus $t^{1/2}$.

DOP (%)	Initial PA3 loading (%)	D (cm ² /s)	Conc. of water (ppm) at t = 360min	Tg (°C)
10	3	-	-	28.9
10	5	-	-	32.8
20	3	5.39e-11	1.22	12.8
20	5	7.26e-11	1.45	13.9
30	1	1.09e-9	1.29	-3.3
30	3	3.01e-10	2.37	-10.6
30	5	1.81e-10	4.61	-8.5
30	7	1.16e-10	5.56	-
30	10	1.65e-10	10.09	-
30	15	9.84e-11	16.92	-

Table 8. 6. Shows the diffusion coefficients for the migration of vanquish (BIT) in plasticised PVC films. The diffusion coefficients were calculated from the plots M_t versus $t^{1/2}$.

DOP (%)	Initial BIT loading (%)	D (cm ² /s)	Conc. of water (ppm) at t = 210min	Tg (°C)
10	3	-	-	
10	5	-	-	
20	1	2.81e-14	0.19	
20	3	1.00e-11	0.22	-
20	5	2.45e-11	0.25	12.3
30	3	1.57e-10	1.69	-16.8
30	5	1.75e-9	2.63	-9.4

The diffusion rates in the 30% plasticised PVC films are much higher than at 20% (at equal amounts of biocides). No leaching was observed from the films containing 10% DOP. Indeed Raman (*figure 5. 25.*) and FTIR-ATR (*table 8. 1.* and *figure 8. 8.*) data show very little or no leaching of fluorfolpet, or vanquish, from films containing only 10% DOP. This could be due to the lower chain mobility of these films (at 25°C) compared to those with higher DOP content. As shown by *table 8. 5.* the Tg is higher than the working temperature (25°C). Therefore the films are not in the rubbery state, and chain mobility is limited, unlike above Tg. Above Tg the polymer molecular structure is “dynamic”, in

that frequent local conformational transitions can serve to create transient adjacent pockets (i.e. additional free volume) into which the penetrant or migrating molecules can jump. Knappe (Knappe 1954) and Grotz (Grotz 1965) in their study of the diffusion of DOP into rigid PVC concluded that the rate-limiting diffusion mechanism is the movement of segments of the polymer chains.

Changes of diffusion rate with DOP :

From *figures 8. 14.* and *8. 15.*, the diffusion coefficients increase with increasing DOP content, for both fluorfolpet and vanquish, and at both concentrations of biocide (3 and 5%). Furthermore, the diffusion coefficient of fluorfolpet in a 20% DOP / PVC matrix is of the same order as the one of vanquish in a 20% DOP / PVC matrix. At 30% DOP concentration however the diffusion coefficients of fluorfolpet and vanquish are very different, about an order of magnitude different. This could be explained by their difference in size, shape and / or molecular structure. Indeed, Storey and many others (Storey et al. 1989 and 1991, Meerwall 1991, Berens and Hopfenberg 1982, Riquet et al. 1991, Kumins and Roteman 1961, Prager and Long 1951, Van Amerongen 1964) have studied the effect of molecular mass or size, and shape of the diffusant on diffusion rate. They found that there was a decrease of D with increase in size, and/or branching of the diffusant molecules. A predominantly longitudinal molecular displacement during diffusion, (i.e. along the direction of least resistance for an elongated molecule) has been suggested by Storey and co-workers (Storey et al. 1989, Mauritz et al. 1990). In addition, if free volume is used to explain diffusion as it is often (Coughlin et al. 1991), our results can be explained by the following scenario.

We have shown that free volume is reduced in the films at 30% DOP concentration. The migration rate of vanquish molecules is higher than that of fluorfolpet molecules (about one order of magnitude) at identical initial biocide loading of 5%. Vanquish molecules can be described as elongated compared to fluorfolpet molecules. Therefore, as the free volume in the polymer matrix is reduced, vanquish molecules may be able to move more easily along the polymer chains. This would explain the difference in diffusion rate observed at

30% DOP content. At 20% DOP concentration, the mean free volume is large (i.e. maximum swelling and high water absorption is observed, chapter 6.), and therefore the size and shape of the diffusing molecules are less important.

Figure 8 .14. Shows the changes in diffusion coefficients with DOP concentration for films containing fluorfolpet (PA3), as obtained from the rotating discs experiments.

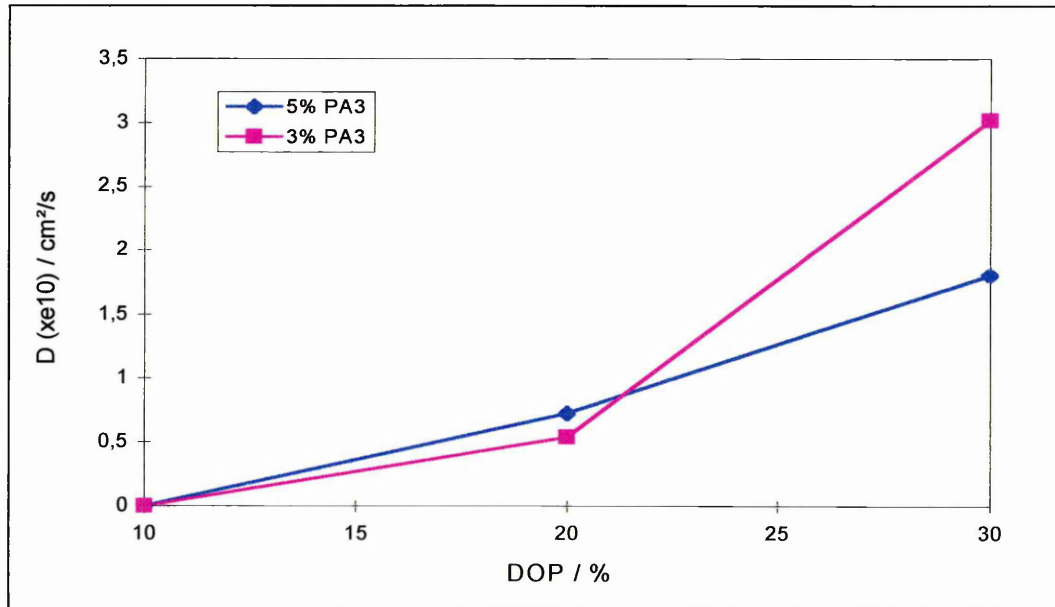
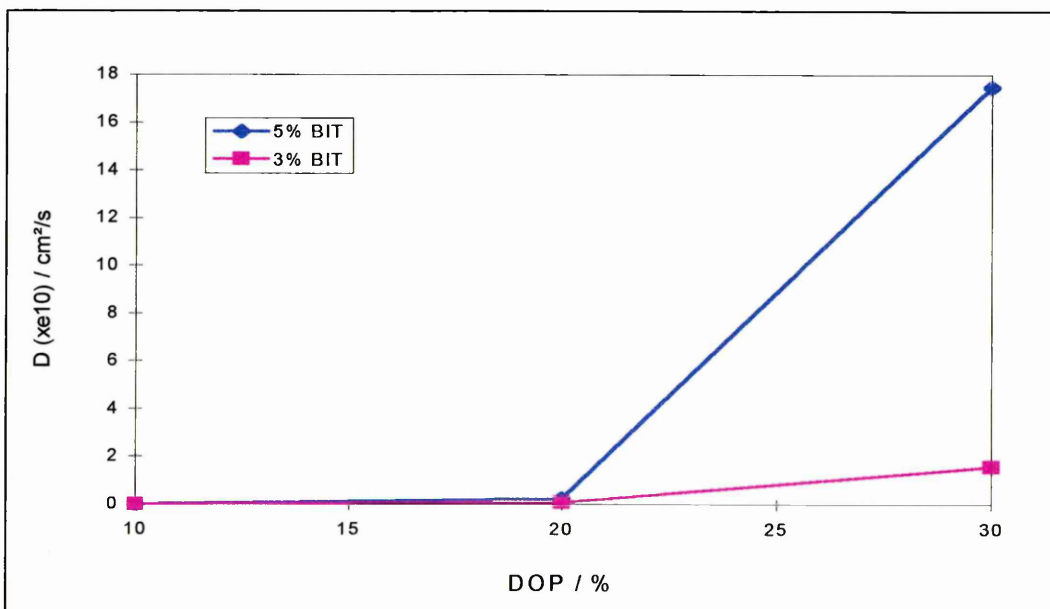


Figure 8 .15. Shows the changes in diffusion coefficients with DOP concentration for films containing vanquish (BIT), as obtained from the rotating discs experiments.



Changes of diffusion rates with initial biocide concentration :

As indicated by **figure 8. 16.** (although the numbers of points are limited), the diffusion coefficients, hence the rates of migration of the vanquish molecules, increase with increasing initial biocide loading at both 20 and 30% DOP concentrations. This is also true for fluorfolpet at 20% DOP concentration (see **figure 8. 17.**)

Figure 8. 16. Shows the change of diffusion coefficient with change in vanquish concentration in the films, at 20% and 30% DOP concentration.

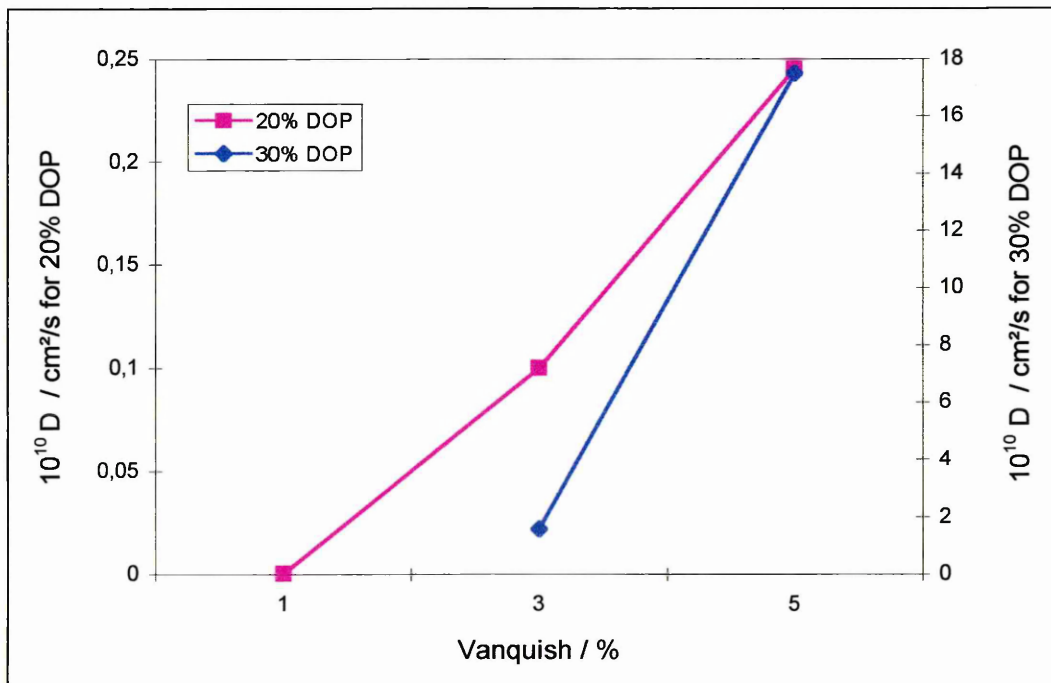


Figure 8. 17. Shows the change of diffusion coefficient with change in fluorfolpet concentration in the films, at 20% DOP concentration.

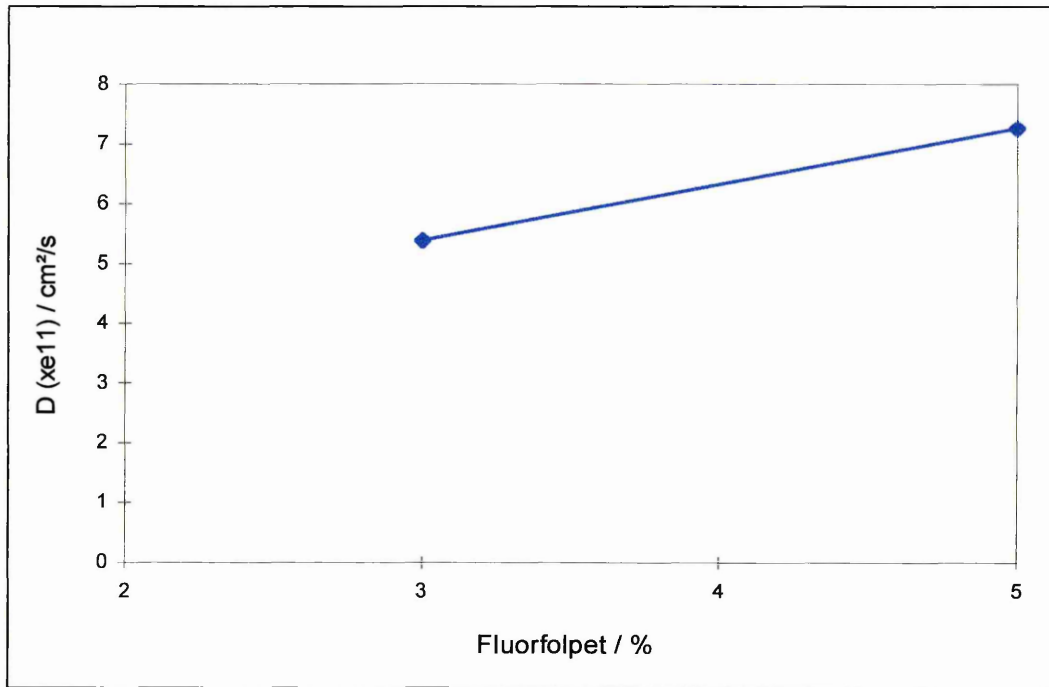
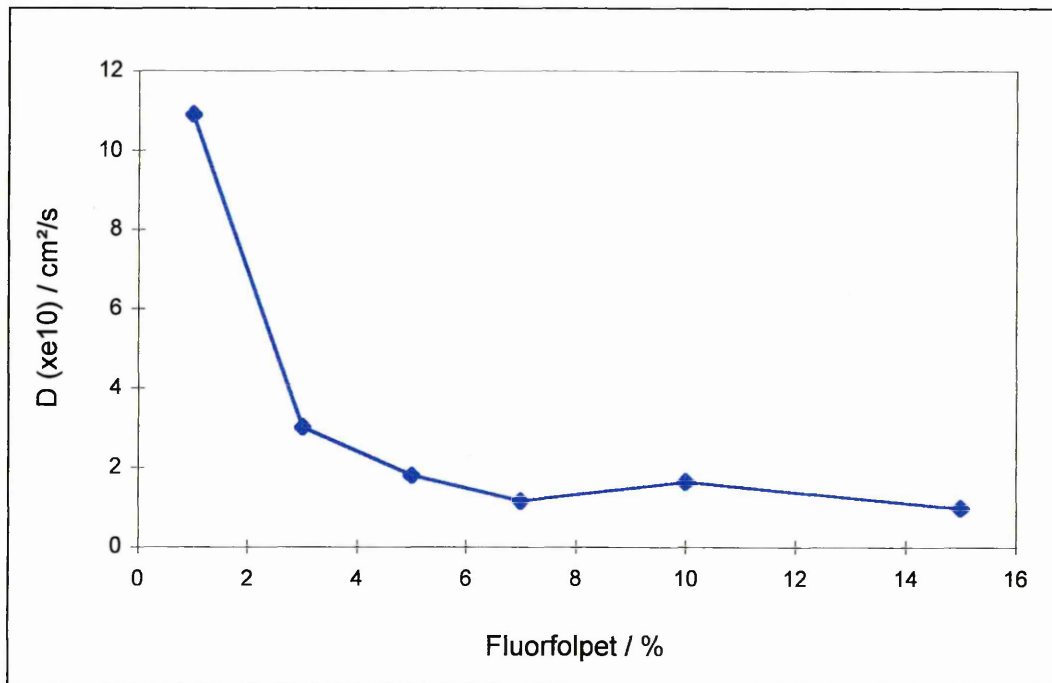


Figure 8. 18. shows the change of diffusion coefficient with change in fluorfolpet concentration in the films, at 30% DOP concentration.



Diffusion rates of fluorfolpet from films containing 30% (in wt) DOP show a strong dependency on initial biocide loading. As initial loading of fluorfolpet

increases, its leaching rate decreases (see **Figure 8 . 18.**). Various factors may be responsible for this very different behaviour at 30% DOP concentration:

- (i) decrease in free volume due to excess biocide molecules and/or size or shape of fluorfolpet compared to that of vanquish molecules,
- (ii) strong and/or increase in number of interactions between the fluorfolpet molecules and the polymer (or plasticiser) chemical groups,
- (iii) saturation of water (by fluorfolpet molecules) (see **table 8. 5.**) : as the initial amount of PA3 in the films increases, the leaching saturates the solvent.

8. 4. SUMMARY AND CONCLUSIONS

It has been demonstrated, that since the PVC matrix swells as water is sorbed, the leaching profiles for fluorfolpet obtained by FTIR-ATR were the result of the convolution of the swelling profile with the true leaching profile. Therefore no direct kinetic measurements can be made. However, to a very good approximation the amount of leachate was obtained from ATR measurements alone. Furthermore, the results confirm the results obtained from Raman mapping. The dependence of leaching upon the concentration of DOP in the films was also clearly demonstrated with both FTIR-ATR and UV analysis showing leaching levels changing in a non-monotonic way with increase of DOP concentration, and reaching a maximum at 25% DOP content.

It was also shown that the concentration of fluorfolpet in the solvent (water) was not a limiting factor for leaching, as saturation was not reached.

The rotating disc method allowed us to access the migration rate of fluorfolpet and vanquish inside the films and explore some of the factors responsible for molecular diffusion. It was shown that migration of these molecules depends on:

- (i) the chain mobility in the polymer, through the degree of plasticisation,
- (ii) the T_g and state of the polymer films, amorphous glassy, or amorphous rubbery. Indeed, no leaching was observed for films (10% DOP) when the working temperature was below their glass transition temperature,
- (iii) the mean free volume and local free volume through the size and shape of the molecules, and loading of both biocide and DOP.

8. 5. REFERENCES

- Amerongen (Van) G. J., *J. of Rubber Chem. and Techn.*, 1964, **37**, 1065.
- Balik C. M., Xu J. R., *J. of Appl. Polym. Sci.*, 1994, **52(7)**, 975.
- Berens A. R., Hopfenberg H. B., *J. of Membr. Sci.*, 1982, **10(2-3)**, 283.
- Coughlin C. S., Mauritz K. A., Storey R. F., *Macromolecules*, 1991, **24**, 1526 - 1534.
- Fayad N. M., Sheikheldin S. Y., AlMalack M. H., ElMubarack A. H., Khaja N., *J. of Environ. Sci. and Health, part A - Environ. Sci. and Eng. and Toxic and Hazard. Subs. Control*, 1997, **32(4)**, 1065.
- Grotz L. C., *J. of Appl. Polym. Sci.*, 1965, **9**, 207.
- Knappe W. Z., *Angew. Phys.*, 1954, **6(3)**, 96.
- Kondyli E., Demertzis P. G., Kontominas M. G., *Food Chem.*, 1992, **45(3)**, 163.
- Kumins C. A., Roteman J., *J. of Polym. Sci.*, 1961, **55**, 683 and 699.
- Lakshmi S., Jayakrishnan A., *Artificial Organs*, 1998, **22(3)**, 222.
- Mauritz K. A., Storey R. F., George S. E., *Macromolecules*, 1990, **23**, 441.
- Meerwall (von) E., Skowronski D., Hariharan A., *Macromolecules*, 1991, **24**, 2441.
- Messadi D., Fertikh N., Gheid A. E. H., *Eur. Polym. J.*, 1991, **27(11)**, 1187.

Messadi D., Gheid A.E.H., *Eur. Polym. J.*, 1994, **30**(2), 167.

Messadi D., Vergnaud J. M., *Eur. Polym. J.*, 1997, **33**(7), 1167.

Papaspyrides C. D., Papakonstantinou V., *J. of Polym. Eng.*, 1996, **15**(12), 153.

Prager S., Long F. A., *J. of the American Chem. Soc.*, 1951, **73**, 4072.

Riquet A. M., Sandray V., Akermann O., Feigenbaum A., *Sciences des Aliments*, 1991, **11**, 341.

Storey R. F., Mauritz K. A., Cole B. B., *Macromolecules*, 1991, **24**, 450.

Storey R. F., Mauritz K. A., Cox B. D., *Macromolecules*, 1989, **22**, 289.

Sadiki A. L., Williams D. T., Carrier R., Thomas B., *Chemosphere*, 1996, **32**(12), 2389.

Taverdet J. M., Hivert M., Vergnaud J. M., *Abstracts of Papers of the American Chem. Soc.*, 1982, **184**(sep), 8 -orpl.

CHAPTER 9. :
FINAL CONCLUSIONS AND FUTURE WORK.

CHAPTER 9. : FINAL CONCLUSIONS AND FUTURE WORK.

The main objectives of this work were to use Raman microscopy and FTIR-ATR spectroscopy to study the distribution and leaching of small molecules from a polymer matrix as a consequence of solvent sorption.

Starting with the work on the distribution of fluorfolpet in a plasticised PVC matrix, the potential of Raman microscopy, via depth profiling and mapping techniques has been demonstrated, as a tool for the study of molecular distribution and leaching.

It was established firstly, that the distribution of both the plasticiser and fluorfolpet molecules may be described as heterogeneous on a microscopic level, but homogeneous on a macroscopic scale. This was true both before and after leaching of fluorfolpet. Secondly, we showed that leaching is strongly dependent upon the plasticiser content, and hence indirectly upon the amount of water penetrating the film. A non-monotonic increase in leaching with increased DOP concentration was observed. Indeed, leaching reaches a maximum at 25% DOP content, probably due to a subsequent reduction of “free” volume in the polymer matrix. The decrease of free volume in the PVC matrix is the consequence of the occupation of voids and/or sites by excess DOP molecules in the film. Finally, it was demonstrated that leaching occurred from the surface (i.e. film/solvent interface) of the films.

More information on the leaching behaviour of fluorfolpet was obtained using FTIR-ATR spectroscopy and a rotating disc apparatus. It was demonstrated that (i) the solubility of the leaching species in the polymer matrix may influence the amount of additive leaving the matrix, but not completely determine the phenomenon, and (ii) the solubility of the leachate in the solvent did not limit the leaching process. The solubility of fluorfolpet in water is crucial, since water dissolves the fluorfolpet molecules, making them more mobile, and therefore activating their migration.

The results obtained strongly suggest that leaching is strongly dependent upon the mean “free” volume in the polymer matrix, and that the rate of migration of

the active molecules is most probably also strongly related to their size and shape.

In addition, it was found that the fluorfolpet molecules are dispersed in the polymer matrix itself, and not (simply) dissolved in the DOP.

The second part of the work was aimed at the analysis of the kinetics of water sorption and the calculation of the diffusion coefficients of the PVC membranes. Two different types of films were studied ; films containing fluorfolpet (at low concentration (5% w/w)) and films not containing fluorfolpet.

A method based on monitoring the time dependent changes in the $\nu(\text{OH})$ vibrational mode of water by ATR was used.

It was established that the diffusion of water into PVC is a two stage process, the first one being more rapid than the second stage. Both stages appear to be pseudo Fickian in the films studied. It therefore follows that the dual-mode model fits the data reasonably well. A dual-mode model was used to describe the diffusion of water in the PVC membranes, and calculate the diffusion coefficients.

It was found that diffusion rates were strongly dependent on DOP concentration. Indeed, they show a non-monotonic evolution with plasticiser concentration and a maximum at 20-25% DOP content.

We have illustrated the importance of chain mobility and free volume in the diffusion process, but also showed that the determining factor is the number of sites available in the matrix for bonding to water molecule. In addition, interactions of the H_2O with the chlorine (Cl) groups of PVC and fluorfolpet is strongly implied, rather than interactions of water with the ester groups of dioctylphthalate (or carbonyl groups of fluorfolpet).

The particular behaviour of $\nu(\text{OH})$ of water, and hence the perturbation of the water molecules in the polymer, was also analysed. Changes in intensities, and band shape with time and plasticiser content were studied. Calculation of the P factor reflected the enhancement of the extinction coefficient when water

molecules are engaged or are released from their hydrogen bonding environment.

The $\nu(\text{OH})$ band between 2950 and 3700 cm^{-1} was decomposed in four main component bands : “free” water, “weakly hydrogen bonded” water, “moderately hydrogen bonded” water, and “strongly hydrogen bonded” water.

It was shown that as water diffuses into the PVC membrane, there is a strengthening of the water hydrogen bonding network, but that it is still weaker than in pure water.

The strength of the hydrogen bonded network of water in the polymer is strongly dependent on the amount of water present in the film. The lower the water content, the weaker the hydrogen bonding network and vice versa. Furthermore, we showed that two stages are involved as water diffuses into the polymer ; (i) at low concentration of water, the network is broken and the water molecules are arranged in small clusters within the polymer microstructure, (ii) as expected, as the amount of water increases in the polymer, the cluster size also increases.

The techniques employed in this work have proven to be highly suitable for the study of polymeric materials and additives in these material. Structural and kinetic information was obtained. They could be used to study interactions in many different, including most, if not all polymer, additive and solvent systems.

Future work on the DOP / PA3/ PVC system could :

- consider the consequence of varying the loading and nature of both biocide and plasticiser on the leaching of the biocide and/or the plasticiser, as well as the diffusion of water,
- examine the consequences of higher temperatures on leaching and diffusion,
- study commercial films prepared by the “plastisol” route,
- explore the perturbation of water molecules as a function of biocide content.

CONFERENCES ATTENDED

1. Zeneca Polymer Club, Academic Collaborations Conference,
Conference Centre, Zeneca Specialties, Runcorn,
24 April 1996.
2. Microspectrometry Applications Group (MAG) Meeting : Sample
Preparation and Data Handling,
Reading Scientific Services Ltd.,
1 May 1996.
3. Process Spectroscopy discussion Group,
ICI's Heath Site at Runcorn,
4 June 1996.
4. Infrared and Raman Discussion Group (IRDG) and IRDG 3rd Martin and
Willis Prize Meeting for students,
Glaxo Wellcome Medicines Research Centre, Stevenage,
16 - 17 October 1996.
5. Microspectrometry Applications Group (MAG) Meeting,
Zeneca Specialties, Blackley, Manchester,
5 November 1996.
6. Microspectrometry Applications Group (MAG) Meeting : 3rd MAG
Award for Young Microspectroscopist,
Perkin Elmer Ltd., Seer Green, Buckinghamshire,
30 April 1997.
7. Polymer Surfaces and Interfaces III, an International Symposium,
Durham University, Durham,
14 - 18 July 1997

8. Infrared and Raman Discussion Group (IRDG)
Leeds University, Leeds,
31 March - 1 April 1998.

9. Gordon Research Conference on Water and Aqueous Solutions (GRC),
Holderness School, New Hampshire, USA,
2 - 7 August 1998.

PUBLICATIONS

Sammon C., Mura C., Yarwood J., Everall N., Swart R., Hodge D.,
FTIR-ATR Studies of the Structure and Dynamics of Water Molecules in
Polymeric Matrixes. A comparison of PET and PVC,
Journal of Physical Chemistry B,
1998, **102**(18), 3402 - 3411.

Mura C., Yarwood J., Swart R., Hodge D.,
Raman Microscopic Studies of the distribution of the Fungicide, Fluorfolpet, in
Plasticised PVC Films,
In print.

Mura C., Yarwood J., Swart R., Hodge D.,
Fluorfolpet Leaching Studies (Using the Rotating Disc Method),
In print.

Mura C., Yarwood J., Swart R., Hodge D.,
Hydration and Dehydration of Plasticised PVC Films,
In print.